

Alma Mater Studiorum – University of Bologna

RESEARCH DOCTORATE

Agricultural Engineering

Course XXII

**Scientific-disciplinary sector/s:** AGR/09

TITLE

**Biomass Gasification - Process analysis and  
dimensioning aspects for downdraft units and gas  
cleaning lines**

*Giovanni Stoppiello*

**Doctorate School Coordinator**

Guarnieri Adriano

**Supervisors**

Caprara Claudio

Fransson Torsten

final exam 2010

## PREFACE

This Doctoral thesis was worked out according to the Rector Decree rules of University of Bologna in order to achieve “Doctor Europaeus” Degree.

At this scope the pertaining research activity was carried out by the author in two different European universities, such as the “Alma Mater Studiorum” University of Bologna (Italy) and the Royal Institute of Technology in Stockholm (Sweden)

The main research idea was developed by the author and his supervisors, which were also the scientific mentors in the study.

The author was the developer of all the analytical procedures adopted in this work and the designer of the technical arrangements presented as practical results.

*Agricultural Economics and Engineering Department,  
Agricultural Engineering Division,  
“Alma Mater Studiorum” University of Bologna*

Viale G. Fanin, 50

40127 Bologna

tel: +39 051 2096192; +39 051 2096189

fax: +39 051 2096178

[www.deiagra.unibo.it/home-ingagraria.html](http://www.deiagra.unibo.it/home-ingagraria.html)

*Department of Energy Technology,  
Heat and Power Technology Division,  
Royal Institute of Technology*

Brinellvagen, 68

SE-100 44 Stockholm

tel: +46 (0)8 790 8921; +46 (0)8 790 7401

fax: +46 (0)8 204161

[www.energy.kth.se](http://www.energy.kth.se)

*“Dai diamanti non nasce niente,  
dal letame nascono i fior”*

F. De André

## ABSTRACT

In such territories where food production is mostly scattered in several small / medium size or even domestic farms, a lot of heterogeneous residues are produced yearly, since farmers usually carry out different activities in their properties. The amount and composition of farm residues, therefore, widely change during year, according to the single production process periodically achieved.

Coupling high efficiency micro-cogeneration energy units with easy handling biomass conversion equipments, suitable to treat different materials, would provide many important advantages to the farmers and to the community as well, so that the increase in feedstock flexibility of gasification units is nowadays seen as a further paramount step towards their wide spreading in rural areas and as a real necessity for their utilization at small scale.

Two main research topics were thought to be of main concern at this purpose, and they were therefore discussed in this work: the investigation of fuels properties impact on gasification process development and the technical feasibility of small scale gasification units integration with cogeneration systems. According to these two main aspects, the present work was thus divided in two main parts.

The first one is focused on the biomass gasification process, that was investigated in its theoretical aspects and then analytically modelled in order to simulate thermo-chemical conversion of different biomass fuels, such as wood (park waste wood and softwood), wheat straw, sewage sludge and refuse derived fuels.

The main idea is to correlate the results of reactor design procedures with the physical properties of biomasses and the corresponding working conditions of gasifiers (temperature profile, above all), in order to point out the main differences which prevent the use of the same conversion unit for different materials.

At this scope, a gasification kinetic free model was initially developed in *Excel* sheets, considering different values of air to biomass ratio and the downdraft gasification technology as particular examined application. The differences in syngas production and working conditions (process temperatures, above all) among the considered fuels were tried to be connected to some biomass properties, such elementary composition, ash and water contents.

The novelty of this analytical approach was the use of kinetic constants ratio in order to determine oxygen distribution among the different oxidation reactions (regarding volatile matter only) while equilibrium of *water gas shift* reaction was considered in gasification zone, by which the energy and mass balances involved in the process algorithm were linked together, as well.

Moreover, the main advantage of this analytical tool is the easiness by which the input data corresponding to the particular biomass materials can be inserted into the model, so that a rapid evaluation on their own thermo-chemical conversion properties is possible to be obtained, mainly based on their chemical composition

A good conformity of the model results with the other literature and experimental data was detected for almost all the considered materials (except for refuse derived fuels, because of their unfitting chemical composition with the model assumptions).

Successively, a dimensioning procedure for open core downdraft gasifiers was set up, by the analysis on the fundamental thermo-physical and thermo-chemical mechanisms which are supposed to regulate the main solid conversion steps involved in the gasification process. Gasification units were schematically subdivided in four reaction zones, respectively corresponding to biomass heating, solids drying, pyrolysis and char gasification processes, and the time required for the full development of each of these

steps was correlated to the kinetics rates (for pyrolysis and char gasification processes only) and to the heat and mass transfer phenomena from gas to solid phase.

On the basis of this analysis and according to the kinetic free model results and biomass physical properties (particles size, above all) it was achieved that for all the considered materials char gasification step is kinetically limited and therefore temperature is the main working parameter controlling this step.

Solids drying is mainly regulated by heat transfer from bulk gas to the inner layers of particles and the corresponding time especially depends on particle size. Biomass heating is almost totally achieved by the radiative heat transfer from the hot walls of reactor to the bed of material.

For pyrolysis, instead, working temperature, particles size and the same nature of biomass (through its own pyrolysis heat) have all comparable weights on the process development, so that the corresponding time can be differently depending on one of these factors according to the particular fuel is gasified and the particular conditions are established inside the gasifier.

The same analysis also led to the estimation of reaction zone volumes for each biomass fuel, so as a comparison among the dimensions of the differently fed gasification units was finally accomplished.

Each biomass material showed a different volumes distribution, so that any dimensioned gasification unit does not seem to be suitable for more than one biomass species.

Nevertheless, since reactors diameters were found out quite similar for all the examined materials, it could be envisaged to design a single units for all of them by adopting the largest diameter and by combining together the maximum heights of each reaction zone, as they were calculated for the different biomasses. A total height of gasifier as around 2400mm would be obtained in this case. Besides, by arranging air injecting nozzles at different levels along the reactor, gasification zone could be properly set up according to the particular material is in turn gasified.

Finally, since gasification and pyrolysis times were found to considerably change according to even short temperature variations, it could be also envisaged to regulate air feeding rate for each gasified material (which process temperatures depend on), so as the available reactor volumes would be suitable for the complete development of solid conversion in each case, without even changing fluid dynamics behaviour of the unit as well as air/biomass ratio in noticeable measure.

The second part of this work dealt with the gas cleaning systems to be adopted downstream the gasifiers in order to run high efficiency CHP units (i.e. internal engines and micro-turbines).

Especially in the case multi-fuel gasifiers are assumed to be used, weightier gas cleaning lines need to be envisaged in order to reach the standard gas quality degree required to fuel cogeneration units. Indeed, as the more heterogeneous feed to the gasification unit, several contaminant species can simultaneously be present in the exit gas stream and, as a consequence, suitable gas cleaning systems have to be designed.

In this work, an overall study on gas cleaning lines assessment is carried out. Differently from the other research efforts carried out in the same field, the main scope is to define general arrangements for gas cleaning lines suitable to remove several contaminants from the gas stream, independently on the feedstock material and the energy plant size

The gas contaminant species taken into account in this analysis were: particulate, tars, sulphur (in H<sub>2</sub>S form), alkali metals, nitrogen (in NH<sub>3</sub> form) and acid gases (in HCl form).

For each of these species, alternative cleaning devices were designed according to three different plant sizes, respectively corresponding with  $8\text{Nm}^3/\text{h}$ ,  $125\text{Nm}^3/\text{h}$  and  $350\text{Nm}^3/\text{h}$  gas flows. Their performances were examined on the basis of their optimal working conditions (efficiency, temperature and pressure drops, above all) and their own consumption of energy and materials.

Successively, the designed units were combined together in different overall gas cleaning line arrangements, *paths*, by following some technical constraints which were mainly determined from the same performance analysis on the cleaning units and from the presumable synergic effects by contaminants on the right working of some of them (filters clogging, catalysts deactivation, etc.).

One of the main issues to be stated in *paths* design accomplishment was the tars removal from the gas stream, preventing filters plugging and/or line pipes clogging. At this scope, a catalytic tars cracking unit was envisaged as the only solution to be adopted, and, therefore, a catalytic material which is able to work at relatively low temperatures was chosen. Nevertheless, a rapid drop in tars cracking efficiency was also estimated for this same material, so that an high frequency of catalysts regeneration and a consequent relevant air consumption for this operation were calculated in all of the cases.

Other difficulties had to be overcome in the abatement of alkali metals, which condense at temperatures lower than tars, but they also need to be removed in the first sections of gas cleaning line in order to avoid corrosion of materials. In this case a dry scrubber technology was envisaged, by using the same fine particles filter units and by choosing for them corrosion resistant materials, like ceramic ones.

Besides these two solutions which seem to be unavoidable in gas cleaning line design, high temperature gas cleaning lines were not possible to be achieved for the two larger plant sizes, as well. Indeed, as the use of temperature control devices was precluded in the adopted design procedure, ammonia partial oxidation units (as the only considered methods for the abatement of ammonia at high temperature) were not suitable for the large scale units, because of the high increase of reactors temperature by the exothermic reactions involved in the process.

In spite of these limitations, yet, overall arrangements for each considered plant size were finally designed, so that the possibility to clean the gas up to the required standard degree was technically demonstrated, even in the case several contaminants are simultaneously present in the gas stream.

Moreover, all the possible *paths* defined for the different plant sizes were compared each others on the basis of some defined operational parameters, among which total pressure drops, total energy losses, number of units and secondary materials consumption.

On the basis of this analysis, dry gas cleaning methods proved preferable to the ones including water scrubber technology in all of the cases, especially because of the high water consumption provided by water scrubber units in ammonia adsorption process. This result is yet connected to the possibility to use activated carbon units for ammonia removal and Nahcolite adsorber for chloride acid. The very high efficiency of this latter material is also remarkable.

Finally, as an estimation of the overall energy loss pertaining the gas cleaning process, the total enthalpy losses estimated for the three plant sizes were compared with the respective gas streams energy contents, these latter obtained on the basis of low heating value of gas only.

This overall study on gas cleaning systems is thus proposed as an analytical tool by which different gas cleaning line configurations can be evaluated, according to the particular practical application they are adopted for and the size of cogeneration unit they are connected to.

# CONTENTS

<b>PREFACE</b> .....	<b>1</b>
<b>ABSTRACT</b> .....	<b>4</b>
<b>LIST OF FIGURES</b> .....	<b>10</b>
<b>LIST OF TABLES</b> .....	<b>13</b>
<b>NOMENCLATURE</b> .....	<b>16</b>
<b>1 INTRODUCTION</b> .....	<b>22</b>
<b>1.1 State of the art</b> .....	<b>22</b>
<b>1.2 Objectives</b> .....	<b>23</b>
<b>1.3 Overall description of the work</b> .....	<b>24</b>

## PART I

### DOWNDRAFT GASIFICATION ANALYSIS AND UNITS DIMENSIONING ASPECTS

<b>2 METHODOLOGY</b> .....	<b>28</b>
<b>2.1 General aspects of process and technology</b> .....	<b>28</b>
2.1.1 Theoretical framework of gasification.....	28
2.1.2 Investigated gasification technology .....	30
<b>2.2 Thermo-chemical model description</b> .....	<b>34</b>
2.2.1 Biomass species .....	34
2.2.2 Moisture vaporization.....	36
2.2.3 Pyrolysis or devolatilization .....	36
2.2.4 Partial oxidation of pyrolysis products (flaming pyrolysis) .....	37
2.2.5 Char Gasification .....	38
2.2.6 Energy balances .....	39
<b>2.3 Principles of gasification units dimensioning</b> .....	<b>42</b>
2.3.1 Physical and chemical processes in char gasification.....	42
2.3.2 Pyrolysis controlling mechanisms .....	46
2.3.3 Fuel drying process.....	50
2.3.4 Biomass heating .....	51
<b>3 RESULTS</b> .....	<b>55</b>
<b>3.1 Outcomes from kinetic free model application on the different biomass fuels</b> .....	<b>55</b>
3.1.1 Main results by thermo-chemical model.....	55
3.1.2 Influence of moisture content and equivalence ratio on gasification model results.....	59
3.1.3 Validation of model results through the comparison with experimental data (woody biomasses).....	62
<b>3.2 Preliminary results for estimating gasification units dimensions</b> .....	<b>65</b>

3.2.1	Results from investigated conversion models for char gasification .....	66
3.2.2	Results from analytical investigation on fuels pyrolysis development .....	68
3.2.3	Moisture vaporization time according to the examined physical resistances ...	72
3.2.4	Required unit surfaces for biomass heating .....	72
3.2.5	Basic dimensions of gasification units .....	74
3.2.6	Influence of char particles properties on gasification zone dimensioning .....	76
3.2.7	Influence of temperature on gasification units dimensioning .....	77
3.2.8	Validation of pyrolysis modelling results through the comparison with experimental data .....	81
<b>4</b>	<b>DISCUSSIONS .....</b>	<b>82</b>
<b>4.1</b>	<b>Possibilities and limitations of thermo-chemical kinetic free model .....</b>	<b>82</b>
<b>4.2</b>	<b>Controlling mechanisms for solid conversion steps .....</b>	<b>83</b>

## PART II

### GAS CLEANING LINES FOR BIOMASS COGENERATION SYSTEMS

<b>5</b>	<b>METHODOLOGY .....</b>	<b>86</b>
<b>5.1</b>	<b>Gas cleaning lines sizes, gas contaminants and tolerance standard limits ....</b>	<b>86</b>
<b>5.2</b>	<b>Gas cleaning units .....</b>	<b>88</b>
5.2.1	Cyclone .....	90
5.2.2	Packed bed filters .....	94
5.2.3	Candle Filters .....	98
5.2.4	Fabric filters .....	101
5.2.5	Catalytic tars cracking unit .....	103
5.2.6	Zn-Ti adsorber for high temperature sulphur removal .....	111
5.2.7	Activated carbon adsorption unit .....	115
5.2.8	Wet scrubber packed column .....	122
5.2.9	Catalytic partial oxidation unit for ammonia decomposition .....	129
5.2.10	HCl dry adsorption unit .....	132
5.2.11	Dry scrubbing of alkali metals .....	135
<b>5.3</b>	<b>Gas cleaning line assembly .....</b>	<b>137</b>
5.3.1	Gas cleaning line temperature profile .....	138
5.3.2	Clogging of pipes and filters by tars condensation .....	140
5.3.3	Materials corrosion .....	141
5.3.4	Catalyst poisoning .....	141
5.3.5	Frequency of regeneration .....	142
<b>6</b>	<b>RESULTS AND DISCUSSIONS .....</b>	<b>143</b>

<b>7</b>	<b>OVERALL CONCLUSIONS .....</b>	<b>152</b>
<b>8</b>	<b>FUTURE WORK.....</b>	<b>156</b>
	<b>REFERENCES .....</b>	<b>157</b>
	<b>APPENDIX .....</b>	<b>162</b>
	A Single efficiencies for packed bed filters: .....	162
	B Jet pulse calculation for cleaning of candle and fabric filters .....	163
	C Dimensioning of fluidized bed reactors for catalytic tars cracking .....	164

## LIST OF FIGURES

<i>Figure 1: energy balance in auto-thermal gasification process (Ramesh and Nekere, 2005)</i>	29
<i>Figure 2: gasification scheme</i>	30
<i>Figure 3: downdraft gasification units at EKV – HPT laboratory (respectively 15-20 and 300 kW<sub>th</sub> sizes)</i>	31
<i>Figure 4: Scheme of a downdraft gasifier (Belgiorno et al., 2003)</i>	32
<i>Figure 5: thermo-chemical scheme of considered air downdraft gasification process</i>	41
<i>Figure 6: Solid carbon particles conversion models</i>	43
<i>Figure 7: Low heating values of product gas as a function of equivalence ratio, for the different biomass fuels</i>	60
<i>Figure 8: Cold gas energy efficiencies of gasification process as a function of equivalence ratio</i>	60
<i>Figure 9: Comparison of residual solid mass fractions and corresponding temperatures between wood pyrolysis experimental tests and calculated model results for woody biomasses</i>	62
<i>Figure 10: Dry syngas compositions as they were calculated by the kinetic free model and as results of experimental tests</i>	63
<i>Figure 11: char gasification times by kinetic resistances according the different conversion models for complete gasification time of solid carbon</i>	68
<i>Figure 12: pyrolysis conversion times of biomass fuels, according to the different controlling mechanisms</i>	71
<i>Figure 13: total heights of biomass gasification units and their distribution among solid conversion steps, in absolute values</i>	74
<i>Figure 14: total heights of biomass gasification units and their distribution among solid conversion steps, in percentage values</i>	75
<i>Figure 15a: total conversion time for softwood char gasification according to the different conversion models and as a function of char particles size</i>	76
<i>Figure 15b: total conversion time for park waste wood char gasification according to the different conversion models and as a function of char particles size</i>	77
<i>Figure 16: variations of pyrolysis and gasification zones heights according to overall temperature decrease inside the reactor</i>	78
<i>Figure 17a: softwood char gasification time as a function of temperature, according to uniform reacting particle model and shrinking core one, for kinetic resistances</i>	79
<i>Figure 17b: park waste wood char gasification time as a function of temperature, according to uniform reacting particle model and shrinking core one, for kinetic resistances</i>	79
<i>Figure 18: comparison between experimental data from wood chips pyrolysis tests and simulated results at the same working conditions</i>	81
<i>Figure 19: Examined gas cleaning units</i>	89
<i>Figure 20a: cyclone pressure drops for unit of 3 – 15 Nm<sup>3</sup>/h gas flow size</i>	91
<i>Figure 20b: cyclone pressure drops for unit of 75 – 250 Nm<sup>3</sup>/h gas flow size</i>	91
<i>Figure 20c: cyclone pressure drops for unit of 250 – 500 Nm<sup>3</sup>/h gas flow size</i>	91

Figure 21a: particles collection efficiency of cyclone at 3 – 15 Nm <sup>3</sup> /h gas flow conditions.	92
Figure 21b: particles collection efficiency of cyclone at 75 – 250 Nm <sup>3</sup> /h gas flow conditions .....	93
Figure 21c: particles collection efficiency of cyclone at 250 – 500 Nm <sup>3</sup> /h gas flow conditions.....	93
Figure 22: overall trend of packed bed filter efficiency as a function of particles size (Wakao and Funazkri, 1978).....	94
Figure 23a: efficiency and dimensions of packed bed filter for 3 –15 Nm <sup>3</sup> /h gas flow unit.	95
Figure 23b: efficiency and dimensions of packed bed filter for 75 –250 Nm <sup>3</sup> /h gas flow unit .....	95
Figure 23c: efficiency and dimensions of packed bed filter for 250 – 500 Nm <sup>3</sup> /h gas flow unit.....	95
Figure 24a: pressure drops and saturation times for 3 –15 Nm <sup>3</sup> /h gas flow filter unit .....	97
Figure 24b: pressure drops and saturation times for 75 – 250 Nm <sup>3</sup> /h gas flow filter unit ...	97
Figure 24c: pressure drops and saturation times for 250 – 500 Nm <sup>3</sup> /h gas flow filter unit .	97
Figure 25a: design parameters and pressure drops for 3 –15 Nm <sup>3</sup> /h gas flow candle filter unit.....	99
Figure 25b: design parameters and pressure drops for 75 – 250 Nm <sup>3</sup> /h gas flow candle filter unit .....	99
Figure 25c: design parameters and pressure drops for 250 – 500 Nm <sup>3</sup> /h gas flow candle filter unit .....	100
Figure 26: fabric filter unit (Proceedings of the 18 <sup>th</sup> DOE Nuclear Airborne Waste Management and Air Cleaning Conference, 1984).....	101
Figure 27a: design parameters and pressure drops fort 3 –15 Nm <sup>3</sup> /h gas flow fabric filter unit.....	102
Figure 27b: design parameters and pressure drops for 75 – 250 Nm <sup>3</sup> /h gas flow fabric filter unit.....	102
Figure 27c: design parameters and pressure drops for 250 – 500 Nm <sup>3</sup> /h gas flow fabric filter unit .....	102
Figure 28a: conversion factor and time on stream analysis for 3 – 15 Nm <sup>3</sup> /h gas flow tars cracking unit.....	106
Figure 28b: conversion factor and time on stream analysis for 75 – 250 Nm <sup>3</sup> /h gas flow tars cracking unit.....	107
Figure 28c: conversion factor and time on stream analysis for 250 – 500 Nm <sup>3</sup> /h gas flow tars cracking unit.....	107
Figure 29a: pressure drops for fixed bed and fluidized bed tars cracking units (3 – 15 Nm <sup>3</sup> /h gas flow size) .....	110
Figure 29b: pressure drops for fixed bed and fluidized bed tars cracking units (75 – 250 Nm <sup>3</sup> /h gas flow size) .....	110
Figure 29c: pressure drops for fixed bed and fluidized bed tars cracking units (250 – 500 Nm <sup>3</sup> /h gas flow size) .....	110
Figure 30a: saturation time for Zn-Ti sorbent bed, according to gas flow and H <sub>2</sub> S concentration (3 – 15 Nm <sup>3</sup> /h unit size) .....	113

Figure 30b: saturation time for Zn-Ti sorbent bed, according to gas flow and H <sub>2</sub> S concentration (75 – 250 Nm <sup>3</sup> /h unit size) .....	113
Figure 30c: saturation time for Zn-Ti sorbent bed, according to gas flow and H <sub>2</sub> S concentration (250 – 500 Nm <sup>3</sup> /h unit size) .....	114
Figure 31a: Saturation times of activated carbon material for separate H <sub>2</sub> S and NH <sub>3</sub> adsorption processes (3 – 15 Nm <sup>3</sup> /h gas flow size) .....	118
Figure 31b: Saturation times of activated carbon material for separate H <sub>2</sub> S and NH <sub>3</sub> adsorption processes (75 – 250 Nm <sup>3</sup> /h gas flow size) .....	118
Figure 31c: saturation times of activated carbon material for separate H <sub>2</sub> S and NH <sub>3</sub> adsorption process (250 – 500 Nm <sup>3</sup> /h gas flow size) .....	118
Figure 32: saturation times for activated carbon units for water vapour adsorption .....	119
Figure 33a: available working time of activated carbon unit for combined contaminants adsorption (3 – 15 Nm <sup>3</sup> /h gas flow size) .....	120
Figure 33b: available working time of activated carbon unit for combined contaminants adsorption (75 – 250 Nm <sup>3</sup> /h gas flow size) .....	120
Figure 33c: available working time of activated carbon unit for combined contaminants adsorption (250 – 500 Nm <sup>3</sup> /h gas flow size) .....	121
Figure 34: tandem arrangement for adsorption units ( <a href="http://www.hdm-stuttgart.de">www.hdm-stuttgart.de</a> ) .....	121
Figure 35: wet scrubber packed column ( <a href="http://www.extolhydro.com">www.extolhydro.com</a> ) .....	122
Figure 36a: saturation time of water stream in 3 – 15 Nm <sup>3</sup> /h gas flow wet scrubber unit .....	127
Figure 36b: saturation time of water stream in 75 – 250 Nm <sup>3</sup> /h gas flow wet scrubber unit .....	128
Figure 36c: saturation time of water stream in 250 – 500 Nm <sup>3</sup> /h gas flow wet scrubber unit .....	128
Figure 37a: conversion factor as a function of gas flow for 3 – 15 Nm <sup>3</sup> /h ammonia decomposition unit .....	131
Figure 37b: conversion factor as a function of gas flow for 75 – 250 Nm <sup>3</sup> /h ammonia decomposition unit .....	131
Figure 37c: conversion factor as a function of gas flow for 250 – 500 Nm <sup>3</sup> /h ammonia decomposition unit .....	131
Figure 38: hydrogen consumption in ammonia partial oxidation process, as percentage of the initial total amount contained in the raw gas stream .....	132
Figure 39a: breakthrough points for HCl adsorption unit of 3 – 15 Nm <sup>3</sup> /h gas flow size ..	134
Figure 39b: breakthrough points for HCl adsorption unit of 75 – 250 Nm <sup>3</sup> /h gas flow size .....	134
Figure 39c: breakthrough points for HCl adsorption unit of 250 – 500 Nm <sup>3</sup> /h gas flow size .....	134
Figure 40: dry scrubbing overall scheme .....	136
Figure 41: determined arrangements for gas cleaning line (paths) .....	143
Figure 42a <sub>1</sub> : high temperature gas stream option (path II) for 8 Nm <sup>3</sup> /h gas flow cleaning line .....	148
Figure 42a <sub>2</sub> : low temperature gas stream option (path V) for 8 Nm <sup>3</sup> /h gas flow cleaning line .....	149

Figure 42b: selected arrangement (pathV) for 125 Nm <sup>3</sup> /h gas flow cleaning line .....	150
Figure 42c: selected arrangement (pathV) for 350 Nm <sup>3</sup> /h gas flow cleaning line.....	151

## LIST OF TABLES

Table 1: Proximate analysis of different biomass species (Liliedahl, 2006). .....	29
Table 2: Requirements for fuel quality and technical characteristics of traditional throated downdraft gasification units (Lettner et al., 2007) .....	33
Table 3: Proximate analysis and elementary compositions of considered biomass fuels (ECN, 2009).....	34
Table 4: Molecular formula, molecular weights and heating values on molar basis of biomass fuels.....	35
Table 5: Standard heats of formation for biomass fuels.....	35
Table 6: Thermo-physical properties of biomass fuels.....	36
Table 7: parameters for gas thermal emissivity calculation.....	47
Table 8: Pyrolysis kinetic parameters and kinetic constants for different biomass species	48
Table 9: Pyrolysis products for the considered biomass fuels (wt%) and their corresponding temperatures according to the kinetic free model application.....	55
Table 10: Air supplies for gasification of biomass fuels according to different ER values..	56
Table 11a: Syngas yields, compositions, temperatures and cold gas energy efficiencies of thermo-chemical process at ER = 0.25.....	56
Table 11b: Syngas yields, compositions, temperatures and cold gas energy efficiencies of thermo-chemical process at ER = 0.30.....	57
Table 11c: Syngas yields, compositions, temperatures and cold gas energy efficiencies of thermo-chemical process at ER = 0.35.....	57
Table 12: Process heats in the different reaction zones, according to biomass nature and equivalence ratio.....	58
Table 13: gas temperatures at the exit of the different reaction zones, according to biomass nature and equivalence ratio .....	58
Table 14: Distribution of combustion heats as heat source for the other endothermic processes involved in biomass gasification .....	59
Table 15: Proximate and ultimate analyses of woody biomasses used for gasification modelling and in experimental tests.....	63
Table 16: Exit syngas temperatures, air / fuel ratios and residual solid mass fractions as analytically estimated and as experimental results on wood biomass gasification tests. ....	63
Table 17: biomass feeding rates, gas yields and flows at the exit of combustion zone, and corresponding units diameters for the different materials gasification applications.....	65
Table 18: solid carbon conversion factors and corresponding conversion times for the different biomass species, according to the uniform reacting particle model, .....	66
Table 19: kinetic parameters and solid carbon total conversion times according to shrinking core model and intrinsic kinetics resistance of single reactions.....	66

<i>Table 20: char gasification times according to shrinking core model and intrinsic kinetics resistance, with both reactions contemporary developed and for each biomass fuel .....</i>	<i>67</i>
<i>Table 21: reacting gas diffusion parameters and corresponding times for char gasification, according to shrinking core model and overall mass transfer resistance, for each single gasification reaction .....</i>	<i>67</i>
<i>Table 22: times for complete gasification of char, according to shrinking core model and overall mass transfer resistance, for reactions simultaneously developed.....</i>	<i>67</i>
<i>Table 23: thermal emissivities of flaming pyrolysis products and the corresponding beam lengths of reactors for the different biomasses gasification applications .....</i>	<i>69</i>
<i>Table 24: biomass sizes corresponding to Biot number as unity (<math>R^*</math>).....</i>	<i>69</i>
<i>Table 25: heat transfer and kinetic parameters regarding biomasses pyrolysis development, and its corresponding conversion times .....</i>	<i>70</i>
<i>Table 26: drying time for the different biomasses, according to shrinking core model and heat transfer resistances analysis.....</i>	<i>72</i>
<i>Table 27: units dimensioning parameters and results for biomass fuels heating process .</i>	<i>73</i>
<i>Table 28: diameters of gasification units and relative heights of reaction zones, for each biomass fuel gasification application.....</i>	<i>74</i>
<i>Table 29a: pyrolysis conversion times for softwood particles as a function of temperature increments, according to kinetics and heat transfer resistances.....</i>	<i>80</i>
<i>Table 29b: pyrolysis conversion times for park waste wood particles as a function of temperature increments, according to kinetics and heat transfer resistances.....</i>	<i>80</i>
<i>Table 30: main components and low heating value of gas stream adopted in cleaning systems analysis (Svensk Maskinprovning. Gengasdrift av en överladdad dieselmotor, 1988).....</i>	<i>86</i>
<i>Table 31: Considered sizes for gas cleaning lines, in terms of syngas flows and corresponding power outputs of cogeneration units .....</i>	<i>86</i>
<i>Table 32: Ranges of gas contaminants concentrations at the gasifier outlet .....</i>	<i>87</i>
<i>Table 33: Standard tolerance limits for gas contaminants (Bauen, 2004; Hasler 1999) ....</i>	<i>88</i>
<i>Table 34: Cyclone dimensions for different syngas flows .....</i>	<i>90</i>
<i>Table 35: physical properties of tars cracking catalysts.....</i>	<i>104</i>
<i>Table 36: catalytic tars cracking units dimensions, for fixed bed and fluidized bed applications.....</i>	<i>106</i>
<i>Table 37: physical properties of <math>H_2S</math> adsorber.....</i>	<i>112</i>
<i>Table 38: Zn-Ti adsorption units dimensions .....</i>	<i>113</i>
<i>Table 39: Langmuir constants for <math>NH_3</math> and <math>H_2S</math> adsorption .....</i>	<i>115</i>
<i>Table 40: physical properties of activated carbon material .....</i>	<i>117</i>
<i>Table 41: Activated carbon adsorption units dimensions.....</i>	<i>117</i>
<i>Table 42: kinetic parameters for water vapour adsorption on activated carbon.....</i>	<i>119</i>
<i>Table 43: Pall rashig rings properties .....</i>	<i>122</i>
<i>Table 44: wet scrubber packed column units dimensions.....</i>	<i>126</i>
<i>Table 45: physical properties of ammonia partial oxidation catalyst .....</i>	<i>129</i>
<i>Table 46: dimensions for catalytic ammonia decomposition units .....</i>	<i>130</i>

<i>Table 47: physical properties of HCl mineral sorbent .....</i>	<i>133</i>
<i>Table 48: HCl adsorption units dimensions.....</i>	<i>133</i>
<i>Table 49: sorbent material mass loadings required for the total adsorption of estimated alkali amounts.....</i>	<i>136</i>
<i>Table 50: considered inlet contaminants concentrations for gas cleaning lines assembly .....</i>	<i>137</i>
<i>Table 51: process heats in different gas cleaning units .....</i>	<i>138</i>
<i>Table 52a: paths analysis for 8 Nm<sup>3</sup>/h gas flow size.....</i>	<i>145</i>
<i>Table 52b: paths analysis for 125 Nm<sup>3</sup>/h gas flow size.....</i>	<i>145</i>
<i>Table 52c: paths analysis for 350 Nm<sup>3</sup>/h gas flow size.....</i>	<i>145</i>

# NOMENCLATURE

## Part I

Term	Sign	Unit
pre-exponential factor of reaction (j)	A	-
Biot number	Biot	-
molar concentration	C	mol/m <sup>3</sup>
specific heat	c <sub>p</sub>	J/(g·K)
internal diameter of reactor, diameter of fuel bed	D <sub>bed</sub>	m
external diameter of internal walls of double-walled gasifier	D <sub>i</sub>	m
molecular diffusion coefficient	ℳ <sub>m</sub>	m <sup>2</sup> /s
effective molecular diffusion coefficient of gas through the solid particle	ℳ <sub>m</sub> <sup>e</sup>	m <sup>2</sup> /s
particle size	d	m
activation energy	E <sub>a</sub>	J/mol
equivalence ratio	ER	-
emissivity coefficient	e	-
convective heat transfer coefficient	h	W/(m <sup>2</sup> K)
standard heat of formation	H <sup>o</sup>	kJ/mole
volumetric kinetic constant (on molar concentration basis)	k	1/s
surface kinetic constant of reaction (j)	k'	m/s
equilibrium constant	K <sub>eq</sub>	-
beam length	L	m
length of reactor involved in heat exchange	L <sub>h</sub>	m
mass	m	g
initial number of moles	n <sup>o</sup>	mol
number of moles at equilibrium	n	mol
Nusselt number	Nu	-
pressure	p	Pa
molecular weight	PM	g/mol
Prandtl number	Pr	-
gas flow	Q	Nm <sup>3</sup> /h
particle radius	R	m
particle radius corresponding to Biot number equal to unity	R*	m

<b>Term</b>	<b>Sign</b>	<b>Unit</b>
Reynolds number	Re	-
thickness of hollow space between internal and external walls of reactor	$s_h$	m
radial shrinkage	$s_r$	-
gas temperature	T	K
standard temperature, 298	$T^\circ$	K
time	t	s
gas velocity through the hollow space of reactor	u	m/s
moisture content on dry biomass basis	U	wt%
moisture content on fresh biomass basis	$U^0$	wt%
solid stream velocity through the reactor	$u_{bed}$	m/s
superficial velocity of gas	v	m/s
diffusion volume of gas molecules	$V_{i/g}$	$m^3/mol$
biomass feeding rate	W	kg/h
mass fraction of fuel component, conversion factor	X	-
fraction of total combustion heat involved in gasification step	Y	-
molar fraction	y	-
distance, length	z	m

### ***Greek symbols***

heat of reaction or physical process	$\Delta H$	kJ/mole, kJ/g
initial thermal radiation	$\Delta H^\circ$	$W/m^2$
thermal absorption coefficient of material	$\alpha$	-
void fraction / bed voidage	$\varepsilon$	-
particle sphericity	$\phi$	-
solid conversion	$\gamma$	-
thermal conductivity	$\lambda$	$W/(m \cdot K)$
gas viscosity	$\mu$	$kg/(s \cdot m)$
molar density	$\rho'$	$mol/m^3$
solid particle density	$\rho$	$kg/m^3$
shrinkage coefficient	$\sigma$	-
Stefan-Boltzmann constant, $5.67 \cdot 10^{-8}$	$\sigma_b$	$W/(m^2 \cdot K^4)$
total conversion time of solid particle, residence time of solid stream	$\tau$	s
heat loss, 0.1 (as fixed)	$\xi$	-

<b>Term</b>	<b>Sign</b>	<b>Unit</b>
<b>Subscripts</b>		
air	<i>air</i>	
ashes	<i>ashes</i>	
biomass	<i>b</i>	
bed / reactor walls	<i>b / w</i>	
solid fuel bed	<i>bed</i>	
solid carbon / char particle	<i>C</i>	
char	<i>char</i>	
combustion	<i>comb</i>	
convective	<i>conv</i>	
diffusion mechanisms	<i>d</i>	
drying	<i>dry, drying</i>	
external diffusion mechanism	<i>ed</i>	
exit, outlet	<i>exit</i>	
fixed carbon	<i>fc</i>	
fresh biomass (including ash and water contents)	<i>fresh</i>	
solid fuel	<i>fuel</i>	
gas	<i>g, gas</i>	
gasification	<i>gasif</i>	
gaseous reactant / product	<i>i</i>	
heating	<i>heat</i>	
internal diffusion mechanism	<i>id</i>	
inlet	<i>inlet</i>	
internal heat transfer	<i>iht</i>	
reaction index	<i>j</i>	
mean, average	<i>m</i>	
solid fuel particle	<i>p</i>	
pyrolysis	<i>pyr</i>	
radiative	<i>rad</i>	
radiative heat transfer	<i>rht</i>	
solid	<i>s</i>	
vaporization	<i>vap</i>	
volatile matter	<i>vm</i>	
moisture / water	<i>w</i>	
reactor walls material	<i>wall</i>	

## Part II

<b>Term</b>	<b>Sign</b>	<b>Unit</b>
sectional area	A	m <sup>2</sup>
specific surface	a	m <sup>2</sup> /m <sup>3</sup>
contaminant concentration	C	mol/m <sup>3</sup> , mg/m <sup>3</sup>
initial concentration	C <sub>o</sub>	mol/m <sup>3</sup>
friction factor for pressure drop	C <sub>d</sub>	-
specific heat capacity	c <sub>p</sub>	kJ/kg K, kcal/kmol°C
diameter of bed or filter	D	m
axial diffusion coefficient	D <sub>L</sub>	m <sup>2</sup> /s
molecular diffusion coefficient of gas	D <sub>m</sub>	m <sup>2</sup> /s
bubble diameter	d <sub>b</sub>	m
size of filter grains / bed material	d <sub>g</sub>	m
particles size	d <sub>p</sub>	m
cut diameter	d <sub>pc</sub>	m
orifice diameter	d <sub>or</sub>	m
single efficiency of packed bed filter	E	-
activation energy	E <sub>a</sub>	J/mol
initial molar flux	F <sub>o</sub>	mol/h, mol/s
gravity acceleration,	g	9,81 m/s <sup>2</sup>
gas mass loading	G <sub>m</sub>	kg/m <sup>2</sup> ·s
bed / filter height	H	m
Henry constant	H <sub>i</sub>	atm
kinetic constant	k	s <sup>-1</sup> , h <sup>-1</sup>
surface kinetic constant	k'	s <sup>-1</sup> , h <sup>-1</sup>
gas (external) mass transfer coefficient	k <sub>g</sub>	m/s
thermal conductivity of gas	k <sub>gas</sub>	W/m·K
liquid mass transfer coefficient	k <sub>l</sub>	m/s
pre-exponential kinetic constant	k <sub>o</sub>	s <sup>-1</sup>
thermal conductivity of solid	k <sub>s</sub>	W/m·K
thermal conductivity of porous material	k' <sub>s</sub>	W/m·K
bed / column length	L, L <sub>bed</sub>	m
liquid mass loading	L <sub>m</sub>	kg/m <sup>2</sup> ·s
molecular weight	M	-
particles mass loading in gas stream (candle and fabric filters)	m	kg/m <sup>3</sup>
mass flow	m'	kg/h

<b>Term</b>	<b>Sign</b>	<b>Unit</b>
number of units	n	-
total pressure	p, P	atm, bar
partial pressure of contaminant <i>i</i>	p <sub>i</sub>	atm
partial pressure of contaminant <i>i</i> at equilibrium	p <sub>i</sub> <sup>*</sup>	atm
amount of adsorbed material	q	mg/g
maximum adsorption capacity	q <sub>m</sub>	mg/g
cleaning gas flow	Q <sub>c</sub>	m <sup>3</sup> /s
gas flow	Q <sub>gas</sub>	m <sup>3</sup> /h, mol/h
water flow	Q <sub>l</sub>	m <sup>3</sup> /h, mol/h
ideal gas constant	R	8,314 J·K <sup>-1</sup> ·mol <sup>-1</sup>
particle radius	r <sub>p</sub>	m
wall / filter thickness	s	m
bed external surface	S <sub>ex</sub>	m <sup>2</sup>
time on stream	t	s, min, h
jet pulse duration	t <sub>p</sub>	s
temperature	T	K, °C
critical temperature	T <sub>c</sub>	K, °C
working average temperature of unit	T <sub>m</sub>	K, °C
face / superficial velocity of gas	u, u <sub>o</sub> , U	m/s
cleaning gas jet pulse velocity	U <sub>c</sub>	m/s
minimum fluidization velocity	U <sub>mf</sub>	m/s
gas velocity through orifice	u <sub>or</sub>	m/s
volume	V	m <sup>3</sup>
specific pore volume	V' <sub>p</sub>	m <sup>3</sup> /kg, cm <sup>3</sup> /g
total volume of reactor	V <sub>r</sub>	m <sup>3</sup>
gas inlet velocity	v <sub>i</sub>	m/s
water velocity through the column	v <sub>w</sub>	m/s
particles re-entrainment factor in candle filters, ≈ 1	x	-
conversion factor	X	-
molar fraction of contaminant <i>i</i> in liquid phase, at equilibrium	x <sub>i</sub> <sup>*</sup>	-
gas molar fraction	y, Y	-
bed (partial) length	z	m

<b>Term</b>	<b>Sign</b>	<b>Unit</b>
<b><i>Greek symbols</i></b>		
$\alpha = 1 - \varepsilon$		
process heat of unit i	$\Delta H'_{i}$	W
heat loss	$\Delta H'_{ex}$	W
pressure drop	$\Delta p$	Pa
initial pressure drop	$\Delta p_o$	Pa
particles sphericity	$\phi$	-
bed porosity	$\varepsilon$	-
bed voidage at minimum fluidization condition	$\varepsilon_{mf}$	-
specific permeability	K	m <sup>2</sup>
permeance of fabric filters, $\approx 6,4 \cdot 10^{-5}$	$\kappa$	m/s*Pa
gas viscosity	$\mu, \mu_g$	kg/m*s
gas viscosity at 20 °C	$\mu_o$	kg/m*s
liquid viscosity	$\mu_l$	kg/m*s
overall efficiency	$\eta$	-
bulk density	$\rho_{bulk}$	kg/m <sup>3</sup>
cake density	$\rho_{cake}$	kg/m <sup>3</sup>
gas density	$\rho_g$	kg/m <sup>3</sup>
liquid density	$\rho_l$	kg/m <sup>3</sup>
molar density of solid	$\rho_m$	mol/m <sup>3</sup>
solid density of collected particles	$\rho_p$	mol/m <sup>3</sup>
solid density of bed particles	$\rho_s$	kg/m <sup>3</sup>
absolute density of bed particles	$\rho'_s$	kg/m <sup>3</sup>
volume ratio between collected particles and total bed of filter	$\sigma$	-
cake detachment stress	$\sigma_c$	Pa
surface tension of solids	$\sigma_s$	N/m
surface tension of water	$\sigma_w$	N/m
saturation time	$\tau$	s, min, h
surface energy of particles	$\vartheta$	N/m

# 1 INTRODUCTION

## 1.1 State of the art

In such territories where food production is mostly scattered in several small / medium size or even domestic farms, a lot of heterogeneous residues are produced yearly, since farmers usually carry out different activities in their properties, from animal farming to different crops growing. The amount and composition of farm residues, therefore, widely change during year, according to the single production process periodically achieved.

The use of high efficiency micro-cogeneration energy systems, integrated with easy handling biomass conversion units suitable to treat different materials, would provide many important advantages to the farmers and to the community, as well. Economy of farms would be improved by the use and/or the sale of self made electricity, by the utilization of heat for internal activities and by the reduction of wastes disposal charges. Moreover, the costs of energy production would not be affected by additional logistics, like fuel transportation and long storage. The advantages for local community would be mainly connected to the reduction of fossil fuels dependence for energy supply, the decrease of land use and soil contamination for waste disposal, the higher efficiency and reliability of a grid connected power net, and, in a larger scale, contribution to air pollution control and global warming reduction.

The increase in flexibility of biomass gasification units regarding feedstock materials would thus be a further step towards their wide spreading and it also sounds like a real necessity for their utilization in rural areas at small scale.

At this purpose, two main research topics seem to be of main concern, such as the investigation of fuels properties impact on gasification process development and the technical suitability of small scale gasification units in being integrated with cogeneration systems.

The theory on gasification of solid fuels is very well developed by now, both in its chemical and thermodynamic fundamentals and for its technological and operational aspects. A lot of analytical models have been already carried out (Ratnadhariya and Channiwala, 2009; Corella and Sanz, 2005; Rao et al., 2004; Marias F., 2003; Di Blasi C., 2000, etc.) with different levels of sophistication. Nevertheless, all these works are necessary based on some initial assumptions and input data, most of which are concerning characteristics of fuel that is considered to be gasified. Elementary composition, ash and water contents, particles size, inner structure are all very important parameters to be estimated a priori, in order to validate and properly use the formulated algorithm for process simulation.

Even design of gasification units is strictly connected with the type of the feeding biomass, whose properties affect dimensioning of reactor and suggest suitable technological solutions for practical operations (ash discharge, feeding system, gas cleaning systems, etc.).

It's therefore clearly assertable that biomass gasification units are commonly modelled, designed and even built up on the basis of the specific material they are suited to gasify. Nevertheless, this also leads to a still little flexibility of current technologies in accepting different biomass fuels, while, as said, economy and sustainability of energy systems exactly go towards the opposite direction, especially in rural scenarios (Pellerano and Pantaleo, 2005).

Moreover, the use of different biomass species as feedstock materials is cause of a wider variety of inorganic, heterocyclic and unsaturated compounds, as well as trace elements and fly ashes in the product gas stream, which act as contaminants of the same gas flow in the case it is assumed to be injected into heat and power cogeneration units.

Indeed, at this scope, very high pureness degrees of product gas need to be reached, in order to especially keep safe the moving parts of cogeneration units from erosion and/or corrosion, as well as to minimize pollutant emissions in the atmosphere from the gas combustion process.

Since the standard permitted concentrations of these contaminants are much lower than the percentages usually yielded at the outlet of traditional gasifiers, a gas cleaning line is necessary to be set between solid conversion unit and cogenerator, by means the desired levels of gas impurities can be achieved.

Nevertheless, in order to make gas cleaning system feasible, reliable and efficient at the same time, many issues have to be face on when it is going to be designed and built up. They are mainly concerning the right functioning of the equipment itself, the nature of gasified biomass (providing type and amount of contaminants), energy and materials consumption as well as wastes production during the same gas cleaning process.

Although a huge number of different units are nowadays available to remove and collect several contaminant species, their assembly in an overall gas cleaning line is not technically regulated yet, and some constraints seem to be overcome only by the use of still novel experimental technologies.

At present, many different gas cleaning systems are connected to gasification plants worldwide, but they are properly designed for the particular application and biomass material. Moreover, even for the same gasification technology, it is possible to see different gas cleaning line arrangements, while only a few efforts have been made to develop some guide lines for their design, to date. [Hasler P. et al., 1999; Sharma S.D. et al., 2008].

## **1.2 Objectives**

The first aim of this work is to detect the level of flexibility for traditional downdraft gasification units in accepting different feedstock materials.

This task can be analytically achieved by the estimation of the reactors basic dimensions (diameter and length) and the volumes of the reaction zones in which gasifiers are schematically subdivided, for all the considered biomass materials and at the same fuel feeding rate. Flexibility is thus evaluated by the comparison of these calculated dimensions.

The definition of the biomass properties and the gasifier working conditions which provide the main differences among the design outcomes for the different solid fuels is also a correlated objective of this part of the work.

Finally, some technical solutions for increasing the flexibility of the designed units are tried to be indicated.

The second goal of the work is to demonstrate the possibility to use multi-fuel gasifiers in small/medium scale cogeneration systems, independently on the nature of gasified material. At this scope, the technical feasibility of such gas cleaning lines suitable to remove several contaminants in the same equipment has to be proved as one of the main issues to be stated.

Moreover, an overall methodology for gas cleaning lines assessment is tried to be accomplished as a general tool to fix proper gas cleaning systems, according to cogeneration unit size, gasification technology and adopted biomass fuel (gas contaminants).

According to these two main objectives, the present work was divided in two main parts (as better explained below). Therefore, the specific operations required to achieve the mentioned aims were also divided in the following two lists.

Part I:

- Checking differences in syngas yield and composition among the different biomass species, especially due to their elementary composition.
- Checking differences in working conditions of gasification unit, as temperature profile along the reactor, among the different materials.
- For each biomass type, estimating thermo-chemical or thermo-physical mechanism, among the considered ones, controlling the rate of the solid conversion steps in which gasification process has been subdivided.
- For each biomass type, estimating solids conversion times, regarding each step involved in gasification process, as residence times of solid stream trough the corresponding reaction zone.
- Defining overall dimensions of each reaction zone of reactor, for the different fuels
- Comparing reactor dimensions for the different fuels, in order to estimate the possibility to use the same unit for more than one feedstock.

Part II:

- According to the contaminant species taken in exam, choosing different gas cleaning units suitable to remove them from gas stream.
- For each considered cogeneration unit size, designing the examined gas cleaning units according to the assumed contaminants concentration ranges of the compounds they are suited to remove or to convert
- Estimating working conditions and operating constraints for the designed gas cleaning units, in order to fix them in overall gas cleaning lines.
- Assessing different gas cleaning line arrangements for each cogeneration system size, by differently combining the designed gas cleaning units in order to always remove all the contaminant species taken in exam and to respect operating constraints previously defined
- Defining some operating parameters related to each gas cleaning unit and as overall indexes for the complete gas cleaning lines in order to compare them from a practical point of view.
- Indicating some preferable gas cleaning line assessments for each cogeneration plant size.

### **1.3 Overall description of the work**

On the basis of the two main topics discussed in this study (see par. 1.1), the present work is divided in two main parts.

The first one is focused on the biomass gasification process, that was investigated in its theoretical aspects and then analytically modelled in order to simulate thermo-chemical conversion of different biomass fuels, such as wood (park waste wood and softwood), wheat straw, sewage sludge and refuse derived fuels.

The main idea is to correlate the results of gasification units design procedures with some of the biomass physical properties and the corresponding working conditions inside the gasifier (temperature profile, above all), in order to point out the main differences among materials which prevent the use of the same conversion unit for all of them.

At this scope, a kinetic free model was initially developed in *Excel* sheets, considering different values of air to biomass ratio and the downdraft gasification technology as particular examined application. Biomass compositions and their typical moisture contents were found in literature, while fuels particles dimensions were chosen as the usual ones for the proposed materials after their own common pre-treatments.

The novelty of this analytical approach was the use of kinetic constants ratio in order to determine oxygen distribution among the different oxidation reactions (regarding volatile matter only) while equilibrium of *water gas shift* reaction was considered in gasification zone, by which the energy and mass balances involved in the process algorithm were linked together, as well.

Moreover, this analytical tool was properly developed in order to easily change the input data relating to the particular biomass materials, so that a rapid evaluation on their own thermo-chemical conversion properties is possible to be obtained, mainly based on their chemical composition

The main results achieved by the simulation model were products yields and gas compositions at the exit of gasifier and in some intermediate sections, gas temperature profile inside the unit and cold gas efficiencies, according to the biomass nature and the equivalence ratio (as 0.25, 0.30, and 0.35).

These results were then validated by the comparison with some experimental data on wood biomass downdraft gasification tests.

As second step of this part of the work, a dimensioning procedure for open core downdraft gasifiers was set up by the analysis on the fundamental thermo-physical and thermo-chemical mechanisms which are supposed to be at the base of the main solid conversion processes involved in the gasification course.

At this purpose, gasification units were schematically subdivided in four reaction zones, respectively corresponding to biomass heating, solids drying, pyrolysis and char gasification processes, and the time required for the full development of each of these steps was correlated to the kinetics rates (for pyrolysis and char gasification processes only) and to the heat and mass transfers phenomena from gas to solid phase.

On the basis of this analysis and according to the kinetic free model results previously obtained, the volumes of the mentioned reaction zones were calculated for each considered biomass fuel, by also investigating on the limiting factors and the key parameters having particular influence on their design.

As partial validation of this analytical approach, the time analysis on wood biomass pyrolysis was compared with the results of pyrolysis experimental tests regarding wood biomass with the same particles size and at the same thermal conditions (heating flux).

Finally, a comparison among the differently fed gasification units was accomplished, regarding their own working conditions and basic dimensions.

The second part of this work deals with the gas cleaning systems to be adopted downstream the gasifiers in order to run high efficiency CHP units (i.e. internal engines and micro-turbines).

Especially in the case multi-fuel gasifiers are assumed to be used at this purpose, weightier gas cleaning lines need to be envisaged in order to reach the standard gas quality degree required to fuel cogeneration units. Indeed, as the more heterogeneous

feed to the gasification unit, several contaminant species can simultaneously be present in the exit gas stream and, as a consequence, suitable gas cleaning systems have to be designed.

The gas contaminant species taken into account in this analysis were: particulate, tars, sulphur (in  $H_2S$  form), alkali metals, nitrogen (in  $NH_3$  form) and acid gases (in  $HCl$  form).

For each of these species, alternative cleaning devices were designed according to three different plant sizes. Their performances were examined on the basis of their optimal working conditions (efficiency, temperature and pressure drops, above all) and their own consumption of energy and materials.

Successively, the designed units were combined together in different overall gas cleaning line arrangements (suitable to eliminate all the considered contaminant compounds from gas stream) by following some technical constraints which were mainly determined from the same performance analysis on cleaning units and from the presumable synergic effects of contaminants on the right working of some of them (filters clogging, catalysts deactivation, etc.).

Finally, on the basis of some defined operating parameters, gas cleaning line arrangements were compared each others and, for each cogeneration unit size, one of them was finally indicated as the preferable one.

The complete study on the gas cleaning lines, including gas cleaning units design, definition of technical restraints for their assembly and determination of some overall operating parameters, can be thus seen as a new general methodology for their assessment at different scales.

**PART I**  
**DOWNDRAFT GASIFICATION ANALYSIS AND UNITS DIMENSIONING**  
**ASPECTS**

## 2 METHODOLOGY

### 2.1 General aspects of process and technology

#### 2.1.1 Theoretical framework of gasification

Gasification of solid fuels is a very complex phenomenon in which several simultaneous or in series mechanisms are involved. They are mainly regarding thermo-physical breakdown of solid particles and chemical reactions, both homogeneous and heterogeneous, whereof development is depending on the operating conditions which are achieved inside the gasifier. These latter are not all easy to regulate during process and they are strictly affected by the specific gasification technology is used at this purpose. The wide variety of potential feedstock materials, with their different composition and structure, adds more complexity and diversification among the different types of gasifiers, as well.

For all these reasons, the real advancement of a solid fuel gasification application is not easy to model and foresee, as well as any generalized analytical assessment is precluded.

Nevertheless, an overall scheme is usually adopted by considering the different steps in which gasification process can be approximately subdivided: heating and drying, pyrolysis or devolatilisation, combustion or partial oxidation, and reduction (or char gasification).

They can be temporary and spatially connected each other in different ways, according to the technology is considered in process modelling. In any case, thermo-chemical conversion of a solid fuel always starts with an heating step, so that its free moisture content is initially vaporized (at around 100°C) and subsequently dry particles are thermally decomposed. Molecular bonds strength, initial particle size, heating rate and process temperature are the main controlling factors of this second phase, such as pyrolysis or devolatilisation. Main products are a mixture of light gases, (CH<sub>4</sub>, CO, H<sub>2</sub>, C<sub>2</sub>H<sub>4</sub>, HCN, generally defined as volatile matter), some other heavier gaseous compounds (tars) with relatively low boiling point (around 450°C), an organic solid residue mainly consisting on solid carbon (fixed carbon or char) and ashes (inert solids).

Although relative yields of pyrolysis products are not depending on composition and structure of materials only, these latter are characterized by the so called *proximate analysis*, where percentages of volatile matter, fixed carbon and ashes are given as results of experimental tests. An example of this analysis is given in table 1, (Liliedahl, 2006).

The other steps of solid conversion scheme are concerning chemical reactions between pyrolysis products and other gaseous agents which are properly fed to the reactor. These gasifying agents are usually air, oxygen, steam, or a mixture of them. When oxygen reacts with char or volatile matter, oxidation reactions occur (combustion). Their products are carbon oxide, carbon dioxide and water vapour, which are added to the other gas components. Because of their high exothermic heat, these reactions also provide for the required energy involved in the other process steps, by maintaining the process thermal sustainability of such reactors, just called auto-thermal ones (see fig. 1).

It can be supposed for some reactor equipments that oxygen initially reacts with volatile matter (especially H<sub>2</sub> and CO), so as increasing the temperature around char particles up to their ignition point, and it subsequently reacts with solid carbon, as well. Since, in the case of gasification, oxygen is fed in such amounts lower than the stoichiometric one required for the complete combustion of biomass, thermal conversion of solid particles proceeds in a reducing atmosphere, where steam and CO<sub>2</sub> reduce char to gaseous compounds, above all. Moreover, recombination of pyrolysis and combustion products, as well as reforming of tars are developed (see figure 2). All these reactions together can be considered as the reduction or char gasification step. Mostly of them are endothermic reactions, so as part of the combustion heat is consumed for their development. Therefore,

a mixture of gas (usually CO, H<sub>2</sub>, CH<sub>4</sub>, CO<sub>2</sub>, H<sub>2</sub>O, N<sub>2</sub>) is obtained as final product, whose outlet temperature is lower than the combustion exhausts one, but the so called syngas still has an energy content as low/medium calorific value (from 4000 to 12000 kJ/kg), by which it can be used as a fuel gas.

	wt%, dry			wt%, dry and ash free		Trace components		
	Volatile matter	Fixed carbon	Ash	Volatile matter	Fixed carbon	Na (ppm)	K (ppm)	Cl (ppm)
<u>Northern woody biomasses</u>								
Wood chips	80.0	19.4	0.60	80.5	19.5	42	983	42
Forest residue	79.3	19.4	1.33	80.4	19.6	76	1377	76
Forest residue	74.1	21.8	1.33	75.1	22.1	640	2604	<50
Saw dust (pine)	83.1	16.8	0.08	83.2	16.8	20	480	<50
Spruce bark	75.2	22.5	2.34	77.0	23.0	89	3003	279
Pine bark	73.0	25.3	1.72	74.3	25.7	29	2133	85
Salix	79.9	18.9	1.18	80.9	19.1	37	4058	37
<u>Agricultural biomasses</u>								
Wheat straw (Denmark)	77.7	17.6	4.71	81.5	18.5	140	5480	1710
Barley straw (Finland)	76.1	18.0	5.88	80.9	19.1	333	12188	2737
Rapeseed	79.2	19.9	2.86	81.5	20.5	166	5768	965
Flax (whole straw)	78.8	18.3	2.93	81.2	18.8	133	5147	588
Flax(shive)	78.6	19.6	1.81	80.0	20.0	87	3362	381
Reed canary grass	73.5	17.6	8.85	80.6	19.4	154	3479	639
<u>European biomasses</u>								
Sweet sorghum(Italy)	77.2	18.06	4.74	81.0	19.00	678	4614	2996
Kenaf (Italy)	79.4	16.97	3.63	82.4	17.60	517	7254	1748
Miscanthus (Italy)	78.5	18.19	3.31	81.2	18.80	259	9702	3266
Cane (Italy)	77.9	18.40	3.70	80.9	19.10	183	9706	2922
Miscanthus (Germany)	79.3	18.40	2.30	81.2	18.80	27	3027	1405

Table 1: Proximate analysis of different biomass species (Liliedahl, 2006).

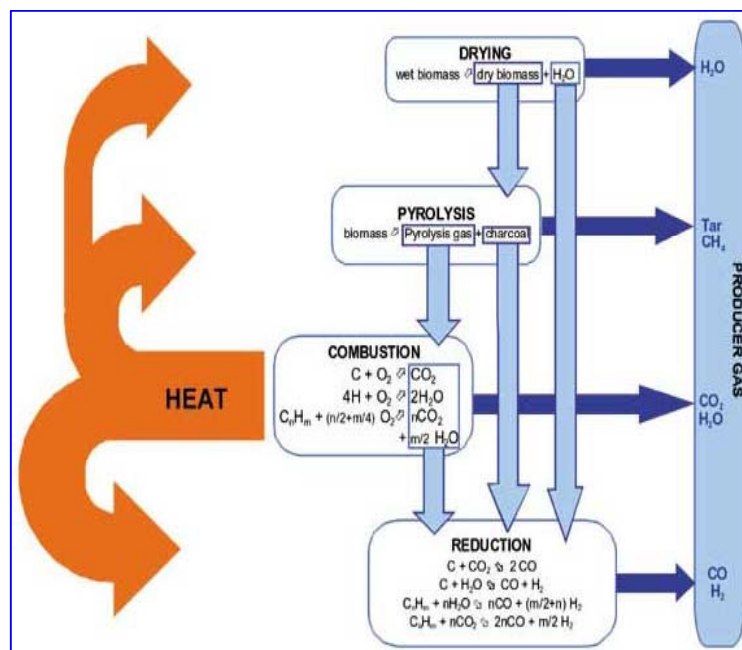


Figure 1: energy balance in auto-thermal gasification process (Ramesh and Nekere, 2005)

While heating, drying and pyrolysis can be always considered as the first steps of gasification process, combustion and reduction ones are spatially and time distributed in the reactor differently, according to the particular gasification technology is used. Required energy for the development of the first two steps can be supplied by combustion heat of reaction, as well, or by means of an indirect heating of the unit, in the case overall process is carried out in different equipments (allothermal gasifiers).

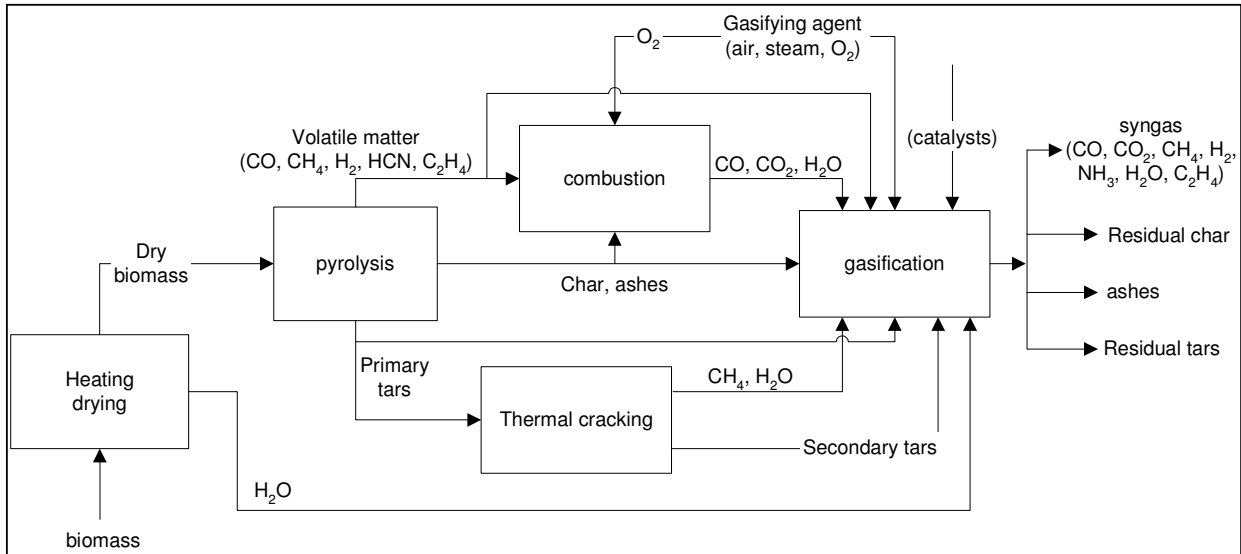


Figure 2: gasification scheme

### 2.1.2 Investigated gasification technology

Since conversion of solid fuels proceeds in so many different ways according to the adopted unit technology, in this work a downdraft air atmospheric reactor was chosen for investigation (In fig. 3, downdraft gasification equipments present in HPT laboratory of Energy Technology Department are shown). It is one of the so called fixed bed reactors, in which there is a fuel bulk filling in the reaction chamber that is sustained by a bottom grate. Fresh biomass is fed from the top, introduced through an opening or sluice on the reactor head, and sinks slowly downwards by gravity as conversion of fuel conversion proceeds.

In the case of downdraft (or co-current) gasifier, the gasifying medium (air in this case) flows through the reactor in the same direction of the sinking bulk filling. It is introduced at some sides above the grate, in the narrowest part of the "throat" that is especially designed to create an high temperature and turbulence zone in combustion zone. The syngas is finally withdrawn under the grate (see fig. 4). The sequence of gasification steps is therefore: heating and drying, pyrolysis, combustion and gasification.

Since drying and pyrolysis zones lie above the oxidation zone, they are mainly heated by radiation (and partly convection) heat from the hearth combustion zone, where volatile matter and part of the char are burnt. Pyrolysis gases also pass through this zone and they react with the input gasification medium (combustion). Beneath the oxidation zone the remaining char and the combustion products pass to the reduction zone where endothermic reactions take place, forming CO and H<sub>2</sub> as main products.

Through these reactions, a portion of the sensitive heat of the gas from combustion is converted into chemical energy of syngas. Thus the gas temperature finally sinks to a level at which no further reactions of the charcoal with the gas phase can be developed.

Consequently, there is always a layer of unreacted char above the grate that has to be discharged with ashes. As a result, even under optimal operating conditions, it is possible to attain solid fuel conversion not over 95% of dry mass (Lettner et al., 2007). Other reasons for this low gasification efficiency can be recognized in the short residence time of char and gas passing through the hottest combustion zone and in the poor penetration of gasifying agent into the inner core of the cross section.

This latter is also the main reason for which up-scaling of downdraft reactors at large scale is usually precluded, but adding particular technical features. In this regard, Bühler and Hasler, 1997, indicated a fuel thermal output of 1 MW<sub>th</sub> as the recommended value for the upper limit of sensible up-scaling of individual gasification reactors.



*Figure 3: downdraft gasification units at EKV – HPT laboratory (respectively 15-20 and 300 kW<sub>th</sub> sizes)*

In recent designs the reactor may be double walled (as it has been thought in the following analysis). The producer gas is conducted through the hollow space between the walls, allowing for heat exchange between the producer gas and the fuel in the pyrolysis and drying zone of the reactor. The effectiveness of this heat exchange is considerably improved when small reactor diameters are applied, thus enlarging the heat exchange surface considerably.

The main advantage for downdraft gasifiers is that pyrolysis tars are forced to pass through the oxidation zone, which is denoted as the “hot treatment zone for tarry compounds” (Lettner et al., 2007), where they are transformed into stable and non condensable gases. This leads to considerably small concentrations of tar compounds in the final product gas. An approximate can be fixed as 1 g/Nm<sup>3</sup> (Lettner et al., 2007). As a consequence, downdraft technology is the commonest in such applications for power production by internal combustion engines.

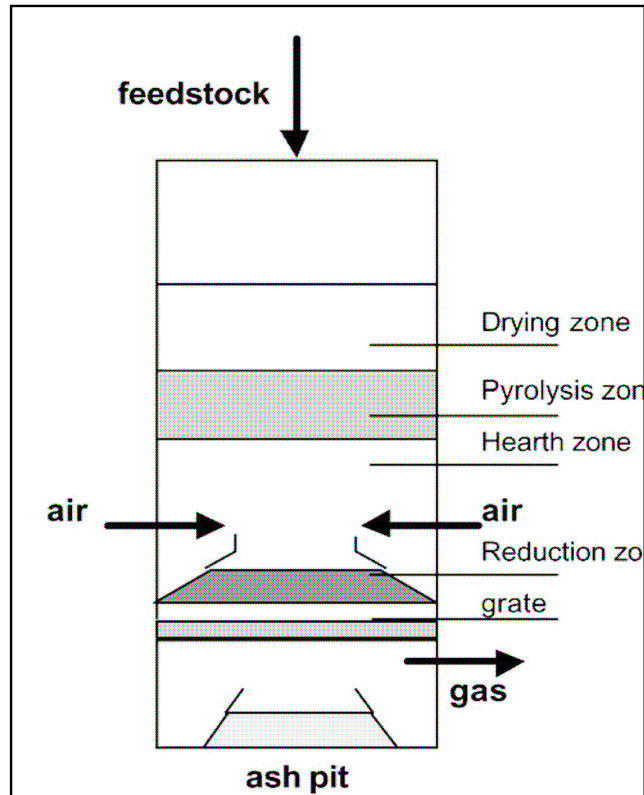


Figure 4: Scheme of a downdraft gasifier (Belgiorno et al., 2003)

As opposite, construction and process engineering principles of downdraft gasifiers make them sensitive to the quality of the fuel that is used. Particular attention must be paid primarily to the water content of the fuel. Steam produced in the drying zone in fact represents a relevant heat loss, since it must be heated up to the temperatures in the oxidation zone, besides its latent heat of vaporization.

More over, heat is also withdrawn from the oxidation zone through the endothermic water gas reactions. As a result, with high amounts of water it is not possible to ensure the high temperatures that are necessary for the solid conversion by the next reduction reactions.

As regards particle size, fine dimensions can have strong influence on uniformity of the gas flow through the solid fuel bed, especially because of channel formation and local different distribution of pressure drops.

Basic data about fuel quality required in traditional, throated downdraft gasifiers applications and technical reactor characteristics are presented in Table 2, (Lettner et al., 2007).

Fuel moisture cont. (wet %)	>10, < 25
Fuel ash content (dry %)	< 6
Size (mm)	20 - 200
Share of fine particles	< 15%mass,wet, ≤ 5mm
Gas exit T (°C)	700
Tars (g/Nm <sup>3</sup> )	< 0,5
Sensitivity to load fluctuations	Sensitive
Turn down ratio	3 – 4
Hot gas efficiency (full load %)	85 - 90
Cold gas efficiency (full load %)	65 – 75
Syngas LHV (kJ/Nm <sup>3</sup> )	4.5 – 5.0

*Table 2: Requirements for fuel quality and technical characteristics of traditional throated downdraft gasification units (Lettner et al., 2007)*

A more recent development of downdraft gasifiers is represented by the so called “*open core*” gasifiers. It is especially designed to gasify fine materials with low bulk density (Bhoi P.R: et al., 2005). Because of the low bulk density of the fuel, indeed, no throat can be applied in order to avoid bridging of the fuel, which would cause hampering or even stopping of the same fuel flow.

Air is sucked over the whole cross section from the top of the bed. This facilitates better oxygen distribution since it will be consumed over the whole cross section of combustion zone, so that the solid bed temperature will not reach the local extremes (hot spots) observed in the oxidation zone of conventional downdraft gasifiers. Moreover, the air nozzles in conventional gasifiers generate caves and create obstacles that may obstruct solid flow specially for solids of low bulk density. Special devices, like rotating grates, may be included to stir the fuel and to remove the ash. The bottom of the gasifier is set in a basin of water by which the ash is removed.

## 2.2 Thermo-chemical model description

A kinetic-free model was developed for simulating biomass gasification process in an air atmospheric downdraft reactor. From the top of gasifier, where biomass fuel is fed, to the bottom grate of reactor, four reaction zones were considered, respectively biomass heating and drying, pyrolysis, combustion (or partial oxidation) and gasification ones.

Gas composition at the exit of each of these zones is one of the main results of the model, which yet doesn't contemplate tars formation during the overall process (according to the usual behaviour and technical characteristics of downdraft units) and it instead envisages total conversion of char during gasification process, in order to simplify analytical procedure.

Temperature profile inside the reactor is the second main result of this analytical approach, as estimation of gas temperatures at the exit of each reaction zone, according to which the different thermo-chemical conversion steps were also modelled.

At this scope mass and energy balances were used as the main analytical tools, while some kinetic constants were considered in combustion zone only, and equilibrium of *water gas shift* reaction was supposed to be achieved during gasification step. In this way, distribution of thermal energy among the different reaction zones was possible to be estimated, as well, and overall energy efficiency was also predicted for each fuel gasification application.

The model was applied to five different biomass materials (park waste wood, softwood, wheat straw, sewage sludge and RDFs) and results were correlated to their proximate analysis and elementary composition. Because of their supposed small particle sizes (see table 6), an open core gasifier was supposed to be used, even if gasifying medium was still supposed to be fed in the middle of gasifier.

### 2.2.1 Biomass species

Five biomass fuels were investigated in this work: park waste wood, stem wood of Swedish spruce (thereinafter simply called softwood), wheat straw, sewage sludge and RDFs (with plastic). Their elementary compositions, heating values and proximate analysis are reported in table 3 (ECN, 2009)

	wheat straw <sup>a</sup>	park waste wood	softwood <sup>b</sup>	sewage sludge	RDF with plastic
<b>HHV (kJ/kg dry ash free)</b>	19876	20172	21114	23231	32592
<b>LHV (kJ/kg dry ash free)</b>	18532	18888	19822	21586	29284
<b>moisture (wt%)</b>	10,3	5,2	9,7	9,9	2,9
<b>ashes (dry wt %)</b>	4,7	3,2	0,3	35	8,9
<b>C (daf wt %)</b>	49,6	51,2	52,7	52,3	68,7
<b>H (daf wt %)</b>	6,2	5,9	6	7,5	15,2
<b>N (daf wt %)</b>	0,61	0,26	0,1	7,2	0,36
<b>S (daf wt %)</b>	0,07	0,05	0	2	0
<b>O (daf wt %)</b>	43,4	42,5	41,2	30,8	15,8
<b>H/C (mass basis)</b>	0,13	0,12	0,11	0,14	0,22
<b>O/C (mass basis)</b>	0,88	0,83	0,78	0,59	0,23
<b>VM (dry wt %)</b>	81,5	77,6	78,2	53,5	85,8
<b>Fixed Carbon (dry wt %)</b>	13,8	19,2	21,5	11,5	5,3

a: other trace elements are present in biomass composition (Cl, F); b: data from Erlich et al., 2006

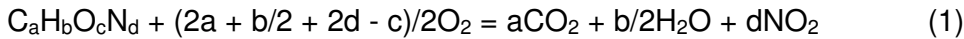
Table 3: Proximate analysis and elementary compositions of considered biomass fuels (ECN, 2009)

Four main elements were considered as components of each kind of biomass (C, O, H, N) and their corresponding molar percentages were calculated on the basis of their elementary *daf* (dry ash free) compositions. An approximate molecular formula was determined for each biomass fuel by fixing subscript of less component (N, in all of the examined cases) equal to unit. Results are showed in table 4

fuel	Molecular formula	Molecular weight	P.C.S. (kJ/mole daf)	P.C.I. (kJ/mole daf)
wheat straw	C <sub>95</sub> H <sub>142</sub> O <sub>62</sub> N	2291	45530	42452
park waste wood	C <sub>230</sub> H <sub>318</sub> O <sub>143</sub> N	5377	108466	101562
softwood	C <sub>615</sub> H <sub>840</sub> O <sub>361</sub> N	14000	295596	277508
sewage sludge	C <sub>8</sub> H <sub>15</sub> O <sub>4</sub> N	189	4401	4089
RDF with plastic	C <sub>223</sub> H <sub>591</sub> O <sub>38</sub> N	3891	126823	113951

*Table 4: Molecular formula, molecular weights and heating values on molar basis of biomass fuels*

Standard heat of formation of solid fuels was calculated by using the following general combustion reaction:



And it was determined as:

$$H^{\circ}_{fuel} = \sum_i (H^{\circ}_i)_{comb} - \Delta H_{comb} \quad (2)$$

The following results were obtained for the four examined materials:

fuel	H <sup>o</sup> <sub>fuel</sub> (kJ/mole)
wheat straw	-12090
park waste wood	-27317
softwood	-66217
sewage sludge	-958
RDF with plastic	-45215

*Table 5: Standard heats of formation for biomass fuels*

Thermo-physical properties of organic materials were found in literature and initial particles sizes were chosen as the typical ones after usual and light pre-treatments for the different biomass species. (In the case of wood, chips of different sizes were considered for the two species, while for refuse derived fuels densified briquettes were taken in exam). A resume of the main thermo-physical properties of biomass fuels is given in the following table 6.

	wheat straw	park waste wood	softwood	sewage sludge	RDF with plastic
particles size (mm)	10	25	11	1	40
sphericity $\phi$ (by geometrical form) <sup>1</sup>	0,8	0,7	0,75	0,9	0,87
particle density $\rho_s$ (kg/m <sup>3</sup> )	410 <sup>(2)</sup>	450 <sup>(3)</sup>	365 <sup>(3)</sup>	1139 <sup>(5)</sup>	1350 <sup>(6)</sup>
bulk density $\rho_{bulk}$ (kg/m <sup>3</sup> )	79 <sup>(6)</sup>	170 <sup>(6)</sup>	170 <sup>(6)</sup>	650 <sup>(6)</sup>	729
bed voidage $\epsilon_{bed}$	0,81	0,62	0,53	0,43	0,46 <sup>(1)</sup>
particle void fraction	0,7	0,7	0,7	0,47	0,5
specific heat (fresh) $c_{p,ar}$ (kJ/kg K)	<sup>a)</sup> $w/(1+w) cp_w + 1/(1+w) cp_{dry}$ <sup>(8)</sup>	2,3 <sup>(9)</sup>	2,3 <sup>(9)</sup>	$w/(1+w) cp_w + 1/(1+w) cp_{dry}$	$w/(1+w) cp_w + 1/(1+w) cp_{dry}$
specific heat (dry) $c_{p,dry}$ (J/kg K)	<sup>b)</sup> $1112 + 4,85 (T - 273)$ <sup>(10)</sup>	$1500+T$ <sup>(11)</sup>	$1500+T$ <sup>(11)</sup>	$1434 + 3,29 T$ <sup>(8)</sup>	$1800$ <sup>(12)</sup>
thermal conductivity $k_s$ (W / m K)	0,08 <sup>(13)</sup>	$0,13+0,0003T$ <sup>(9)</sup>	$0,13+0,0003T$ <sup>(9)</sup>	<sup>c)</sup> $0,653X_m + 0,25X_m + 0,15X_{ic} + 0,05X_{ash}$ <sup>(14)</sup>	0,17 <sup>(12)</sup>
solid emissivity $e_s$	0,9	0,95	0,95	0,95	0,95
thermal absorption coefficient $\alpha$ <sup>(15)</sup>	0,81	0,77	0,77	0,72	0,8

a) w = water content mass fraction of biomass

b) T = solid temperature (K)

c)  $X_m$  = moisture mass fraction,  $X_{ic}$  = volatile matter mass fraction,  $X_{ic}$  = fixed carbon mass fraction,  $X_{ash}$  = ashes mass fraction

1) Kunii and Levenspiel, 1991; 2) Zhou et al., 2005; 3) Erlich et al., 2006 4) Di Blasi et al., 2001; 5) Hartman et al., 2005;

6) Eco-Engineering, 2009; 7) ECN, 2009; 8) Arlabosse et al., 2005; 9) Sadhukan, 2009; 10) Jalan and Srivastava, 1998;

11) Bellais M., 2007; 12) Savage, 1989; 13) Fjellerup et al., 2003; 14) Yang et al., 2008; 15) Perry, 2007

Table 6: Thermo-physical properties of biomass fuels

## 2.2.2 Moisture vaporization

Water content of initial (fresh) biomass material was determined through the moisture mass percentage included in its proximate analysis (see table 3) and referred to one mole of *daf* biomass. Heat of moisture vaporization was calculated by the following formula (Galvano et al., 2004):

$$\Delta H_{vap} = 3.348 - 13.085U + 60.262U^2 - 95.778U^3 \text{ (kJ/g), if } U \leq 0,3 \quad (3)$$

$$\Delta H_{vap} = 2.260 \text{ (kJ/g), if } U \geq 0,3 \quad (4)$$

## 2.2.3 Pyrolysis or devolatilization

Pyrolysis of biomass materials was simulated by following the original model of Østberg (Østberg et al., 1998), that was initially developed for coal devolatilisation. According to this model and considering biomass general formula as  $C_aH_bO_cN_d$ , char is considered as  $C_xN_{x*d/a}$  and volatile matter is defined as  $C_{a-x}H_bO_cN_{(a-x)*d/a}$ . Devolatilization is supposed to be carried out until the whole mass percentage of volatile matter expressed in the proximate analysis of fuels is released as gaseous species, such as CO, H<sub>2</sub>, CH<sub>4</sub>, C<sub>2</sub>H<sub>4</sub>, HCN and soot. In order to fit the original model on biomass pyrolysis, water vapour (H<sub>2</sub>O) was added to the gaseous products and soot was instead neglected.

General expression for pyrolysis step can be hence written as follows:



Through the total mass balance on one mole of initial solid *daf*-fuel, as well as by mass balance on each element included in biomass composition (C, H, O, N), the number of moles of pyrolysis products were obtained.

Heat of pyrolysis was calculated by the following equation:

$$\Delta H_{\text{pyr}} = \sum_i (H^{\circ}_i)_{\text{pyr}} - H^{\circ}_{\text{fuel}} \quad (6)$$

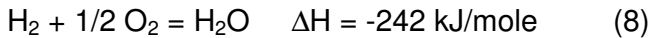
Standard heat of formation of char ( $C_xN_{x \cdot d/a}$ ) was considered as zero in this calculation.

For all the biomass species the same temperature was chosen as the one at which solids devolatilization begins. According to literature data on experimental tests of different materials (Pantoleontos G. et al., 2009), an average temperature of 300°C was fixed as initial pyrolysis one.

## 2.2.4 Partial oxidation of pyrolysis products (flaming pyrolysis)

According to the regular fluid-dynamic behaviour of a downdraft gasifier (such as co-current flux of solid fuel and gasifying medium), partial oxidation of gaseous pyrolysis products was supposed to be achieved in the combustion zone of reactor (flaming pyrolysis, Giltrap et al., 2003), in spite of char burning. Carbon monoxide and hydrogen were supposed to be the main components reacting with oxygen, while the other pyrolysis products ( $CH_4$  and  $C_2H_4$  above all) were considered to be oxidized by residual oxygen only (due to their relatively low combustion kinetic rates and low yields).

Two main oxidation reactions were thus initially taken in exam:



Kinetic rates of these two reactions are expressed by second order Arrhenius' laws, showing the same value of activation energy for both of them ( $E_a = 99.8 \text{ kJ/mole}$ , Kim et al., 2000).

Therefore, oxygen supply was shared between the two mentioned reactions according to the ratio of their pre-exponential factors, which are respectively  $A_{CO}=8,83 \cdot 10^{11}$  and  $A_{H_2}=3,09 \cdot 10^{11}$ , until the total consumption of one of the gas reactants ( $CO$  or  $H_2$ ).

In the case both  $CO$  and  $H_2$  were completely oxidized, residual oxygen were supposed to be reacting with  $CH_4$  and  $C_2H_4$ , according to the following reactions:



(In this case, the ratio between their heats of reactions was considered as parameter for oxygen distribution, since their kinetic rates show different dependences on temperature).

Total heat of combustion was finally calculated as the sum of the heats of all the mentioned reactions, each of them by the number of corresponding fuel gas reacting moles.

For all the considered biomass species air gasification was assumed to be accomplished and process development was investigated as a function of the equivalence ratio ( $ER$ ) by setting values of this parameter as 0.25, 0.30 and 0.35. According to them, air supplies per kilogram of raw material were calculated, on the basis of elementary composition, water and ashes contents.

## 2.2.5 Char Gasification

In the bottom zone of a downdraft reactor, char gasification is the main occurring process, together with thermal cracking and reforming of tars (which were neglected in this analysis) and adjustment of syngas composition through homogeneous reactions.

In this case, char gasification was considered through the following two reactions (considering carbon bound-nitrogen releasing in the combustion zone as  $N_2$ ):



$\alpha$  and  $\beta$  are numerical coefficients whose sum is equal to the total number of moles of solid carbon released during pyrolysis step ( $n^{\circ}_C$ ). This means carbon was supposed to be completely gasified in this zone:

$$\alpha + \beta = n^{\circ}_C \quad (13)$$

The other two reactions considered in gasification step were:



Reaction (14) was supposed to be completely developed towards the right side, while reaction (15), such as *water gas shift* reaction, was considered at equilibrium. On the basis of this latter assumption,  $\alpha$  and  $\beta$  numerical values and final composition of syngas were possible to be calculated.

Equilibrium of reaction (15) was written as:

$$K_{eq} = \frac{P_{CO_2} \cdot P_{H_2}}{P_{CO} \cdot P_{H_2O}} = \frac{n_{CO_2} \cdot n_{H_2}}{n_{CO} \cdot n_{H_2O}} \quad (16)$$

where:

- $n_{CO_2} = n^{\circ}_{CO_2} - \beta + \chi$
- $n_{H_2} = n^{\circ}_{H_2} + \alpha + \chi$
- $n_{CO} = n^{\circ}_{CO} + 2\beta + \alpha - \chi + n^{\circ}_{HCN}$
- $n_{H_2O} = n^{\circ}_{H_2O} - \alpha - \chi - n^{\circ}_{HCN}$
- $\chi =$  number of CO moles reacting in reaction (15)

In order to calculate the values of parameters  $\alpha$ ,  $\beta$  and  $\chi$ , equations (13) and (16) were put into system together with the following expression, showing the dependence on temperature of equilibrium constant  $K_{eq}$  (Bellais, 2007):

$$K_{eq} = 0.0265 \cdot e^{\left(\frac{32987}{R \cdot T}\right)} \quad (17)$$

R as ideal gas constant, 8.3145 [J/mol·K]

Since  $K_{eq}$  is depending on temperature, eq. (13), (16) and (17) were also linked to the overall energy balance (including all the reaction zones of gasifier, see par. 2.2.6), by which temperature of syngas at the outlet of gasification zone was calculated (supposing ashes at the same temperature of gas).

Mass and energy balances were thus correlated by means of equations (16) and (17) in this analysis. Since they are depending on each other, an iterative procedure was adopted in order to calculate final gas composition and its gasification temperature.

The necessary heat for gasification step was finally calculated by summing heats of reactions (11), (12), (14) and (15), each of them by the corresponding number of reacting moles.

## 2.2.6 Energy balances

In order to estimate gas temperatures in the different reaction zones of the downdraft unit, different energy balances were set up, each of them including one or more zones of the reactor. Thermal energy released by oxidation reactions in combustion zone (see table 14) was supposed to meet energy demands for the other process steps, such as moisture vaporization, pyrolysis and gasification, as well as to heat up gas and solid components to the corresponding process temperatures. Moreover, an heat loss as 10% of combustion heat was added to the overall balance.

For all the proposed energy balances the same algorithm was used, such as the difference of sensible heat contents between inlet and outlet species of the reference frame (volume of the investigated part of reactor) was put equal to the sum of heat loss and process heats involved in the same considered frame.

The first considered energy balance is regarding the whole volume of reactor, and it thus takes in exam all the reaction zones. Gas temperature at the exit of gasification zone is therefore calculated (supposing ashes at the same temperature). The energy balance can be written as follows:

$$\sum_i (m_i \cdot cp_i \cdot (T_{gasif} - T^0))_{gasif} - m_{fresh} \cdot cp_{fresh} \cdot (T_{dry} - T^0) - m_{air} \cdot cp_{air} \cdot (T_{air} - T^0) + m_{ashes} \cdot cp_{ashes} \cdot (T_{gasif} - T_{dry}) = \Delta H_{comb} \cdot (1 - \xi) - \Delta H_{gasif} - \Delta H_{pyr} - \Delta H_{vap} \quad (18)$$

( $cp_i$  was calculated as integral mean between gasification and standard temperatures,  $cp_{fresh}$  as integral mean between drying and standard temperatures and  $cp_{air}$  as integral mean between air inlet and standard temperatures. Air inlet temperature was set to 473K. Heat loss was fixed to 0,1)

In equation (18) the unknown value is  $T_{gasif}$  only. Nevertheless,  $m_i$  values are also determined on the basis of this temperature, according to equations (16) and (17). Therefore, as already said,  $T_{gasif}$  was obtained through an iterative calculation which also involves equations (13), (16) and (17).

The second energy balance includes drying, pyrolysis and combustion zones only. Thus, the outlet species from the reference frame are flaming pyrolysis (combustion) products and ashes. It can be written as follows:

$$\sum_i (m_i \cdot cp_i \cdot (T_{comb} - T^0))_{comb} + m_{ashes} \cdot cp_{ashes} \cdot (T_{comb} - T_{dry}) - m_{air} \cdot cp_{air} \cdot (T_{air} - T^0) - m_{fresh} \cdot cp_{fresh} \cdot (T_{dry} - T^0) = \Delta H_{comb} \cdot (1 - \xi) - \Delta H_{pyr} - \Delta H_{vap} \quad (19)$$

(in this case  $cp_i$  was calculated as integral mean between combustion and standard temperatures).

According to equation (19),  $T_{\text{comb}}$  as temperature at the exit of combustion zone was possible to be estimated.

Successively, In order to know temperature at the outlet of pyrolysis zone, energy balance on the only combustion one was set up, by considering that gasification heat is provided by the cooling of flaming pyrolysis products and solids devolatilization starts at temperature of 573K for all the biomass fuels (see par. 2.2.3). Therefore, thermal energy for heating solids up to this value is also subtracted from combustion heat. The overall balance was written as follows:

$$\sum_i (m_i \cdot c_{p_i} \cdot (T_{\text{comb}} - T^0))_{\text{comb}} - \sum_j (m_j \cdot c_{p_j} \cdot (T_{\text{pyr}} - T^0))_{\text{pyr}} - m_{\text{air}} \cdot c_{p_{\text{air}}} \cdot (T_{\text{air}} - T^0) + m_{\text{ashes}} \cdot c_{p_{\text{ashes}}} \cdot (T_{\text{comb}} - T_{\text{pyr}}) = \Delta H_{\text{comb}} \cdot (1 - \xi) - \Delta H_{\text{pyr}} - \Delta H_{\text{vap}} - \Delta H_{\text{heat}} \quad (20)$$

( $c_{p_i}$  was calculated as integral mean between combustion or pyrolysis temperatures and standard one, for combustion and pyrolysis products respectively, while  $c_{p_{\text{ashes}}}$  was determined as integral mean between combustion and pyrolysis temperatures)

As a graphical representation of proposed thermo-chemical model development, and for better comprehension of the adopted theoretical assumptions, figure 5 is shown below.

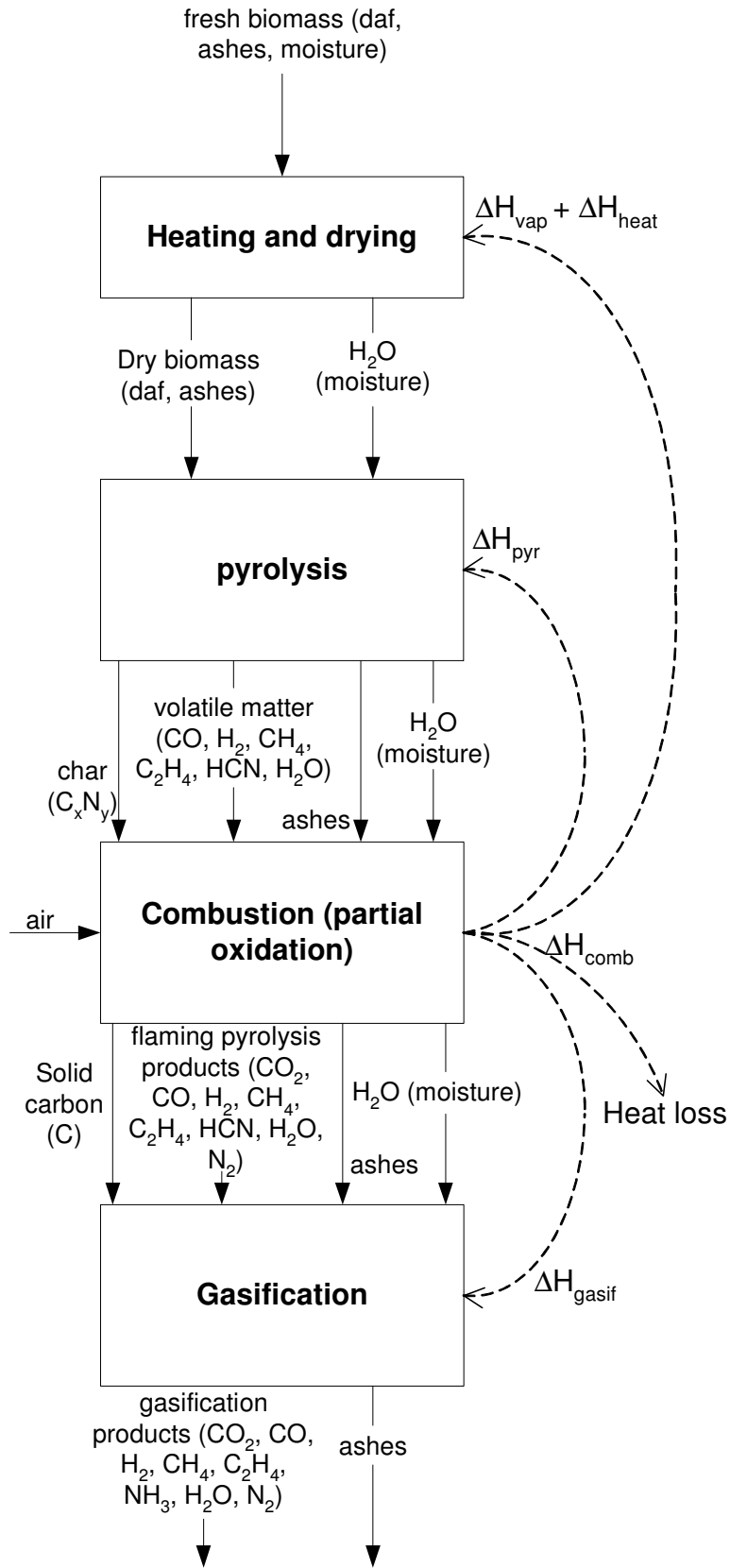


Figure 5: thermo-chemical scheme of considered air downdraft gasification process

## 2.3 Principles of gasification units dimensioning

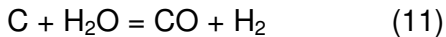
On the basis of the results achieved from thermo-chemical model and according to the thermo-physical properties of solid fuels (table 6), some basic calculations regarding gasification unit dimensioning were carried out, especially by focusing on heterogeneous reactions and gas-solid physical interactions analysis.

Indeed, mass and heat transfers between gas and solid phases were investigated and they were correlated to the intrinsic kinetics of the processes. The scope was to determine the controlling mechanism for each process step and to consequently estimate the necessary minimum residence time ( $\tau$ ) of solid stream through the corresponding reaction zone (assumed to be in perfect plug flow regime), in order that the same step can be totally developed.

As regards the combustion zone, homogeneous reactions of volatile matter oxidation are considered immediate in respect with the other heterogeneous processes of pyrolysis and char gasification. Therefore, time for combustion was not calculated in this analysis. Time to reach equilibrium of homogeneous *water gas shift* reaction was neglected, too. Because of the unreliable results regarding thermo-chemical conversion of refuse derived fuels (especially process temperatures, see par. 3.1.2), park waste wood, wheat straw and sewage sludge were only considered as solid fuels in this second part of work.

### 2.3.1 Physical and chemical processes in char gasification

As stated in par. 2.2.5, the heterogeneous reactions which were supposed to take place in the gasification zone are reactions (11) and (12), such as



Initial amount of solid carbon, as well as  $\text{H}_2\text{O}$  and  $\text{CO}_2$  concentrations, were previously calculated as flaming pyrolysis products in thermo-chemical model simulations. By leading the analysis to the single particle conversion mechanism back, mass transfer from bulk gas to the reacting sites of solid carbon particles was investigated as possible limiting factor of heterogeneous reactions, and two different solid conversion models were investigated, such as shrinking core model and uniform reacting particle one (see fig. 6).

According to this latter, reacting gas is supposed to be present evenly throughout the solid particle at each moment, and it reacts with active sites uniformly and simultaneously (Kunii and Levenspiel, 1991). Gas mass transfer resistance was thus not estimated in this case but an overall equation suggested by Groeneweld and Van Swaaij (Di Blasi, 2009) was used for the calculation of solid carbon conversion time  $\tau_{ur}$ :

$$\frac{dX_c}{dt} = \frac{2.88 \cdot 10^{7.5}}{(T_{gasif})^{0.7}} \cdot e^{\left(\frac{-217}{RT_{gasif}}\right)} \cdot (p_{CO_2} + p_{H_2O})^{0.7} \cdot (1 - X_c) \quad (21)$$

$X_c$  as conversion factor of char.

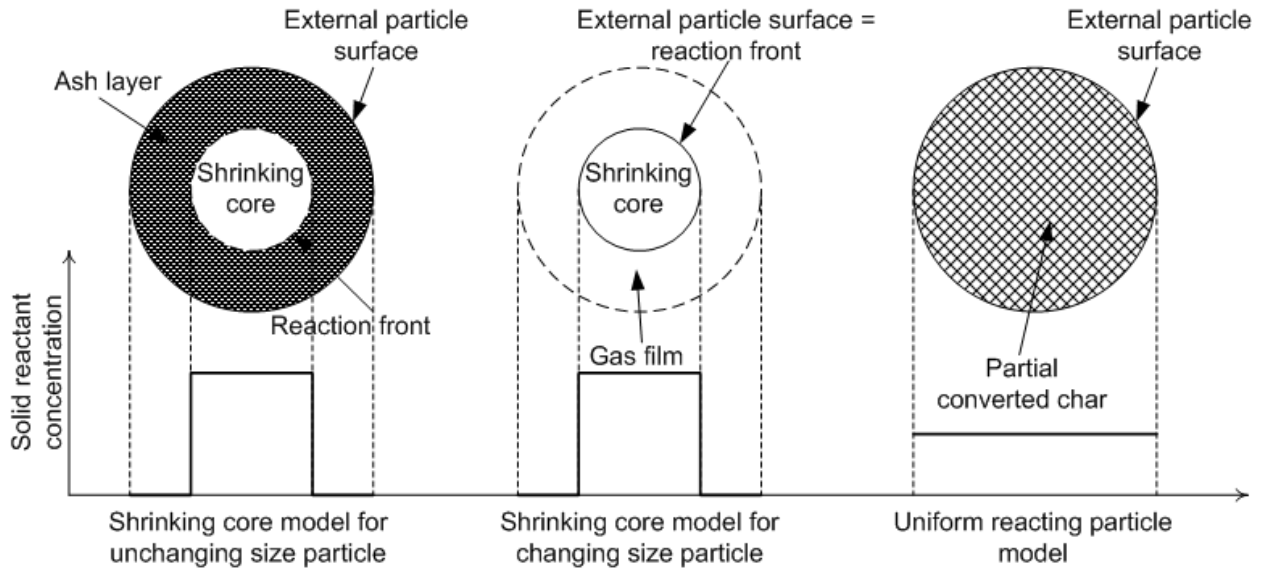


Figure 6: Solid carbon particles conversion models

By solving eq. (21) in respect with  $X_C$  and fixing its final value as 0,999, the time for uniform reaction and closely complete carbon conversion was obtained. Partial pressures of  $\text{CO}_2$  and  $\text{H}_2\text{O}$  were calculated on the basis of flaming pyrolysis products composition (total pressure as 1 bar) and they were considered time constants.

According to the shrinking core model, instead, a spherical reaction front, on which reactions (11) and (12) take place, advances from the external surface of solid particle to its inner core, which hence shrinks during process and it finally disappears.

If shrinking core model is applied to an unchanging size particle, reaction front can be supposed to leave behind a layer of converted char (ashes), through which reacting gas needs to penetrate and diffuse before reacting on solid active sites, while product gas diffuses to the external particle surface the opposite way. Neglecting this second diffusion phenomenon, the limiting factors for char gasification process can be in this case the intrinsic surface kinetics of reactions (11) and (12), or the reacting gas diffusion through the inner pores of converted char.

For each of these two conditions, a chemical or physical resistance to the reaction front advancement was respectively calculated, as well as the necessary time for complete carbon conversion.

In the case intrinsic kinetic was considered as limiting factor, the resistance to front advancement,  $r_k$ , was given as:

$$r_k = 1 / k'_{(j)} \quad [\text{s/m}] \quad (22)$$

Surface kinetic constants,  $k'_{(j)}$ , were obtained for each of two reactions from the relative volumetric kinetic constants,  $k_{(j)}$ , through the following relation:

$$k'_{(j)} = k_{(j)} \cdot R_c / 3 \quad (23)$$

Carbon particle radius  $R_c$  was calculated from initial biomass particle size,  $R_p$  (as spherical, such as decreased by sphericity,  $\phi$ ), by considering radial particle shrinkage during pyrolysis (Davidsson and Pettersson, 2002).

Indeed:

$$R_c = R_p \cdot \phi \cdot s_r \quad (24)$$

$$s_r = \sigma \cdot \gamma^2 \quad (25)$$

$$\sigma = -2.62 \cdot 10^{-6} (T_{pyr})^2 + 0.00395 \cdot T_{pyr} - 1 \quad (26)$$

$$\gamma = X_{vm} / (X_{vm} + X_{fc}) \quad (27)$$

Volumetric kinetic constants were obtained from literature data (Babu and Sheth, 2005) and they were adjusted on molar concentration basis as follows ( $\text{mol/m}^3 \cdot \text{s}$ ):

$$k_{11} = 1.517 \cdot 10^4 e^{\left(\frac{-121620}{RT}\right)} \cdot \frac{P_{H_2O}}{C_{H_2O}} \quad (28)$$

$$k_{12} = 3.616 \cdot 10 e^{\left(\frac{-77390}{RT}\right)} \cdot \frac{P_{CO_2}}{C_{CO_2}} \quad (29)$$

Solid carbon total conversion time  $\tau_k$ , was initially calculated for each reaction separately, by means of the following expression (Kunii and Levenspiel, 1991):

$$\tau_{k(i)} = \frac{\rho'_c \cdot R_c \cdot r_{k(i)}}{C_{(i)}} \quad [\text{s}] \quad (30)$$

Finally, In order to know total char gasification time in the case both of the reactions are contemporary developed, the following expression was used:

$$\tau_k = \frac{1}{\frac{1}{t_{k11}} + \frac{1}{t_{k12}}} \quad [\text{s}] \quad (31)$$

In the case of internal diffusion mechanism of reacting gases through the inner pores of converted char layers, the physical resistance to the reaction front advancement was written for both of the gasification reactions ( $i$ ) as follows:

$$r_{id(i)} = R_c / (6 \cdot \mathcal{D}_m^e)_i \quad [\text{s/m}] \quad (32)$$

Total carbon conversion time was then calculated by means of the following equation for each reaction separately (Kunii and Levenspiel, 1991):

$$\tau_{id(i)} = \frac{\rho'_c \cdot R_c \cdot r_{id}}{C_{(i)}} \quad [\text{s}] \quad (33)$$

$(\mathcal{D}_m^e)_i$  was estimated as follows:

$$(\mathcal{D}_m^e)_i = (\mathcal{D}_m)_i \cdot \varepsilon_c \quad [\text{m}^2/\text{s}] \quad (34)$$

$(\mathcal{D}_m)_i$ , molecular diffusion coefficient of reacting gas ( $i$ ) [ $\text{m}^2/\text{s}$ ], was calculated for  $\text{CO}_2$  and  $\text{H}_2\text{O}$  by using an analytical expression adopted for binary gas mixtures (Inglezakis and Pouloupoulos, 2006), in which one of the components is the diffusing reactant gas ( $i$ ) and the other includes all the other gaseous compounds resulted in flaming pyrolysis products composition.

$$D_{m_i} = 0.01 \cdot \frac{(T_{\text{gasif}})^{1.75} \cdot M_R^{0.5}}{p \cdot (V_i^{1/3} + V_g^{1/3})^2} \quad (35)$$

$$M_R = \frac{1}{PM_i} + \frac{1}{PM_g} \quad (36)$$

Shrinking core model was also used for changing size carbon particles, in the case fuel ash content is not enough to form a layer of converted char behind the advancing reaction front. In this case, this latter always coincides with the external surface of particle that shrinks during the gasification process, so as diffusion of reactant gas through the converted char layer cannot be considered.

Therefore, besides the intrinsic kinetic chemical resistance, as limiting factor for carbon conversion process, the diffusion mechanism of reacting gases from bulk to external surface of particle was investigated. Indeed, a gas film is always supposed to be established around the solid carbon particle, where a radial gas concentration gradient is developed, representing the driving force (or equivalently the physical resistance) to process advancement. This resistance is usually neglected in the case of unchanging size particle conversion, since it is normally lower than gas diffusion resistance trough the inner pores of solid. Nevertheless, they can also be coupled together as in series mechanisms, when their effects on conversion time are comparable.

External gas film resistance,  $r_{ed}$ , was calculated for each reacting gas, as follows:

$$r_{ed(i)} = R_c \cdot y_i / \mathcal{D}_{m(i)} \quad [\text{s/m}] \quad (37)$$

Corresponding time for total carbon conversion was then:

$$\tau_{ed(i)} = \frac{\rho_c \cdot R_c \cdot r_{ed}}{2 \cdot C_{(i)}} \quad [\text{s}] \quad (38)$$

In this analysis, since their comparable resistances, internal and external mass transfers were coupled together as in series phenomena for all the biomasses species. Unchanging size particles were therefore always considered as a more conservative case for char gasification time calculation.

The resulting overall physical resistance for each gasification reaction was hence calculated as:

$$r_{d(i)} = r_{id(i)} + r_{ed(i)} \quad [\text{s/m}] \quad (39)$$

while the corresponding solid carbon conversion time by the overall diffusion mechanism was calculated as:

$$\tau_{d(i)} = \frac{\rho_c \cdot R_c \cdot r_{d(i)}}{C(i)} \quad [\text{s}] \quad (40)$$

Finally, in order to take into account the simultaneous development of the two gasification reactions, eq.(31) was still used, by only changing  $\tau_k$  values with  $\tau_d$  ones.

Overall diffusion mechanism corresponding time was successively compared with the ones resulting from kinetics analysis, according to both the uniform reacting particle and shrinking core models.

The maximum estimated value among these all results was thus assumed to be the necessary time for complete char gasification in that particular application.

### 2.3.2 Pyrolysis controlling mechanisms

Shrinking core model for single particles conversion was used in biomass pyrolysis analysis, too. Nevertheless, as pyrolysis is a thermo-physical process in which no gas reactants take place (reaction of solids alone, as stated by Kunii and Levenspiel, 1991), intrinsic surface kinetic was compared with heat transfer mechanism as possible limiting factor of the process, instead of gas mass transfer. Since in downdraft units the gasifying medium (air, in this case) is supposed to be directly fed to the combustion zone and gaseous products flow downwards, convective heat exchange between flaming pyrolysis products (as heat source) and biomass particles was not considered in this analysis, but conductive and radiative ones only.

Conductive heat exchange was considered in the case of unchanging size particles, whereof the converted char layer represents the internal resistance to the same heat transfer. Indeed, the external surface of particle is supposed to be at combustion temperature while reaction front is at pyrolysis one. A thermal gradient is then established inside the particle and it represents the driving force for the reaction front, in this case.

The conductive heat transfer coefficient was calculated as:

$$h_{\text{cond}} = \lambda_{\text{char}} / (R_p \cdot \phi) \quad [\text{W} / \text{m}^2 \cdot \text{K}] \quad (41)$$

$\lambda_{\text{char}}$ , thermal conductivity of char, was estimated from literature data. It was assumed as 0,11 for woody biomasses (Gupta et al., 2003) and as 0.06 for unwoody biomasses (Suuberg et al., 2001), corresponding to cellulose char thermal conductivity.

Finally, the time for complete pyrolysis of biomass particle, in the case of internal heat transfer limitation, was calculated as follows:

$$\tau_{iht} = \frac{(R_p \cdot \phi)^2 \cdot \Delta H_{\text{pyr}} \cdot \rho_s}{2 \cdot \lambda_{\text{char}} \cdot \Delta T} \quad (42)$$

$$\Delta T = T_{\text{comb}} - T_{\text{pyr}} \quad [\text{K}] \quad (43)$$

Radiative heat transfer was instead considered as an external thermal resistance for still unchanging size particles conversion (in order to take in exam both of the resistances in pyrolysis time estimation)), whose outer surface, in this case, was supposed to be at

pyrolysis temperature and flaming pyrolysis products were envisaged as the radiative heat source at combustion temperature.

Their thermal emissivity was calculated by following an analytical procedure which is usually called the *mixed grey gas model*, (Rhine and Tucker, 1990): hot gas is considered as a mixture of three main grey components (CO<sub>2</sub>, H<sub>2</sub>O, N<sub>2</sub>, in this case) with the addition of an auxiliary clear gas.

Thermal emissivity for each of these components is given as:

$$e_g = 1 - e^{(-k_g pL)} \quad (44)$$

$k_g$  is the thermal absorption coefficient [ $\text{atm}^{-1} \cdot \text{m}^{-1}$ ], empirically estimated (as zero for clean gas).

Total emissivity of the gas mixture is then given by a weighted sum of the single components emissivities, whose weighting coefficients,  $a_g$ , were also empirically estimated (Rhine and Tucker, 1990). Their analytical expression is:

$$a_g = b_1 + b_2 \cdot T \quad (45)$$

Numerical values of these coefficients are reported in the table 7.

	$b_1$	$b_2$	$k_g$
clear gas	0,423	4,33E-05	0
component 1	0,285	5,13E-05	0,890
component 2	0,227	-6,76E-05	15,5
component 3	0,065	-2,70E-05	240,0

Table 7: parameters for gas thermal emissivity calculation

In equation (44) beam length  $L$  also appears. For its estimation, a reactor characteristic dimension was needed to be determined and at this scope an infinite cylinder was considered as theoretical geometrical model for radiative heat transfer. In this case, beam length  $L$  is defined as the diameter of cylinder (as characteristic reactor dimension) by the reciprocal factor,  $F$  (as 0,9 from Colombo, 2007).

Radiative heat transfer coefficient was calculated as follows (Di Blasi, 2008):

$$h_{\text{rad}} = e_g \cdot \sigma_b \cdot (T_{\text{comb}} + T_{\text{pyr}}) \cdot (T_{\text{comb}}^2 + T_{\text{pyr}}^2) \quad [\text{W} / \text{m}^2 \cdot \text{K}] \quad (46)$$

And time for complete pyrolysis of biomass particles, in the case of radiative heat transfer limitation, was calculated as:

$$\tau_{\text{rht}} = \frac{(R_p \cdot \phi) \cdot \Delta H_{\text{pyr}} \cdot \rho_s}{h_{\text{rad}} \cdot \Delta T} \quad (47)$$

In order to evaluate the relative weights of heat transfer resistances on pyrolysis development, *Biot* number was calculated, as the ratio between radiative and conductive heat transfer coefficients:

$$Biot = h_{\text{rad}} / h_{\text{cond}} = (R_p \cdot \phi) \cdot e_g \cdot \sigma_b \cdot (T_{\text{comb}} + T_{\text{pyr}}) \cdot (T_{\text{comb}}^2 + T_{\text{pyr}}^2) / \lambda_{\text{char}} \quad [-] \quad (48)$$

For  $Biot > 10$ , conductive heat transfer process was investigated as possible pyrolysis limiting factor only.

For  $Biot < 0.1$ , radiative heat transfer process was considered as possible limiting factor only.

For  $0.1 < Biot < 10$ , both of the thermal resistances were taken into account to estimate time for complete pyrolysis development.

As definition, for  $Biot$  number equal to unity, conductive and radiative heat transfer coefficients are the same, and the corresponding thermal resistances thus have the same relevance in pyrolysis development. For each biomass fuel, therefore, the appropriate particle size corresponding to this condition ( $R^*$ ), was also calculated for better analysis.

Besides thermal resistances, intrinsic surface kinetics was investigated as the main resistance to solid devolatilization, too. In fact, although pyrolysis is a thermo-physical process rather than a real chemical reaction, it is very common to find in the literature some analytical expressions similar to the kinetic rate equations, usually derived from experimental tests on different fuels conversion. The analytical formula that was used for solid conversion factor  $X_b$  in this analysis is:

$$\frac{dX_b}{dt} = k_{pyr} \cdot (1 - X_b) \quad (49)$$

where  $k_{pyr}$  is the pyrolysis kinetic constant [ $s^{-1}$ ], according to what mentioned above. For all the biomass materials, the Arrhenius' expression was adopted:

$$k_{pyr} = k^0 \cdot e^{\left(\frac{-E_a}{RT_{pyr}}\right)} \quad (50)$$

Values of kinetic parameters and their corresponding kinetic constants (at pyrolysis temperature) are listed in the table 8, as they were found in the literature for the different biomass fuels:

fuel	$T_{pyr}$ (K)	$k^0$ (1/s)	$E_a$ (kJ/mole)	$k_{pyr}$ (1/s)	$k'_{pyr}$ (m/s)	Reference
wheat straw	712	1,56E+10	138	1,174	0,00391	Zhou et al., 2005
park waste wood	674	1,90E+12	177	0,037	0,00031	Bellais, 2007
softwood	711	1,90E+12	177	0,189	0,00069	Bellais, 2007
sewage sludge	702	3,00E+03	69	0,022	0,00001	Yang et al., 2008

Table 8: Pyrolysis kinetic parameters and kinetic constants for different biomass species

For woody biomasses, the same kinetic expression was used (Bellais, 2007) in order to better investigate the effects of the other physical properties of the same materials on the overall pyrolysis development.

By solving eq. (49) in respect with  $X_b$  and fixing its value as 0,999, the time for closely complete development of particles pyrolysis was finally calculated.

The relative weight of intrinsic kinetic resistance on pyrolysis development was compared with both of the thermal ones through the analysis of the so called *Thiele* number,  $Th$ , as ratio of the respective heat transfer rates.

Since conductive or radiative heat transfer resistances could be in turn considered, two different expressions of *Thiele* number were used (Di Blasi et al., 2001):

$$Th_{cond} = \frac{k_{pyr}^* \cdot \rho_s \cdot cp_b \cdot (\phi \cdot R_p)^2}{\lambda_{char}} \quad (51)$$

$$Th_{rad} = \frac{k_{pyr}^* \cdot \rho_s \cdot cp_b \cdot (\phi \cdot R_p)}{h_{rad}} \quad (52)$$

According to the values obtained for *Biot* and *Thiele* numbers, the following procedure was finally adopted:

If  $Biot > 10$ ,  $Th_{cond}$  was only taken in exam for the comparison and combination of solid conversion resistances, and in this case:

- for  $Th_{cond} > 10$ , internal conductive heat transfer resistance was considered the only limiting factor of pyrolysis process and  $\tau_{iht}$  was chosen as solid conversion time.
- for  $Th_{cond} < 0.1$ , intrinsic kinetic resistance was considered the only limiting factor of pyrolysis process and total solid conversion time was calculated by means of eq. (49).
- for  $0.1 < Th_{cond} < 10$ , internal conductive heat transfer resistance and intrinsic kinetic one were both considered as limiting factors of pyrolysis process. For simplicity, their corresponding solid conversion times were only added together in order to estimate time for total pyrolysis achievement

If  $Biot < 0.1$ ,  $Th_{rad}$  was only considered for the comparison and combination of solid conversion resistances. In this case:

- for  $Th_{rad} > 10$ , external radiative heat transfer resistance was considered as the only limiting factor of pyrolysis process and  $\tau_{rht}$  was chosen as solid conversion time.
- for  $Th_{rad} < 0.1$ , intrinsic kinetic resistance was considered the only limiting factor of pyrolysis process and total solid conversion time was calculated by means of eq. (49)
- for  $0.1 < Th_{rad} < 10$ , external radiative heat transfer resistance and intrinsic kinetic one were both considered as limiting factors of pyrolysis process. For simplicity, their corresponding solid conversion times were only added together in order to estimate total pyrolysis time.

If  $0.1 < Biot < 10$ ,  $Th_{cond}$  and  $Th_{rad}$  were both considered for the combination of solid conversion resistances and the procedure described above was applied for both of them, such as:

- for both *Thiele* numbers  $> 10$ , thermal resistances were only considered as pyrolysis limiting factors and their corresponding conversion times were added together in order to obtain total conversion time.
- for both *Thiele* numbers  $< 0.1$ , kinetic resistance was considered as only pyrolysis limiting factor.
- If one or both of the *Thiele* numbers came out in the range from 0.1 to 10, their corresponding thermal resistances were coupled with the kinetic one, and their relative solid conversion times were added together

### 2.3.3 Fuel drying process

Drying of solid fuels was investigated according to the same analytical procedure adopted for pyrolysis conversion step, such as by the analysis of internal and external heat transfer mechanisms for a solid particle. In addition, moisture diffusion (as water vapour) from the inner core to the external surface of particle was also considered as possible process limiting factor.

In this latter case, the time for complete drying of fuels was calculated by means of the following equation (Kunii and Levenspiel, 1991), fixing  $X_w = 0,999$  independently on initial moisture content of biomass ( $n$  assumed as 1,2,3)..

$$1 - X_w = \frac{6}{\pi^2} \cdot \sum_{n=1}^{\infty} \frac{1}{n^2} \cdot \exp \left[ - (n\pi^2) \cdot \frac{D_{m_w} \cdot t}{R_p^2} \right] \quad (53)$$

$\mathcal{D}_{m_w}^*$  is the vapour effective molecular diffusion coefficient in air [ $m^2/s$ ], and it was calculated as:

$$\mathcal{D}_{m_w}^* = \mathcal{D}_{m_w} \cdot \varepsilon_b \quad (54)$$

Solids drying process was then supposed to be heat transfer limited, too. Internal conductive heat transfer and radiative one were still considered, and shrinking core model was still adopted.

As regard radiative heat transfer, biomass particles surface was supposed to be at drying temperature and pyrolysis products were in this case considered as heat source, at their corresponding pyrolysis temperature (CO, H<sub>2</sub> and H<sub>2</sub>O were chosen as gas mixture for emissivity estimation, in this case). Radiative heat transfer coefficient,  $h_{rad}$ , was then calculated according to eq. (46) by only changing  $T_{comb}$  and  $T_{pyr}$  with  $T_{pyr}$  and  $T_{drying}$  respectively.

The analytical expression of drying time of solid fuels,  $(\tau_{dry})_{rht}$ , is shown below (Kunii and Levenspiel):

$$(\tau_{dry})_{rht} = \frac{\rho_s \cdot (R_p \cdot \phi) \cdot U^0 \cdot \Delta H_{vap}}{6 \cdot h_{rad} \cdot \Delta T} \quad (55)$$

$$\Delta T = T_{pyr} - T_{drying} \text{ [K]} \quad (56)$$

In the case of internal heat conduction mechanism, instead, heat transfer coefficient was calculated as follows:

$$h_{cond} = \lambda_b / (R_p \cdot \phi) \quad [\text{W} / \text{m}^2 \cdot \text{K}] \quad (57)$$

$\lambda_b$  is the thermal conductivity of biomass particle in this case, whose values were found in literature for the different biomass fuels, as well (see table 6).

Time for particle drying was then calculated through the following equation:

$$(\tau_{dry})_{iht} = \frac{(R_p \cdot \phi)^2 \cdot \Delta H_{vap} \cdot U^0 \cdot \rho_s}{2 \cdot \lambda_b \cdot \Delta T} \quad (58)$$

As for pyrolysis, internal and external heat transfer resistances were then compared through the *Biot* number estimation, for which, in this case, the following expression was assumed:

$$Biot_{dry} = h_{rad} / h_{cond} = (R_p \cdot \phi) \cdot \epsilon_g \cdot \sigma_b \cdot (T_{pyr} + T_{dry}) \cdot (T_{pyr}^2 + T_{dry}^2) / \lambda_b \quad [-] \quad (59)$$

### 2.3.4 Biomass heating

In order to complete the analysis on the main steps to be envisaged for a correct dimensioning of a downdraft gasifier, heating of solid fuels was investigated, too.

On the contrary of the other examined processes, biomass bed inside the reactor was thought as a single macro-fluid, considering solids and air as components of an homogeneous material, whose density and heat capacity were thus defined as:

$$cp_{bed} = cp_{fresh} \cdot (1 - \epsilon_{bed}) + cp_{air} \cdot \epsilon_{bed} \quad [J/g K] \quad (60)$$

$$\rho_{bed} = \rho_{bulk} \quad [kg/m^3] \quad (61)$$

Three main mechanisms were studied and combined together for biomass heating analysis: convective heat transfer between the leaving product syngas and the fresh feeding material through the cavity walls of a double-walled reactor, radiative heat exchange from the hot inner walls of reactor, and still radiative heat exchange by flaming pyrolysis products to the upper bed of material. These mechanisms were supposed to accomplish the biomass heating process from unit inlet up to pyrolysis temperature. Moisture vaporization was instead neglected in this section, since it was already treated in the previous paragraph, supposing to be achieved by radiative and conductive heat transfers only.

Thermal power from convective heat exchange,  $\Delta H_{conv}$ , was estimated by the following expression (Colombo, 2007):

$$\Delta H_{conv} = \frac{\pi \cdot \Delta T^m \cdot L_h}{\frac{1}{h_{bed} \cdot D_{bed}} + \ln\left(\frac{D_i}{D_{bed}}\right) \cdot \frac{1}{2\lambda_w} + \frac{1}{h_{gas} \cdot D_i}} \quad (62)$$

$\Delta T^m$  is the logarithmic temperature difference [K] between externally flowing syngas and inner biomass bed. It was calculated as (Colombo, 2007):

$$\Delta T^m = \frac{(T_{gasif} - T_{pyr}) - (T_{exit}^g - T_{in}^b)}{\ln\left(\frac{T_{gasif} - T_{pyr}}{T_{exit}^g - T_{in}^b}\right)} \quad (63)$$

$h_{gas}$  is the convective heat transfer coefficient at the gas side and it was calculated as:

$$h_{gas} = Nu_{gas} \cdot \lambda_{gas} / s_h \quad [W/m^2 K] \quad (64)$$

$Nu_{gas}$  is Nusselt number of gas flow, calculated as (Holman, 1990):

$$Nu_{gas} = 1,86 \cdot \left( \frac{Re_{gas} \cdot Pr_{gas} \cdot s_h}{L_h} \right)^{\frac{1}{3}} \quad \text{per } Re_{gas} < 4000 \quad (65)$$

$$Nu_{gas} = 0,023 \cdot Re_{gas}^{0,8} \cdot Pr_{gas}^{\frac{1}{3}} \quad \text{per } Re_{gas} > 4000 \quad (66)$$

$$Re_{gas} = \frac{u \cdot \rho_{gas} \cdot s_h}{\mu_{gas}} \quad (67)$$

$$Pr_{gas} = \frac{cp_{gas} \cdot \mu_{gas}}{\lambda_{gas}} \quad (68)$$

Heat transfer coefficient at biomass side,  $h_{bed}$ , was instead calculated as the combination of two different in series terms, respectively regarding heat transfer from solid bed to reactor walls and radial thermal diffusion through the same biomass bed (Kunii and Levenspiel, 1991).

Conductive heat transfer coefficient from bed to reactor walls was estimated by means of the following expression, where convective term is neglected, since the very low bed material velocity through the reactor (Kunii and Levenspiel, 1991):

$$h_{b/w} = \frac{2 \cdot \lambda_{bed}}{d_p \cdot \phi} \quad [\text{W/m}^2 \text{ K}] \quad (69)$$

$\lambda_{bed}$  is the thermal conductivity of bed [W/m K], estimated by coupling solid and air thermal conductivities through the following expression (Kunii and Levenspiel, 1991):

$$\lambda_{bed} = \varepsilon_{bed} \cdot \lambda_{air} + (1 - \varepsilon_{bed}) \cdot \lambda_b \cdot \left[ \frac{1}{\phi_w \left( \frac{\lambda_b}{\lambda_{air}} \right) + \frac{1}{3}} \right] \quad (70)$$

$\Phi_w$  is the thickness of bed film (as dimensionless ratio with  $d_p$ ) through which the conductive heat exchange is supposed to be developed. It is calculated according to the ratio  $\lambda_b/\lambda_{air}$ , that was estimated as 0.35 for wood, 0.34 for straw, and as 0.30 for sewage sludge (Kunii and Levenspiel, 1991).

Thermal diffusion within the bed and towards the inner walls of reactor was instead calculated as:

$$h^0_{bed} = 1.13 \cdot \left[ \frac{\lambda_b \cdot \rho_b \cdot cp_b \cdot (1 - \varepsilon_{bed}) \cdot u_{bed}}{L_h} \right] \quad (71)$$

Finally, total heat transfer coefficient at the bed side,  $h_{bed}$ , was calculated as:

$$h_{bed} = \frac{1}{\frac{1}{h_{b/w}} + \frac{1}{h_{bed}^0}} \quad (72)$$

$h_{gas}$  and  $h_{bed}$  were then inserted in eq. (62), as they were obtained by eq. (64) and (72) respectively.

Besides convective heat transfer, two radiative exchange terms were also considered, as said. The first is regarding the radiative heat emission from the hot walls of reactor, which are externally heated by the syngas stream which brushes their external surface while leaving from reactor..

At this purpose, temperature of reactor walls was calculated by considering convective heat exchange  $\Delta H_{conv}$  from flowing gas to the inner wall surface only.  $\Delta T_w^m$  was first estimated as corresponding logarithmic mean temperature:

$$\Delta T_w^m = \frac{\Delta H_{conv}}{2\pi R_m \cdot L_h \cdot \frac{1}{\frac{2R_m}{h_{gas} \cdot D_i} + \frac{R_m}{\lambda_w} \cdot \ln\left(\frac{D_i}{D_{bed}}\right)}} \quad (73)$$

$$R_m = \frac{\frac{D_i - D_{bed}}{2}}{\ln\left(\frac{D_i}{D_{bed}}\right)} \quad (74)$$

$T_w$  was thus possible to be estimated through the following equation:

$$T_w = \frac{T_{gasif} - T_{exit}^g \cdot e^{\left(\frac{T_{gasif} - T_{exit}^g}{\Delta T_w^m}\right)}}{1 - e^{\left(\frac{T_{gasif} - T_{exit}^g}{\Delta T_w^m}\right)}} \quad (75)$$

Radiative heat exchange from reactor walls was finally calculated as:

$$\Delta H_{rad}^w = \frac{2\pi R_m L_h \cdot \sigma_b \cdot (T_w^4 - T_{bed}^m{}^4)}{\frac{1}{e_w} + \frac{1}{e_b} - 1} \quad (76)$$

$$T_{bed}^m = (T_{pyr} + T_{in}^b)/2 \quad (77)$$

Radiative heat exchange from hot flaming pyrolysis product gases was envisaged, too. It was calculated as thermal radiation absorption by the biomass bed taking up the pyrolysis zone.

The thermal radiation passing a fluid or solid layer through, at a distance  $z$  from energy source,  $\Delta H_{bed}^{rad}$ , is expressed by the Lambert-Beer's law (Bass M. et al., 1995):

$$\Delta H_{rad}^{bed} = \Delta H^o e^{(-\alpha \cdot z)} \quad (78)$$

In the case of a downdraft gasifier,  $\Delta H^o$  can be seen as the thermal radiation by flaming pyrolysis products and, therefore, thermal power absorbed by biomass bed can be written as:

$$\Delta H_{rad}^{bed} = \frac{\pi D_{bed}^2}{4} \cdot F \cdot \varepsilon_g \cdot \sigma_b \cdot T_{comb}^4 \cdot (1 - e^{-\alpha L_h}) \quad (79)$$

Equations (62), (76) and (79) were finally coupled together in order to formulate the energy balance on biomass fuel to be heated from drying to pyrolysis temperature. It was written as:

$$\rho_{bed} \cdot \frac{\pi \cdot D_{bed}^2}{4} \cdot u_{bed} \cdot c_{p_{bed}} \cdot (T_{pyr} - T_{drying}) = \Delta H_{conv} + \Delta H_{rad}^w + \Delta H_{rad}^{bed} \quad (80)$$

In equation (79) the only two unknown values are  $L_h$  and  $T_{exit}^g$  (bed diameter was chosen the same as gasification zone one, according to the open core configuration). As a consequence, in order to find them out, thermal energy balance on syngas stream was also added:

$$\rho_g \cdot c_{p_g} \cdot Q_g \cdot (T_{gasif} - T_{exit}^s) = \Delta H_{conv} \quad (81)$$

### 3 RESULTS

#### 3.1 Outcomes from kinetic free model application on the different biomass fuels

##### 3.1.1 Main results by thermo-chemical model

According to the biomass gasification kinetic free model described in par. 2.2, the results on thermo-chemical conversion processes of considered biomass fuels are presented in this paragraph.

From the Østberg's pyrolysis model application (Østberg et al., 1998), the following components and yields at the exit of pyrolysis zone were estimated for the examined biomass species. Their corresponding temperatures ( $T_{pyr}$ ) are also reported as they were calculated according to eq. (20):

wt%	wheat straw	park waste wood	softwood	sewage sludge	RDF with plastic
<b>Char (C<sub>x</sub>N<sub>y</sub>)</b>	12,45	18,24	19,42	10,87	5,15
<b>CO</b>	65,36	67,31	57,08	33,37	24,51
<b>H<sub>2</sub></b>	4,97	5,34	3,79	3,26	4,13
<b>CH<sub>4</sub></b>	0,04	0,00	3,65	1,26	14,53
<b>C<sub>2</sub>H<sub>4</sub></b>	2,36	0,01	0,96	5,87	39,80
<b>HCN</b>	0,72	0,28	0,10	6,09	0,56
<b>H<sub>2</sub>O (moisture + pyrolysis)</b>	9,86	5,78	14,72	6,66	2,65
<b>ashes</b>	4,24	3,04	0,27	32,62	8,66
<b>T<sub>pyr</sub> (K)</b>	712	674	711	702	664

*Table 9: Pyrolysis products for the considered biomass fuels (wt%) and their corresponding temperatures according to the kinetic free model application*

By relating these first outcomes to the proximate and ultimate analyses of biomass fuels (table 3), it can be noted that oxygen/carbon ratio (O/C) in biomass elementary composition plays a very important role in determining volatile matter components. Indeed, for low O/C ratios (in the case of sewage sludge and refuse derived fuels above all), high mass percentages of methane and ethylene are obtained in spite of CO and H<sub>2</sub> yields.

The reason of this result is due to the same assumption of Østberg's model for pyrolysis simulation (initially developed for coal devolatilisation), and its relatively limited number of considered gas components as possible products. In fact, according to this analytical approach, in the case the examined fuel shows a low O/C ratio, carbon element that is not involved in char production is necessary linked to hydrogen, thus leading to a high production of CH<sub>4</sub> and C<sub>2</sub>H<sub>4</sub> and relatively low fractions of CO. As a consequence, even low yields of molecular hydrogen are obtained, since it is mainly consumed in the formation of the same hydrocarbon compounds.

In real cases, besides CH<sub>4</sub> and C<sub>2</sub>H<sub>4</sub>, different compounds are also produced during pyrolysis (especially tars and heavier hydrocarbons) which are successively thermally cracked or dry and steam reformed in the further steps of gasification.

In this proposed solid conversion model, instead, CH<sub>4</sub> and C<sub>2</sub>H<sub>4</sub> are the only considered hydrocarbons in pyrolysis products and they are even assumed to be stable components of final syngas composition.

Therefore, O/C ratio in fuel elementary composition represents a limiting key parameter for the reliability of the model simplifying assumptions, since they can be accepted only for fuels with relatively high O/C values.

As regards char production during pyrolysis, it was assumed to be as the same amount of fixed carbon reported in fuels proximate analyses.

In table 9, the high mass percentage of ashes as solid pyrolysis products of sewage sludge obviously causes the decrease of the other gas yields, which therefore show lower values than the other biomass materials.

As stated in par. 2.2.4, air gasification was assumed to be carried out for all the biomass materials. Equivalence ratios as 0.25, 0.30 and 0.35 were fixed in this analysis and different air / fuel ratios were consequently calculated for each biomass fuel, as reported in table 10.

fuel	kg <sub>air</sub> / kg <sub>fresh biom</sub>			kg <sub>air</sub> / kg <sub>daf biom</sub>		
	ER = 0.25	ER = 0.3	ER = 0.35	ER = 0.25	ER = 0.3	ER = 0.35
wheat straw	1,28	1,54	1,80	1,50	1,80	2,10
park waste wood	1,40	1,68	1,96	1,52	1,83	2,13
softwood	1,42	1,71	1,99	1,58	1,90	2,22
sewage sludge	1,19	1,43	1,66	2,03	2,44	2,84
RDF with plastic	2,75	3,30	3,85	3,11	3,73	4,35

Table 10: Air supplies for gasification of biomass fuels according to different ER values

By following the analytical procedure described in paragraphs 2.2.4, 2.2.5 and 2.2.6, final process products were estimated as ashes and gaseous components leaving the gasification zone. Gas components percentages and total yields are listed in tables 11a, 11b and 11c according to the equivalence ratios cited above, for all the biomass species. Corresponding temperatures at the exit of gasification zone (as calculated from eq. (18)) and cold gas energy efficiencies are also included.

vol% (ER = 0.25)	wheat straw	park waste wood	softwood	sewage sludge	RDF with plastic
<b>CO</b>	22,96	29,46	25,98	17,47	-
<b>H<sub>2</sub></b>	26,96	26,95	22,33	18,52	-
<b>CH<sub>4</sub></b>	0,02	0,002	2,17	0,99	-
<b>C<sub>2</sub>H<sub>4</sub></b>	0,84	0,004	0,33	2,65	-
<b>CO<sub>2</sub></b>	10,73	7,05	8,74	10,48	-
<b>N<sub>2</sub></b>	35,24	35,69	37,06	43,13	-
<b>H<sub>2</sub>O</b>	2,97	0,74	3,37	3,91	-
<b>NH<sub>3</sub></b>	0,27	0,10	0,04	2,85	-
<b>LHV (kJ/Nm<sup>3</sup>)</b>	6350	6645	6663	6525	-
<b>T<sub>gasif</sub> (K)</b>	782	684	895	849	-
<b>gas yield (Nm<sup>3</sup>/kg<sub>fresh</sub>)</b>	2,24	2,41	2,36	1,72	-
<b>process efficiency</b>	0,90	0,92	0,88	0,89	-

Table 11a: Syngas yields, compositions, temperatures and cold gas energy efficiencies of thermo-chemical process at ER = 0.25

vol% ( $ER = 0.3$ )	wheat straw	park waste wood	softwood	sewage sludge	RDF with plastic
<b>CO</b>	21,70	26,63	23,89	15,83	0,23
<b>H<sub>2</sub></b>	21,44	22,49	17,42	13,17	5,28
<b>CH<sub>4</sub></b>	0,02	0,002	2,02	0,91	3,89
<b>C<sub>2</sub>H<sub>4</sub></b>	0,78	0,003	0,30	2,44	8,22
<b>CO<sub>2</sub></b>	9,78	7,45	8,43	9,93	11,44
<b>N<sub>2</sub></b>	39,50	39,97	41,40	47,59	57,10
<b>H<sub>2</sub>O</b>	6,52	3,36	6,51	7,51	13,71
<b>NH<sub>3</sub></b>	0,25	0,09	0,03	2,62	0,13
<b>LHV (kJ/Nm<sup>3</sup>)</b>	5560	5804	5802	5558	6861
<b>T<sub>gasif</sub> (K)</b>	986	932	1110	1067	604
<b>gas yield (Nm<sup>3</sup>/kg<sub>fresh</sub>)</b>	2,40	2,58	2,54	1,86	3,55
<b>process efficiency</b>	0,84	0,86	0,82	0,82	0,94

Table 11b: Syngas yields, compositions, temperatures and cold gas energy efficiencies of thermo-chemical process at  $ER = 0.30$

vol% ( $ER = 0.35$ )	wheat straw	park waste wood	softwood	sewage sludge	RDF with plastic
<b>CO</b>	20,39	24,60	21,84	14,01	0,93
<b>H<sub>2</sub></b>	16,81	18,14	13,37	9,01	4,00
<b>CH<sub>4</sub></b>	0,02	0,002	1,89	0,85	2,77
<b>C<sub>2</sub>H<sub>4</sub></b>	0,74	0,003	0,28	2,26	7,05
<b>CO<sub>2</sub></b>	9,15	7,36	8,39	9,88	10,76
<b>N<sub>2</sub></b>	43,23	43,72	45,18	51,40	59,45
<b>H<sub>2</sub>O</b>	9,43	6,10	9,01	10,16	14,93
<b>NH<sub>3</sub></b>	0,23	0,09	0,03	2,43	0,12
<b>LHV (kJ/Nm<sup>3</sup>)</b>	4863	5077	5048	4725	5717
<b>T<sub>gasif</sub> (K)</b>	1162	1130	1294	1255	832
<b>gas yield (Nm<sup>3</sup>/kg<sub>fresh</sub>)</b>	2,56	2,75	2,71	2,01	3,97
<b>process efficiency</b>	0,78	0,81	0,77	0,75	0,88

Table 11c: Syngas yields, compositions, temperatures and cold gas energy efficiencies of thermo-chemical process at  $ER = 0.35$

As it can be seen from table 11a, values for RDFs corresponding to  $ER = 0.25$  are not indicated. In fact, at this condition, total energy balance of the overall gasification process was not satisfied, such as air supply was not enough to thermally sustain the thermo-chemical endothermic processes (moisture vaporization, pyrolysis and char gasification) by providing the necessary heat from combustion reactions. Indeed, as reported in table 12, a very high pyrolysis heat was calculated for RDFs, according to pyrolysis products composition and solid fuel heating value (eq. (6)). For this reason, thermal energy supply and demands were not balanced in the case of  $ER = 0.25$ . Moreover, for  $ER$  as 0.30 and 0.35, estimated combustion and gasification temperatures (see table 13) also resulted too low in respect with the usual values at which their corresponding processes are expected to be developed.

Moreover, the high yields of methane and ethylene calculated in pyrolysis zone and resulting from the low O/C ratios of their elementary compositions, are still present as high volumetric percentages in final syngas compositions both for sewage sludge and

especially for RDFs, since these compounds are assumed to be not involved in the further combustion and gasification steps.

Besides, RDFs are also featured by a little char production during pyrolysis step, that is instead assumed to be the only compound to be converted to H<sub>2</sub> and CO in the gasification zone. As a consequence, very low percentages of these two combustible gases are presented in the final syngas composition.

For the two woody biomasses, syngas low heating values resulted almost the same, although their compositions were quite different. Because of its lower O/C ratio (see table 3), softwood shows an higher percentage of methane in final gas composition and a slightly lower syngas yields.

The highest bound nitrogen content in sewage sludge elementary composition is then the reason for the highest ammonia percentages in its corresponding final syngas compositions.

fuel	$\Delta H_{\text{vap}}$ (kJ/kg <sub>daf</sub> )	$\Delta H_{\text{pyr}}$ (kJ/kg <sub>daf</sub> )	$\Delta H_{\text{comb}}$ (kJ/kg <sub>daf</sub> )			$\Delta H_{\text{gasif}}$ (kJ/kg <sub>daf</sub> )		
			ER = 0.25	ER = 0.3	ER = 0.35	ER = 0.25	ER = 0.3	ER = 0.35
wheat straw	329	2362	-5967	-7160	-8353	1705	1851	1986
park waste wood	168	2095	-6048	-7257	-8467	2494	2585	2700
softwood	309	1308	-6283	-7540	-8744	2637	2763	2823
sewage sludge	316	3452	-7968	-9400	-10832	1805	1790	1747
RDF with plastic	95	10633	-	-12836	-14721	-	480	490

Table 12: Process heats in the different reaction zones, according to biomass nature and equivalence ratio

ER = 0.25	wheat straw	park waste wood	softwood	sewage sludge	RDF with plastic
$T^{\text{pyr}}$ (K)	712	674	711	702	-
$T^{\text{comb}}$ (K)	1216	1345	1510	1208	-
$T^{\text{gasif}}$ (K)	782	684	895	849	-
ER = 0.3	wheat straw	park waste wood	softwood	sewage sludge	RDF with plastic
$T^{\text{pyr}}$ (K)	712	674	711	702	664
$T^{\text{comb}}$ (K)	1409	1525	1669	1371	656
$T^{\text{gasif}}$ (K)	986	932	1110	1067	604
ER = 0.35	wheat straw	park waste wood	softwood	sewage sludge	RDF with plastic
$T^{\text{pyr}}$ (K)	712	674	711	702	664
$T^{\text{comb}}$ (K)	1569	1674	1791	1509	888
$T^{\text{gasif}}$ (K)	1162	1130	1294	1255	832

Table 13: gas temperatures at the exit of the different reaction zones, according to biomass nature and equivalence ratio

By comparing the maximum estimated temperatures inside the gasifier (such as at the exit of combustion zone) at the same equivalence ratio and for all the biomass materials (except for RDFs), they seem to be depending on biomass ash content more than on air to biomass supply (as inert nitrogen gas conveyor). Indeed, sewage sludge shows the lowest combustion temperature and the highest ash content, and combustion temperatures for all the materials decrease with the rise of ash amounts. The same trend can be also observed by considering the two woody biomasses only, whose elementary compositions are very similar and only ash and moisture content are changed.

Woody biomasses also show the highest gasification heat,  $\Delta H_{gasif}$ , at each  $ER$  condition (see table 12). This is also an expected result since these materials are characterized by the highest fixed carbon contents, which are assumed to give similar char contents during pyrolysis step and then to be totally converted in the gasification zone.

As an indirect result of the previous computations, an estimation of combustion heat distribution among the other endothermic processes was achieved, according to equivalence ratio. Besides heat loss (fixed to 10% of total combustion heat), two other terms were considered: heat for processes occurring before combustion, (air and feedstock heating, biomass drying and pyrolysis), and heat for endothermic gasification reactions, afterwards partial oxidation. Their respective amounts,  $X$  and  $Y$ , as ratio to total combustion heat, are reported in following table 14:

$ER = 0.25$	wheat straw	park waste wood	softwood	sewage sludge	RDF with plastic
$\xi$	0,1	0,1	0,1	0,1	-
$X$	0,58	0,48	0,36	0,58	-
$Y$	0,32	0,42	0,54	0,32	-
$ER = 0.30$	wheat straw	park waste wood	softwood	sewage sludge	RDF with plastic
$\xi$	0,1	0,1	0,1	0,1	0,1
$X$	0,47	0,44	0,30	0,56	0,89
$Y$	0,43	0,46	0,60	0,34	0,01
$ER = 0.35$	wheat straw	park waste wood	softwood	sewage sludge	RDF with plastic
$\xi$	0,1	0,1	0,1	0,1	0,1
$X$	0,41	0,34	0,26	0,43	0,77
$Y$	0,49	0,56	0,64	0,47	0,13

Table 14: Distribution of combustion heats as heat source for the other endothermic processes involved in biomass gasification

### 3.1.2 Influence of moisture content and equivalence ratio on gasification model results

Gas temperatures at the exit of pyrolysis zone are not affected by equivalence ratio, as well as pyrolysis products. This is an obvious result, since solids devolatilization is a thermo-physical process that is carried out without any oxidizing gas reactants, and, in a downdraft gasification configuration, gasifying medium is fed downwards pyrolysis zone.

As expected,  $CO$  and  $H_2$  percentages instead decrease with the rise of equivalence ratio, while  $CO_2$  and water contents increase as combustion products of reactions (7) and (8) prevalently. This obviously leads to a consequent increase of syngas heating values for

lower  $ER$  values (see fig. 7). Moreover, in spite of the greater syngas yields corresponding to higher equivalence ratios, even cold gas energy efficiencies show the same trends as gas low heating values as a function of  $ER$  (see fig. 8).

Nevertheless, these results are deeply influenced by the initial simplifying assumptions of complete conversion of char in gasification zone and fixed energy loss as 10% of combustion heat, by neglecting tars formation at each working condition. In practical applications, on the contrary, air / fuel ratio plays a very important role in char conversion and final yield of tars, so as cold gas energy efficiencies could even show opposite trends from the analysis of experimental results.

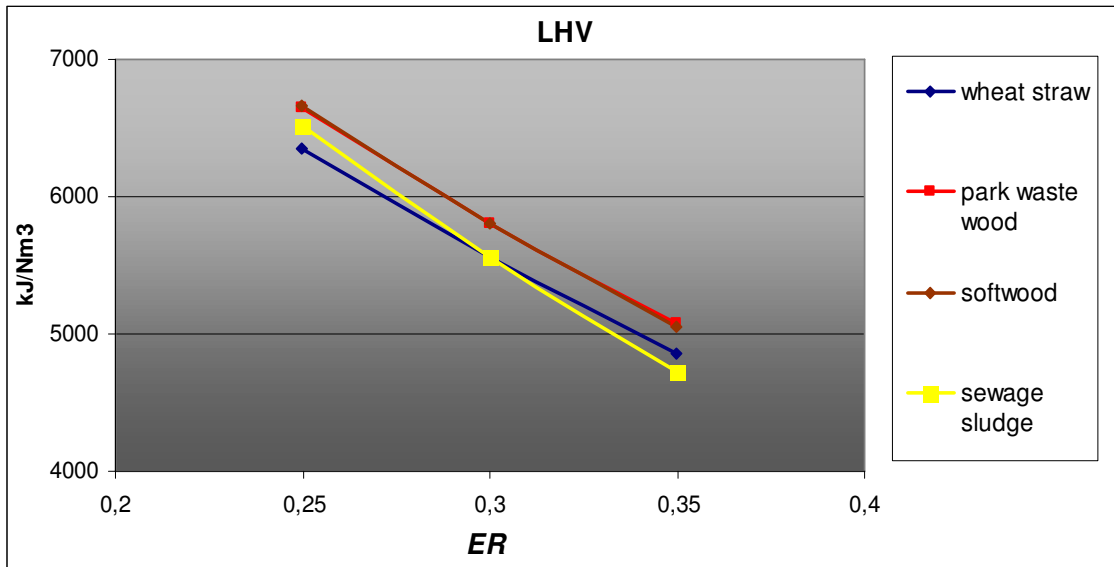


Figure 7: Low heating values of product gas as a function of equivalence ratio, for the different biomass fuels

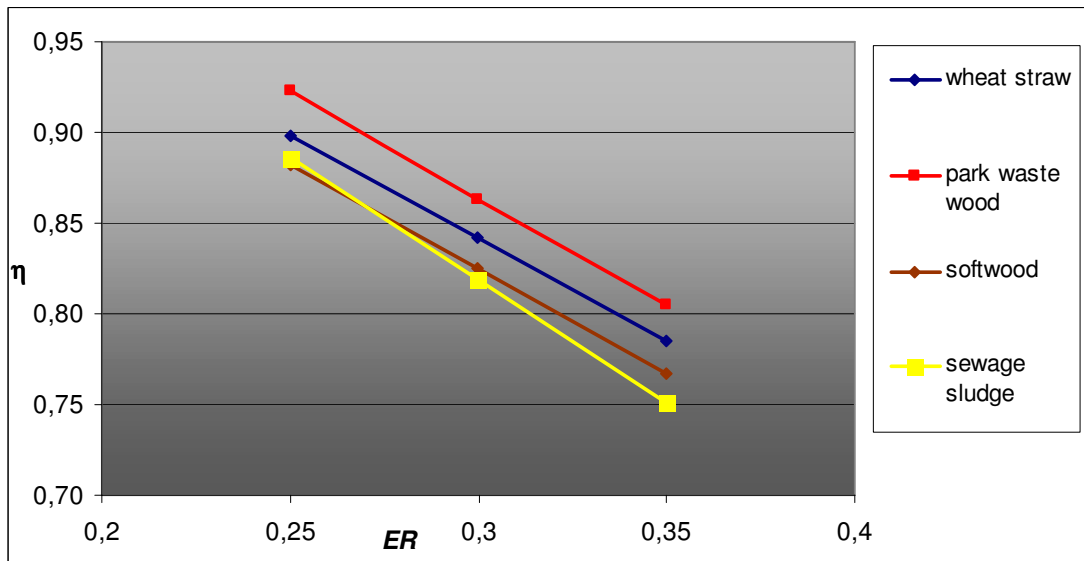


Figure 8: Cold gas energy efficiencies of gasification process as a function of equivalence ratio

As the enhanced exothermic oxidation reactions (7) and (8), also combustion heat,  $\Delta H_{comb}$  (in absolute terms), increases with equivalence ratio, and, as a consequence, temperatures in combustion and gasification zones as well, since the more energy supply (see table 13).

Besides, as the rise of temperature in the gasification zone, the exothermic *water gas shift* reaction (15), ( $\Delta H = -41$  kJ/mole) is not favoured for higher *ER* values, so that the overall process heat of gasification step,  $\Delta H_{gasif}$  (as endothermic process), also results increased at higher equivalence ratio conditions.

Water vapour percentages in final syngas compositions are clearly dependant on the moisture contents of corresponding fuels, as it can be especially seen from the analysis of park waste wood syngas composition according to its lowest initial water content.

The same dependence is not so evident in the case of  $H_2$  syngas percentage, instead. It could be thus deducted that, at least for the considered biomasses, low moisture contents (until 5%, at least) don't represent a limiting factor for solid carbon conversion (eq. (11)), which is on the contrary mainly carried out by the oxidation reactions products ( $H_2O$  and  $CO_2$ ) released in the combustion zone.

The addition of auxiliary steam for increasing process efficiency and heating value of syngas seems therefore to be not necessary in the case of the biomasses taken in exam.

Fuel moisture content seems also to be affecting gas temperature at the exit of gasification zone. In fact, by considering the two woody biomasses only, at the same *ER* condition, gasification temperatures resulted higher for softwood than for park waste wood, although this latter shows the lowest moisture content. This can be explained from the assumption of *water gas shift* reaction equilibrium in the gasification zone. Indeed, by also considering complete conversion of char by reactions (11) and (12), a greater  $H_2O$  concentration in final syngas composition, especially due to the higher initial water content of fuel (as in this case of softwood), gives a lower value of equilibrium constant (see eq. (16)), and, according to eq. (17), it consequently make a rise of equilibrium temperature.

### 3.1.3 Validation of model results through the comparison with experimental data (woody biomasses)

Results of the proposed analytical model were well validated from the comparison with experimental data regarding wood processing, for which a great number of thermo-chemical conversion tests are reported in literature.

Gas temperatures and solid mass fractions (char + ashes) calculated at the exit of pyrolysis zones (see table 9) were compared with the same parameters registered during wood pyrolysis tests, considering their measured constant values at the end of solid devolatilization trial (fig. 9).

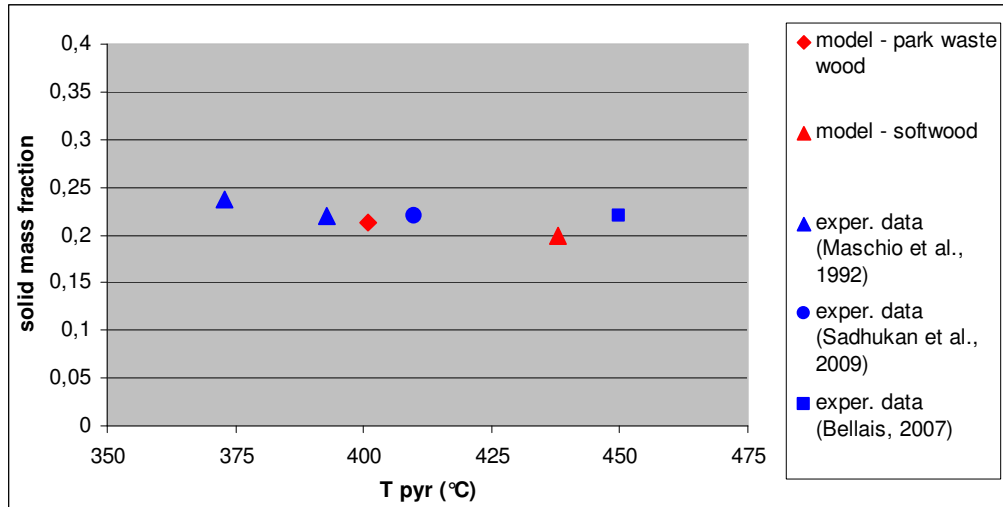


Figure 9: Comparison of residual solid mass fractions and corresponding temperatures between wood pyrolysis experimental tests and calculated model results for woody biomasses.

From figure 9, it can be stated that experimental and analytical results are in quite a good accordance. Indeed, in spite of the different wood species used for pyrolysis modelling and experimental tests, a maximum error of 11% was estimated for residual mass fraction between model and experimental results. Since properties of woods used for experiments were not clearly indicated in the corresponding literature, no further analysis on this result was possible. Anyway, the assumption of char content as final pyrolysis product equal to the fixed carbon amount of initial solid fuel composition seems to be an acceptable modelling simplification.

Estimated syngas compositions and gasification temperatures were also examined on the basis of experimental results on wood downdraft gasification tests (Jayah et al., 2003). Since still different woody biomasses were used for experiments and gasification modelling, their proximate and ultimate analyses are reported in table 15 for better comparison.

Figure 10 shows dry syngas compositions as they were calculated by the kinetic free model and as measured at the exit of wood downdraft gasifier. Corresponding air / fuel ratios, exit syngas temperatures and final solid mass fractions are listed in table 16, as main working conditions and further outcomes.

	park waste wood	softwood	rubber wood (exper. tests)*
<b>proximate analysis</b>			
VM (d.b. %)	77,6	78,2	80,1
FC (d.b. %)	19,2	21,5	19,2
ashes (d.b. %)	3,2	0,3	0,7
moisture (d.b. %)	5,5	10,7	16
<b>ultimate analysis</b>			
C (%)	49,6	52,5	50,6
H (%)	5,7	6,0	6,5
N (%)	0,3	0,1	0,2
O (%)	41,1	41,1	42
S (%)	0,0	0,0	-
ash (%)	3,2	0,3	0,7

\* Jayah et al., 2003

Table 15: Proximate and ultimate analyses of woody biomasses used for gasification modelling and in experimental tests

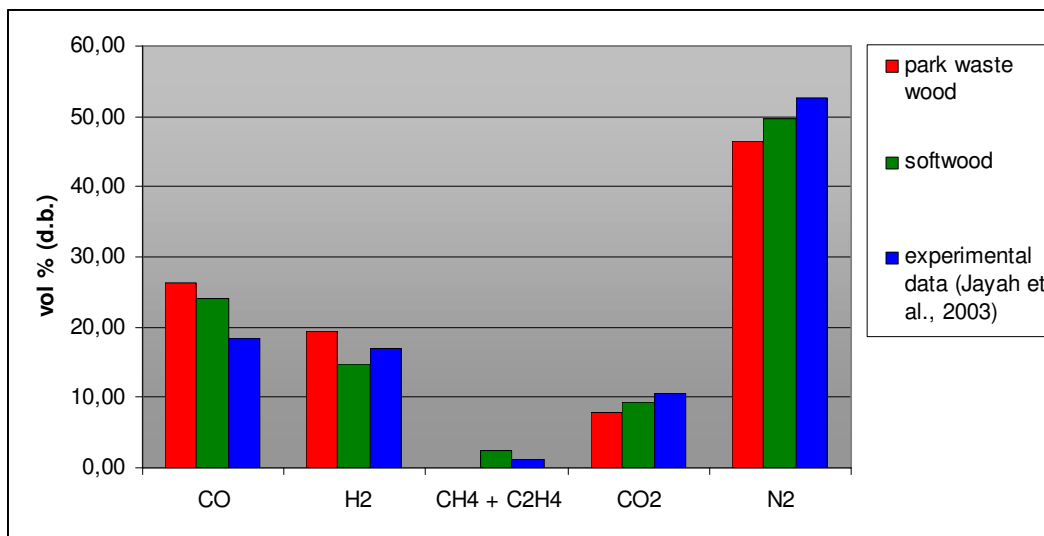


Figure 10: Dry syngas compositions as they were calculated by the kinetic free model and as results of experimental tests

	park waste wood	softwood	exper. data (Jayah et al., 2003)
$T_{\text{gasif}}$ (°C)	857	1021	890
air/fuel ratio	1,96	1,99	1,96
mass fraction (char + ashes, % d.b.)*	3,2	0,3	4,3

\* percentage on initial dry fuel feed

Table 16: Exit syngas temperatures, air / fuel ratios and residual solid mass fractions as analytically estimated and as experimental results on wood biomass gasification tests.

As stated in the previous paragraphs, complete gasification of char was considered in the kinetic free model development, although it is clearly not achieved during experimental tests. Indeed, residual mass fraction collected at the end of wood gasification experiments (see table 16) is much greater than initial ash content of fuel (see table 15). Therefore, unconverted char is measured at the end of downdraft gasification trials.

This main gap between analytical and experimental results can be also considered as the main reason for the lower CO percentage and the higher CO<sub>2</sub> one of experimental data in respect with model results.

In fact, as solid carbon is not completely converted in practical applications, it can be deduced that especially the following reaction (12)



is not totally carried out during experiments, maybe because of a too low working temperature or short gas residence time in gasification zone.

The higher N<sub>2</sub> percentage in experimental data in respect with the analytical results, even at the same air / fuel ratio, reveals a lower yield of dry syngas, maybe due to the higher moisture content of tested fuel (see table 16) or still because of the incomplete conversion of solid carbon.

Moreover, although the greatest moisture content of rubber wood, its corresponding gas temperature at the exit of gasification zone is not higher than the estimated ones for the other two materials. It can be hence deduced that in real experiments (in this case at least) *water gas shift* equilibrium is not achieved.

### 3.2 Preliminary results for estimating gasification units dimensions

As stated in par. 2.3, heterogeneous char gasification reactions, solid fuel devolatilization, moisture vaporization and initial feedstock heating were considered as the main processes affecting the dimensioning of gasification units, through the analysis of the respective times required for their complete development inside the reactor. These time periods were indeed used as residence times of solid phases in the corresponding zones, considering a perfect plug flow regime.

With the scope of estimating the volumes of reaction zones for each biomass fuel considered in this analysis (except for refuse derived fuels, whose results by thermo-chemical gasification model were not satisfactory), some initial assumptions were made.

As regard the units size, an initial fresh biomass feeding rate ( $W$ ) as 100 kg/h was considered for all of the species, and an open core downdraft configuration was used in all of the cases.

Among the different investigated air feeding conditions ( $ER$ ), the ones providing the best cold gas efficiencies were chosen, but maintaining an exit syngas temperature not less than 950K. Indeed, according to a previous study by Sharma, 2008, critical temperatures above which complete gasification of biomass char can be only achieved were calculated as 932K and 950K, according to the different models adopted.

This result was therefore considered as an initial assumption in this present analysis and, as a consequence, equivalence ratio as 0.3 was used as air feeding condition for wheat straw, softwood and sewage sludge, while for park waste wood  $ER = 0,35$  was used (see table 13).

In this way, for the two woody biomasses, working conditions providing almost the same cold gas efficiencies were taken in exam, as well (see table 11b and 11c).

On the basis of these assumptions, gas flows through the gasifiers could be calculated for each biomass fuel and in each reaction zone. According to their values at the inlet of gasification zones ( $Q$ ), units diameters were calculated by choosing a gas superficial velocity as 0.5 m/s, as suggested by Reed et al., 1999.

Numerical values of the quantities mentioned above are shown in the following table 17, for each considered biomass type.

fuel	$W_{\text{fresh}}$ (kg/h)	$W_{\text{daf}}$ (kg/h)	$Q_g$ (Nm <sup>3</sup> /kg <sub>daf</sub> )	$Q_g$ (Nm <sup>3</sup> /h)	$v$ (m/s)	$D$ (m)
wheat straw	100	85,48	2,54	217	0,50	0,39
park waste wood	100	91,77	2,63	241	0,50	0,41
softwood	100	90,03	2,41	217	0,50	0,39
sewage sludge	100	58,57	2,89	169	0,50	0,35

Table 17: biomass feeding rates, gas yields and flows at the exit of combustion zone, and corresponding units diameters for the different materials gasification applications

### 3.2.1 Results from investigated conversion models for char gasification

For char gasification by reactions (11) and (12), kinetic and gas mass transfer resistances were compared each others as possible limiting factors of the process, and two conversion models were adopted, such as uniform reacting particle model and shrinking core one.

For the first one, as definition of the same model, mass transfer of reacting gas towards the inner active sites of fuel particles is negligible, so that only kinetic resistance is considered. At this scope eq. (21) was used, where kinetics of reactions (11) and (12) are coupled in one expression only, according to partial pressures of H<sub>2</sub>O and CO<sub>2</sub>.

Results regarding temperatures and initial partial pressures of reactants, as well as char conversion factors and corresponding gasification times are presented in the following table 18, for the different biomass species:

fuel	T <sub>gasif</sub> (K)	p <sub>CO<sub>2</sub></sub> (Pa)	p <sub>H<sub>2</sub>O</sub> (Pa)	X <sub>c</sub>	τ <sub>ur</sub> (s)
wheat straw	986	17181	11644	0,999	2146
park waste wood	1130	19630	9847	0,999	84
softwood	1110	19024	15086	0,999	123
sewage sludge	1067	15287	17030	0,999	298

*Table 18: solid carbon conversion factors and corresponding conversion times for the different biomass species, according to the uniform reacting particle model,*

In the case of shrinking core model, reactions (11) and (12) were initially taken in exam separately, and successively their corresponding times for total char gasification were combined together by means of eq.(31).

In table 19, kinetic parameters and corresponding char gasification times are reported for the two reactions separately and for each biomass material. Table 20, instead, shows the total conversion times for char gasification as they were obtained by considering the two gasification reactions simultaneously

C + H <sub>2</sub> O = CO + H <sub>2</sub>	R <sub>p</sub> (mm)	R <sub>c</sub> (mm)	T <sub>gasif</sub> (K)	k <sub>11</sub> (1/s)	k' <sub>11</sub> (m/s)	r <sub>k(11)</sub> (s/m)	τ <sub>k(11)</sub> (s)
wheat straw	5,00	1,42	986	58	0,027	37	590
park waste wood	12,5	2,66	1130	454	0,402	2	211
softwood	5,5	1,23	1110	361	0,148	7	133
sewage sludge	0,50	0,15	1067	174	0,008	118	349

C + CO <sub>2</sub> = 2CO	R <sub>p</sub> (mm)	R <sub>c</sub> (mm)	T <sub>gasif</sub> (K)	k <sub>12</sub> (1/s)	k' <sub>12</sub> (m/s)	r <sub>k(12)</sub> (s/m)	τ <sub>k(12)</sub> (s)
wheat straw	5,00	1,42	986	30	0,014	70	761
park waste wood	12,5	2,66	1130	120	0,106	9	401
softwood	5,5	1,23	1110	104	0,042	24	366
sewage sludge	0,50	0,15	1067	61	0,003	337	1114

*Table 19: kinetic parameters and solid carbon total conversion times according to shrinking core model and intrinsic kinetics resistance of single reactions*

fuel	$\tau_k$ (s)
wheat straw	332
park waste wood	138
softwood	97
sewage sludge	266

Table 20: char gasification times according to shrinking core model and intrinsic kinetics resistance, with both reactions contemporary developed and for each biomass fuel

As said, char gasification was investigated as mass transfer limited, too. In this case, char particles were alternatively considered as changing and unchanging size ones, so that external and internal mass transfer resistances by reacting gases were estimated, according to shrinking core conversion model again.

As a more conservative case, however, gasification of unchanging size char particles was considered for the estimation of total carbon conversion time, so as internal and external mass transfer resistances were in series combined (eq.(39)), by initially considering both of the gasification reactions separately. Their corresponding char gasification times were thus calculated by eq.(40) and finally they were coupled together by means of eq.(31).

Estimations of the main parameters involved in gas diffusion mechanisms analysis, and the corresponding overall times for complete gasification of char are reported in table 21, for each considered gasification reaction and for all the examined biomass species

$C + H_2O = CO + H_2$	$R_c$ (mm)	$T_{gasif}$ (K)	$\mathcal{D}_m$ (m <sup>2</sup> /s)	$\epsilon_c$	$\mathcal{D}_m^e$ (m <sup>2</sup> /s)	$r_d$ (s/m)	$\tau_d$ (s)
wheat straw	1,42	986	0,00124	0,7	0,00087	0,4046	7
park waste wood	2,66	1130	0,00166	0,7	0,00117	0,5368	46
softwood	1,23	1110	0,00163	0,7	0,00114	0,2922	6
sewage sludge	0,15	1067	0,00115	0,7	0,00080	0,0523	0,2

$C + CO_2 = 2CO$	$R_c$ (mm)	$T_{gasif}$ (K)	$\mathcal{D}_m$ (m <sup>2</sup> /s)*	$\epsilon_c$	$\mathcal{D}_m^e$ (m <sup>2</sup> /s)	$r_d$ (s/m)	$\tau_d$ (s)
wheat straw	1,42	986	0,00076	0,7	0,00053	0,7664	8
park waste wood	2,66	1130	0,00102	0,7	0,00071	1,1347	48
softwood	1,23	1110	0,00100	0,7	0,00070	0,5277	8
sewage sludge	0,15	1067	0,00069	0,7	0,00048	0,0835	0,3

Table 21: reacting gas diffusion parameters and corresponding times for char gasification, according to shrinking core model and overall mass transfer resistance, for each single gasification reaction

In table 22, instead, times for complete gasification of char according to gas diffusion mechanisms and simultaneous development of gasification reactions are reported for the different biomass species.

fuel	$\tau_d$ (s)
wheat straw	4
park waste wood	23
softwood	3
sewage sludge	0,1

Table 22: times for complete gasification of char, according to shrinking core model and overall mass transfer resistance, for reactions simultaneously developed.

It can be noted that for char gasification process thermo-physical resistances of gas reactants diffusion from bulk gas to the inner active sites of solid carbon particles are almost negligible in respect with kinetic ones. Diffusion mechanisms are clearly depending on char particles size, while for kinetics resistances gasification temperature is the only parameter affecting the solid carbon conversion time determination. Therefore, at present conditions, kinetics of reactions (11) and (12) can be considered as the only limiting factors of the process.

Their corresponding conversion times were then compared according to the conversion models were used for their estimation, such as uniform reacting particle model and shrinking core one. Results for the different biomass materials are presented in figure 11.

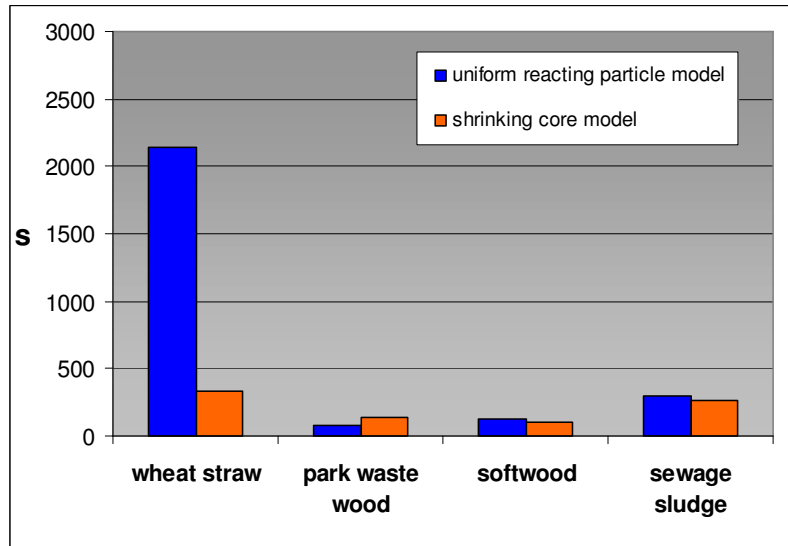


Figure 11: char gasification times by kinetic resistances according the different conversion models for complete gasification time of solid carbon

A deep difference can be seen for wheat straw char conversion times, such as for the biomass presenting the lowest gasification temperature (see table 18), and a great dependence on temperature can be noted for all the results pertaining uniform reacting particle model, according to eq.(21). Shrinking core model, instead, shows narrower ranges for the different biomass species and gasification temperatures, maybe because of the general assumption of char as solid carbon only, so as the same theoretical gasification reactions are used.

On the contrary, since eq.(21) was empirically determined from wood char gasification tests by Groeneweld and Van Swaji (Di Blasi, 2009), it could be maybe not properly fitting for other biomass fuels conversion simulations or it could be only working in a limited range of temperatures (around 1000K – 1100K).

### 3.2.2 Results from analytical investigation on fuels pyrolysis development

For biomass pyrolysis shrinking core model was considered only, and heat transfer resistances were compared with kinetic ones, as stated in par. 2.3.2. Unchanging size particles were considered as a more conservative case, in order to take into account both internal and external resistances.

For this latter, thermal emissivity of flaming pyrolysis products needed to be estimated in order to calculate radiative heat exchange coefficient  $h_{rad}$ . (see eq.(46)). Since gas thermal

emissivity depends on the reactor characteristic dimension,  $L$ , (see eq.(44)), its values could be only estimated on the basis of the reactor diameters previously designed, such as by considering an initial feeding rate for each considered fuel.

Gas thermal emissivities at the exit of combustion zone and the relative parameters involved in their estimation are shown in the following table 23, for each biomass fuel:

fuel	$T_{comb}$ (K)	D (m)	F	L (m)	$e_g$
wheat straw	1409	0,39	0,9	0,35	0,228
park waste wood	1674	0,41	0,9	0,37	0,217
softwood	1669	0,39	0,9	0,35	0,216
sewage sludge	1371	0,35	0,9	0,31	0,233

Table 23: thermal emissivities of flaming pyrolysis products and the corresponding beam lengths of reactors for the different biomasses gasification applications

As also explained in par. 2.3.2, internal and external thermal resistances to pyrolysis development were compared each other by means of the *Biot* number, such as the ratio between their respective heat transfer coefficients, as it is expressed by eq. (48).

According to the initial selected particles sizes of biomass fuels, *Biot* number resulted greater than unity for all the biomass fuels except for sewage sludge (see table 25), whose particles are very small (1mm). This means that internal heat transfer resistance can be considered greater than external one in most of the practical applications, at least for downdraft gasification technology.

For better analysis, the sizes by which *Biot* number corresponds to unity in the different fuels gasification applications ( $R^*$ ) were also calculated, meaning the initial biomass size for which conductive and radiative heat transfer resistances achieve the same relevance on biomass pyrolysis advancement. Values are reported in table 24, for each biomass material.

fuel	$R^*$ (mm)
wheat straw	2,2
park waste wood	3,3
softwood	3,1
sewage sludge	2,0

Table 24: biomass sizes corresponding to *Biot* number as unity ( $R^*$ )

*Biot* number came out in the range 0.1 to 10 for all the biomass fuels. Therefore, as explained in par. 2.3.2, both heat transfer resistances were considered and compared with kinetic one in order to finally estimate pyrolysis conversion time. At this scope, *Thiele* numbers were also determined, according to eq. (51) and (52), for conductive and radiative heat transfer mechanisms respectively.

Both  $Th_{cond}$  and  $Th_{rad}$  came out in the range 0.1 to 10 for woody biomasses, so that conversion times regarding internal and external heat transfer resistances, as well as kinetic one, were all considered and summed together in order to estimate the overall time for pyrolysis complete development. They were calculated according to eq. (42), (47) and (49) respectively.

For wheat straw both *Thiele* numbers were greater than 10, so that kinetic resistance was neglected in the estimation of solid conversion time, which was thus obtained by the sum of the times resulting from heat transfers analysis only.

Finally, in the case of sewage sludge, conductive *Thiele* number,  $Th_{cond}$ , was less than 0,1, meaning a poor internal thermal resistance to pyrolysis development. Therefore, its corresponding time was neglected for the calculation of the overall solid conversion time (even if its value was still comparable with the one resulting by external heart transfer analysis)

In the following table 25, heat transfer coefficients, *Biot* and *Thiele* numbers, single conversion times and overall pyrolysis ones are reported for the examined biomass fuels.

	wheat straw	park waste wood	sewage sludge	softwood
$T_{comb}$ (K)	1409	1674	1371	1669
$T_{pyr}$ (K)	712	674	702	711
$R_p$ (mm)	5,0	12,5	0,5	5,5
sphericity $\phi$	0,8	0,7	0,9	0,75
conductive heat transfer coefficient, $h_{cond}$ [W/m <sup>2</sup> K]	15	13	133	27
radiative heat transfer coefficient, $h_{rad}$ [W/m <sup>2</sup> K]	68	94	65	96
<i>Biot</i> number	4,55	7,49	0,49	3,60
conductive <i>Thiele</i> number, $Th_{cond}$	99,72	7,74	0,09	7,20
radiative <i>Thiele</i> number, $Th_{rad}$	21,90	1,03	0,18	2,00
intrinsic kinetic conversion time [s]	18	530	1000	104
internal heat transfer conversion time [s]	185	328	10	39
radiative heat transfer conversion time [s]	81	88	41	21
total conversion time [s]	267	946	1041	164

Table 25: heat transfer and kinetic parameters regarding biomasses pyrolysis development, and its corresponding conversion times

In order to better point out the differences among heat transfer and kinetic resistances in the devolatilization process of examined solid fuels, their relative conversion times are still reported in figure 12, as they were calculated by eq. (42), (47) and (49).

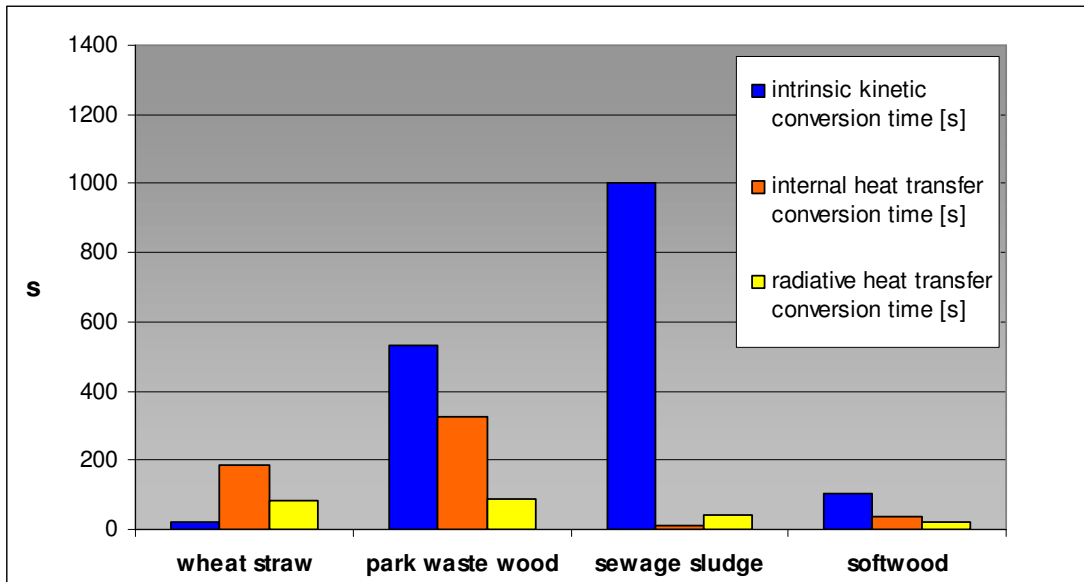


Figure 12: pyrolysis conversion times of biomass fuels, according to the different controlling mechanisms.

It can be especially noted that the nature of biomass plays a very important role in pyrolysis development, both in the case thermal resistances are examined only and for single kinetics mechanism analysis.

For wheat straw, sewage sludge and softwood above all, in spite of their very similar pyrolysis temperatures (see table 25), the analysis of their own kinetics resistances gave completely different solid conversion times, the highest one for sewage sludge, whose pyrolysis temperature is only a bit lower than the others (respectively 702 K against 711 K and 712 K). Moreover, by comparing conversion times by thermal resistances for wheat straw and softwood, high values for the first material can be noted, although their very similar pyrolysis temperatures and particle sizes. This result has hence to be mainly ascribed to the different pyrolysis heats for the two materials and therefore to their nature, as well.

Form the comparison between the two woody biomasses only, it can still be noted that pyrolysis kinetics (Bellais, 2007) is deeply influenced by temperature, with a great increase of conversion time (around five times more) corresponding to a slightly decrease of temperature (from 674 K to 711 K).

The relevance of biomass particles size can be instead observed by comparing the conversion times by heat transfer resistances, still for the two examined woody biomasses. Indeed, by roughly doubling particle size (from 11mm for softwood to 25mm for park waste wood), conversion time by external radiative heat transfer resistance is increased by around four (from 21s to 88s), while pyrolysis time by internal conductive heat transfer resistance is increased by even eight (from 39s to 328s).

### 3.2.3 Moisture vaporization time according to the examined physical resistances

Internal and external heat transfers from bulk gas to solid phase as well as water vapour diffusion through the pores of particles were considered as fuel drying mechanisms in this analysis (see par. 2.3.3).

As regard water vapour diffusion, according to eq. (53), very low and negligible times of moisture vaporization were calculated, so as they were not taken into account in fuels drying analysis and they were not reported in this section, as well.

On the contrary, heat transfer resistances investigation gave more conservative results, still based on shrinking core model, according to eq. (55) and (58). Their relative relevancies on fuel drying process control were still estimated by *Biot* number, as for pyrolysis process. In this case, *Biot* number was calculated by means of eq. (59) and it came out less than one for all the materials, as it can be seen from table 26. This means that radiative heat exchange has a greater effect on drying process development in respect with conductive heat transfer, for each considered biomass treatment application.

For sewage sludge, since its very small particles size, *Biot* number was even less than 0.1. Therefore, radiative heat transfer resistance was only considered for moisture vaporization time estimation. Results are reported in table 26 for all the biomass species.

fuel	$(\tau_{dry})_{iht}$ [s]	$(\tau_{dry})_{rht}$ [s]	<i>Biot</i>	$(\tau_{dry})_{TOT}$ [s]
wheat straw	36	39	0,61	75
park waste wood	38	62	0,40	100
softwood	11	34	0,21	45
sewage sludge	0,5	13	0,02	13

Table 26: drying time for the different biomasses, according to shrinking core model and heat transfer resistances analysis

### 3.2.4 Required unit surfaces for biomass heating

As reported in par. 2.3.4, biomass heating process was considered to be accomplished by three different heat exchange phenomena: convective heat exchange between fresh biomass stream and syngas flux flowing upwards through the hollow space of the double-walled reactor, radiative heat exchange from inner walls of reactor and radiative heat exchange from flaming pyrolysis gases to the upper bed of solid material.

The analysis on these simultaneous heat transfer mechanisms led to the calculation of overall available heat exchange surfaces, from which suitable gasification units lengths were estimated in order to achieve the heating of fuels up to their corresponding final pyrolysis temperatures.

At this task, biomass feeding rates and reactors diameters were firstly to be fixed (see table 17), and biomass stream was considered as a single macro-fluid moving downward through the gasifier. Its velocity,  $u_{bed}$ , was then possible to be estimated according to the bulk densities of materials.

In the following table 27 the main results from the analytical procedure explained in par. 2.3.4, as well as the gasification units lengths required for the overall heat exchange development are reported for each biomass fuel heating application.

	wheat straw	park waste wood	sewage sludge	softwood
$T_{\text{gasif gas}} (\text{°C})$	713	857	794	837
$T_{\text{exit gas}} (\text{°C})$	700	839	756	822
$T_{\text{in bed}} (\text{°C})$	20	20	20	20
$T_{\text{pyr bed}} (\text{°C})$	439	401	429	438
$T_{\text{comb gas}} (\text{°C})$	1136	1401	1098	1396
$T_w (\text{°C})$	645	705	631	726
$Q_{\text{gas}} (\text{m}^3/\text{h})$	789	1034	655	941
$W_{\text{fresh}} (\text{kg}/\text{h})$	100	100	100	100
$\rho_{\text{bed}} (\text{kg}/\text{m}^3)$	79	170	650	170
$cp_{\text{bed}} (\text{kJ}/\text{kg K})$	1,26	1,29	1,68	1,36
$D_{\text{bed}} (\text{m})$	0,39	0,41	0,35	0,39
$D_i (\text{m})$	0,41	0,43	0,37	0,41
$s_n (\text{m})$	0,02	0,02	0,02	0,02
$R_m (\text{m})$	0,20	0,21	0,18	0,20
$u_{\text{bed}} (\text{m}/\text{s})$	0,0030	0,0012	0,0004	0,0014
$u (\text{m}/\text{s})$	8	10	7	10
$h_{\text{bed}} (\text{W}/\text{m}^2 \text{K})$	3	9	7	6
$h_{\text{gas}} (\text{W}/\text{m}^2 \text{K})$	21	29	19	26
$\Delta H_{\text{conv}} (\text{W})$	1160	1815	2936	1589
$e_b$	0,9	0,95	0,95	0,95
$\alpha_b$	0,81	0,77	0,72	0,77
$e_g$	0,228	0,217	0,233	0,216
$\Delta H_{\text{rad}}^w (\text{W})$	18962	12691	21075	18333
$\Delta H^0 (\text{W})$	5525	11663	4051	10225
$\Delta H_{\text{rad}}^{\text{bed}} (\text{W})$	2463	2663	1980	3136
$L_n (\text{m})$	0,73	0,34	0,93	0,48

Table 27: units dimensioning parameters and results for biomass fuels heating process

### 3.2.5 Basic dimensions of gasification units

As one of the objectives of this part of the work and as a resume of the outcomes reported in the previous paragraphs, basic dimensions of gasification units, such as diameters and relative heights of each reaction zone of gasifier, are listed in table 28, for each examined biomass fuel. Total heights of units are also reported, of course.

	wheat straw	park waste wood	sewage sludge	softwood
<b>D<sub>bed</sub> (mm)</b>	<b>390</b>	<b>413</b>	<b>350</b>	<b>390</b>
H <sub>drying</sub> (mm)	217	122	6	61
H <sub>heating</sub> (mm)	729	337	931	476
H <sub>pyrolysis</sub> (mm)	665	1058	277	200
H <sub>gasification</sub> (mm)	121	41	185	48
<b>H<sub>TOT</sub> (mm)</b>	<b>1732</b>	<b>1557</b>	<b>1400</b>	<b>786</b>

Table 28: diameters of gasification units and relative heights of reaction zones, for each biomass fuel gasification application

In order to better point out the differences among the biomass fuels regarding their corresponding units dimensioning, their relative reaction zones heights are also reported in fig. 13 and fig. 14, as absolute and percentage values respectively.

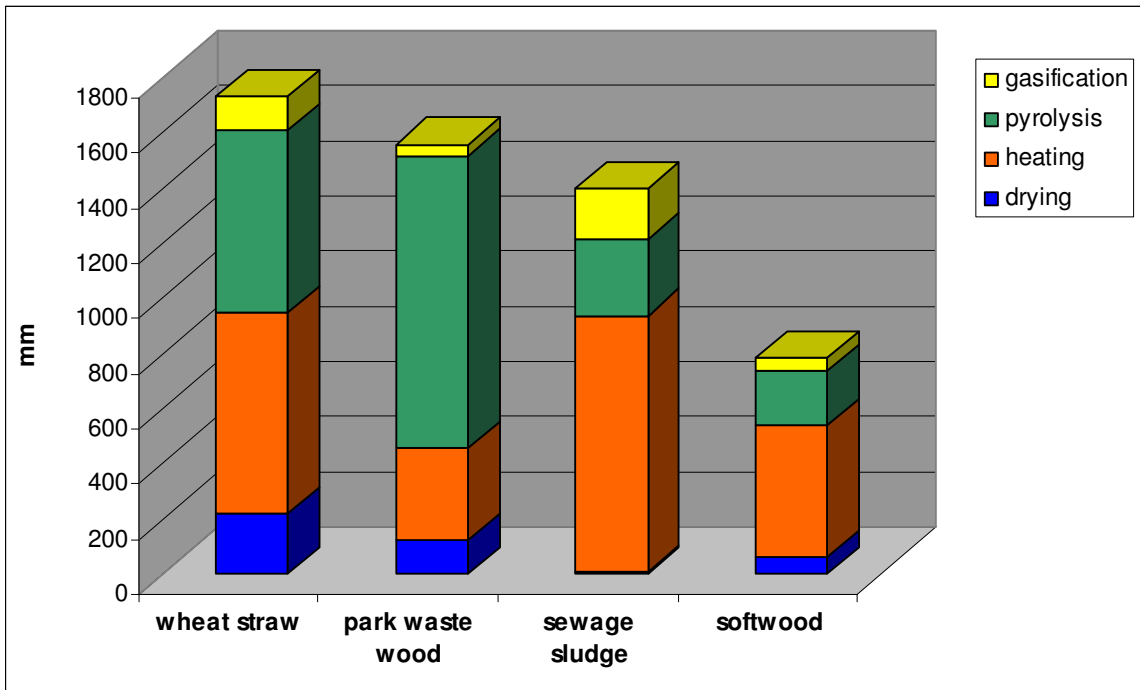


Figure 13: total heights of biomass gasification units and their distribution among solid conversion steps, in absolute values

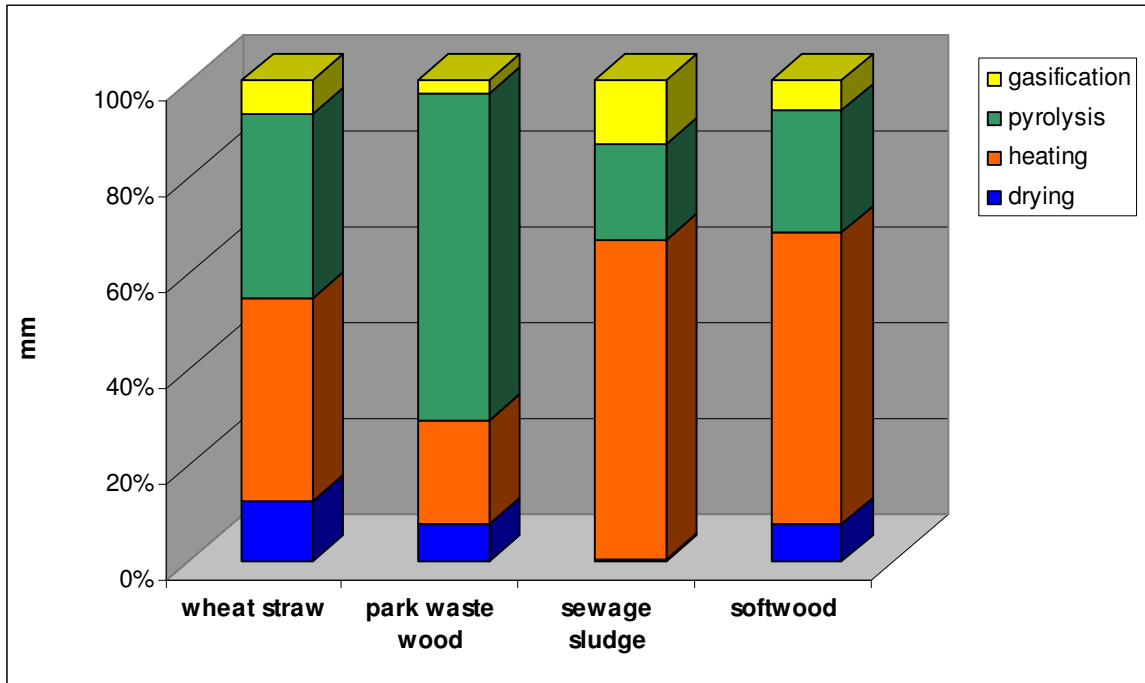


Figure 14: total heights of biomass gasification units and their distribution among solid conversion steps, in percentage values

Although its relatively small particles size (see table 6), wheat straw shows the highest gasification unit among the considered fuels (fig. 13), with an overall height more than twice the one calculated for softwood, which even presents almost the same initial particles size. One of the reasons for this result can be due to the straw lowest solid bulk density ( $79 \text{ kg/m}^3$ ) which obviously provides for larger volumes at the same biomass feeding rate.

Moreover, in comparison with the woody biomasses, straw and sewage sludge show larger gasification zone volumes, especially due to their lower gasification temperatures (in the case of wheat straw, the result by shrinking core model was considered, since the unacceptably high char gasification time by uniform reacting particle model)

On the contrary, the weight of fuel initial particles size is especially remarkable on pyrolysis zone dimensioning, for which thermal heat transfer resistances are comparable with kinetics one for all the materials, except for sewage sludge (since its very small particles).

From the comparison between the woody biomasses only (with the same pyrolysis kinetics), it can be noted an higher pyrolysis zone for park waste wood than for softwood one, according to the larger particles size of the first material (25mm against 11mm). In fact, although a lower temperature at the exit of pyrolysis zone was estimated for park waste wood (affecting kinetics rate), this result is mainly to be attributed to the internal heat transfer resistance, which deep increases with particles size.

Moisture vaporization process is also much more affected by initial biomass particles size than by initial moisture content of fuels. Therefore, It can even be considered negligible for sewage sludge gasification unit design. Maybe because of its greater specific heat (see tables 6) sewage sludge instead shows the highest unit height for biomass heating.

### 3.2.6 Influence of char particles properties on gasification zone dimensioning

As stated in par. 2.3.1., biomass particles shrinkage during pyrolysis was modelled according to the analytical procedure by Davidsson and Pettersson, 2002, with the scope of estimating char particles size at the inlet of gasification zone.

This parameter, however, did not have any influence on gasification zone dimensioning, since intrinsic kinetics resistance (which doesn't depend on char particles size) was found out as limiting factor of the process for each biomass fuel, according to the estimated gasification temperatures, initial biomass particles sizes and char particles densities obtained from literature data.

Nevertheless, in this paragraph an analysis on char gasification time variability according to char properties is carried out by considering woody biomasses only, as the materials which uniform reacting particle model expression was empirically deduced for.

As previously said, kinetic resistances to char gasification (and their corresponding times, as a consequence) are not affected by char particles size in both the conversion models are used for their estimation (see fig. 15a and 15b). These latter have different relative weights on char gasification for the two biomass fuels yet. Indeed, uniform reacting particle model provides the longer char gasification time in softwood application, while shrinking core one presents a more conservative result in park waste wood analysis. This is mainly due to the difference in char particle density between the mentioned materials, since this quantity has a major effect on shrinking core model results in respect with the uniform reacting particle ones.

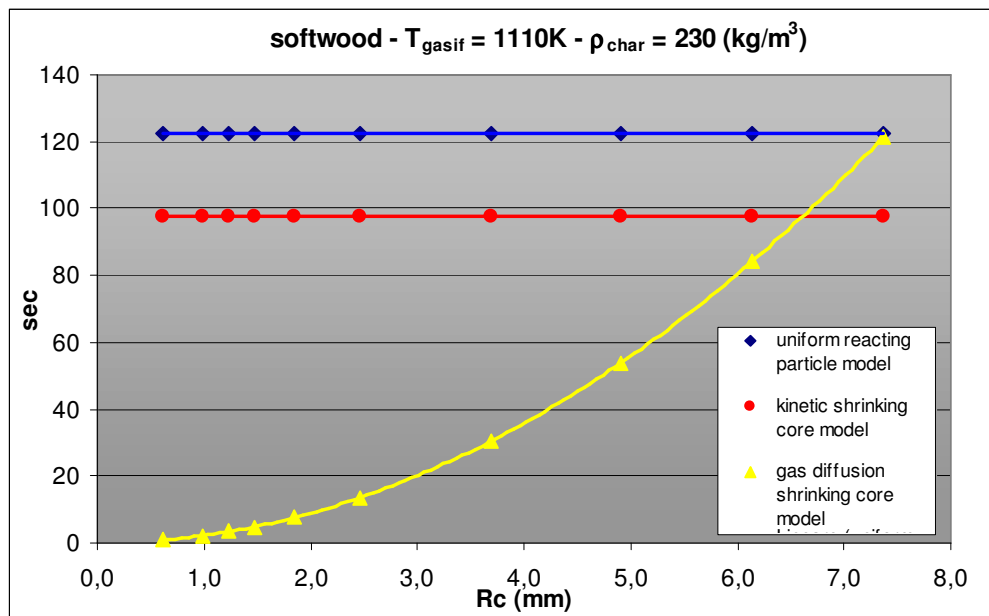


Figure 15a: total conversion time for softwood char gasification according to the different conversion models and as a function of char particles size

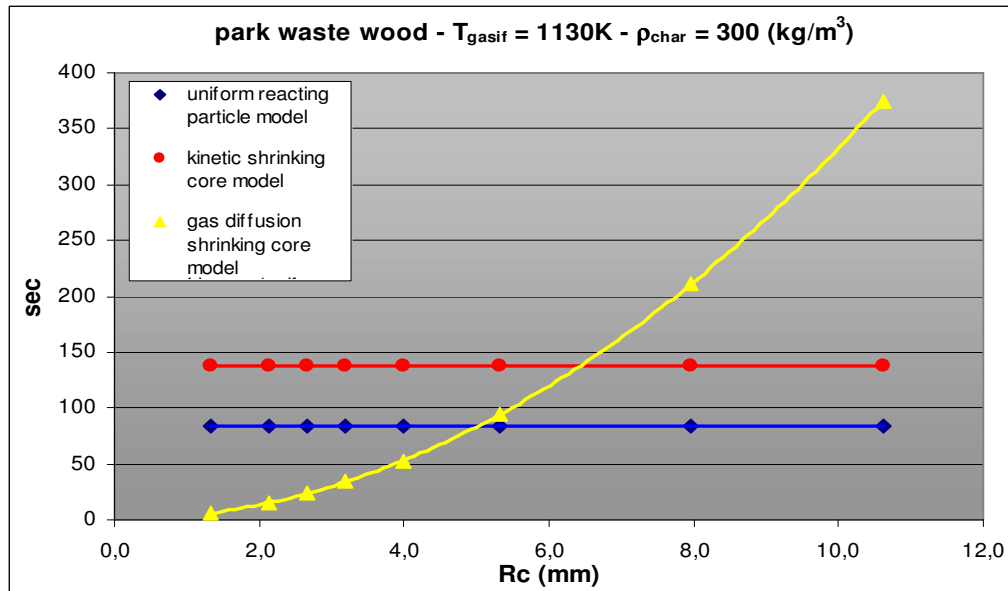


Figure 15b: total conversion time for park waste wood char gasification according to the different conversion models and as a function of char particles size

A quadratic relation with char particle size can be instead detected for solid conversion time in the case gas diffusion mechanism is considered as limiting factor and shrinking core model is still applied.

Char particles sizes for softwood and park waste wood were respectively calculated as 1.2 and 2.7 mm, so that their corresponding gasification times according to physical resistances were much lower than the ones estimated by considering kinetics of gasification reactions.

Besides, an error of +/-20% in char particles size estimation (from the calculated values) leads to an absolute maximum variation of conversion time as about 45%, that is still not relevant for the overall analysis of char gasification time, since the higher values obtained from the analysis of kinetic resistance.

Indeed, as it can be seen from figures 15a and 15b, char particles sizes at which mass diffusion resistance results equal to the kinetics one (considering both the conversion models) are 7.4mm for softwood and 6.4mm for park waste wood. For higher values, mass diffusion mechanisms come out as the controlling factors for char gasification.

### 3.2.7 Influence of temperature on gasification units dimensioning

In this paragraph, the dependence on temperature of units dimensioning analytical procedure was investigated for the two woody biomasses. At this scope, the temperature values initially obtained at the exit of each reaction zone through the thermo-chemical model simulations (see table 13) were arbitrary changed and their effects on the corresponding solid conversion times and units dimensions were observed.

In two cases, temperatures at the exit of reaction zones were decreased all at once, respectively by 5% and 10% in respect with the model results.

For both the materials, unit height for biomass heating process rose of about 10% and 25% for temperature decreases as 5% and 10% respectively, while unit height for drying process rose of around 20% and 50% according to the same temperature changes.

Nevertheless, very high increases were detected for pyrolysis and gasification zones, above all. Indeed, by maintaining the same reactor diameters in all of the cases, pyrolysis height increases by about twenty times more (20.5 times for park waste wood and 19.5 times for softwood) according to a temperature decrease of 10% only, and by about four times more (3,8 and 3.7 times, respectively) according to a temperature decrease of 5%.

As regard gasification zone, reactor height increases by 12 and 8 times according to a temperature decrease of 10%, and by 8 and 2 times according to a temperature decrease of 5%, respectively for softwood and park waste wood. Figure 16 shows these results:

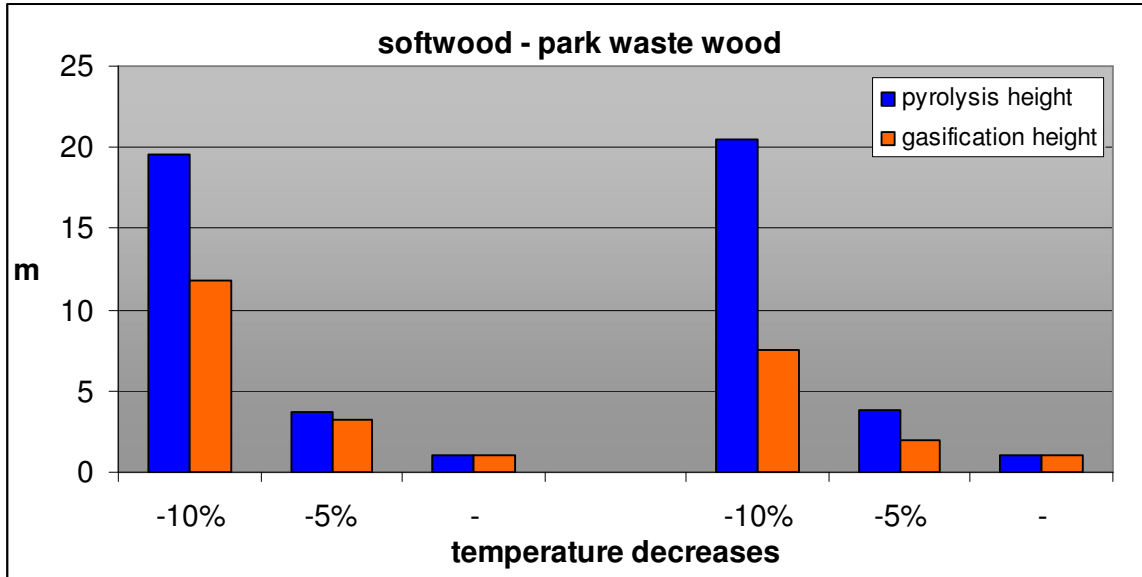


Figure 16: variations of pyrolysis and gasification zones heights according to overall temperature decrease inside the reactor

These very high fluctuations are mainly due to the changes of solid conversion times pertaining kinetics resistances, which come out as limiting factors for char gasification process and give the highest contributes to the estimation of pyrolysis conversion times.

From figures 17a and 17b char gasification times as a function of gasification temperature (in the range +/-10% from the values calculated by the kinetic free model) can be observed as they were estimated according to the uniform particle reacting model and shrinking core one, for kinetics resistances.

It can be noted that uniform particle reacting model, according to eq.(21), has a deeper dependence on temperature than the shrinking core model (eq.(30) and eq.(31)), and corresponding char gasification times assume very high values at gasification temperature lower than 1000 K. For temperatures higher than about 1100 K, instead, shrinking core model shows more conservative results, even if the difference between the two analytical approaches are quite low.

However, according to their trends with temperature, both of the models lead to an high increase of process time for even low temperature decreases, but less remarkable effects if temperature rises of the same quantities.

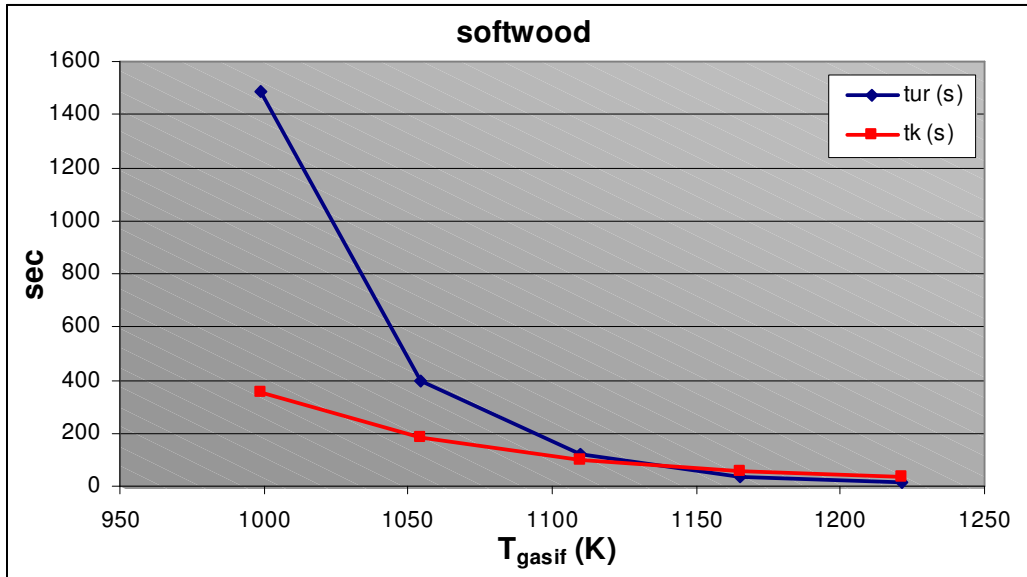


Figure 17a: softwood char gasification time as a function of temperature, according to uniform reacting particle model and shrinking core one, for kinetic resistances

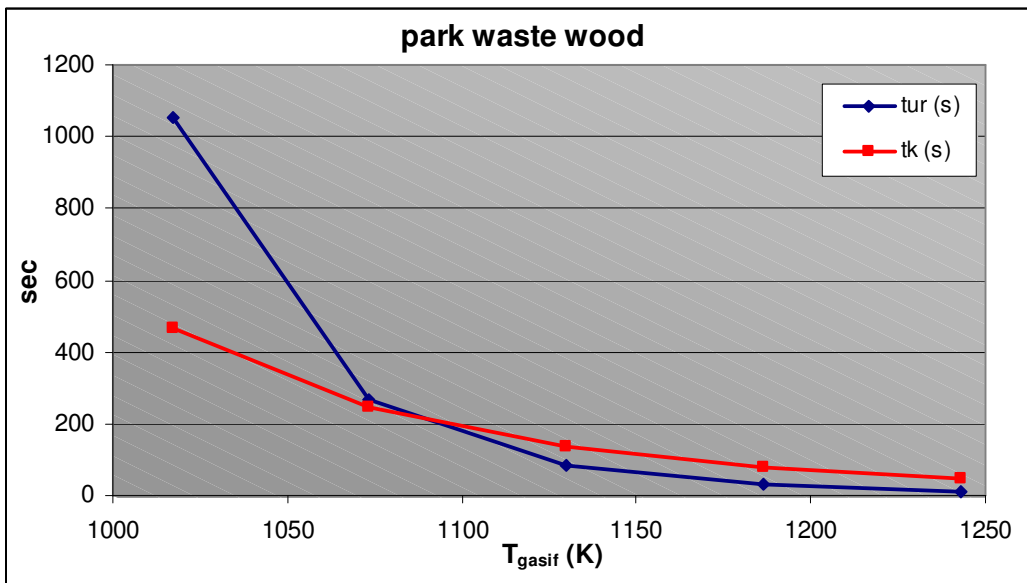


Figure 17b: park waste wood char gasification time as a function of temperature, according to uniform reacting particle model and shrinking core one, for kinetic resistances

As regard pyrolysis, by still considering temperature changes in the range +/-10% from the calculated values during thermo-physical pyrolysis simulation, it can be noted that kinetics shows a deep dependence on temperature in this case too, according to the exponential form of eq.(50). Therefore, for even short temperature decreases, pyrolysis conversion times considerably rise, as it can be seen from tables 29a and 29b. On the contrary, by increasing temperature, heat transfer physical resistances have greater effects on solid conversion time.

Nevertheless, these latter show a relatively low dependence on pyrolysis temperature, with changes in solid conversion times of about 8% and 7%, respectively for softwood and park waste wood, according to a temperature variation of 10%.

They only show a slightly increasing trend with pyrolysis temperature since the reduction of  $\Delta T$  between combustion and pyrolysis ones, as driving force for heat transfers.

<b>softwood pyrolysis</b>					
<b>temperature (K)</b>	640	675	711	747	782
<b>temperature variation (%)</b>	-10%	-5%	-	5%	10%
<b>intrinsic kinetic conversion time [s]</b>	3164	555	104	26	8
<b>internal heat transfer conversion time [s]</b>	36	37	39	40	42
<b>radiative heat transfer conversion time [s]</b>	21	21	21	22	22

*Table 29a: pyrolysis conversion times for softwood particles as a function of temperature increments, according to kinetics and heat transfer resistances*

<b>park waste wood pyrolysis</b>					
<b>temperature (K)</b>	607	640	674	708	741
<b>temperature variation (%)</b>	-10%	-5%	-	5%	10%
<b>intrinsic kinetic conversion time [s]</b>	18664	3215	530	128	31
<b>internal heat transfer conversion time [s]</b>	307	317	328	339	351
<b>radiative heat transfer conversion time [s]</b>	87	87	88	88	89

*Table 29b: pyrolysis conversion times for park waste wood particles as a function of temperature increments, according to kinetics and heat transfer resistances*

### 3.2.8 Validation of pyrolysis modeling results through the comparison with experimental data

Results on pyrolysis modelling were partially checked out by the comparison with some experimental data regarding wood pyrolysis tests. At this purpose, park waste wood was only taken in exam and the specific working condition by which process temperatures were decreased by 5% in respect with the ones previously calculated through the kinetic free model was considered (so that  $T_{pyr} = 640K$ ,  $T_{gasif} = 1074K$  and  $T_{comb} = 1590K$ ).

Indeed, in this case, an external heating flux to biomass particles in pyrolysis zone was calculated as the same adopted for one of the experimental investigated data sets (Galgano and Di Blasi, 2004), such as  $80 \text{ KW/m}^2$ . Moreover, the equivalent particles sizes considered in pyrolysis modelling simulation and the ones adopted in the experimental tests were almost the same (17,5 mm against 16 mm, respectively), while an higher initial moisture content was registered for the tested material (11% against 5.2% for park waste wood).

For the second set of experimental data (Sadhukan et al., 2009), pyrolysis temperature was  $410^\circ\text{C}$  (against a simulated one as  $367^\circ\text{C}$ ) and the particles size was 10 mm.

A comparison between model and experimental results is then reported in figure 18.

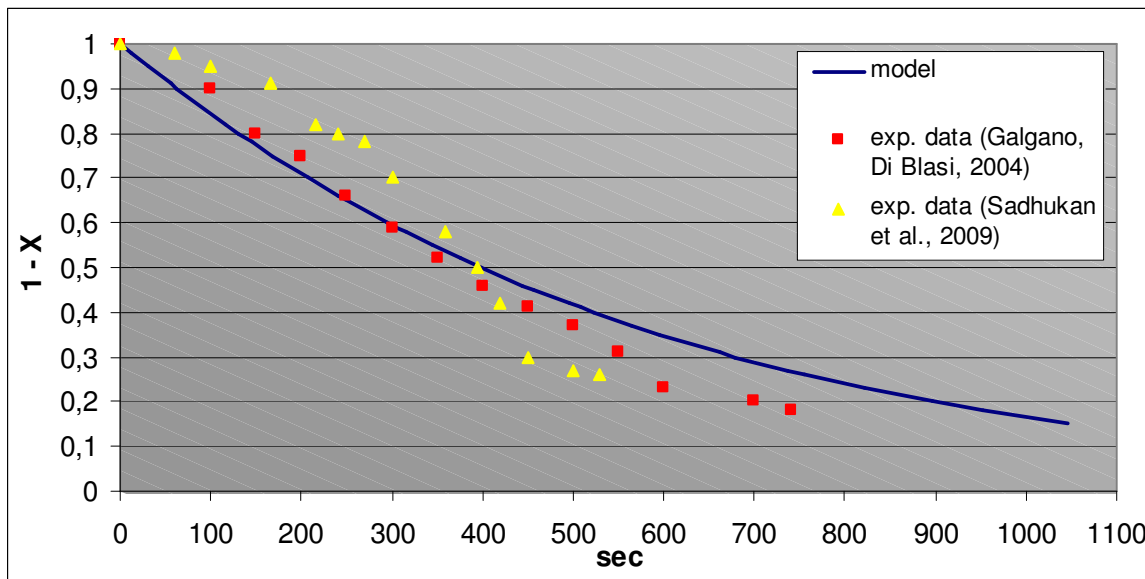


Figure 18: comparison between experimental data from wood chips pyrolysis tests and simulated results at the same working conditions

It can be seen that the simulated results well fit the experimental data in the case of the same external heating fluxes in pyrolysis zone, and almost the same particles sizes (blue line and red symbols). In the first steps, such as for low solid conversion degrees, analytical simulation shows slightly lower conversion times then the real ones, maybe because, in real cases, moisture vaporization is combined to solid devolatilization so that the time for solid mass losing is increased.

On the contrary, at high conversion degrees, simulated conversion times are longer than the ones measured during the experiments. This could be due to the splitting of partially converted particles during the last phase of pyrolysis, in spite of a perfect shrinking core behaviour until their complete devolatilization. Smaller particles would in fact accelerate their conversion in this case.

## 4 DISCUSSIONS

### 4.1 Possibilities and limitations of thermo-chemical kinetic free model

On the basis of ultimate and proximate analysis of biomass fuels, the developed gasification kinetic free model is able to predict the corresponding product gas yields, compositions and heating values, according to the feeding amount of gasifying medium (equivalence ratio).

An estimation of temperature profile inside the gasifier is also possible to be achieved, considering energy balance for the different reaction zones in which the unit is schematically subdivided.

Finally, cold gas efficiency and distribution of process heats among the different reaction zones are possible to be appraised.

Therefore, an analytical evaluation on fuels thermo-chemical conversion properties is thus possible to be obtained, mainly based on their chemical composition.

As regard this latter, the fundamental parameter to be checked out in order to achieve correct simulation results is the O/C ratio. Indeed, for relatively low values of this parameter (about less than 0.6), the kinetic free model gives gas compositions and process temperatures unacceptably different from the experimental data on the same materials and out of the ranges by which model assumptions can be still considered valid.

This model limitation was verified in the case of refuse derived fuels and it is mainly due to the assumption of Østberg's model for pyrolysis simulation (initially developed for coal devolatilisation), by which a limited number of considered gas components are considered.

Presumably, other heavier compounds with lower H/C ratio should be considered in pyrolysis step instead of CH<sub>4</sub> and C<sub>2</sub>H<sub>4</sub> only, and a different formula for solid residue should be envisaged instead of C<sub>x</sub>N<sub>x+d/a</sub>, in order to lead to an higher H<sub>2</sub> percentage in gas pyrolysis products and to low down heat of pyrolysis at the same time. Besides, thermal cracking and steam reforming of these heavier compounds should be considered in gasification zone, so as to increase the percentages of CO and H<sub>2</sub> in final syngas composition.

The other main simplifying assumptions of the proposed kinetic free model are the fixed temperature at which solids devolatilization begins (573K), the development of combustion process by the partial oxidation of carbon monoxide and hydrogen only, the total conversion of solid char and the equilibrium of *water gas shift* reaction in the gasification zone, and a total energy loss fixed to 10% of total combustion heat.

On the basis of these hypotheses, the proposed analytical tool seems to well fit the experimental results and other literature data for all the other considered biomass fuels.

Particularly for woody biomass, model results were compared with experimental data (at the same working conditions) and a good conformity could be observed. Some differences are only due to the assumption of total char gasification which is on the contrary not achieved in those particular gasification tests.

The same assumption leads to high cold gas efficiencies for all the biomass species, especially at low equivalence ratios. In this case, the incomplete char gasification should be envisaged for more verisimilar results.

Moreover, in some cases (as sewage sludge, for example), cold gas efficiency is still increased by the presence in final syngas composition of some compounds like ethylene and ammonia. Nevertheless, in real applications, ethylene would be presumably reformed during gasification step to other compounds with lower heating value (as CO, H<sub>2</sub>) and

ammonia is usually removed from syngas stream, since it is detrimental for power generation devices (usually adopted next to the solid conversion unit) and it is responsible of NO<sub>x</sub> emissions from syngas combustion. Therefore, the estimated cold gas efficiencies should be considered still lower in the optics of biomass cogeneration systems assessment.

## 4.2 Controlling mechanisms for solid conversion steps

Since char from pyrolysis was assumed to be solid carbon for all the examined biomass species, differences in gasification zone could only be due to the operating temperatures and particles sizes.

As expected, time for complete char gasification decreases as process temperature rises. Among the considered solid fuels, wheat straw thus shows the highest char conversion time (see tables 18, 20 and fig. 11) since its temperature in gasification zone proved the lowest. A very deep difference is detected from the other materials, especially if the results from uniform reacting particle model are observed.

In fact, as also come out from the analysis of wood char gasification time as a function of temperature, uniform particle reacting model shows noticeable higher gasification times than shrinking core model ones at temperatures about less 1100K. Since eq.(21), which uniform particle reacting model is based on, is an empirically expression, it could be possible it has a limited range of applicability. For this reason, for dimensioning wheat straw gasification zone, the corresponding time resulting from shrinking core model was adopted, instead of the longest one.

In any case, process temperature is far the most important parameter affecting char gasification development, at least for the initial biomass particle dimensions chosen in this analysis. Indeed intrinsic kinetics resistances came out as process limiting factors for all the materials.

A noticeable variability of gasification times with temperature was also detected, so that a good estimation of temperature profile inside the gasifier is necessary for a correct dimensioning.

Reacting gases diffusion resistances resulted negligible and not comparable with kinetic ones, since the small biomass particles sizes considered in this work, as said. From the analysis carried out according to shrinking core model, and as expected by the same definition of gas diffusion mechanism (especially through the inner layers of char particle), mass diffusion resistances increase with particle size, as it can hence be seen from the results regarding the different biomass materials (see tables 21 and 22).

Char dimensions by which gas diffusion mechanisms have similar weights in gasification process development as intrinsic kinetics were found out as about 6.4mm and 7.4mm, respectively for park waste wood and softwood at their corresponding calculated gasification temperatures.

These dimensions are much greater than the ones calculated for the initial wood particles sizes, according to the shrinkage model by Davidsson and Pettersson, 2002, which, nevertheless, should be validated by experimental tests carried out at the same working conditions and with the same biomass materials.

Moreover, these results are affected by char void fraction parameter  $\epsilon_c$ , which is difficult to predict for practical applications and therefore it was assumed as biomass particles void fraction in this case, that is however characterized by great variability, as well.

As regard pyrolysis, process temperature and biomass particles size play different roles in solids devolatilization advancement according to the considered biomass fuel. In fact, for sewage sludge, because of its very small particles dimension (1 mm), physical resistances by heat transfer mechanisms were almost negligible in respect with kinetic ones, while, on the contrary, wheat straw kinetics is so fast (at corresponding estimated temperature) as it can be neglected for the estimation of pyrolysis time. For woody biomasses, finally, kinetic and physical resistances have comparable weights in pyrolysis development, as it is also confirmed by *Biot* and *Thiele* numbers evaluation.

*Biot* numbers came out included in the range 0.1 – 10 for all the materials, as well, so that it could be deducted that internal conductive heat transfer resistance and external radiative one have to be considered combined together in all of the cases, such as at almost each particles size and working temperature.

From the analysis of pyrolysis dependence on temperature for the woody biomasses only, it can be said that, within the considered temperature ranges ( $\pm 10\%$  from the values obtained by kinetic free model), pyrolysis kinetics is remarkably affected by temperature while conductive heat transfer resistances only show short increments, and radiative heat transfer ones can even be considered constant with temperature.

Nevertheless, since physical heat transfer mechanisms are mainly regulated by the temperature difference between combustion and pyrolysis zone, which is in this case one order of magnitude higher than the considered temperature intervals, the previous result will be presumably changed if these temperature ranges of investigation are enlarged.

It is also important to point out that process temperature and particles size are not only the main parameters to be considered for pyrolysis zone dimensioning. Nature of biomass, with its proper kinetics expression and heat of pyrolysis also have great effect on pyrolysis time estimation.

On the basis of these previous considerations, and as an overall conclusion about the two main thermo-chemical processes occurring within a biomass gasifier fed with small/fine particle materials, it could be stated that char gasification is in most of the cases affected by kinetic factors and therefore it is regulated by operating temperature above all, while, for pyrolysis, the different factors taken in exam, such as temperature, particles size and nature of biomass fuel, can have different weights in process advancement according to the particular application.

As regards solids drying, moisture diffusion through the solid particles proved almost immediate, so that corresponding drying time was considered negligible for each kind of material. Heat transfer resistances were instead found out to be more effective, giving vaporization times of the same order of magnitude than pyrolysis ones (always by heat transfer resistances, of course) *Biot* number was calculated lower than one for each material, so that radiative heat transfer seems to be slower than conductive one, in this case. However, drying process can be anyway neglected in sewage sludge gasification unit dimensioning, according to the proposed analysis.

For biomass heating, radiative flux from hot walls of reactor resulted as the main thermal energy source, while convective heat exchange and thermal radiation from hot gases were about one order of magnitude less. This led to an only short decrease of exit gas temperature in respect with gasification one, which is not always achieved in practical applications, yet.

## **PART II**

### **GAS CLEANING LINES FOR BIOMASS COGENERATION SYSTEMS**

## 5 METHODOLOGY

### 5.1 Gas cleaning lines sizes, gas contaminants and tolerance standard limits

As said in par.1.3, gas cleaning systems for gasified biomass were investigated in this second part of the work, in order to use the product gas as suitable fuel for high efficiency CHP units (i.e. internal engines and micro-turbines).

Of course, the same air downdraft gasification technology was supposed to be adopted in practical applications but the outgoing gas composition was in this case obtained from literature data on wood gasification tests (see table 30) and different cogeneration units sizes were considered in this analysis.

CO (vol%)	CO <sub>2</sub> (vol%)	CH <sub>4</sub> (vol%)	H <sub>2</sub> (vol%)	N <sub>2</sub> (vol%)	H <sub>2</sub> O (vol%)	LHV (kJ/kg)	LHV (kJ/Nm <sup>3</sup> )	Biomass consumption (kg/Nm <sup>3</sup> <sub>gas</sub> )*
16	10	3	15	41	15	5000	5500	0,60

\*data from gasification tests at HPT laboratory

*Table 30: main components and low heating value of gas stream adopted in cleaning systems analysis (Svensk Maskinprovning. Gengasdrift av en överladdad dieselmotor, 1988)*

These latter were considered in terms of three different syngas streams flowing through the envisaged cleaning lines (thereinafter called *design values* in this work). They were obtained by considering the fuel gas heating value as reported in table 30 and net power efficiencies of generators as 20% for the medium size and 30% for the largest one (as respectively pertaining to micro-turbines and natural gas engines, EPA, 2008) The smallest size was instead chosen as the same of the laboratory scale downdraft gasifier existing at HPT laboratory of Energy Technology Department in KTH University (see fig.3), for which gas cleaning system was tried to be designed, as well.

Moreover, for all the considered cleaning line sizes, a variability range of gas flows design values was fixed, in order to check the gas cleaning units behaviour out according to the fluctuations of gas production or to the refitting from gasification equipment. Considered gas flows are then shown in table 31. In the same table the estimated power outputs are also reported for the three corresponding cogenerators sizes.

Design value (Nm <sup>3</sup> /h)	Variability range (Nm <sup>3</sup> /h)	Design value (kW <sub>e output</sub> )	Variability range (kW <sub>e output</sub> )
8	3 – 15	3	1,15 – 6
125	75 – 250	40	23 – 75
350	250 – 500	160	115 – 750

\*considering net power efficiency as 25%

*Table 31: Considered sizes for gas cleaning lines, in terms of syngas flows and corresponding power outputs of cogeneration units*

Since biomass elementary composition usually shows several inorganic components (ashes), and as the thermo-chemical solid conversion steps are often not completely developed inside the gasifier, many other different substances are also present in the gas stream, besides the main components reported in table 30.

As already said, the presence of these substances is one of the main technical barriers for the overspread of energy cogeneration systems from biomass, since they need to be removed from the gas stream in order to run cogeneration units.

Indeed, these equipments require a very high pureness degree of gaseous fuel, in order to especially avoid problems regarding erosion and corrosion of the moving parts, as well as to reach standard operating parameters of efficiency and reliability.

Besides, these same substances are also cause of toxic and harmful emissions in the atmosphere, mainly produced during gas combustion steps for power generation.

The main secondary products which were considered as gas contaminants and therefore corresponding removal techniques were investigated are listed below:

- Particulate: solid residues of micron and sub-micron size due to biomass inorganic components (ash), incomplete gasification process (char) and/or secondary polymerization of hydrocarbons (coke and soot). They are main responsible for erosion of moving part of cogeneration units and harmful emissions into the atmosphere.
- Tars: heavy aromatic and/or unsaturated hydrocarbons (molecular weight higher than benzene, as definition) with boiling point relatively high. They are mainly produced during pyrolysis step or by incomplete reactions of gasification. They tend to condense at temperatures lower than 700 K, causing filters clogging/blinding and plugging of valves and pipes when condensing simultaneously with particles deposition.
- Sulphur (as H<sub>2</sub>S): produced by reduction of solid-bound sulphur. It provokes materials corrosion and harmful emissions.
- Alkali metals: inorganic compounds, especially sulphates and chlorates of K and Na. They are main cause of materials corrosion.
- Nitrogen (as NH<sub>3</sub>): produced by reduction of solid-bound nitrogen. It provokes NO<sub>x</sub> formation during gas combustion processes.
- Halides (as HCl): acid components of gas stream, causing materials corrosion.

Their concentrations in the gas downstream are obviously related to the type of biomass is going to be used for energy purposes and they also depend on gasification technology. In this work, biomass nature is not specified but large ranges of contaminants concentrations are examined in order to cover different kinds of materials potentially used. These values are listed in the following table 32:

particulate	5 – 10	g/Nm <sup>3</sup>
tars	10 – 50	g/Nm <sup>3</sup>
Sulphur (H <sub>2</sub> S)	100 – 1000	ppmv
Nitrogen (NH <sub>3</sub> )	2000 – 6000	ppmv
Chlorine (HCl)	30 – 150	ppmv
Alkali metals	600 – 4000	mg/kg <sub>biom</sub>

*Table 32: Ranges of gas contaminants concentrations at the gasifier outlet*

Finally, the standard tolerance limits for the same compounds are shown in the table 33, as the lowest permitted ones for micro-turbines or gas engines appliances.

particulate	0,03 (0 for $d_p > 3\text{mm}$ )	$\text{g/Nm}^3$
tars	3	$\text{g/Nm}^3$
Sulphur ( $\text{H}_2\text{S}$ )	20	ppmv
Nitrogen ( $\text{NH}_3$ )	100	$\text{mg/Nm}^3$
Chlorine ( $\text{HCl}$ )	0,6	ppmv
Alkali metals	0,1	ppmv

*Table 33: Standard tolerance limits for gas contaminants (Bauen, 2004; Hasler 1999)*

## 5.2 Gas cleaning units

Gas cleaning units examined in this work are shown in the figure 19, according to the contaminant species they are suitable to treat and their usual best working temperatures.

Their dimensioning was carried out according to the three gas flow design values previously defined, and their efficiency and operating conditions (pressure drop, convective heat loss and working temperature, above all) were investigated within the corresponding flow ranges cited before (see table 31).

Units regeneration frequency was calculated on the basis of maximum pressure drops and/or materials consumption during online operations. These latter were estimated according to the same gas flows values and the initial contaminants amounts or concentrations listed in table 32.

A short description of all of the units and their corresponding analytical procedures adopted for design are presented in the following paragraphs

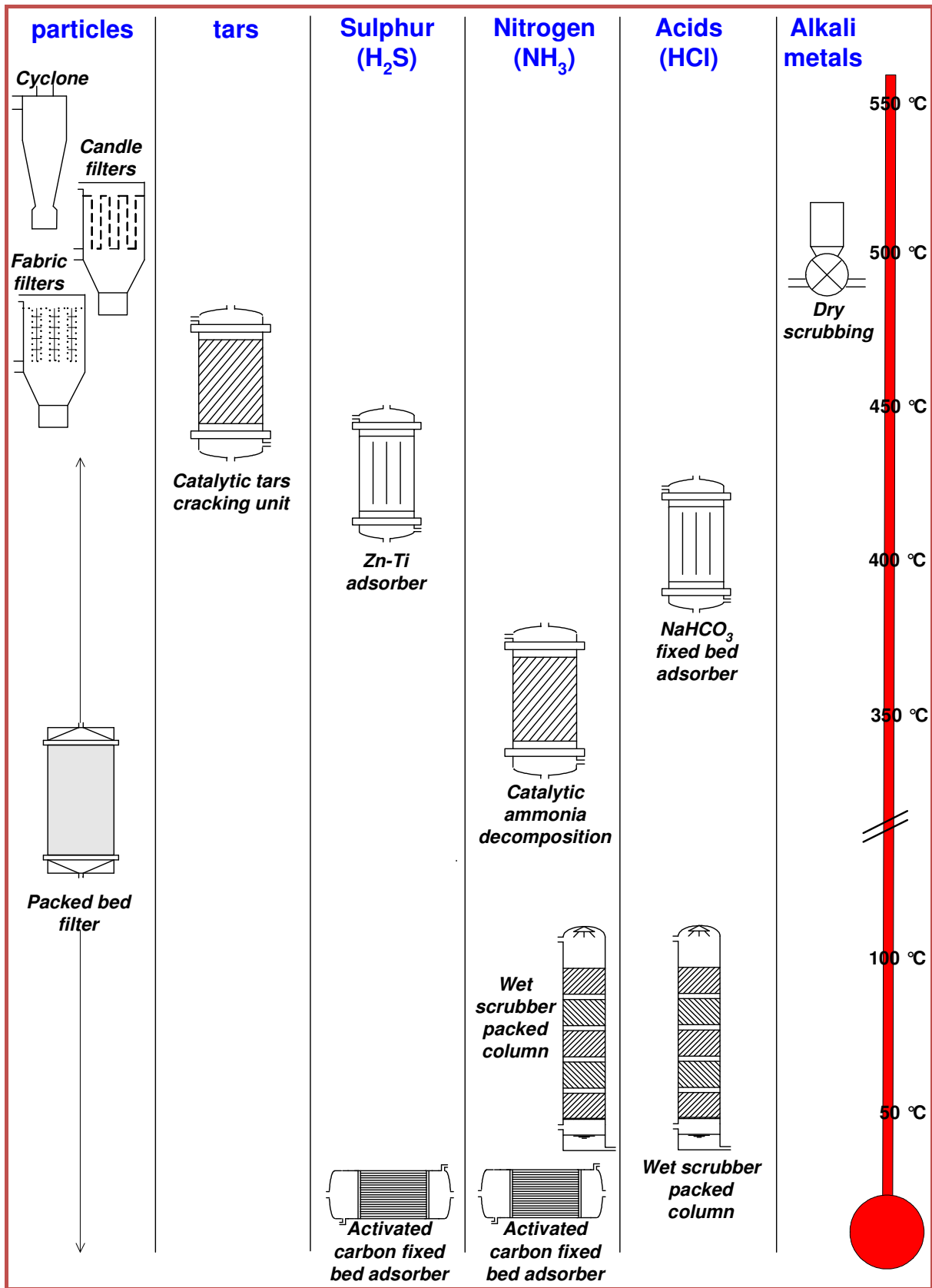


Figure 19: Examined gas cleaning units

## 5.2.1 Cyclone

Cyclone is commonly the first unit included in the gas cleaning line, downstream the gasifier. Its role is to collect and remove any large solids are still conveyed by the gas stream, in order to avoid they could damage or have negative effects on the right functioning of the following gas cleaning devices, as well as to minimize pressure drops.

Nevertheless, its intrinsic particles collection efficiency is not enough to reach the desired low concentrations, especially in the case of sub micron particles (see fig. 21a, 21b and 21c), so that other units are usually inserted downstream at this purpose.

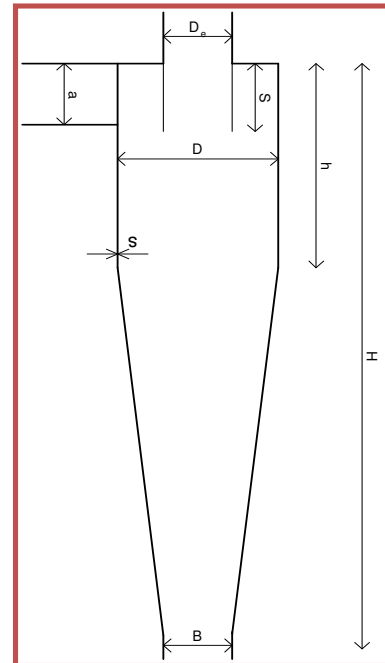
Since it is almost maintenance less, cheap and easy to built, cyclone is always present in any biomass gasification equipment.

Its dimensioning was carried out according to the empirical procedure by Arena et al., 1991. According to this approach, particles are removed from the gas stream by the centrifugal force they are subjected to, that pushes them towards the inner walls of cyclone. This force is due to the vortical motion of the gas stream that is developed inside the cyclone by the tangential injection of the gas.

The main design parameter is thus the inlet tangential gas velocity, whose value is normally set to 25 m/s. From this input data, inlet cross section can be calculated according to the gas flow, and, subsequently, all other dimensions of the cyclone can be obtained on the basis of fixed ratios between them and the same inlet section previously calculated. Results for the different unit sizes are shown below:

	3 – 15 Nm <sup>3</sup> /h (8 Nm <sup>3</sup> /h)	75 – 250 Nm <sup>3</sup> /h (125 Nm <sup>3</sup> /h)	250 – 500 Nm <sup>3</sup> /h (350 Nm <sup>3</sup> /h)
<b>A (mm)</b>	17	68	114
<b>B (mm)</b>	16	62	104
<b>D (mm)</b>	39	155	259
<b>D<sub>e</sub> (mm)</b>	16	62	104
<b>h (mm)</b>	55	217	363
<b>H (mm)</b>	153	604	1011
<b>S (mm)</b>	20	77	130
<b>s (mm)</b>	3	3	3

Table 34: Cyclone dimensions for different syngas flows



Two main verifications are then operated in order to check cyclone behaviour out. They are regarding pressure drops and the so called “*saltation velocity*” [Arena, 1991].

Pressure drops are calculated by the following equations:

$$\Delta p = 0.0030 \rho_g v_i^2 N_H \quad (1)$$

$$N_H = 11,3 \left( \frac{\pi a^2}{4 * D e^2} \right)^2 + 3,3 \quad (2)$$

The following results are then obtained:

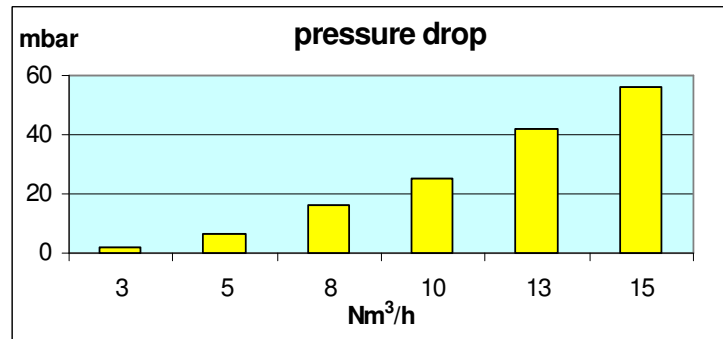


Figure 20a: cyclone pressure drops for unit of 3 – 15 Nm³/h gas flow size

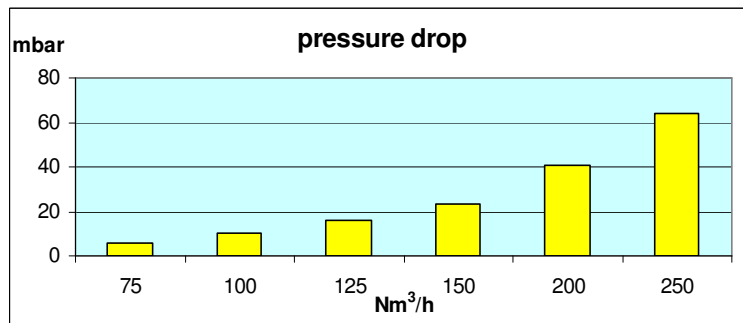


Figure 20b: cyclone pressure drops for unit of 75 – 250 Nm³/h gas flow size

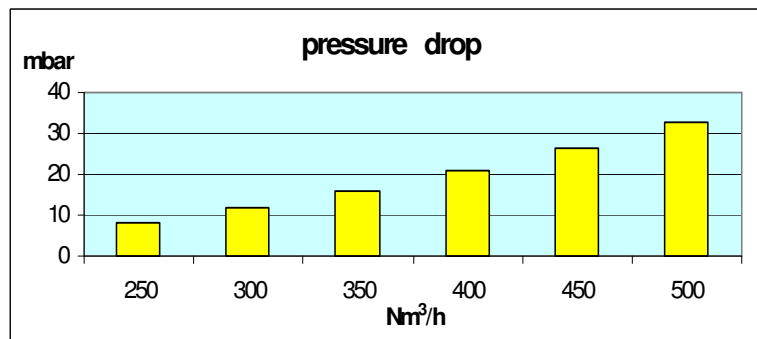


Figure 20c: cyclone pressure drops for unit of 250 – 500 Nm³/h gas flow size

The *Saltation velocity* (or critical velocity) is the maximum gas velocity at the inlet of the cyclone by which particles can be still removed from the stream. For higher values, indeed, turbulence inside the cyclone is too high to permit particles segregation.

Its value is calculated by the following relation:

$$v_c = 1.25 \left[ 2.055 \left( \frac{4g\mu(\rho_s - \rho_g)}{3\rho_g^2} \right)^{1/3} \frac{(b/D)^{0.4}}{(1-b/D)^{1/3}} D^{0.067} v_i^{2/3} \right] \quad (3)$$

As the ingoing gas velocity is present in the right side of this formula, the condition  $v_c > v_i$  is verified by an iterative procedure.

Finally, efficiency of cyclone is calculated as follows:

$$\eta = \frac{1}{1 + \left(\frac{d_{pc}}{d_p}\right)^2} \quad (4)$$

Where  $d_{pc}$ , *cut diameter*, is defined as the particle size for which cyclone efficiency is equal to 0,5. It is calculated by:

$$d_{pc} = \sqrt{\frac{9\mu b}{2\pi N_e v_i (\rho_s - \rho_g)}} \quad (5)$$

$$N_e = \frac{h + (H - h)/2}{a} \quad (6)$$

Cyclone efficiencies for different gas flows and according to particles size are shown below:

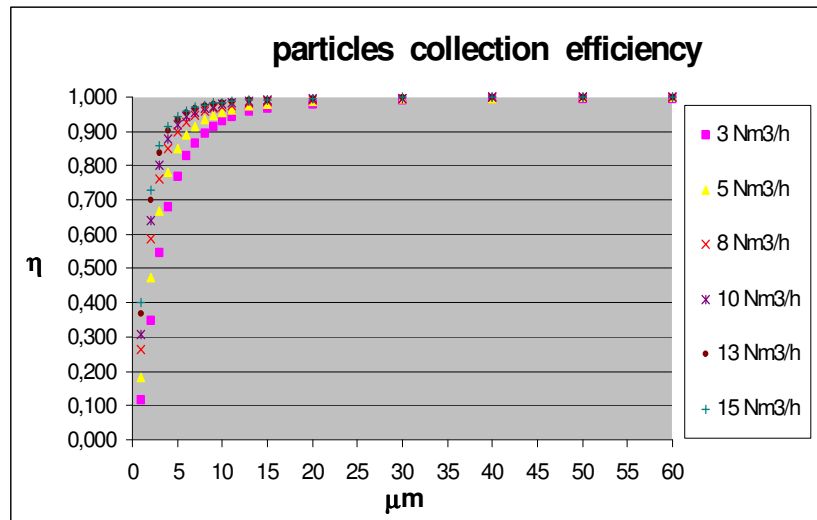


Figure 21a: particles collection efficiency of cyclone at 3 – 15 Nm<sup>3</sup>/h gas flow conditions

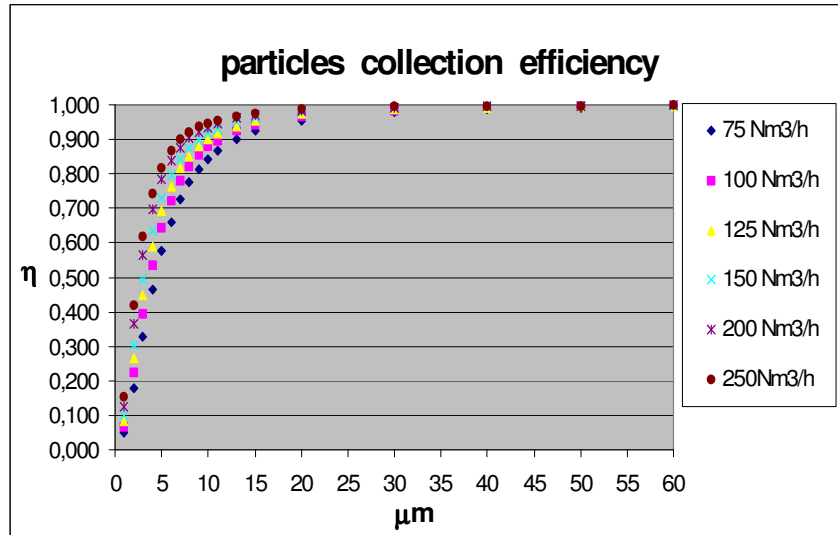


Figure 21b: particles collection efficiency of cyclone at 75 – 250 Nm<sup>3</sup>/h gas flow conditions

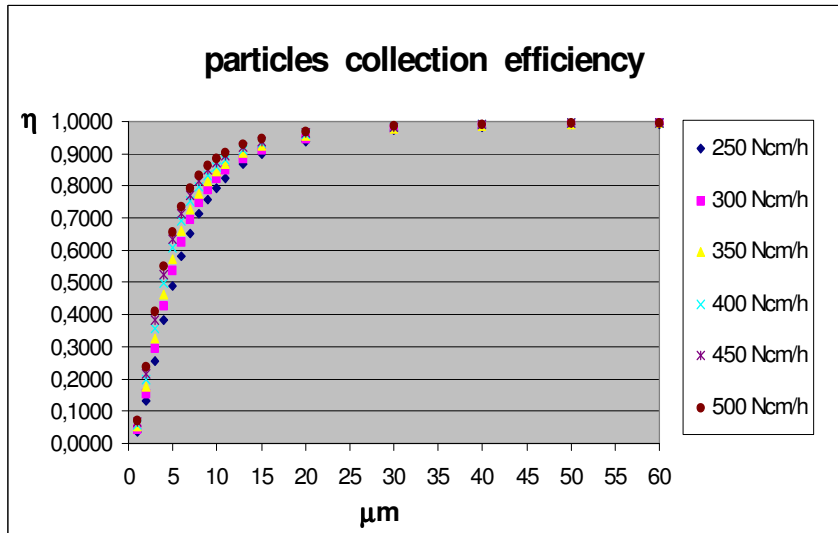


Figure 21c: particles collection efficiency of cyclone at 250 – 500 Nm<sup>3</sup>/h gas flow conditions

It can be seen that both pressure drops and particles collection efficiencies increase with gas flow rate. Therefore, a compromise solution is usually adopted in cyclone design between these two parameters (by fixing a right value of gas tangential velocity at the inlet of the cyclone).

For particles sizes larger than 20 $\mu\text{m}$  the efficiency is almost the same for all the gas flow rates, in each designed cyclone unit. This size can be therefore considered as an inherent lower limit for these units for which they still show an acceptably high collection efficiency (more than 95%, at least) in a wide range of working conditions.

As the vortical fluid dynamics that is established inside the cyclone, pressure drops show relatively high increments in the considered gas flow ranges. Therefore they sound like the parameter to better check out in respect with the collection efficiency.

### 5.2.2 Packed bed filters

Packed bed filters are usually cylindrical vessels filled up with granular material (usually sand) of relatively small size (50 – 500 μm). Gas is conveyed through the channels of this bed where several particles retention mechanisms occur [Lee, 2001]. Neglecting the electrostatic forces between particles and bed material, the other main phenomena involved in particles collection process are:

- Brownian diffusion
- Interception
- Inertial impaction
- Gravitational settling

Each of these mechanisms shows its own trapping efficiency according to the particles size (see Appendix A), so that the overall efficiency for a single collection layer of the filter can be assumed to be [Lee, 2001]:

$$E_i = 1 - (1 - E_i^{gravity})(1 - E_i^{inertial})(1 - E_i^{interception})(1 - E_i^{diffusion}) \quad (7)$$

where  $i$  = particle size

The retention efficiency for the whole filter, ( $\eta_i$ ), whose height is  $H$ , is then given by:

$$\eta_i = 1 - \exp\left[\frac{-4 \cdot E_i \cdot \alpha \cdot H}{\pi \cdot d_g \cdot (1 - \alpha)}\right] \quad (8)$$

The corresponding overall trend for particles collection efficiency as a function of particles size shows an usual drop in the range 0,1 – 1 micron, as it is shown in fig. 22 and as it was also estimated for the different syngas flows and particulate concentrations considered in this work (figure 23a, 23b, 23c).

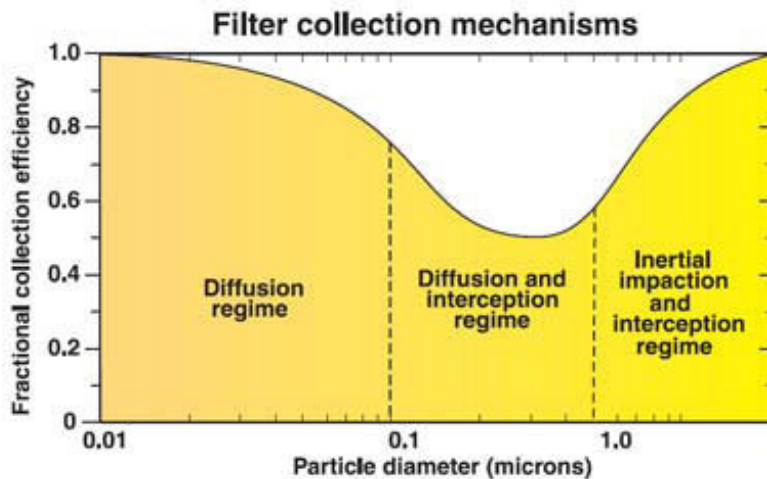


Figure 22: overall trend of packed bed filter efficiency as a function of particles size (Wakao and Funazkri, 1978)

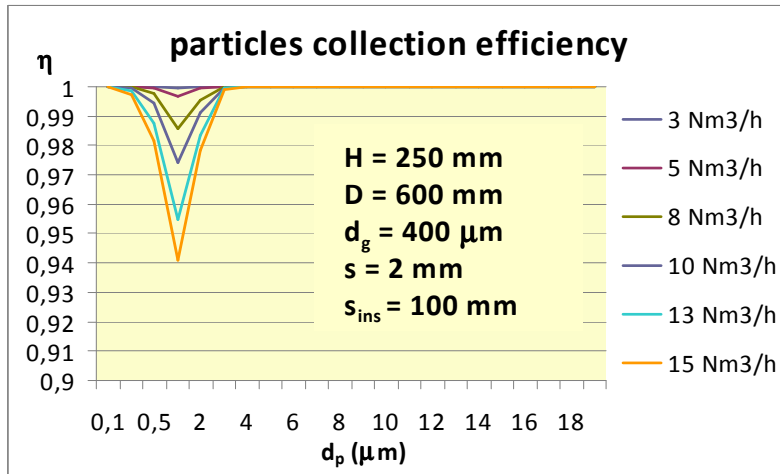


Figure 23a: efficiency and dimensions of packed bed filter for 3 –15 Nm<sup>3</sup>/h gas flow unit

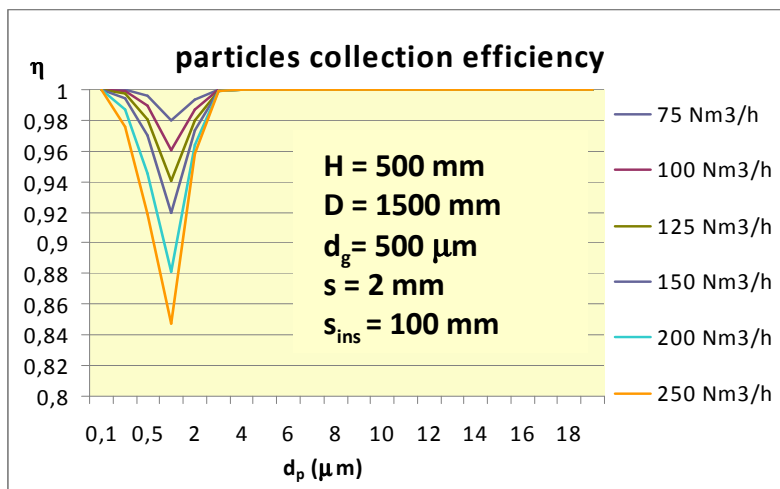


Figure 23b: efficiency and dimensions of packed bed filter for 75 –250 Nm<sup>3</sup>/h gas flow unit

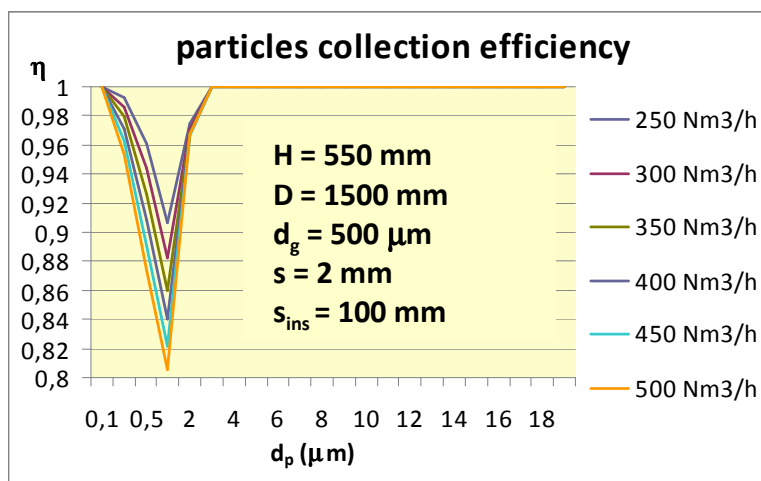


Figure 23c: efficiency and dimensions of packed bed filter for 250 – 500 Nm<sup>3</sup>/h gas flow unit

Dimensioning of packed bed filters was carried out by fixing an initial total efficiency of 99,99% for 3  $\mu\text{m}$  size particles. During filtration, this efficiency increases thanks to the positive effect by the retained particles which act as a barrier for the following gas stream. This effect was not considered in this analysis but for pressure drop estimation. The initial one was indeed calculated according to the following *Ergun's* formula [Kunii et al., 1969]:

$$\Delta p_o = 150 \frac{(1-\varepsilon)^2}{\varepsilon^3} \cdot \frac{\mu \cdot u}{(\phi \cdot d_g)^2} + 1,75 \frac{1-\varepsilon}{\varepsilon^3} \cdot \frac{\rho \cdot u^2}{\phi \cdot d_g} \quad (9)$$

Its rise was then estimated by the following empirical correlation [Yongwon et al., 1991]:

$$\frac{dp/dz}{dp_o/dz} = 1 + \beta_1 \cdot \sigma^{\beta_2} \quad (10)$$

$$\left[ \frac{dp/dz}{dp_o/dz} - 1 \right]_{\sigma=10^{-3}} = 0,3484 St^{-1,199} \cdot N_R^{0,8568} \quad (11)$$

$$N_R = \frac{d_p}{d_g} \quad (12)$$

$$St = \frac{Cu \cdot \rho_p \cdot d_p^2 \cdot u}{18\mu d_g} \quad (13)$$

where  $\sigma$  is the ratio between the volume already filled by retained particles and the total volume of the bed. At the filter saturation condition, this value was set as  $10^{-3}$  [Yongwon et al., 1991], and, according to the analytical procedure reported above, maximum pressure drops and allowable filters operational times were calculated, by considering an initial particulate concentration of  $10 \text{ g/Nm}^3$  (see fig. 24a, 24b and 24c).

It can be noted very high pressure drops (in respect with the other filter units described below) and very short operating times, especially for the larger size of filters. This clearly suggests the necessity to envisage an on line filter regeneration process, maybe achieved by the temporary fluidization of the filters beds. In some cases, especially for the higher flow rates, the utilization of packed bed filters for the proposed applications seems to be absolutely prevented.

Nevertheless, the analytical approach described above seems to be too much conservative against the real applications. Indeed, Seville J.P.K., 1997, gives a saturation times for sand filters in the same gas flow regimes and with the same bed material sizes as less than one hour, against the calculated times as tens or even a few minutes.

Finally, the use of some lighter bed materials (like organic ones, such as bio-filters) could be envisaged to reduce pressure drops. In this case, yet, gas stream should be cooled upstream the filters or they should be arranged at the end of the gas cleaning line.

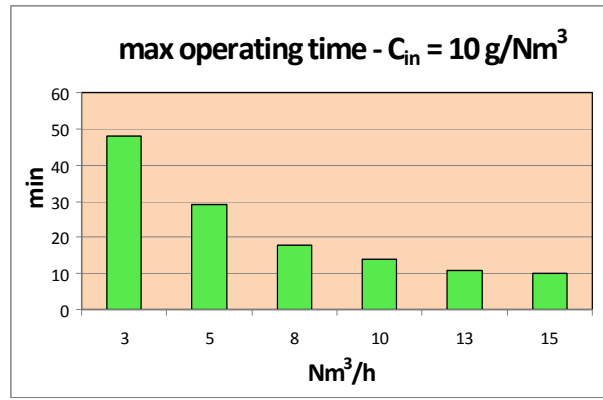
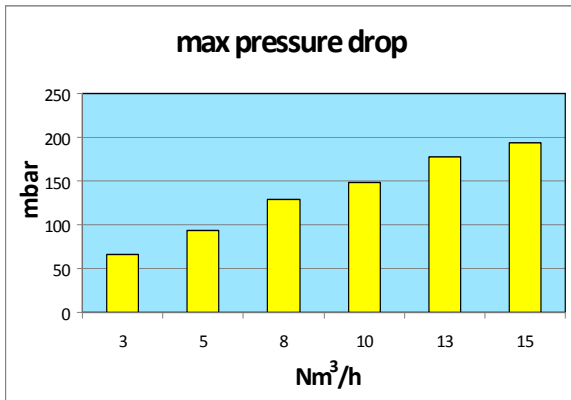


Figure 24a: pressure drops and saturation times for 3 – 15 Nm<sup>3</sup>/h gas flow filter unit

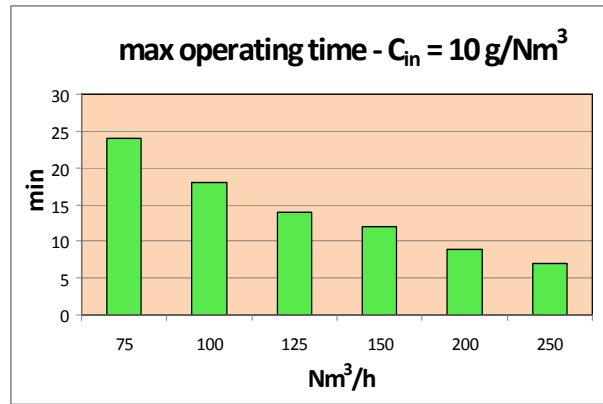
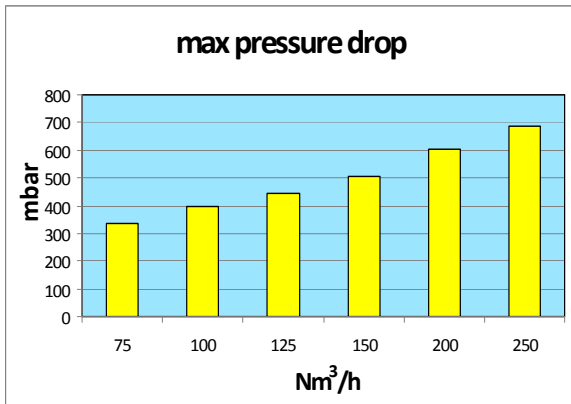


Figure 24b: pressure drops and saturation times for 75 – 250 Nm<sup>3</sup>/h gas flow filter unit

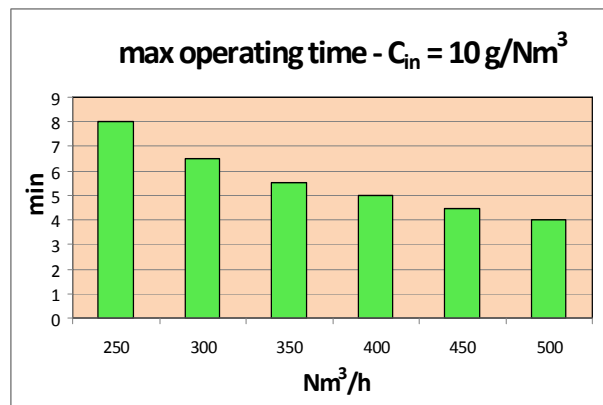
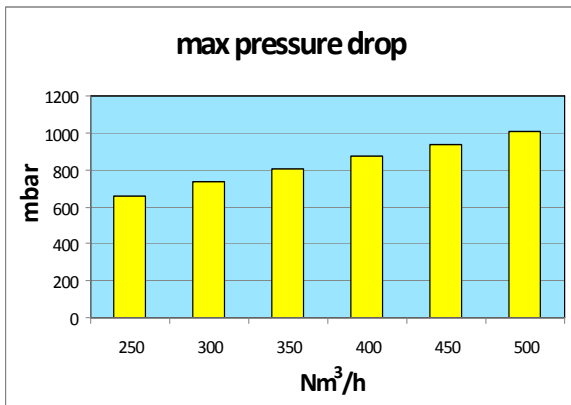


Figure 24c: pressure drops and saturation times for 250 – 500 Nm<sup>3</sup>/h gas flow filter unit

### 5.2.3 Candle Filters

On the contrary of packed bed filters, candle filters are surface filtration units. They consist on several blind cylindrical rigid elements (candles) made of porous materials (usually ceramic or sintered metal), through which raw gas usually flows from the outside to their inner layers, so that mostly of the particles are deposited on their external surface.

Because of this particles deposition, a layer of collected material, commonly called *cake*, sticks and grows up during filtration around the filter. This cake acts as a filter element itself, by deeply improving the retention capacity of the unit. On the other hand, it is also responsible for the increase in pressure drops during operating time.

The design parameter for candle filters is the so called *face velocity*, such as the ratio between the total gas flow and the total area available for filtration (2 – 6 cm/s, [Seville, 1997]), which corresponds to the total (external) surface of candles. From this data the number of required candles is obtained, since their dimensions are usually standardized by manufacturers.

As already mentioned, because of the increase of cake thickness around the candles surface, pressure drops are also increasing in time. When a maximum allowable value is reached, candles are on line cleaned by injecting a gas jet pulse in the opposite direction of syngas flow, so as cake is detached from the elements and collected in a bottom vessel.

The frequency of the filter cleaning steps (usually carried out by injecting nitrogen or even recycled clean gas) is set according to the maximum acceptable pressure drop and the same consumption of cleaning gas.

Pressure drops are calculated as the sum of two different terms. The first one corresponds to the pressure drop for filter elements themselves, and it usually increases with the number of regeneration cycles ( $N$ ). Indeed, since some particles penetrate into the porous structure of candles during filtration phase, they are not removed anymore from their positions, even during regeneration of filter.

Therefore, pressure drops for clean filters is given by [Seville,1997]:

$$\Delta p_{o \text{ candle}} = \frac{\mu \cdot u \cdot s}{K} \quad (14)$$

and its value after a certain number of regeneration cycles ( $N$ ) is:

$$\Delta p'_{\text{candle}} = \frac{\mu \cdot u \cdot s}{K} \cdot N^r \quad (15)$$

where  $r$  is an empirical coefficient usually given by manufacturers (in this case,  $r = 0,06$  [Pall Corporation Inc.]

The second term for pressure drops is regarding cake resistance to gas flow and it is time depending:

$$\Delta p_{\text{cake}} = k' \cdot x \cdot m \cdot u^2 \cdot \tau \quad (16)$$

$$k' = \frac{\mu}{\rho_{\text{cake}} \cdot K_{\text{cake}}} \quad (17)$$

In this application, candle filters were designed according to the design values of gas flows (unit sizes) by choosing the less number of candle elements corresponding to a face velocity still lower than 2 cm/s,.

Pressure drops were then calculated within the total ranges of gas flow variability, in correspondence to an operating filtration time of 30 min, and particles mass loading as 10 g/Nm<sup>3</sup>.

Candle filter units DIA SCHUMALITH 05-20 DS by *Pall Corporation Inc.* were considered.

Indeed, because of the special materials which candles are made of and the proper technologies are used, their particles collection efficiencies and their specific permeability are usually not easy to be estimated but they are furnished as filters properties, together with the overall dimensions of candles, by the same manufacturers.

Dimensioning results and pressure drops estimations for the different units sizes are shown in the following charts 25a, 25b and 25c:

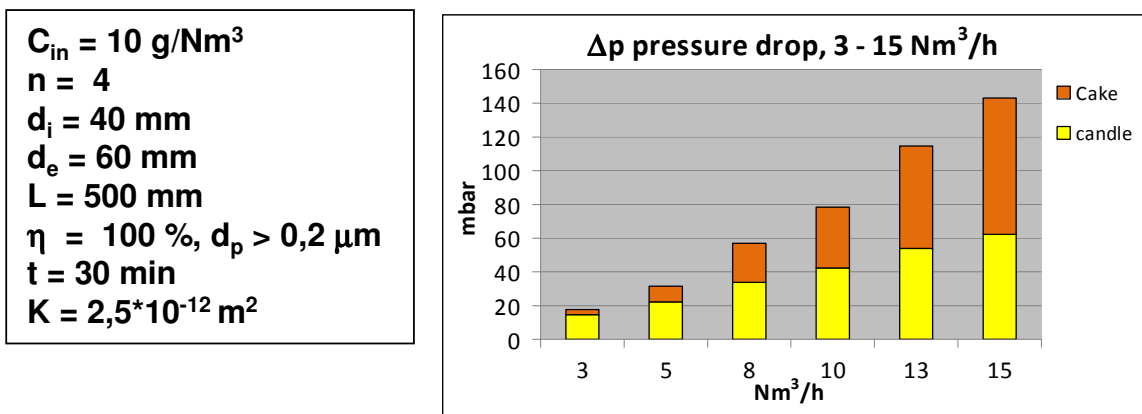


Figure 25a: design parameters and pressure drops for 3 –15 Nm<sup>3</sup>/h gas flow candle filter unit

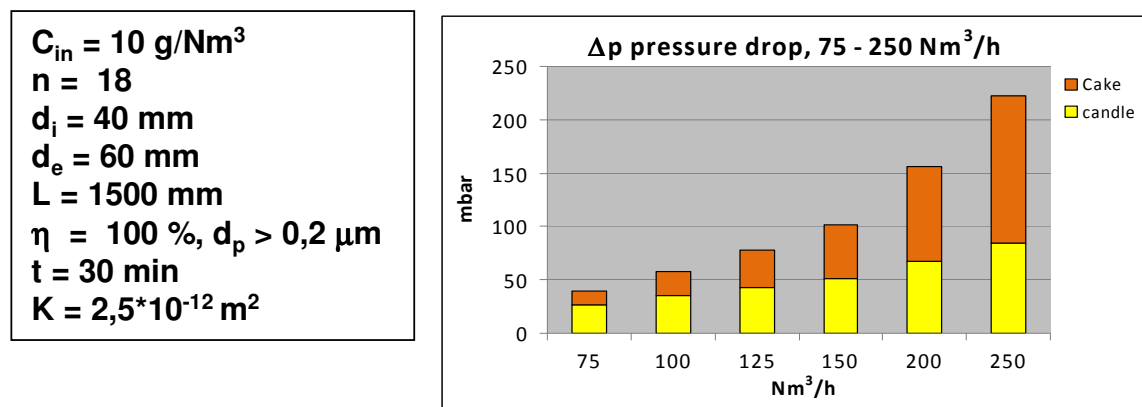


Figure 25b: design parameters and pressure drops for 75 – 250 Nm<sup>3</sup>/h gas flow candle filter unit

$C_{in} = 10 \text{ g/Nm}^3$   
 $n = 48$   
 $d_i = 40 \text{ mm}$   
 $d_e = 60 \text{ mm}$   
 $L = 1500 \text{ mm}$   
 $\eta = 100 \%$ ,  $d_p > 0,2 \mu\text{m}$   
 $t = 30 \text{ min}$   
 $K = 2,5 \cdot 10^{-12} \text{ m}^2$

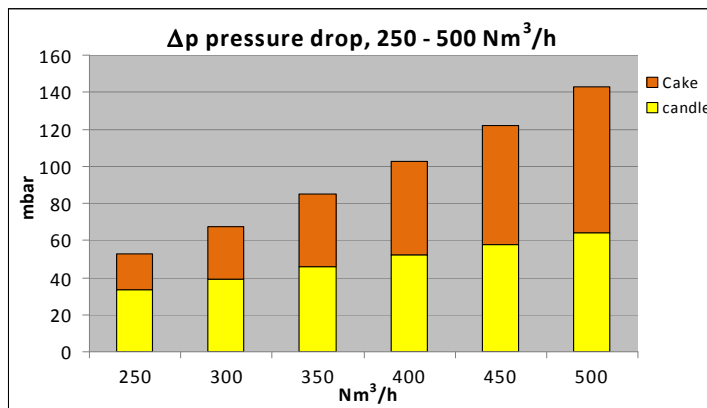


Figure 25c: design parameters and pressure drops for 250 – 500 Nm<sup>3</sup>/h gas flow candle filter unit

It can be seen that, even for a very low face velocity (< 2 cm/s), pressure drops of filter elements are of the same magnitude as cake ones reached in 30 min. Their effects on total pressure drops development are hence comparable each other.

Finally, jet pulse velocities and cleaning gas flows were calculated according to the tensional stress required to detach the cake from filters. This allowed to know cleaning gas consumption during the life time of the overall syngas cleaning line (see Appendix B).

Besides their very high particles collection efficiencies, other main advantages of candle filters utilization are the high working temperatures they can reach (600-800 °C for metal filters, up to 1200°C for ceramic ones) and their on line regeneration methods.

Main disadvantages are the little resistance to thermal shocks for ceramic filters and the corrosion for metal ones, especially in reducing gas atmosphere. They can also be irreversibly clogged by tars when the working temperatures decrease below the boiling point of these compounds.

## 5.2.4 Fabric filters

Fabric filters are also surface filtration units for fine particles collection. They differ from candle filters for the filtration elements only. Indeed, these latter are not rigid elements but they are made of special woven fibres supported by rigid metallic frames. A scheme of usual fabric filter unit is shown in fig. 26.

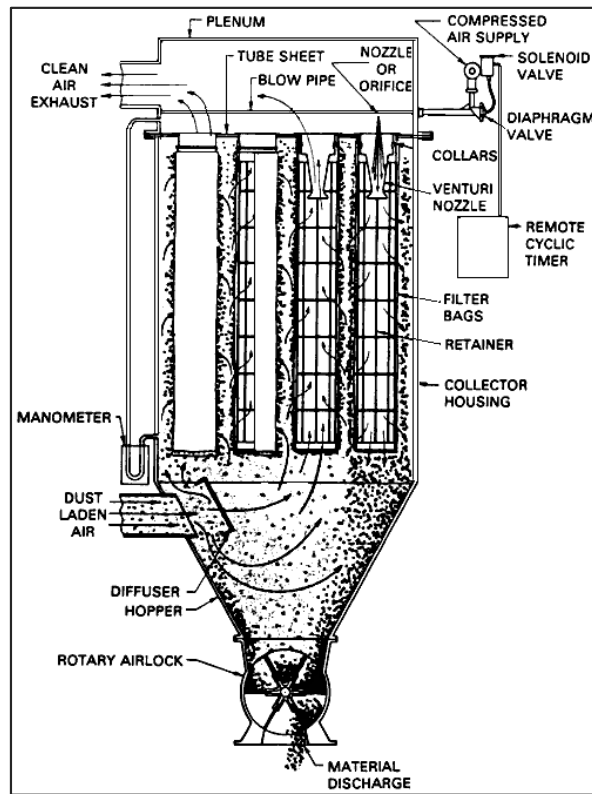


Figure 26: fabric filter unit (*Proceedings of the 18<sup>th</sup> DOE Nuclear Airborne Waste Management and Air Cleaning Conference, 1984*).

In these arrangements, pressure drops for the filter woven elements are generally lower than the ones achieved for rigid filters, and the overall weight of the filtration unit is also reduced. Moreover, filters pressure drops can be considered constant with regeneration cycles (N).

On the other hand, working temperatures for fabric filters are much lower than for candle ones, since they can work at temperatures up to 450 – 500 °C, according to the special materials they are made of (usually ceramics). They are also more subjected to thermal and mechanical degradation, this latter especially due to jet pulse cleaning cycles.

Face velocity is usually included from 12 to 24 mm/s and pressure drops are estimated by the following equation [Ergudenler et al., 1996]:

$$\Delta p_{fabric} = \frac{\mu}{\mu_o} \cdot \frac{u}{K} \quad (18)$$

For cake pressure drops, equations (16) and (17) are still used.

In this application, fabric filters 312 by NEXTEL 3 M Company were considered, especially because of their capability to work at high temperature (around 500 °C). Inlet particles concentration was still set to 10 g/Nm<sup>3</sup> and working time before filters regeneration was

still fixed as 30 min. Dimensioning results and pressure drops calculations are shown below (figure 27a, 27b and 27c)

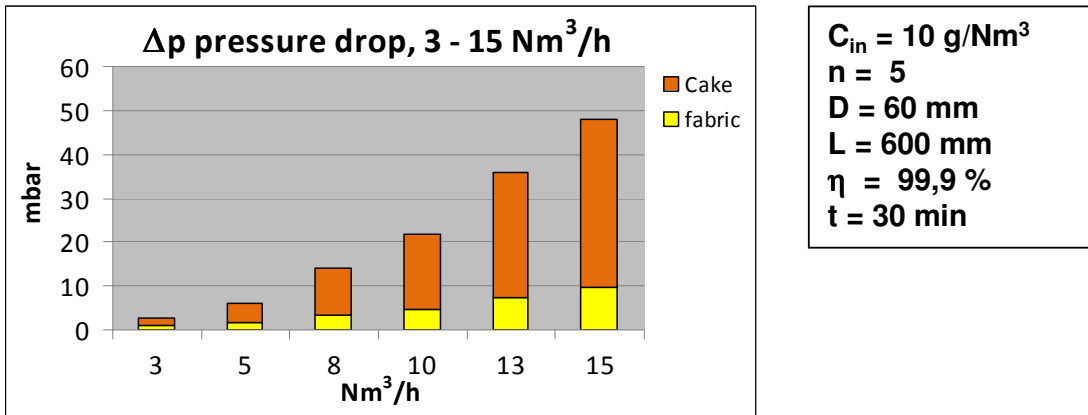


Figure 27a: design parameters and pressure drops for 3 – 15 Nm<sup>3</sup>/h gas flow fabric filter unit

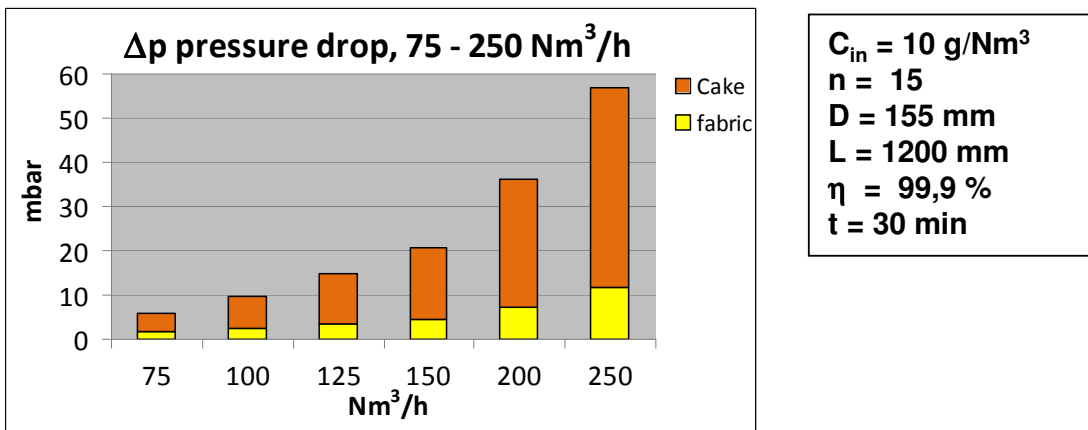


Figure 27b: design parameters and pressure drops for 75 – 250 Nm<sup>3</sup>/h gas flow fabric filter unit

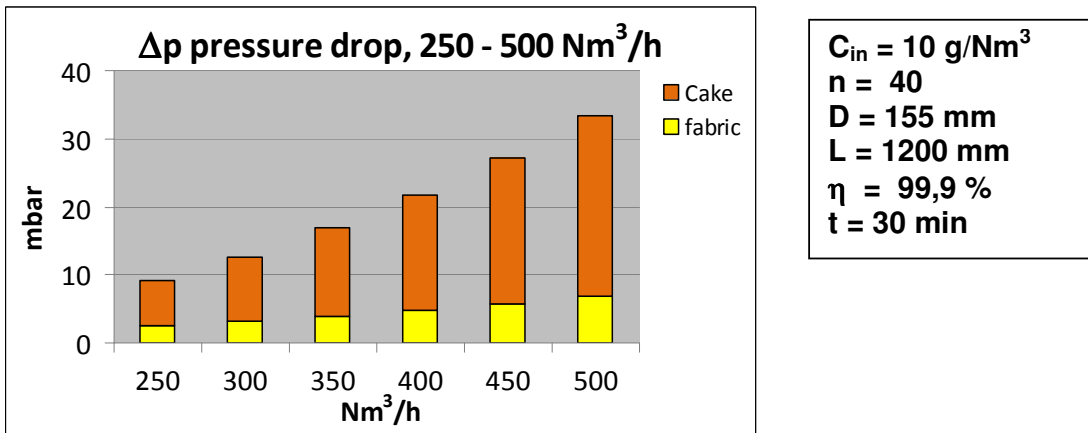


Figure 27c: design parameters and pressure drops for 250 – 500 Nm<sup>3</sup>/h gas flow fabric filter unit

It can be noted that pressure drops for the filter elements are lower than the ones relating to the cake deposition, in this case. Therefore, as already mentioned, fabric filters generally show pressure drops lower than candle ones. This can be considered one of their main advantages. Disadvantages are instead relating to maintenance issues and to a lower collection efficiency for sub-micron particles (the values shown in charts above are regarding 10  $\mu\text{m}$  size particles, [Ergudenler et al., 1996]).

As for candle filters, regenerating jet pulse velocities and cleaning gas flows were calculated according to the raw gas stream and particles concentration, in order to still estimate the consumption of cleaning gas. Results showed an higher consumption for fabric filters in respect with candle ones at the same operating conditions.

### 5.2.5 Catalytic tars cracking unit

As the large number of elementary steps which the overall gasification process is made of and because of the complexity of involved thermal conversion processes, many different heavy hydrocarbons are also recovered as final products, especially produced by thermal cracking of solids during pyrolysis, or through secondary partial oxidation reactions in gasification phase [Corella et al., 2004]. A great number of different compounds is usually found out (mostly polyaromatics and heterocyclics), so as their single detailed analysis and treatment are usually avoided in practical applications, but they are all considered as an only product of gasification, commonly called *tars*.

For their high molecular weight (tars are also defined as hydrocarbon species whose molecular weight is higher than benzene), the main practical issue related to tars is their relatively high boiling point (up to 750 K), for which they are liquid at room temperature (they are also called bio-oils) and they start to condense in a range of temperature from 400K to 700K, usually the same temperature interval at which gas cleaning lines for air downdraft gasified biomass work.

Their condensation downstream the gasifier is the main cause of plugging for the narrower and colder connection parts of the gas cleaning line (valves, elbows, inlet sections, etc.). Indeed, tars droplets usually trap solid particles still present in the gas stream as well, and they together form a sticky material that deposits on the colder walls of the instruments.

For the same reason, they also cause packed bed filters clogging and they are also able to penetrate and condense into the ceramic and metal filters, blinding them irreversibly.

Moreover, they also present some operational difficulties in being used in gas engines, so that they need to be eliminated from the gas stream.

One of the commonest methods for their collection is to enhance their condensation in a dedicated unit, such as a water scrubber, where they condense by the contact with cold water. This latter is then used for tars dilution and removal from the gas stream as well, together with collected solid particles.

Nevertheless, water scrubber have not a very high efficiency in tars removal [Hasler et al., 1999] and it also shows different operational issues to be faced on. One of these is regarding the necessity to keep the temperature of gas cleaning line higher than the boiling point of tars for all the units coming ahead the scrubber. Because tars start to condense at temperature relatively high, heating system for these units is usually required.

On the other hand, at the exit of scrubber, gas temperature is too low for any other high temperature treatments downstream, so that these applications are not permitted but by re-heating the gas stream.

Finally a lot of water is consumed for this process and its handling and regeneration result very difficult and expensive.

Another new technology for tars removal is the so called *OLGA process* that is based on wet scrubber of tars by oils instead of water. In this case, the waste-oil stream results much easier to handle and temperature of gas is still higher than the water dew point at the scrubber outlet, so that no waste water is produced [www.renewableenergy.nl]

In this work, the only method that was considered for tars abatement is the catalytic cracking process, by which tars are not removed from the gas stream but they are decomposed in lighter non condensable products through steam reforming reactions or simply by thermal cracking enhanced by catalysts.

In this way tars condensation is avoided at all, energy content of product gas results increased and its temperature is kept still high for further applications.

The chosen catalysts were Y zeolite materials (LZ-Y82 from *Union Carbide*), whereof main characteristics are shown in the following table 35:

<b>zeolite LZ-Y82</b>	
pore volume (ml/g)	0,35
$\rho_{\text{bulk}}$ (kg/m <sup>3</sup> )	610
sphericity $\phi$	0,7
$\epsilon$ bed	0,5
$\epsilon_{\text{mf}}$ bed	0,55
$\rho_s$ (kg/m <sup>3</sup> )	1220
void ratio	0,30
$\rho'_s$ (kg/m <sup>3</sup> )	1741
$k_s$ (W/m <sup>2</sup> *K)	1,7
$k'_s$ (porous material) (W/m <sup>2</sup> *K)	0,57

Table 35: physical properties of tars cracking catalysts (Lopez J.M. et al.,1994)

They were selected especially for their working temperature (700-800K), high cracking efficiency and resistance to sulphur poisoning [Hopkins et al., 1996].

Nevertheless, cracking activity of catalysts is quickly reduced by means of *coke* formation, such as a mixture of still heavy and solid hydrocarbons (mainly C<sub>n</sub>H<sub>2n-26</sub>, [Doka Nassionou et al.,1998]) which are produced as sub-products of cracking reactions themselves, and they are able to neutralize the active sites of catalysts as well as to deposit on their external surface [Hopkins et al., 1996; Lopez et al., 1994].

The main problem regarding tars cracking catalysts utilization is then their rapid loss in efficiency and their high frequency of regeneration consequently required.

For this reason, in industrial applications, tar cracking is often carried out in fluidized bed reactors, where a continuous recirculation of solids is possible, so as an online regeneration of catalysts is also achieved. Besides, hot spots inside the reactor are avoided, preventing catalysts destabilization. Nevertheless, fluidized bed reactors usually show a lower efficiency in respect with fixed bed reactors, in terms of required amount of catalysts.

In this case, a comparison in efficiency between the two technologies was accomplished in order to especially estimate their difference according to the units sizes.

Molecular formula for tars and coke were respectively chosen as C<sub>6</sub>H<sub>6,2</sub>O<sub>0,2</sub> [Okuga] and C<sub>4</sub>H<sub>8</sub> [Doka Nassionou et al.,1998], and the time depending intrinsic kinetics of tars cracking was considered as follows [Lopez, 1994]:

$$k = 12,8 \cdot e^{(-18,98 \cdot t)} + 3,407 / (1 + 0,95 \cdot t) \quad [\text{s}^{-1}] \quad (19)$$

Since this equation has been obtained empirically, it can be considered as an apparent kinetic constant, such as an only comprehensive constant that includes all the elementary reactions of tars cracking, as well as mass transfer phenomena of gas throughout the pores of catalysts. It is then inserted in an Arrhenius first order law.

In the case of fixed bed technology, apparent kinetic resistance in respect with external gas mass transfer one was checked out by means of the following relation [Levenspiel, 1962]:

$$k_g \cdot S_{ex} > k \cdot V_r \quad (20)$$

where  $k_g$  is the external film mass transfer coefficient and it is estimated by the following equation [Wakao N., 1978]:

$$k_g = \frac{Sh \cdot D_m}{d_g} \quad (21)$$

$$Sh = 2 + 1,1 \cdot Sc^{1/3} \cdot Re^{0,6} \quad (22)$$

$$Re = \frac{u \cdot \rho_g \cdot d_g}{\mu} \quad (23)$$

$$Sc = \frac{\mu}{\rho_g \cdot D_m} \quad (24)$$

Dimensioning of tars cracking unit was initially accomplished for the fixed bed technology, by setting a tars conversion factor as 0,9 after two hours of catalytic activity by zeolites, and considering gas flow design values as units sizes parameters (see table 31).

Units efficiencies were then investigated according to the gas flow changes within the variability fixed ranges (see table 31), by calculating the corresponding operating time of catalysts after which tars conversion factor drops to 0,9, or, equivalently, in terms of efficiency drop after two fixed hours of catalytic activity.

The same amount of catalysts calculated for fixed bed units was then investigated as material for bubbling bed reactors, working at the same temperature (723K) and at the same gas flow conditions. Analysis of efficiency trend was carried out in the same way previously described and graphs for the two technologies were finally compared each others. Units dimensions for the two technologies and corresponding results are reported on table 36 and figures 28a, 28b and 28c.

Fixed bed				Fluidized bed		
3 – 15 Nm <sup>3</sup> /h (8 Nm <sup>3</sup> /h)	75 – 250 Nm <sup>3</sup> /h (125 Nm <sup>3</sup> /h)	250 – 500 Nm <sup>3</sup> /h (350 Nm <sup>3</sup> /h)		3 – 15 Nm <sup>3</sup> /h (8 Nm <sup>3</sup> /h)	75 – 250 Nm <sup>3</sup> /h (125 Nm <sup>3</sup> /h)	250 – 500 Nm <sup>3</sup> /h (350 Nm <sup>3</sup> /h)
950	2050	2250	H (mm)	770	1410	1400
300	750	1200	D (mm)	370	950	1600
7	7	7	d <sub>g</sub> (mm)	0,2	0,5	0,5
41	552	1551	Kg cat	41	552	1551
30	30	30	C <sub>in</sub> (g/Nm <sup>3</sup> )	30	30	30
0,9	0,9	0,9	X <sub>design</sub>	0,9	0,9	0,9
2	2	2	t <sub>design</sub> (h)	2	2	2
air	air	air	reg. agent	air	air	air
-	-	-	TDH (mm)	760	1210	1210

Table 36: catalytic tars cracking units dimensions, for fixed bed and fluidized bed applications

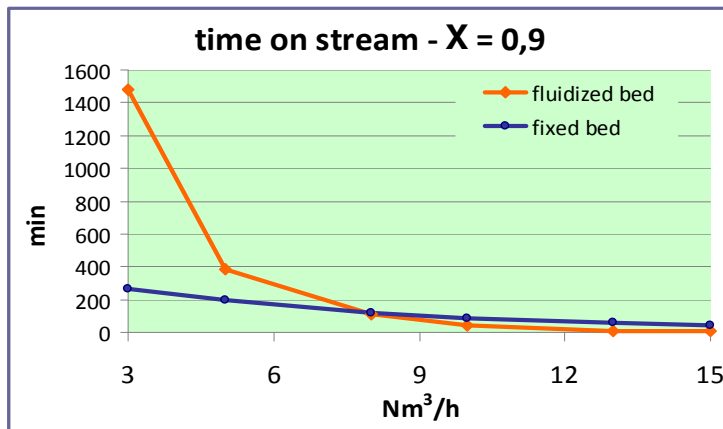
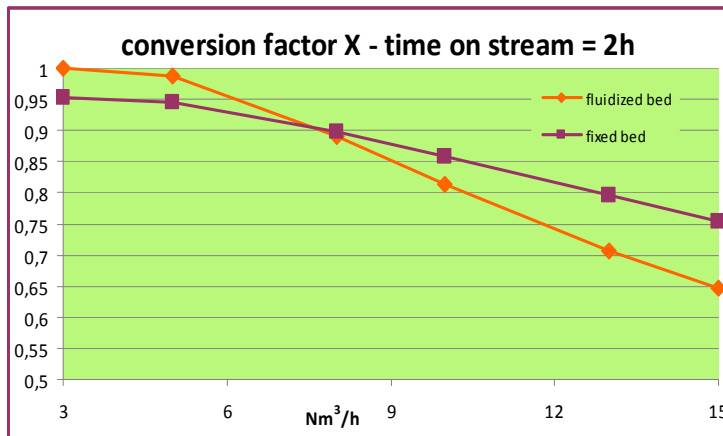


Figure 28a: conversion factor and time on stream analysis for 3 – 15 Nm<sup>3</sup>/h gas flow tars cracking unit

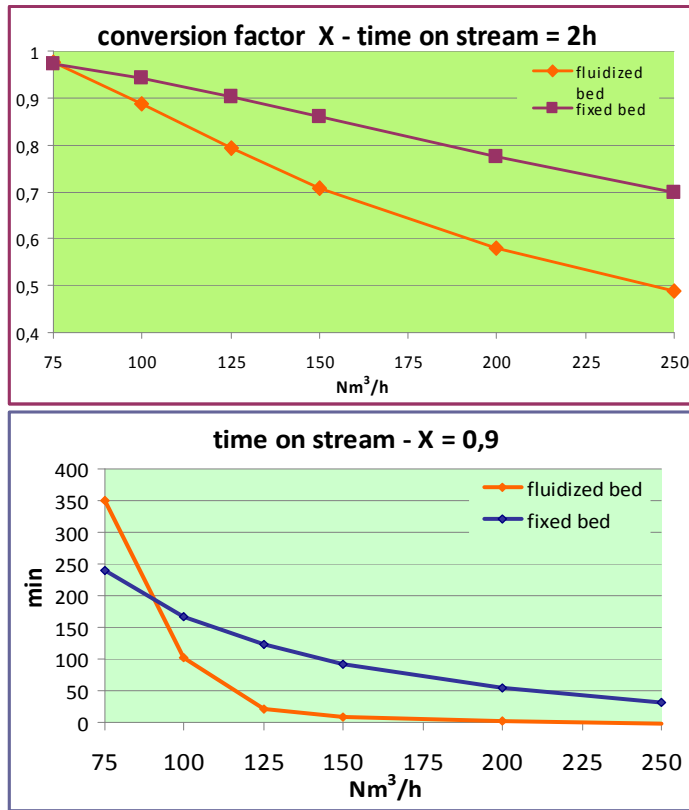


Figure 28b: conversion factor and time on stream analysis for 75 – 250 Nm<sup>3</sup>/h gas flow tars cracking unit

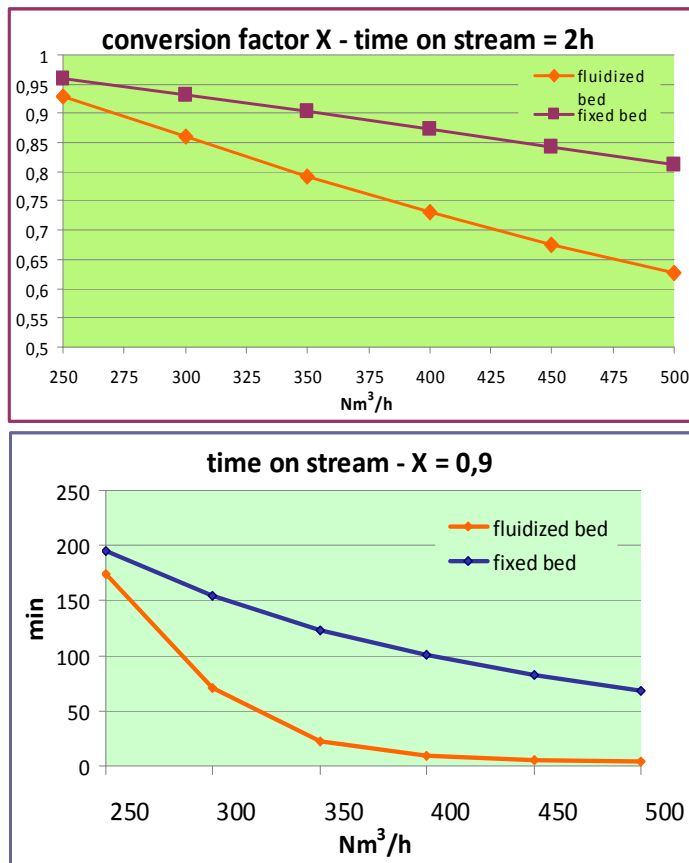


Figure 28c: conversion factor and time on stream analysis for 250 – 500 Nm<sup>3</sup>/h gas flow tars cracking unit

In the case of 500 $\mu\text{m}$  fluidized bed material size (125 and 350  $\text{Nm}^3/\text{h}$  gas flow units), it was calculated that tars cracking efficiencies are similar for the two different technologies (fixed bed and fluidized bed ones) if the ratio between gas superficial velocity and minimum fluidization velocity is about 2. Nevertheless, for lower values of this ratio, (such as lower than 2), the bubbling bed model adopted in this analysis (see appendix C) proves close to the analytical limits for its applicability.

For bed material size as 200 $\mu\text{m}$  (8  $\text{Nm}^3/\text{h}$  unit size), tars cracking efficiencies are the same for the two technologies if ratio between gas superficial velocity and minimum fluidization velocity is about 4 (the value that was also used for bubbling bed reactor design).

For fixed bed reactors dimensioning, plug flow axial dispersion model was used. According to this theoretical approach, available volume for cracking reactions is estimated by the following equation [Levenspiel, 1962]:

$$V = \frac{F_o}{C_o \cdot k} \left[ \ln \left( \frac{1}{1-X} \right) \right] \quad (25)$$

In the case of catalytic reactions, this volume ( $V$ ) is the total pore volume of catalysts, so as these other equations are used in order to calculate catalysts amount and bed volume, respectively:

$$kg_{cat} = V / V'_p \quad (26)$$

$$V_{bed} = kg_{cat} / \rho_{bulk} \quad (27)$$

According to the axial dispersion model, the reaction front of a plug flow reactor is not uniform in the cross sectional area at any time, but it shows a fluctuating distribution of products concentration, as well as of conversion factor. For this reason, an additional segment of reactor as transition zone needs to be added to the calculated volume, in order to assure the same desired conversion factor at each point of the outlet section.

Therefore, total volume of reactor is increased by a factor according to the following relation:

$$V_r = V \cdot \left( 1 + \frac{k}{D_L \cdot u^2} \right) \quad (28)$$

where  $D_L$  is the axial diffusion coefficient [ $\text{m}^2/\text{s}$ ] and it is calculated as follows [Yonghou X. et al., 2007]

$$\frac{\varepsilon \cdot D_L}{D_m} = 20 + 0,5 \cdot Sc \cdot Re \quad (29)$$

It can be seen that the transition zone increases as the superficial velocity of gas decreases. Therefore, tars conversion factor is influenced by this parameter as well, according to eq. (25), since very low gas superficial velocities reduce the effective reactor volume available for reactions ( $V$ ).

On the basis of this consideration and according to the pressure drops estimation, diameter of fixed bed reactors were assumed, once the total volume of reactor was calculated. Bed heights were thus obtained as a consequence.

For fluidized bed dimensioning a two phase bubbling model was chosen [Kunii et al., 1969]. According to this analytical approach, the reacting gas is prevalently flowing through the bed as bubbles, which grow and accelerate from the bottom of the bed to its upper surface. Solid catalysts are on the contrary almost completely contained in the emulsion phase (part of the bed out of bubbles, that includes solids and gas at minimum fluidization condition), where catalytic reactions are assumed to take place. Therefore, gas mass transfer from bubbles to emulsion phase has to be considered for unit design. Besides, bubbles are supposed to be surrounded by a zone of high solid concentration, called *cloud*, whose thickness depends on the same bubbles size and velocity. In the region immediately behind the bubbles another high solids concentration zone is established, as well, because of the pressure decrease. It also depends on bubbles sizes and it is usually called *wake*. In series mass transfer phenomena are hence to be investigated for bubbling bed behaviour analysis..

As the two phase bubbling bed model was considered for catalytic tars cracking units design only, as well as because of the complexity of required calculations, fluidized bed units dimensioning procedure is only reported as Appendix C, in this work (moreover, fixed bed technology was finally chosen as the one to be inserted in gas cleaning lines, as well).

Pressure drops for fixed bed units were calculated by means of eq. (9) while they were estimated as bed material weight in the case of fluidized bed ones [Kunii et al., 1969]. Successively, pressure drops from gas distributors were also added in both of the cases. Perforate plates were assumed to be used and the following equation was used (considering design values of gas flow):

$$\Delta p_{plate} = \frac{1}{2} \cdot \left( \frac{u_{or}}{C_d} \right)^2 \cdot \rho_g \quad (30)$$

In order to achieve an uniform gas distribution through the bed, a minimum value as  $0,1\Delta p_{bed}$  is suggested for  $\Delta p_{plate}$  and not less than 3,4 kPa [Kunii et al., 1969]. In this way  $u_{or}$  can be calculated as follows:

$$u_{or} = \sqrt{\frac{2 \cdot \Delta p_{plate}}{\rho_g}} \cdot C_d \quad (31)$$

By choosing an orifice diameter value,  $d_{or}$  (in this case,  $d_{or} = 1$  mm), the number of holes per unit area  $N_{or}$  can be calculated:

$$N_{or} = \frac{u_o}{u_{or} \cdot \frac{\pi d_{or}^2}{4}} \quad (32)$$

For a square distribution of holes on the perforate plate, the distance between two of them is calculated as:

$$l_{or} = \sqrt{\frac{1}{N_{or}}} \quad (33)$$

Dimensioning of gas distributor was initially accomplished for fluidized bed reactors. Successively the same values of  $N_{or}$ ,  $d_{or}$  and  $l_{or}$  were used for fixed beds, as well.

Results on total pressure drops are shown below, in the case of the two different considered technologies:

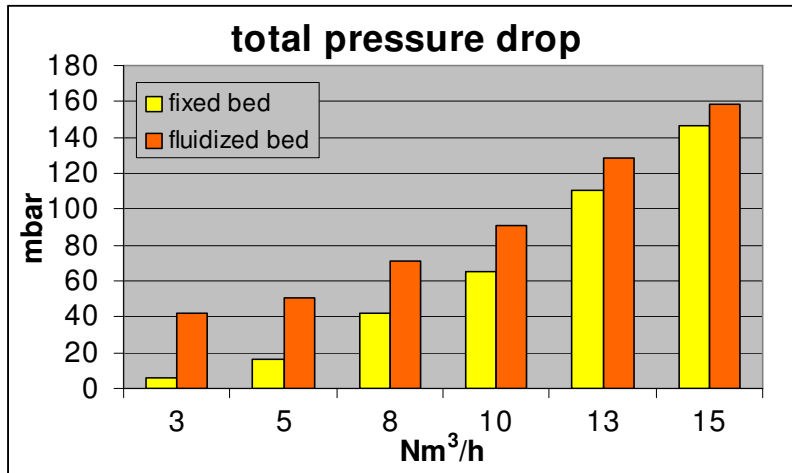


Figure 29a: pressure drops for fixed bed and fluidized bed tars cracking units (3 – 15 Nm<sup>3</sup>/h gas flow size)

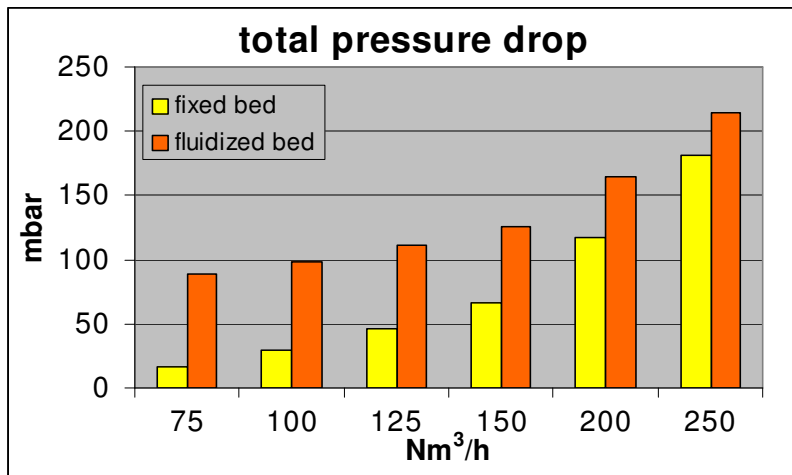


Figure 29b: pressure drops for fixed bed and fluidized bed tars cracking units (75 – 250 Nm<sup>3</sup>/h gas flow size)

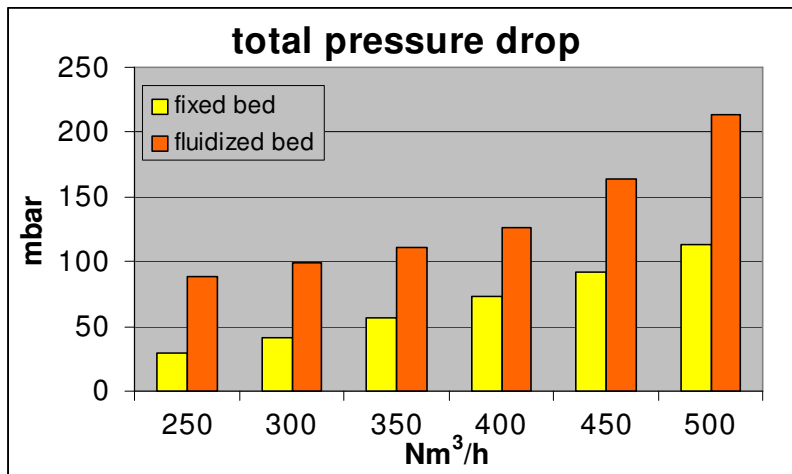


Figure 29c: pressure drops for fixed bed and fluidized bed tars cracking units (250 – 500 Nm<sup>3</sup>/h gas flow size)

Because of the different bed material sizes (see table 36), fixed bed units show pressure drops always lower than fluidized bed ones, although they become comparable for high gas flow rates.

Regeneration of catalysts was considered in terms of air consumption estimation, only. Indeed, catalysts are regenerated by enhancing coke combustion reactions with air. In this phase, operational issues are regarding the uniformity and the rise of combustion temperature inside the reactor and the oxygen distribution for correct regeneration. Indeed, hot spots should be avoided in order to keep catalysts safe from destabilization.

For the air consumption calculation, different values of initial tars concentration were considered in the range from 10 to 50 g/Nm<sup>3</sup> and 70% of tars amount was supposed to be converted to coke during cracking activity.

### 5.2.6 Zn-Ti adsorber for high temperature sulphur removal

The total sulphur content of biomass fuel is assumed to be converted to hydrogen sulphide, H<sub>2</sub>S, during gasification process. COS formation is therefore neglected in this work. Hydrogen sulphide is a corrosive substance that can damage materials of traditional gas cleaning lines as well as cogeneration units. Besides, it is the main cause of SO<sub>2</sub> formation during combustion processes of syngas, whose emissions into the atmosphere are not permitted but in very low concentrations.

Many different methods for H<sub>2</sub>S removal from fuel gas streams are already developed. Some of them are carried out by liquid absorption of H<sub>2</sub>S in ammonia or alkanolamine solutions, others are accomplished by oxidation (*Claus process*) and many different solid adsorbers are also used [Kohl et al., 1997]

In this latter case, two main categories for solid adsorbers can be distinguished: regenerable sorbents and non regenerable sorbents. These latter are usually cheap and disposable materials whose reaction with H<sub>2</sub>S is irreversible. Their activity is enhanced at high temperature, yet [Schimdt et al., 1996].

Other sorbents work at lower temperature (700 – 900K) and they can be regenerated, usually by oxidation, once they are completely exhausted by sulphur. Among them, one of the most promising materials for H<sub>2</sub>S adsorption is Zinc-titanate oxide.

Indeed, zinc is one of the most reactive element with sulphur but it shows a little thermal resistance to sulfidation-regeneration cycles (regeneration is carried out at about 900K up to 1100K). Therefore, a stronger material (like Titan) is used as a binder in order to increase thermal stability of the material.

This compound was considered for H<sub>2</sub>S adsorption in this work, too. It was chosen for its suitable working temperature (700 – 750K) above all, and dry adsorption was preferred in order to avoid water and other secondary materials consumption.

The specific chosen material is named ZT-4 and it was developed by Research Triangle Institute and U.S. Department of Energy (USA) [Gupta et al., 1996]. Its molecular formula is (ZnO)<sub>1,5</sub>TiO<sub>2</sub> and its main physical properties are shown in table 37.

ZT- 4 (ZnO) <sub>1,5</sub> -TiO <sub>2</sub>	
pore volume (cm <sup>3</sup> /g)	0,22
$\rho_{\text{bulk}}$ (kg/m <sup>3</sup> )	1260
sphericity $\phi$	0,6
$\varepsilon$ bed	0,4
$\rho_s$ (kg/m <sup>3</sup> )	2100
void ratio	0,316
$\rho_m$ (moles/cm <sup>3</sup> )	0,0104
$k_s$ (W/m <sup>2</sup> *K)	13,13
$k'_s$ (porous material) (W/m <sup>2</sup> *K)	4,21

Table 37: physical properties of H<sub>2</sub>S adsorber (Gupta et al., 1996)

Fixed bed unit was examined for this application and 1 mm bed material size was chosen. As already mentioned, the reacting component is Zinc oxide only, so that the sulfidation reaction can be written as [Yrjas et al., 1996]:



Kinetic constant for this reaction was found out as  $k = 221 \text{ cm}^3/\text{mol}\cdot\text{s}$  ( $T = 400^\circ\text{C}$ ) [Mojtahedi et al., 1996] in respect with solid sorbent consumption.

For heterogeneous reactions developed in fixed bed units, the time for the complete saturation of solid bed can be divided in two different steps: the necessary time for complete development of reaction front in the first layer of the bed (whose amplitude depend on the solid reactivity,  $k$ ), and the time that the same reaction front takes to cover the full height of the bed and reach the exit sectional area [Wang et al. 1989].

In this case, only the second term for solid bed exhausting time was considered, in order to simplify dimensioning procedure and as a security factor for the outlet contaminant concentration. Indeed, by neglecting the necessary time for reaction front formation inside the bed, it can be supposed that, after the calculated saturation time, contaminant concentration at the outlet section of the bed is still zero.

The constant velocity of reaction front along the bed is obtained as [Wang et al. 1989]:

$$u_{rf} = \frac{b \cdot C_0 \cdot u}{[\rho_m \cdot (1 - \varepsilon)]} \quad (35)$$

where  $b$  is the stoichiometric coefficient of the overall heterogeneous reaction.

Adsorption units were dimensioned by choosing mass space velocities as  $0,30 \text{ h}^{-1}$  for each gas flow design value. In this way, sorbent amounts inside the beds were obtained for the three gas cleaning line sizes.

Bed diameters were chosen according to the admitted pressure drops (from 100 to 150 mbar), which were calculated as the sum of fixed bed (eq. (9)) and gas distributor ones (see par. 5.2.5). Eq. (28) was still used in order to consider gas dispersion impact on outlet contaminant concentration. Dimensioning results are shown in table 38:

<b>Fixed bed</b>	<b>3 – 15 Nm<sup>3</sup>/h (8 Nm<sup>3</sup>/h)</b>	<b>75 – 250 Nm<sup>3</sup>/h (125 Nm<sup>3</sup>/h)</b>	<b>250 – 500 Nm<sup>3</sup>/h (350 Nm<sup>3</sup>/h)</b>
<b>H (mm)</b>	640	650	700
<b>D (mm)</b>	200	800	1300
<b>d<sub>g</sub> (mm)</b>	1	1	1
<b>Kg ads</b>	25	411	1170
<b>mass space vel. (h<sup>-1</sup>)</b>	0,30	0,30	0,30
<b>reg. agent</b>	air	air	air

Table 38: Zn-Ti adsorption units dimensions

The saturation (or working available) time for sorbent was estimated by applying eq. (35) to the dimensioned bed heights,  $H$ , and a range of contaminant concentration was chosen from 100 to 1000 ppmv. Results are shown in the following charts:

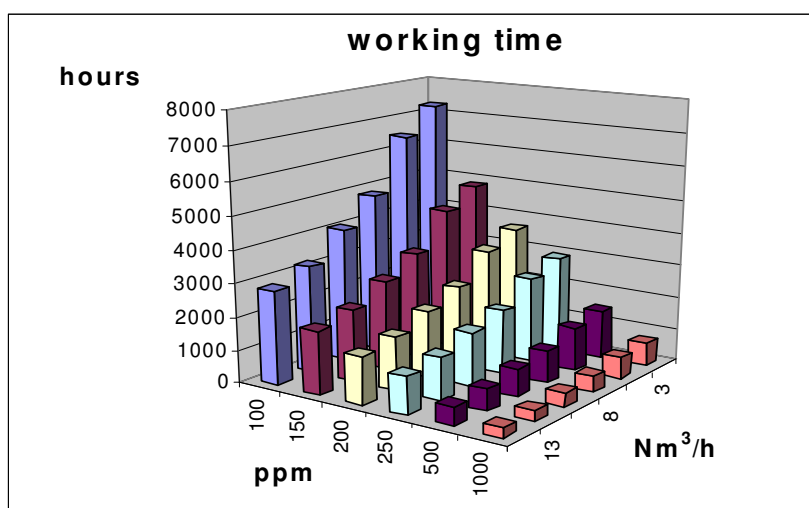


Figure 30a: saturation time for Zn-Ti sorbent bed, according to gas flow and H<sub>2</sub>S concentration (3 – 15 Nm<sup>3</sup>/h unit size)

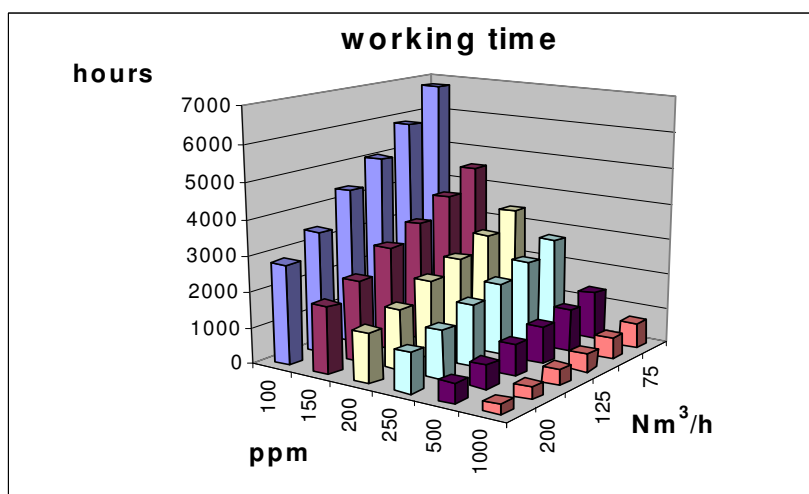


Figure 30b: saturation time for Zn-Ti sorbent bed, according to gas flow and H<sub>2</sub>S concentration (75 – 250 Nm<sup>3</sup>/h unit size)

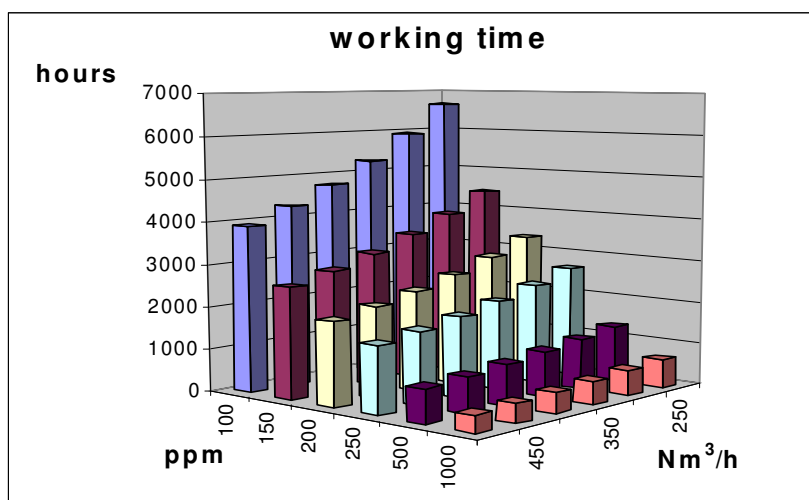


Figure 30c: saturation time for Zn-Ti sorbent bed, according to gas flow and H<sub>2</sub>S concentration (250 – 500 Nm<sup>3</sup>/h unit size)

A great variability is detected according to both gas flow and especially H<sub>2</sub>S concentration. Two orders of magnitude are indeed covered from the harder conditions (high gas flows and high contaminant concentrations) to the lighter ones.

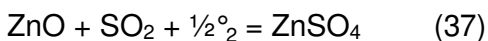
Nevertheless, an high adsorption efficiency of material can be generally estimated. Indeed, saturation time is higher than 1000 hours for each designed unit and at all gas flow conditions, for contaminant concentrations lower than 250 ppm. At the lighter conditions (such as at the lower limits of considered gas flow ranges and with contaminant concentration as 100 ppm), even more than 6500 hours can be reached before regenerating the sorbent material. Therefore, except for the higher concentration values as 500 ppm and 1000 ppm (in such a case an increase of units dimensions could be also envisaged), a few regeneration steps per year can be foreseen in this application.

Sorbent regeneration is then carried out by oxidation, according to the following reaction [Yrjas et al., 1996]:



Oxidation temperature is usually between 900 and 1000 K [Mojtahedi et al., 1996]. Nevertheless, because of the high exothermic behavior of this reaction, temperature of reactor tends to reach higher values during regeneration, so as stability of adsorption material is damaged. For this reason, temperature control devices are usually required for this application.

Another operational issue regarding sorbent regeneration is the possibility to achieve ZnSO<sub>4</sub> formation instead of clean regenerated sorbent, according to the following reactions:



Air consumption for sorbent regeneration was finally calculated in the different working conditions (gas flows and contaminant concentrations) by means of eq. (36).

### 5.2.7 Activated carbon adsorption unit

Activated carbon is one of the commonest material for the adsorption of several species (especially organic compounds, VOCs, benzene, etc.), and it is already well in use in such air purification applications where trace elements need to be eliminated from gas streams.

Many experimental works have been carried out in order to check the feasibility of activated carbon utilization in gasified biomass cleaning systems, too. Some of them have shown good results in H<sub>2</sub>S and ammonia capture [Rodriguez et al., 2007; Yonghou X. et al., 2007] so that activated carbon adsorption unit was especially investigated in this work for the removal of these two main contaminants.

When syngas stream flows through the bed of the adsorbing particles, gaseous components are retained on the carbon surface by means of a physical adsorption mechanism, in this case, such as mainly due to Van der Waals forces and polar attraction between gas components and active sites of carbon. This process is temperature depending and it is enhanced at low temperature values.

According to Langmuir theory, an equilibrium relation can be written between contaminant concentration in the gas stream and contaminant amount retained on the carbon particle surface, for each value of temperature (Langmuir isotherm):

$$q = \frac{q_m \cdot K_L \cdot C_{in}}{1 + K_L \cdot C_{in}} \quad (39)$$

q is the real quantity of gas contaminant adsorbed per mass unit of material, (mg/g), q<sub>m</sub> is the maximum admitted quantity of contaminant per mass unit of carbon at the same temperature (mg/g), K<sub>L</sub> is an equilibrium constant (m<sup>3</sup>/mg) and C<sub>in</sub> is the inlet contaminant concentration in the gas stream (mg/m<sup>3</sup>). Some values of these Langmuir parameters are shown below, for both H<sub>2</sub>S and NH<sub>3</sub> (Rodriguez et al., 2007; Yonghou X. et al., 2007).

<b>Langmuir constants</b>	<b>q<sub>m</sub> (mg/g)</b>	<b>K<sub>L</sub> (m<sup>3</sup>/mg)</b>	<b>T (°C)</b>
<b>NH<sub>3</sub></b>	<b>4,2</b>	<b>0,00047</b>	<b>40</b>
<b>H<sub>2</sub>S</b>	<b>2,7</b>	<b>0,014</b>	<b>30</b>

Table 39: Langmuir constants for NH<sub>3</sub> and H<sub>2</sub>S adsorption

The first step for adsorption unit dimensioning was to calculate q values for different inlet contaminants concentrations. Concentration ranges were chosen between 100 and 1000 ppmv for H<sub>2</sub>S and between 2000 and 6000 ppmv for NH<sub>3</sub> (in the case of coupled contaminants treatment, the highest considered concentration of H<sub>2</sub>S was 500 ppmv).

Fixed bed technology with 1mm carbon material size was chosen in this case, and breakthrough model was adopted for units design. According to this, a curve of contaminant concentration in the gas stream passing through the bed (or equivalently of adsorbate concentration on the bed surface) can be detected along the bed length (breakthrough curve). Since the shape of this curve doesn't change during the adsorption process but it is depending on Langmuir constants only, a gas concentration front (whose value depends on its position on the curve) can be detected as moving towards the exit section of the bed, While the slope of breakthrough curve is depending on Langmuir constants only (such as temperature), the reaction front velocity is affected by the sorbent amount in the bed and the inlet initial contaminant concentration in the gas stream.

Therefore, by fixing bed dimensions a priori, it is possible to estimate the saturation time for the adsorption unit by choosing a maximum contaminant concentration in the exit gas stream and calculating the time that the corresponding reaction front takes to cover the total length of the bed, according to its pre-determined velocity (Breakthrough point).

The following equation is used at this purpose:

$$\frac{C}{C_o} = \frac{1}{2} \left\{ 1 + \operatorname{erf} \left[ \left( \frac{u \cdot z}{4 \cdot D_L} \right)^{\frac{1}{2}} \cdot \frac{(t - t_{\min})}{(t \cdot t_{\min})^{\frac{1}{2}}} \right] \right\} \quad (40)$$

In this case, C is the admitted contaminant concentration at the exit section of the adsorbing bed.

$D_L$  is the axial dispersion coefficient of gas and it is calculated through eq. (23), (24), (29).

t is the saturation time corresponding to the admitted contaminant concentration C

$t_{\min}$  is the saturation time corresponding to the contaminant concentration equal to the initial one in the raw gas stream, such as it is the minimum time after which the same concentrations at the inlet and outlet of the adsorbing unit are detected. It is calculated as:

$$t_{\min} = \left[ 1 + \left( \frac{\varepsilon}{1 - \varepsilon} \right) \cdot \frac{C_{eq}}{C_o} \right] \frac{z}{u} \quad (41)$$

$C_{eq}$  is the contaminant concentration on carbon surface at equilibrium with the initial gas concentration, on volumetric basis ( $\text{mg}/\text{m}^3$ ), and it is obtained by multiplying Langmuir q value by bulk density of the bed.

Erf is a statistical error analytical function whose expression is:

$$\operatorname{erf} = \frac{2}{\sqrt{\pi}} \int_0^x e^{-x^2} \quad (42)$$

Gas superficial velocity through the activated carbon bed was chosen between 4 cm/s and 6 cm/s (4 cm/s for the smaller unit sizes, 6 cm/s for the larger ones). Diameters of beds were then calculated according to the gas flow design values for the three unit sizes.

Bed heights were differently dimensioned, depending on if activated carbon unit was supposed to be used for  $\text{H}_2\text{S}$  adsorption only, or even for simultaneous removal of  $\text{H}_2\text{S}$  and  $\text{NH}_3$ .

In the first case, bed heights proved different for the three unit sizes, respectively as:

$L_{\text{bed}} = 1\text{m}$  for  $8 \text{ Nm}^3/\text{h}$  gas flow unit size

$L_{\text{bed}} = 1,5\text{m}$  for  $125 \text{ Nm}^3/\text{h}$  gas flow unit size

$L_{\text{bed}} = 2\text{m}$  for  $350 \text{ Nm}^3/\text{h}$  gas flow unit size

They were calculated according to the admitted pressure drops for adsorption units. These latter were estimated (in all of the gas flow ranges defined for the three unit sizes) by means of eq. (9) and by adding gas distributors ones, as determined in par. 5.2.5. The bed heights reported above were then determined by setting a maximum pressure drop as 30 mbar for the small unit and as 40 and 45 mbar for the two other units respectively, according to the gas flow design values.

On the contrary, in the case of simultaneous removal of H<sub>2</sub>S and NH<sub>3</sub>, bed heights were always fixed as 2 m, as a maximum acceptable height for the adsorption unit. Pressure drops were thus calculated as 37 mbar for the small size unit and 46 mbar for both the larger ones, still corresponding to gas flow design values.

Physical properties of activated carbon material [Yonghou X. et al., 2007] and adsorption units estimated dimensions are reported in table 40 and 41 respectively.

activated carbon	
pore volume (ml/g)	0,27
$\rho_{\text{bulk}}$ (kg/m <sup>3</sup> )	390
$\phi$	0,8
$\varepsilon$ bed	0,4
$\rho_s$ (kg/m <sup>3</sup> )	650
void ratio	0,15
Dm (cm <sup>2</sup> /s)	1,30
$k_s$ (W/m*K)	0,26
$k'_s$ (W/m*K)	0,063

Table 40: physical properties of activated carbon material

<b>Fixed bed</b>	<b>3 – 15 Nm<sup>3</sup>/h (8 Nm<sup>3</sup>/h)</b>	<b>75 – 250 Nm<sup>3</sup>/h (125 Nm<sup>3</sup>/h)</b>	<b>250 – 500 Nm<sup>3</sup>/h (350 Nm<sup>3</sup>/h)</b>
<b>H (mm)</b>	2000	2000	2000
<b>D (mm)</b>	265	876	1476
<b>d<sub>g</sub> (mm)</b>	1	1	1
<b>Kg ads</b>	43	469	1333
<b>C<sub>out</sub> NH<sub>3</sub> (g/Nm<sup>3</sup>)</b>	0,1	0,1	0,1
<b>C<sub>out</sub> H<sub>2</sub>S (ppmv)</b>	20	20	20
<b>reg. agent</b>	steam (130°C)	steam (130°C)	steam (130°C)
<b>Kg vapor / kg H<sub>2</sub>S</b>	10	10	10

Table 41: Activated carbon adsorption units dimensions

Once the adsorption units dimensions were determined, available working times before their regeneration were calculated through eq.(40), according to the gas flows and inlet contaminant concentrations, as well as by choosing exit permitted concentrations as 20 ppmv for H<sub>2</sub>S and 100 mg/Nm<sup>3</sup> for NH<sub>3</sub>. Results are shown in figures 32a, 32b and 32c, in the case of single contaminants abatement.

As regard H<sub>2</sub>S, the same trend of saturation time detected for chemical adsorption units can be noted in this case as well, but with an overall decrease as about one order of magnitude. As it could be expected, hence, physical adsorption is less efficient than chemical one, although its corresponding sorbent regeneration process is generally easier to be accomplished (see below).

Ammonia is much less adsorbed on activated carbon than H<sub>2</sub>S, as it can be also noted from their relative equilibrium constants  $K_L$  (see tab. 39). Except for the small unit, the saturation time is not higher than 60 hours, even at the lighter conditions of gas flow and contaminant concentration.

Nevertheless, for the highest considered ammonia concentration in the gas stream, such as 6000 ppm, saturation time is still higher than 10 hours at each gas flow condition and for all the designed units. It can be still considered a reasonable operating time, according to the designed units dimensions and the proposed application.

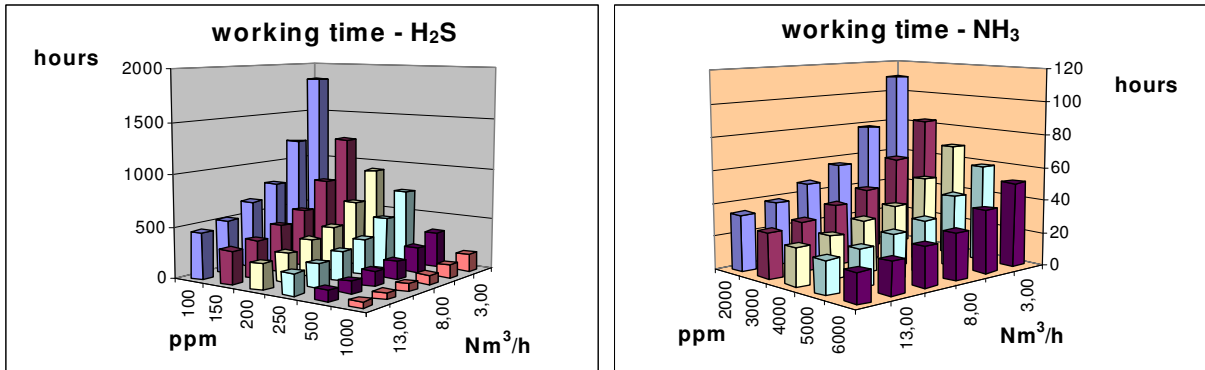


Figure 31a: Saturation times of activated carbon material for separate  $H_2S$  and  $NH_3$  adsorption processes (3 – 15  $Nm^3/h$  gas flow size)

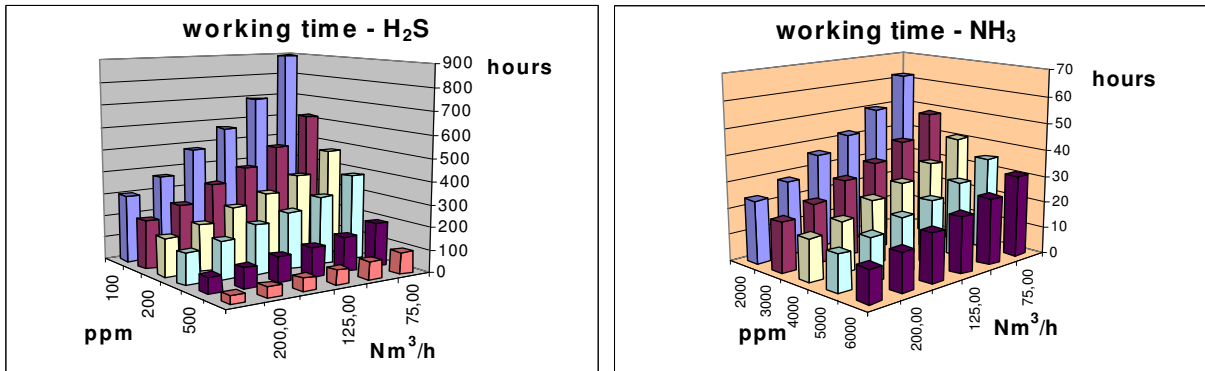


Figure 31b: Saturation times of activated carbon material for separate  $H_2S$  and  $NH_3$  adsorption processes (75 – 250  $Nm^3/h$  gas flow size)

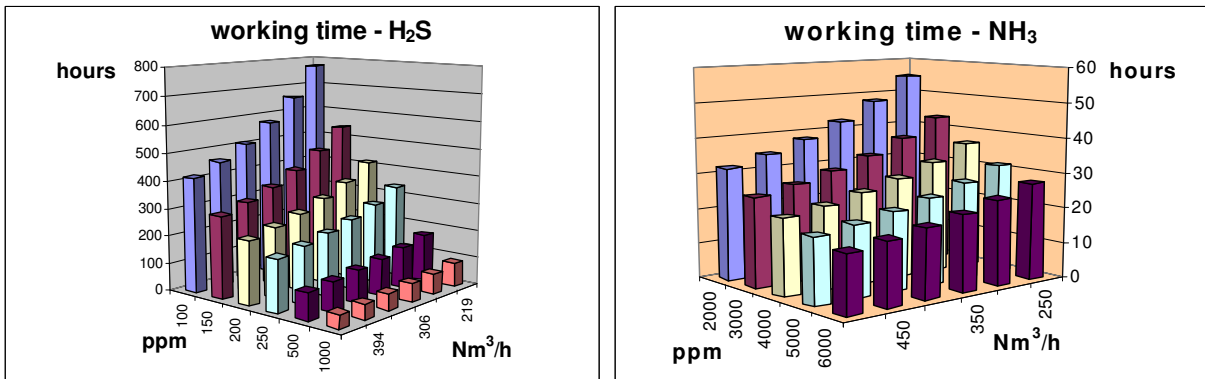


Figure 31c: saturation times of activated carbon material for separate  $H_2S$  and  $NH_3$  adsorption process (250 – 500  $Nm^3/h$  gas flow size)

Activated carbon is able to adsorb water vapour, as well. [Dubinin,1981; Barton et al. 1991]. Although this is obviously not listed as contaminant for the gas stream, vapour adsorption was also considered in this application, in order to estimate its influence on activated carbon bed exhausting time.

The relative adsorption isotherm can be written as follows [Dubinin, 1981]:

$$h = \frac{a}{\left[ c \cdot (a_o + a) \cdot \left( 1 - \frac{c-1}{c} \cdot \frac{a}{a_s} \right) \right]} \quad (43)$$

$h$  is the ratio between the vapor pressure in the exit gas stream and the saturation one on active sites of carbon. Therefore, for complete saturation of the bed, this value has to be 1.

$c$  is a kinetic parameter

$a_o$  and  $a_s$  are respectively the initial adsorbing active sites concentration and the maximum one at the working temperature (mmol/g), since different adsorption layers can be assumed to be developed during adsorption process.

$a$  is the concentration of water vapor adsorbed on the bed surface (very close to  $a_s$ , for  $h$  value equal to 1), (mmol/g)

Values for these parameters have been empirically found out by Barton at al. [1991] and they are shown in the following table:

vapor adsorption	$c$ (-)	$a_o$ (mmol/g)	$a_s$ (mmol/g)	$T$ (°C)
	1,62	1,44	19,4	25

Table 42: kinetic parameters for water vapour adsorption on activated carbon

By using  $a$  value as equilibrium concentration in eq. (41) and by fixing  $C / C_o$  ratio as 0,001 in eq. (40), ( $C_o$  is supposed to be the saturation vapour pressure at the bed inlet temperature), exhausting time of carbon bed by vapour adsorption was calculated.

Results regarding the same dimensioned units for  $H_2S$  and  $NH_3$  adsorption processes are reported below, as saturation times by vapour retention.

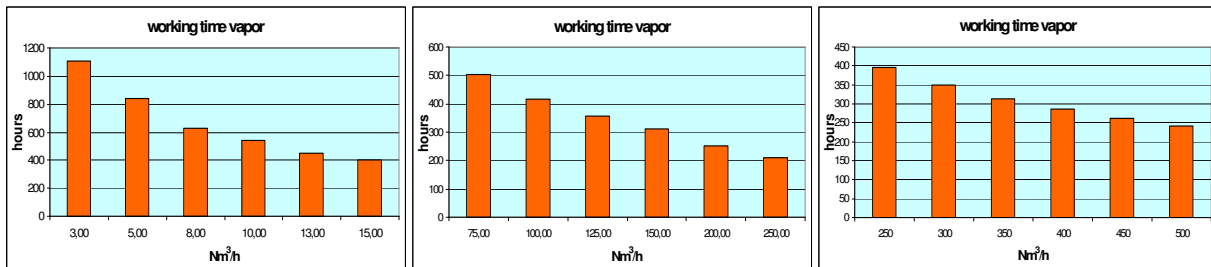


Figure 32: saturation times for activated carbon units for water vapour adsorption

In the case different contaminants were assumed to be simultaneously adsorbed by the same gas cleaning unit, the corresponding total saturation time (of activated carbon bed, in this case) was calculated as follows:

$$\tau = \frac{1}{\sum_i \frac{1}{t_i^s}} \quad (44)$$

$t_i^s$  = saturation time for single contaminant adsorption (hour).

As an example, results regarding the simultaneous removal of H<sub>2</sub>S and NH<sub>3</sub> by the activated carbon units previously dimensioned are reported in the following figures. In this case, the inlet contaminants concentrations were coupled together by following the same increase order for both the contaminants.

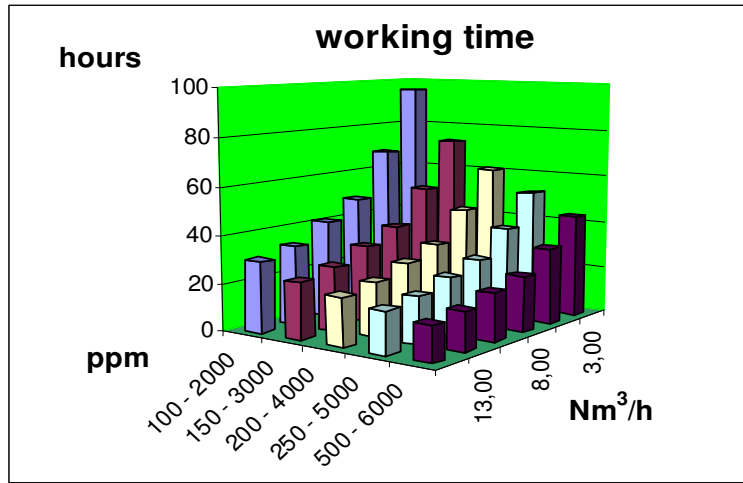


Figure 33a: available working time of activated carbon unit for combined contaminants adsorption (3 – 15 Nm<sup>3</sup>/h gas flow size)

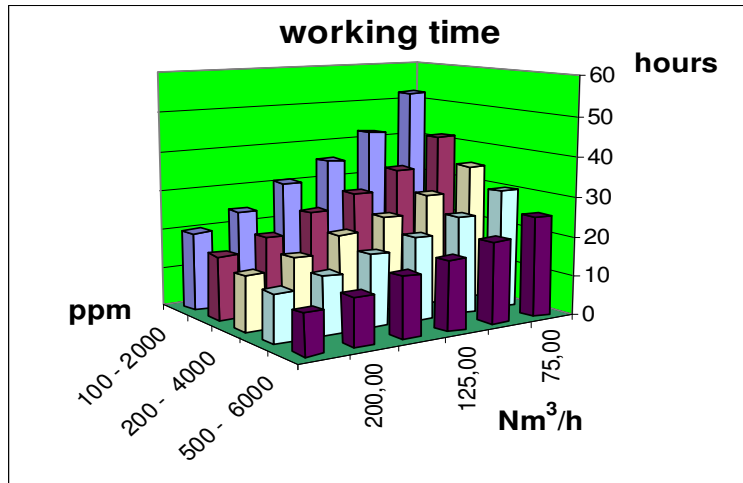


Figure 33b: available working time of activated carbon unit for combined contaminants adsorption (75 – 250 Nm<sup>3</sup>/h gas flow size)

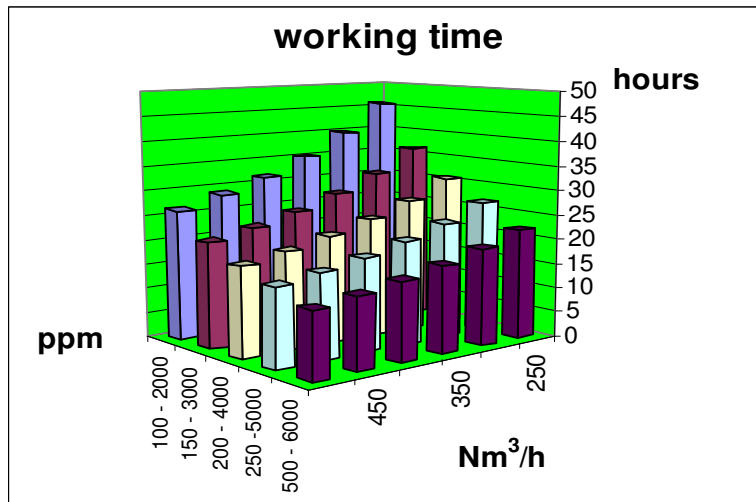


Figure 33c: available working time of activated carbon unit for combined contaminants adsorption (250 – 500 Nm<sup>3</sup>/h gas flow size)

As it can be seen, in this case the saturation times are very close to the ones calculated for single ammonia adsorption, such as for the material which is worse adsorbed by the carbon. Since they can be even less than 24 hours (as operating limit for off line regeneration methods) tandem arrangements are usually set up for this technology.

This means that two identical adsorption units are used, alternatively working in adsorption and regeneration phases. In this way, a continuous adsorption operation can be achieved in the overall gas cleaning line, although several carbon regeneration cycles are required. An operational scheme of this arrangement is shown below.

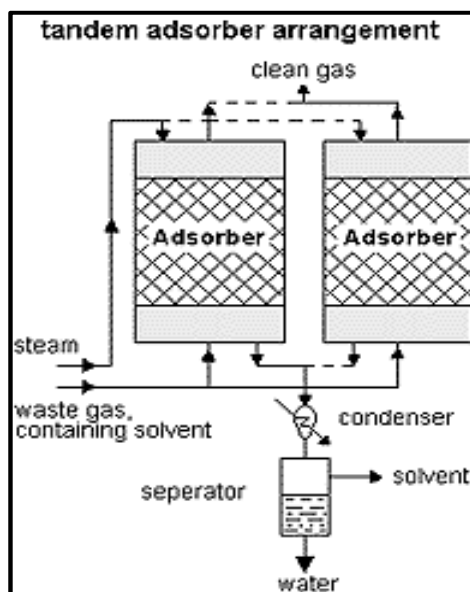


Figure 34: tandem arrangement for adsorption units ([www.hdm-stuttgart.de](http://www.hdm-stuttgart.de))

Carbon regeneration is carried out by steam injection. Steam temperature is suggested to be 130°C and a ratio of 10kg steam per kg adsorbate is reported in literature [Germerdonk, 1993]. On the basis of this parameter, steam consumption for regeneration of dimensioned carbon bed adsorbing units was calculated in each operating condition, and for all the three considered unit sizes.

### 5.2.8 Wet scrubber packed column

Wet scrubber can be considered as the most adopted technology in gas cleaning systems. It is based on the transfer of gas contaminants from the syngas stream to a cleaning water flux, whose contact with gas is achieved in different arrangements (venturi scrubbers, tray columns, spray columns, packed bed columns, etc.).

Depending on the nature of contaminants are supposed to be treated, water stream can play different roles in the gas cleaning line: particles trapping for particulate collection, enhancement of tars and oil condensation, or chemical absorption of different gaseous species, such as acids, some organic materials and other inorganic soluble compounds (especially  $\text{NH}_3$ ).

For the present study water scrubber was considered for the last case only, such as for chemical absorption of acids (HCl) and ammonia ( $\text{NH}_3$ ). For particulate and tars collection, indeed, different units are assumed to be used, because of their higher efficiencies (Hasler et al., 1999) and in order to avoid some operational problems usually occurring from the use of water scrubber for tars condensation (see par. 5.2.5).

Wet scrubber packed column was the investigated unit in this case, since it is mainly distinguished by a good quality of contact between gas and liquid phases, in respect with the other arrangements. It roughly consists on a cylindrical vessel in which some packing materials are filled in, whereof main role is exactly to increase available contact surface between gas and water streams, as well as to rise gas flow residence time for adsorption. In this case, plastic rashig rings from *Pall Corporation Inc.* were chosen. Their characteristics are presented below.

Rashing rings					
$d_r^e$ (m)	0,006	$a$ ( $\text{m}^2/\text{m}^3$ )	packing factor (Cf)	$\sigma_s$ surface tension (N/m)	free space e
$d_r^e$ (mm)	5,625	320	315	0,036	0,7

Table 43: Pall rashig rings properties

Water is sprayed or distributed from the top of the column (and in some other middle sections, if necessary) and it is percolating downward while wetting the raschig rings. Gas stream flows upward to the opposite direction, so as a counter current fluid-dynamic flow is developed. A figure of traditional wet scrubber packed column is shown below.



Figure 35: wet scrubber packed column ([www.extolhydro.com](http://www.extolhydro.com))

Absorption process is defined by the Henry's law, that states the equilibrium condition between gas and liquid phases concentrations is reached according to system temperature and it can be expressed by the following equation:

$$p_i^* = H_i \cdot x_i^* \quad (45)$$

Contaminant can be therefore transferred from one phase to the other (in this case from gas to water stream) until equilibrium is reached.

As already mentioned, HCl and NH<sub>3</sub> were considered as the main contaminants to be removed in water scrubber unit.

For HCl, Henry constant was calculated by means of the following empirical formula [Zhang et al., 2006]:

$$\ln H_{HCl} = h_0 / T + h_1 \cdot \ln T + h_2 \cdot T + h_3 \quad [\text{kPa}] \quad (46)$$

where  $h_0$ ,  $h_1$ ,  $h_2$ ,  $h_3$  are empirical constant parameters for water-hydrochloric acid system.

For NH<sub>3</sub>, this other formula was used [Hand et al., 1999]:

$$\log H_{NH_3} = -\Delta H / RT + J \quad (47)$$

where  $\Delta H$  is the adsorption energy and  $J$  is an empirical constant. For NH<sub>3</sub>,  $\Delta H = 3,75 \cdot 10^3$  kcal/kmol and  $J = 6,31$ .

Working temperature was chosen as the average between the gas and water values, both of them calculated in the middle section of the column (therefore as the mean value between the inlet and outlet temperatures of the unit, for both of the streams).

Dimensioning of wet scrubber packed column followed a standard procedure [Hand et al., 1999]. From the contaminant mass balance on the overall column, the minimum required water flux for absorption was calculated, by assuming equilibrium of water and gas phases at the exit section of the same water stream (at the bottom of the column) and supposing inlet contaminant concentration in water as zero.

$$Q_l^{\min} = \frac{Q_{gas} \cdot (y_{in} - y_{out}) \cdot H}{y_{in} \cdot P} \quad (48)$$

$y_{in}$  and  $y_{out}$  are respectively the molar fractions of contaminant compound in the gas stream at the inlet and outlet sections of the column.

As inlet concentrations, a range of values was chosen for the two considered species, such as 2000 ÷ 6000 ppmv for NH<sub>3</sub> and 50 ÷ 150 ppmv for HCl. The outlet concentrations were instead fixed to 132 ppmv (100mg/Nm<sup>3</sup>) for NH<sub>3</sub> and 0,6 ppmv (1mg/Nm<sup>3</sup>) for HCl.

$Q_l^{\min}$  was increased by a factor of 3 ÷ 5 (in this case 5) in order to obtain the real water flow through the column.

Diameter of the column was instead dimensioned according to the gas stream pressure drops and the flooding point limitations regarding gas and water mass loadings ratio. Flooding point is indeed the undesired condition by which the column is totally full of liquid and gas bubbles in it. It is mainly due to an incorrect regulation of water and gas flows inside the column.

After choosing acceptable pressure drops per unit length  $\Delta p/L$ , gas mass loading rate  $G_m$  ( $\text{kg}/\text{m}^2 \cdot \text{s}$ ) is initially calculated through the following equations:

$$G_m = \sqrt{\frac{M \cdot \rho_g (\rho_l - \rho_g)}{C_f (\mu_l)^{0.1}}} \quad (49)$$

$$\log_{10}(M) = a_0 + a_1 \cdot E + a_2 \cdot E^2 \quad (50)$$

$$E = -\log_{10} \left[ \left( \frac{Q_g}{Q_l} \right) \sqrt{\left( \frac{\rho_g}{\rho_l} \right) - \left( \frac{\rho_g}{\rho_l} \right)^2} \right] \quad (51)$$

$$a_0 = -6,6599 + 4,3077 \cdot F - 1,3503 \cdot F^2 + 0,15931 \cdot F^3 \quad (52)$$

$$a_1 = 3,0945 - 4,3512 \cdot F + 1,6240 \cdot F^2 - 0,20855 \cdot F^3 \quad (53)$$

$$a_2 = 1,7611 - 2,3394 \cdot F + 0,89914 \cdot F^2 - 0,11597 \cdot F^3 \quad (54)$$

$$F = \log_{10} \left( \frac{\Delta P}{L} \right) \quad (55)$$

Water mass loading rate,  $L_m$  ( $\text{kg}/\text{m}^2 \cdot \text{s}$ ), is then calculated as follows:

$$L_m = \frac{G_m}{\left( \frac{Q_g}{Q_l} \right) \left( \frac{\rho_g}{\rho_l} \right)} \quad (56)$$

and finally sectional area and diameter of the column are obtained:

$$A = \frac{Q_l \cdot \rho_l}{L_m} \quad (57) \quad D = \sqrt{\frac{4 \cdot A}{\pi}} \quad (58)$$

As usually, these calculations were carried out by considering gas flow design values (as gas cleaning line sizes), and pressure drops were subsequently estimated within all the fixed ranges of variability for gas flows.

The height of the column is calculated as the product by two different factors, respectively called *height of transfer unit* and *number of transfer units* [Fair et al., 1985].

The first term is regarding mass transfer resistances in gas or in liquid phases (respectively indicated as  $H_G$  or  $H_L$ ) and it can be considered constant for diluted streams (indicated as  $H_{OG}$  or  $H_{OL}$ ), since in this case mass transfer coefficients can be assumed proportional to gas or liquid streams velocities only.

It assumes different expressions depending on if mass transfer resistance is referred to gas or water phase. In this case, gas phase was considered, so as:

$$H_{OG} = \frac{Q_{gas}}{K_G \cdot a \cdot p \cdot A} \quad (59)$$

$$\frac{1}{K_G \cdot a} = \frac{1}{k_g \cdot a} + \frac{H}{k_l \cdot a_w} \quad (60)$$

H = Henry constant (atm · m<sup>3</sup> / mol)

a<sub>w</sub> is the wet specific surface of the bed provided by the rashig rings (m<sup>2</sup>/m<sup>3</sup>), such as the effective specific surface of the bed that is covered by water stream. It is calculated through the following relation [Onda et al., 1967]:

$$a_w = a \left\{ 1 - \exp \left[ -1,45 \cdot \left( \frac{\sigma_s}{\sigma_w} \right)^{0,75} \cdot \left( \frac{L_m}{a \cdot \mu_l} \right)^{0,1} \cdot \left( \frac{L_m^2 \cdot a}{\rho_l^2 \cdot g} \right)^{-0,05} \cdot \left( \frac{L_m^2}{\rho_l \cdot a \cdot \sigma_w} \right)^{0,2} \right] \right\} \quad (61)$$

σ<sub>w</sub> = surface tension of water (dyn/cm) = 132,674 · (1 - T / T<sub>c</sub>)<sup>0,955</sup>

k<sub>g</sub> and k<sub>l</sub> are mass transfer coefficients respectively for gas and liquid sides. Their expressions were determined empirically [Onda et al., 1967]:

$$k_g = 5,23 \left( G_m / a \cdot \mu_g \right)^{0,7} \cdot \left( \mu_g / \rho_g \cdot D_g^m \right)^{\frac{1}{3}} \cdot \left( a \cdot d_r^e \right)^{-2} \cdot \left( \frac{a \cdot D_g^m}{RT} \right) \quad (62)$$

$$k_l = 0,0051 \left( \frac{L_m}{a_w \cdot \mu_l} \right)^{\frac{2}{3}} \cdot \left( \frac{\mu_l}{\rho_l \cdot D_l^m} \right)^{-0,5} \cdot \left( \frac{\rho_l}{\mu_l \cdot g} \right)^{-\frac{1}{3}} \cdot \left( a \cdot d_r^e \right)^{0,4} \quad (63)$$

D<sub>g</sub><sup>m</sup> and D<sub>l</sub><sup>m</sup> are molecular diffusion coefficients for contaminant compound in gas and liquid phases (values are found in literature).

The second term for the column height dimensioning (*number of transfer units*) is regarding the quantity of material that is assumed to be transferred from gas to liquid phase and, therefore, it obviously depends on gas and water mass loading rates, as well as on the inlet and outlet contaminant concentrations in both of the phases [Fair et al., 1985]:

$$N_{OG} = \frac{1}{1 - (mG_m / L_m)} \ln \left[ \left( 1 - \frac{mG_m}{L_m} \right) \cdot \left( \frac{y_{in} - mx_{in}}{y_{out} - mx_{in}} \right) + \frac{mG_m}{L_m} \right] \quad (64)$$

m = Henry constant, as ratio between contaminant molar fractions in gas and liquid phases, at equilibrium conditions (-)

G<sub>m</sub> and L<sub>m</sub> are mass loading rates of gas and water streams (kg/m<sup>2</sup>·s)

y and x are the real contaminant molar fractions respectively in gas and liquid phase (-). In dimensioning procedure, x<sub>in</sub> is usually set to zero (clean initial water flux).

As already mentioned, wet scrubber packed column height is finally calculated as:

$$H_{column} = H_{OG} \cdot N_{OG} \quad (65)$$

Pressure drops are then obtained as the product of  $\Delta p/L$  by  $H_{column}$ , with the addition of an empirical term referring to concentrated head losses inside the column (depending on gas velocity):

$$\Delta p_{TOT} = \Delta p/L \cdot H_{column} + 275 \cdot u_{gas}^2 \quad (66)$$

In this analysis, wet scrubber packed column is supposed to be used for simultaneous removal of  $NH_3$  and  $HCl$ . For this reason, design was initially carried out for the two contaminants separately. Dimensions, pressure drops and other operating parameters (i.e. water flux) were calculated according to the procedure described above for each raw gas flow and single contaminant concentration.

Successively a single unit was dimensioned for both of the species: the minimum water fluxes separately calculated for the two contaminant species (by means of eq.(48)) were summed and multiplied by a factor of 5. According to the gas flow design values, pressure drops for unit length were chosen as 100 Pa/m for the small unit size and 10 kPa/m for the larger ones.

On the basis of these assumptions, diameters of the column for each unit size were obtained through eqs. (49) – (58). Column height was arbitrarily set as 2m and  $H_{OG}$  was recalculated on the basis of the new water flux value ( $L$  or  $L_m$ ) according to eqs. (59) – (63).

Finally, by means of eq. (64), the obtained outlet contaminants concentrations in the gas stream were compared with the standard limits for the same contaminants, in order to check out efficiency of water scrubber unit at each operating condition (such as gas flows and inlet gas concentrations).

Main dimensions and operating parameters of wet scrubber packed columns are presented in the following table.

	<b>3 – 15 Nm<sup>3</sup>/h (8 Nm<sup>3</sup>/h)</b>	<b>75 – 250 Nm<sup>3</sup>/h (125 Nm<sup>3</sup>/h)</b>	<b>250 – 500 Nm<sup>3</sup>/h (350 Nm<sup>3</sup>/h)</b>
<b>H (mm)</b>	<b>2000</b>	<b>2000</b>	<b>2000</b>
<b>D (mm)</b>	<b>107</b>	<b>164</b>	<b>275</b>
<b>Water flow (l/s)</b>	<b>0,033</b>	<b>0,614</b>	<b>1,79</b>
<b>T<sub>in</sub> gas (C°)</b>	<b>120</b>	<b>120</b>	<b>120</b>
<b>T<sub>out</sub> gas (°C)</b>	<b>30</b>	<b>30</b>	<b>30</b>
<b>T<sub>in</sub> water (°C)</b>	<b>30</b>	<b>30</b>	<b>30</b>
<b>C<sub>out</sub> NH<sub>3</sub> (mg/Nm<sup>3</sup>)</b>	<b>100</b>	<b>100</b>	<b>100</b>
<b>C<sub>out</sub> HCl (ppm)</b>	<b>0,6</b>	<b>0,6</b>	<b>0,6</b>
<b>Packing material</b>	<b>Raschig rings</b>	<b>Raschig rings</b>	<b>Raschig rings</b>
<b>V tank (liters)</b>	<b>200</b>	<b>1000</b>	<b>2000</b>

*Table 44: wet scrubber packed column units dimensions*

As it can be seen, temperature at the gas inlet section is around kept at 120°C, in order to avoid cleaning water vaporization during the contact with the same gas stream. As a consequence, this latter has normally to be cooled down before entering the packed

column, so as losing part of its enthalpy. Moreover, an heat exchanger needs to be inserted into the gas cleaning line at this purpose.

Absorption heats were calculated according to eq.(47), as well. Nevertheless, in the case the total heat capacity of water,  $L_m \cdot c_p^w$ , is much higher than gas one,  $G_m \cdot c_p^g$ , it can be supposed adsorption heat is totally transferred to water stream, while gas is leaving the column at the same temperature of the inlet water stream (in this case, 30°C).

Water stream is then assumed to be recycled through the column until the contaminant concentration reaches the equilibrium value ( $x^*_{out}$ ) corresponding with the one in the exit gas stream (such as the permitted contaminant concentration,  $y_{out}$ ), according to Henry's law.

As a consequence, available water re-circulating time and the number of possible cycles were estimated, as well. At this scope, the volumes of tanks to collect the total amounts of water were arbitrarily chosen a priori. For the small unit size a 200 litres tank was assumed to be used, while for the other two units a 1000 litres tank was considered. Assuming that water stream is clean at the beginning of the first cycle (free of contaminant) and by calculating the total amount of contaminant moles which are transferred to the water stream during the single cycle, their required number to saturate the water stream was possible to be estimated.

Besides, the real velocity of liquid flux through the column was also calculated by means of the following equation:

$$v_w = Q_l \cdot a / (A \cdot \varepsilon \cdot a_w) \quad (67)$$

and therefore the required time for each water cycle was estimated as:

$$t_{cycle} = H_{column} / v_w \quad (68)$$

Finally, the total exhausting time was obtained as the factor of  $t_{cycle}$  by the number of cycles previously estimated.

These calculations were initially achieved for both of the contaminants ( $NH_3$  and  $HCl$ ) separately. Successively, in order to calculate the total saturation time of water stream eq.(44) was used. Results are shown below.

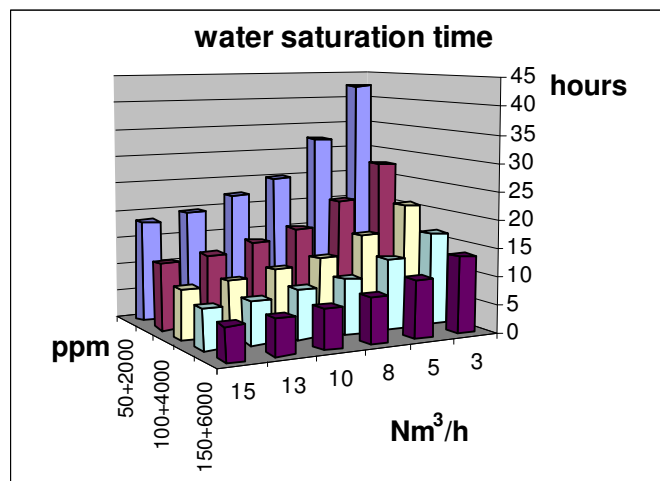


Figure 36a: saturation time of water stream in 3 – 15 Nm<sup>3</sup>/h gas flow wet scrubber unit

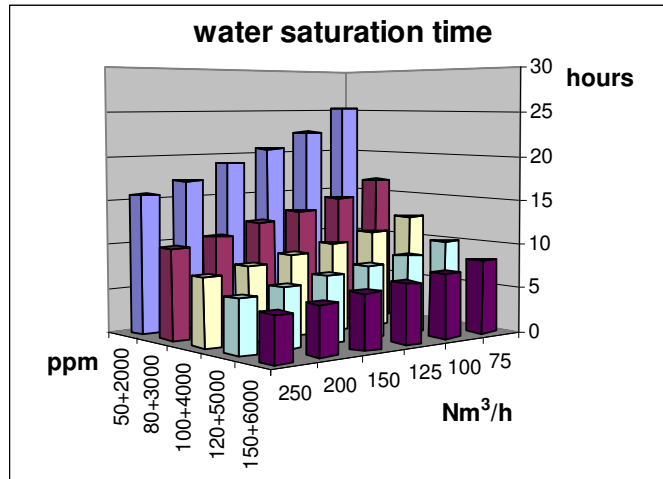


Figure 36b: saturation time of water stream in 75 – 250 Nm<sup>3</sup>/h gas flow wet scrubber unit

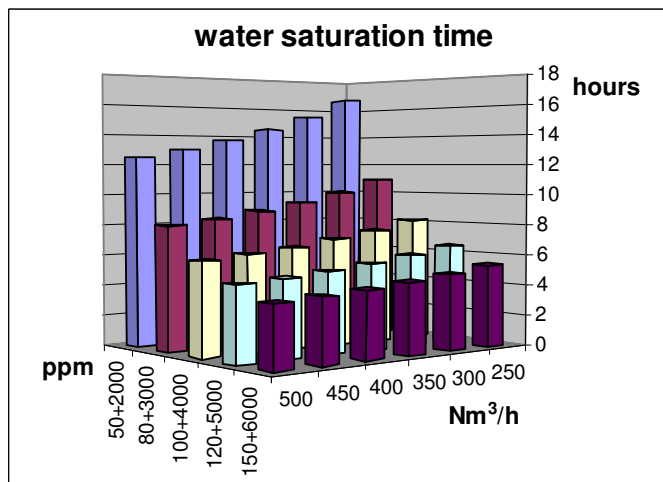


Figure 36c: saturation time of water stream in 250 – 500 Nm<sup>3</sup>/h gas flow wet scrubber unit

Although the water saturation times for the single contaminants absorption are not presented here, it could be checked ammonia is even in this case the contaminant compound that is worse removed from gas stream in respect with the other considered species, such as chloride acid. Therefore, the water saturation times reported in fig. 36a, 36b and 36c can be considered really similar to the ones estimated for the only absorption of ammonia.

According to the water tanks volumes previously defined, they have to be thought very short, especially in the case of the larger cleaning units. Indeed, since water is considered as a non regenerable material in this analysis, on the basis of these results a lot of water consumption would be yearly produced in such applications.

This is mainly due to the high absorption efficiency required to reach the low standard limit of ammonia concentration in the gas stream (100mg/Nm<sup>3</sup>). In order to avoid an high water consumption, it could be thus envisaged to reduce the water scrubber designed efficiency (at least for ammonia removal) and to put downstream an higher performance unit at the same scope.

In this optics, coupling water scrubber and activated carbon adsorption units could be an effective solution, even for the simultaneous removal of the other considered contaminants.

### 5.2.9 Catalytic partial oxidation unit for ammonia decomposition

An alternative method to remove ammonia from gas stream is given by its decomposition through partial oxidation, that is usually carried out in catalytic reactors (selective partial oxidation).

Many catalysts have been already tested for this task even in simulated gasification conditions (such as with adopted gas mixture similar to gasified biomass products) [Jones et al., 2005; Darvell et al., 2003]. One of the most promising catalysts seems hence to be a copper alumina supported material (Cu/Al<sub>2</sub>O<sub>3</sub>) [Jones et al., 2005; Gang Lu et al., 2000].

Indeed, it shows an high ammonia cracking efficiency even at low temperatures (550 – 650K), it is resistant to sulphur deactivation (reaction seems to be even enhanced by H<sub>2</sub>S content at low concentrations [Jones et al., 2005]) and it can be also considered as a stable catalyst during operation [Gang Lu et al., 2000]. Best performances have been registered with Copper loading in the catalyst composition between 7% and 10% mass percentages [Jones et al., 2005; Darvell et al., 2003].

Physical properties of this considered catalytic material are shown below.

<b>Cu/Al<sub>2</sub>O<sub>3</sub> catalyst</b>	
pore volume (ml/g)	0,8
$\rho_{\text{bulk}}$ (kg/m <sup>3</sup> )	800
sphericity $\phi$	0,7
$\epsilon$ bed	0,45
$\rho_s$ (kg/m <sup>3</sup> )	1455
void ratio	0,54
$\rho'_s$ (kg/m <sup>3</sup> )	3147
$k_s$ (W/m*K)	22
$k'_s$ (porous material) (W/m*K)	12

Table 45: physical properties of ammonia partial oxidation catalyst

A fixed bed of 300 $\mu$ m catalyst particles ( $d_g$ ) was considered in this application, in order to achieve operating conditions close to the ones of experimental tests cited above.

The main catalytic reaction can be written as follows:



Its kinetic constant was determined from experimental data [Jones et al., 2005], by assuming first order Arrhenius' law (apparent kinetic constant). Consequently, the formula which were used are:

$$k = k_0 \exp\left(\frac{-E_a}{RT}\right) \quad (70)$$

$$k = -\ln\left[\frac{(1-X)}{t}\right] \quad (71)$$

X is the ammonia conversion factor at different temperatures, whose values were obtained from the experimental tests reported in literature. Time  $t$  corresponding to the same experimental tests was calculated as 0,21s, from the mass space velocity and bed material amount adopted in the empirical procedure.

By plotting  $k$  values versus  $1/T$  in a logarithmic scale,  $k_0$  and  $E_a$  parameters were obtained, respectively as  $E_a = 34272 \text{ J/mol}$  and  $K_0 = 1068\text{s}^{-1}$ . According to the operating temperature at which catalytic unit is assumed to work in the gas cleaning line (around  $350^\circ\text{C}$ ), kinetic constant  $k$  was calculated. This value was then decreased by a factor as 0,9 in order to take in account the efficiency loss that is usually detected during the first hours of catalytic activity [Gang Lu et al., 2000].

Dimensioning of catalytic units was carried out according to the plug flow axial dispersion model (see par. 5.2.5). Eq.s (23) – (29) were still used in order to estimate fixed bed volume, considering a constant ammonia conversion factor as 0,98 for each gas flow design value. Indeed, Initial ammonia concentration in the gas stream was still chosen in a range of 2000 – 6000 ppmv and standard emission limit was still kept at 132 ppmv ( $100\text{mg/Nm}^3$ ), so that  $X = 0,98$  resulted as the required efficiency value in order to reach the standard concentration limit with the maximum initial contaminant concentration in the gas stream (6000ppmv).

Bed diameters were still estimated according to pressure drops limitations (200mbar for the small unit and 250mbar for the larger ones), and eq.(9) was still used for their estimation, with the addition of gas distributors head losses.

The main results on catalytic units dimensioning for partial oxidation of ammonia are reported in table 46.

	<b>Fixed bed</b>		
	<b>3 – 15 Nm<sup>3</sup>/h (8 Nm<sup>3</sup>/h)</b>	<b>75 – 250 Nm<sup>3</sup>/h (125 Nm<sup>3</sup>/h)</b>	<b>250 – 500 Nm<sup>3</sup>/h (350 Nm<sup>3</sup>/h)</b>
<b>H (mm)</b>	280	260	250
<b>D (mm)</b>	500	940	1620
<b>d<sub>g</sub> (mm)</b>	0,3	0,5	0,5
<b>Kg cat</b>	25	144	412
<b>C<sub>in</sub> (ppmv)</b>	4000	4000	4000
<b>X<sub>design</sub></b>	0,98	0,98	0,98
<b>O<sub>2</sub>/NH<sub>3</sub> vol.</b>	<b>7</b>	<b>7</b>	<b>7</b>

Table 46: dimensions for catalytic ammonia decomposition units

An analysis on ammonia conversion factor as a function of gas flow (within the variability gas flow ranges) was also carried out for the dimensioned units, as it is reported the following figures 37a, 37b and 37c.

It can be seen that conversion factor analysis shows a downwards parabolic curve for each dimensioned unit, so that this has a maximum point in correspondence with a particular gas flow value. For other even lower gas flows, conversion factor proved decreased in spite of the lower mass contaminant loadings, as well. This unexpected trend can be maybe explained by the assumption of plug flow axial dispersion model, according to which larger transition zones of bed volume have to be considered for lower gas superficial velocities, so that the effective available volume for catalytic reactions is reduced, so as conversion factor.

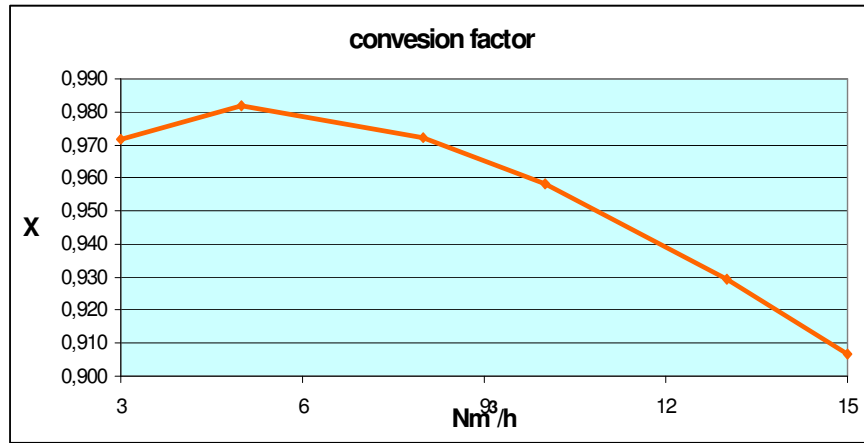


Figure 37a: conversion factor as a function of gas flow for 3 – 15 Nm<sup>3</sup>/h ammonia decomposition unit

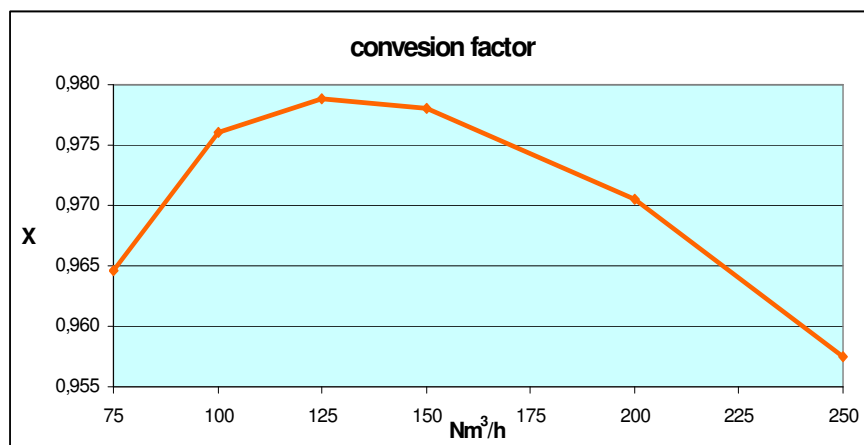


Figure 37b: conversion factor as a function of gas flow for 75 – 250 Nm<sup>3</sup>/h ammonia decomposition unit

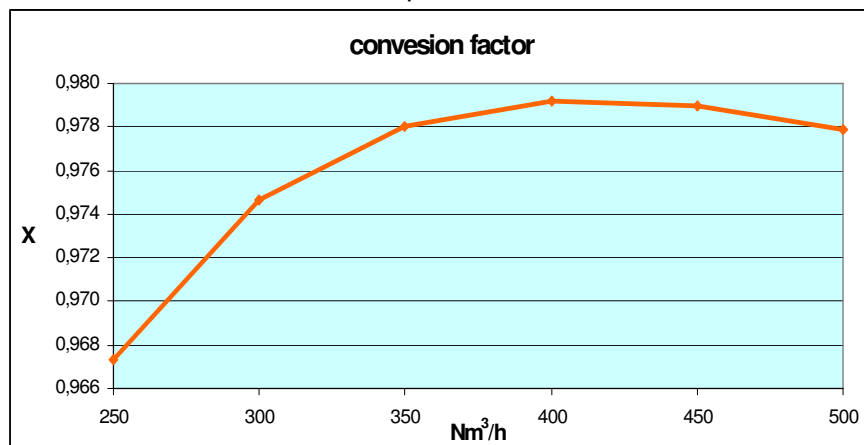


Figure 37c: conversion factor as a function of gas flow for 250 – 500 Nm<sup>3</sup>/h ammonia decomposition unit

As already said and as it can also be seen from reaction (69), ammonia decomposition is obtained by partial oxidation. Although the stoichiometric coefficient of the mentioned reaction is 0,75, an O<sub>2</sub>/NH<sub>3</sub> volumetric ratio as 7 is suggested to be adopted in practical applications (Gang Lu et al., 2000) in order to achieve the complete development of reaction.

Moreover, copper catalyst is able to enhance hydrogen oxidation too, according to the following reaction:



Therefore, an unavoidable consumption of hydrogen has also to be accounted when partial oxidation of ammonia is accomplished.

According to the predicted values of ammonia concentrations in the product gas stream (see table 32), this consumption was estimated as percentage of the total hydrogen content of gas, as it was calculated from its composition reported in table 30.

From figure 38 a very high hydrogen consumption can be noted. For the highest considered ammonia concentration (6000ppm), even half of the initial total amount of hydrogen is indeed oxidized. Therefore, it can be concluded that ammonia partial oxidation technology can be better envisaged as a gas refining method than a proper removal technology, such as it can be mainly taken into account in such applications where contaminant concentrations are one or two orders of magnitude less than the considered ones.

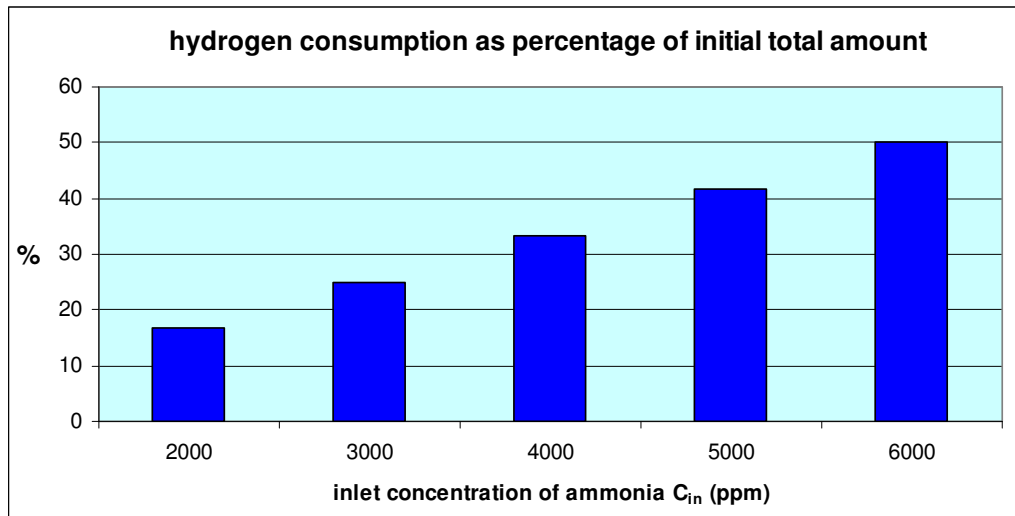


Figure 38: hydrogen consumption in ammonia partial oxidation process, as percentage of the initial total amount contained in the raw gas stream

### 5.2.10 HCl dry adsorption unit

In biomass gasification applications, one of the most usual products derived from the fuel chloride content is chloride acid, HCl, such as a reactive, very corrosive and toxic gas. Therefore, both for environmental pollution control and for protection of cogeneration unit devices (from corrosion, above all) it needs to be removed from raw syngas stream.

Besides wet scrubber (see par. 5.2.8), another effective method for HCl abatement is the chemical dry adsorption, especially adopted in such applications where high syngas temperature are still required at the exit of gas cleaning system.

Most of HCl sorbents are non regenerable minerals (alumina, alkaline earth carbonates or oxides, activated carbons, etc.). On the basis of some successful experimental tests [Krishnan et al., 1996] achieved in this application, Nahcolite (or Sodium bi-carbonate,  $\text{NaHCO}_3$ ) mineral was considered as material bed for the fixed bed adsorption units in this work. Bed material size was assumed as 5mm, like mineral particles dimension already used in the experimental analysis. The other mineral properties are shown in the following table 47.

<b>Nahcolite NaHCO<sub>3</sub></b>	
pore volume (ml/g)	0,35
$\rho_{\text{bulk}}$ (kg/m <sup>3</sup> )	540
$\phi$	0,7
$\varepsilon$ bed	0,5
$\rho_s$ (kg/m <sup>3</sup> )	1080
void ratio	0,500
$\rho'_s$ (kg/m <sup>3</sup> )	2159
Dm (cm <sup>2</sup> /s)	2,52
$k_s$ (W/m <sup>2</sup> *K)	1
$k'_s$ (W/m <sup>2</sup> *K)	0,55

Table 47: physical properties of HCl mineral sorbent

HCl concentrations in the raw gas stream were considered in the range 30 –150 ppmv and standard limit was fixed as 0,6 ppmv (1mg/Nm<sup>3</sup>).

Gas superficial velocities in adsorption units were set as 10cm/s for the small size unit (8 Nm<sup>3</sup>/h gas flow) and 15 cm/s for the larger ones, in order to almost achieve the same working conditions of experimental tests ( $u = 13,3$  cm/s). On the basis of these values, units diameters were calculated according to gas flow design values, as usually. Bed heights were arbitrarily fixed as 10cm for the small unit and 15cm for the larger ones, in order to always have the same mass space velocity (2,4h<sup>-1</sup>). Units dimensions resulting from these assumptions are presented in table 48.

Eq.(28) was still used to estimate the effective volume of the bed, while the following equation (73) was used as breakthrough curve expression [Krishnan et al., 1996] in order to predict the units available working time before the concentration limit is reached at the exit section of the bed (breakthrough points)

$$\frac{Y_{out}}{Y_{in}} = \frac{\exp \frac{k \cdot P \cdot Y_{in} \cdot t}{S_{max} \cdot M_{Cl}^{-1}}}{\exp \frac{k \cdot P \cdot Y_{in} \cdot t}{S_{max} \cdot M_{Cl}^{-1}} + \exp \frac{k \cdot \rho_s \cdot R \cdot T \cdot z}{u} - 1} \quad (73)$$

$S_{max}$  is the maximum sorption capacity of solid (0,58 g<sub>Cl</sub>/g<sub>s</sub>) and k is the apparent first order kinetic constant (5,2 mol<sub>HCl</sub> · atm<sup>-1</sup> · g<sup>-1</sup> · h<sup>-1</sup>).

	<b>Fixed bed</b>		
	<b>3 – 15 Nm<sup>3</sup>/h (8 Nm<sup>3</sup>/h)</b>	<b>75 – 250 Nm<sup>3</sup>/h (125 Nm<sup>3</sup>/h)</b>	<b>250 – 500 Nm<sup>3</sup>/h (350 Nm<sup>3</sup>/h)</b>
<b>H (mm)</b>	100	150	150
<b>D (mm)</b>	260	880	1500
<b>d<sub>g</sub> (mm)</b>	5	5	5
<b>Kg ads.</b>	3	51	143
<b>mass space vel. (h<sup>-1</sup>)</b>	2,4	2,4	2,4
<b>C<sub>out</sub> HCl (ppmv)</b>	0,6	0,6	0,6

Table 48: HCl adsorption units dimensions

Estimated breakthrough points as a function of gas flows and Inlet contaminant concentrations are shown in the following charts, for the three dimensional unit sizes.

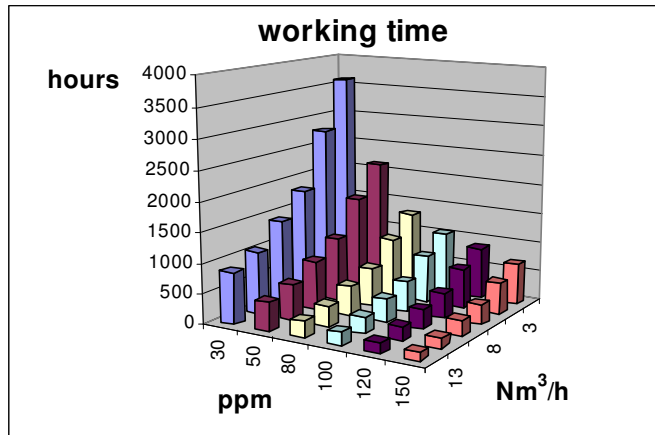


Figure 39a: breakthrough points for HCl adsorption unit of 3 – 15 Nm<sup>3</sup>/h gas flow size

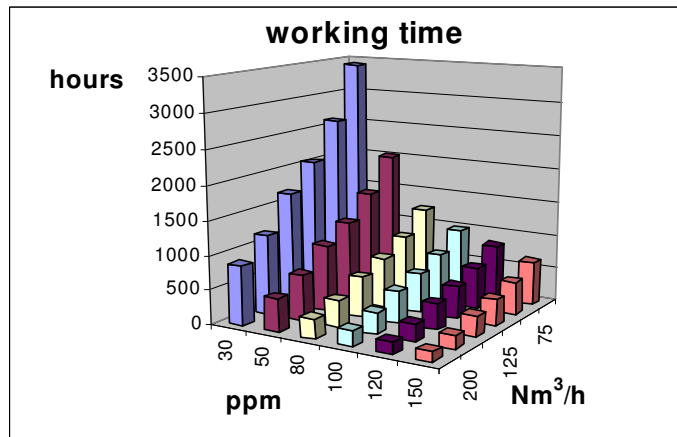


Figure 39b: breakthrough points for HCl adsorption unit of 75 – 250 Nm<sup>3</sup>/h gas flow size

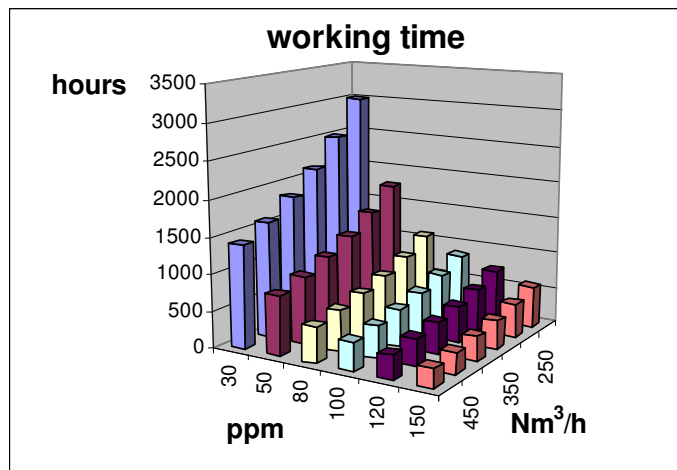


Figure 39c: breakthrough points for HCl adsorption unit of 250 – 500 Nm<sup>3</sup>/h gas flow size

### 5.2.11 Dry scrubbing of alkali metals

The alkali species which are of main concern in biomass gasification applications (especially in the case of non woody biomasses conversion) are Sodium and Potassium. At the usual gasification temperatures, these elements are released to the syngas stream as alkali sulphates or alkali chlorites, according to the relative contents of chlorine and sulphur in solid fuel elementary composition [Uberoi M et al., 1990].

Nevertheless, both alkali sulphates and alkali chlorites are characterized by a great corrosion capacity towards the traditional materials which gasifiers and gas cleaning devices are made of. Indeed, through their nucleation as metal aerosols (sub micron particles and droplets), they also act as a binder for fly ashes, by giving them a sticky behaviour and by decreasing their melting point, as well. Therefore, a corrosive ash deposition along gas cleaning line equipments is usually detected when fuels with high alkali metals contents are gasified.

The only practical difference between alkali sulphates and alkali chlorites is due to their condensation temperatures. Sulphates condense at temperatures below 600 °C, so that they are supposed to already nucleate around solid particles surface (char and ashes) at the exit section of gasification unit. As a consequence, they are also supposed to be removed from the raw gas stream in the same units adopted for particulate collection (cyclone and filters). In this case, ash deposition on the inner walls of cyclone could be only found out as an operational issue to be faced to. If so, *in situ* (inside the gasifier) alkali removal techniques would be required.

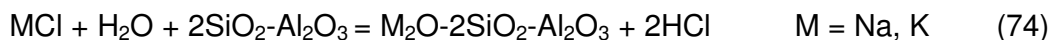
On the contrary, alkali chlorites condense at lower temperature, so that they are the main cause of corrosion and ash deposition along the other gas cleaning line equipments, as well as on the moving parts of cogeneration units.

For this reason alkali metals were all considered as alkali chlorites in this analysis, and their concentration was related to the maximum chlorine content of biomass fuel. By choosing one of the highest values of chlorine content for woody biomasses, the resulting alkali concentration in raw gas stream was estimated as 0,45g/Nm<sup>3</sup>

In order to achieve alkali abatement in the first sections of the overall gas cleaning line, as well as to avoid the use of further single units at this scope, dry scrubbing technology was considered for chemical adsorption of alkali metals from syngas.

It practically consists on the injection of solid particles of alkali adsorber materials upstream the candle or fabric filters arranged in the same gas cleaning line, so that they are able to adsorb alkali metal gases on their external surface and successively they are in turn trapped by the same filters used for particulate collection (see fig. 41).

According to some experimental tests on alkali adsorption capacity [Turk B.S et al., 1996; Uberoi M et al., 1990], kaolinite mineral (2SiO<sub>2</sub>-Al<sub>2</sub>O<sub>3</sub>) seems to be the best promising sorbent material. Therefore it was considered as the alkali getter for this application, too. Its corresponding adsorption reaction can be hence written as follows:



It can be seen that HCl is also produced by this reaction. Therefore, some dedicated units are to be foreseen for the abatement of this secondary product, as well (see par. 5.2.8 – 5.2.10).

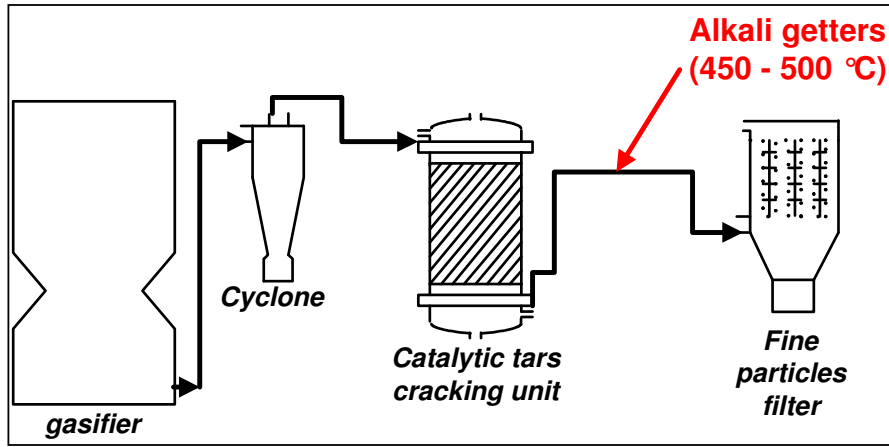


Figure 40: dry scrubbing overall scheme

The maximum adsorption capacity of kaolinite was found to be  $0,023 \text{ mol}_{\text{MCl}}/\text{cm}^3_{\text{s}}$  [Uberoi M et al., 1990] and its particle density was estimated as  $2160 \text{ kg/m}^3$  (from literature). According to these parameters and considering a constant initial contaminant concentration in the raw gas stream as  $0,45 \text{ g/Nm}^3$ , the adsorber material mass loadings required for the total adsorption of alkali metals were calculated for the three gas cleaning line sizes and at the different gas flow conditions, as it is reported in table 49.

$C_{\text{MCl}} \text{ (g/Nm}^3\text{)}$	$\text{g/h } 2\text{SiO}_2\text{-Al}_2\text{O}_3$						
<b>0,45</b>	14	23	<b>38</b>	47	61	70	<b>3 – 15 Nm<sup>3</sup>/h (8 Nm<sup>3</sup>/h)</b>
	442	589	<b>737</b>	884	1179	1473	<b>75 – 250 Nm<sup>3</sup>/h (125 Nm<sup>3</sup>/h)</b>
	1601	1921	<b>2242</b>	2562	2882	3202	<b>250 – 500 Nm<sup>3</sup>/h (350 Nm<sup>3</sup>/h)</b>

Table 49: sorbent material mass loadings required for the total adsorption of estimated alkali amounts

These values were successively added to the particulate mass loadings considered in candle and fabric filters dimensioning (see par. 5.2.3 – 5.2.4), in order to re-calculate the effective pressure drops for these latter units.

Moreover, the time for complete alkali adsorption was also estimated according to the supposed initial concentrations in gas stream, and it was then compared with the filters regeneration frequency (fixed as 30min, for both candle and fabric filters). The adsorption time was thus checked to be lower than the cake formation one on the external surface of filters. For this calculation, the following two formula were used [Levenspiel O., 1962]:

$$\tau = \frac{\rho_m \cdot r_p}{k' \cdot C_o} \quad (75)$$

where  $\tau$  is the time for complete conversion of solid sorbent and  $k'$  is the surface kinetic constant estimated from experimental data.

In order to know the alkali adsorption time,  $t_{\text{ad}}$ , this second relation was also considered [Levenspiel O., 1962]:

$$\frac{t_{\text{ad}}}{\tau} = 1 - (1 - X)^{\frac{1}{3}} \quad (76)$$

where  $X$  is the solid conversion ratio, calculated in this case as maximum adsorption capacity of kaolinite divided by its molar density.

### 5.3 Gas cleaning line assembly

As second step of the analysis on gasified biomass cleaning systems, the development of a simple methodology by which previously analyzed gas cleaning units can be assembled together was achieved, with the scope of arranging overall gas cleaning lines which are suitable to clean the product gas up to the standard quality degree required for cogeneration units utilization (see tab. 33).

This methodology was simply set up by detecting some operational constraints which limit the right functioning of the cleaning system. Some of them are dealing with the best working conditions for single gas cleaning units (temperature, above all) while others are mainly concerning the correct settlement of their relative positions in the overall gas cleaning line arrangement.

Moreover, some assumptions on gas cleaning line design were also considered in order to reduce the field of investigation and focusing on some simpler configurations only.

One of these initial assumptions is that any gas (re)heating system is not inserted in the gas cleaning line, so as the maximum gas stream temperature is registered at the exit of gasification unit (500°C, [Svensk Maskinprovning. Gengasdrift av en överladdad dieselmotor, 1988]) and a decreasing temperature profile is developed along the cleaning equipments. Possible heat exchangers are assumed to be gas coolers only, and cleaning devices temperature is kept constant by the only mean of insulation materials, when necessary.

In the following paragraphs, the main technical barriers which were taken into account for gas cleaning line configurations set up are shortly described, by focusing on the solutions which were adopted for their overcoming.

As a simplification, in this second part of the analysis, gas flow design values corresponding to the three gas cleaning line sizes were considered only, and initial contaminant concentrations were fixed as follows:

<b>Initial contaminants concentration</b>		
<b>particulate</b>	<b>10</b>	<b>g/Nm<sup>3</sup></b>
<b>tars</b>	<b>30</b>	<b>g/Nm<sup>3</sup></b>
<b>Sulphur (H<sub>2</sub>S)</b>	<b>200</b>	<b>ppmv</b>
<b>Nitrogen (NH<sub>3</sub>)</b>	<b>4000</b>	<b>ppmv</b>
<b>Chlorine (HCl)</b>	<b>100</b>	<b>ppmv</b>
<b>Alkali metals</b>	<b>0,45</b>	<b>g/Nm<sup>3</sup></b>

Table 50: considered inlet contaminants concentrations for gas cleaning lines assembly

### 5.3.1 Gas cleaning line temperature profile

As already mentioned, one of the main constraints according to which gas cleaning line arrangements were fixed is the achievement of the optimal working temperatures for each gas treatment unit. Since the maximum raw gas temperature in the cleaning line is registered at the exit of gasifier (fixed as 500°C), all the cleaning devices were chosen among the ones whose working temperature is lower than this predetermined value.

Once their relative positions in the overall arrangement were defined (according to the other operational issues described below, as well), corresponding inlet and outlet gas temperatures were estimated by calculating convective heat loss to the external environment. It was therefore checked out that the mean gas temperature inside each unit was close to the optimal one for the right working conditions (see fig. 19). If this condition was not verified, insulation material was assumed to be used or even unit position was changed.

As said, working temperature of each single unit was always considered as the average of inlet and outlet temperature of gas stream flowing through it ( $T_m$ ). Outlet temperature,  $T_{out}$ , was calculated by means of the following energy balance:

$$\dot{m} \cdot c_{p, gas} \cdot (T_{in} - T_{out}) = \Delta H'_i + \Delta H'_{ex} \quad (77)$$

$\Delta H'_i$  = process heat, related to the gas treatment process accomplished inside the unit [W]

$\Delta H'_{ex}$  = heat loss by external convective exchange [W]

Assumed  $\Delta H_i$  (kJ/mol or kJ/kg) for the different cleaning processes are presented in the following table:

	$\Delta H_i$	reference
Particles collection	-	-
Tars cracking	-42 (kJ/kg)	From the analysis of heats of formation
Chemical adsorption of H <sub>2</sub> S (Zn-Ti adsorber)	-74,1 (kJ/mol)	[Yrjas et al., 1996]
Physical adsorption of H <sub>2</sub> S, NH <sub>3</sub> (activated carbon adsorber)	-45 (kJ/mol), -40 (kJ/mol)	.....
Ammonia partial oxidation	-314,65 (kJ/mol)	Jones et al., 2005
Chemical adsorption of HCl (Nahcolite)	-224,5 (kJ/mol)	.....
Alkali chemical adsorption (kaolinite)	-	-
NH <sub>3</sub> absorption (water scrubber)	-36,15 (kJ/mol)	Analytical estimation from Henry constant values
HCl absorption (water scrubber)	-78,1 (kJ/mol)	Analytical estimation from Henry constant values

Table 51: process heats in different gas cleaning units

For fixed bed units,  $\Delta H_{ex}$  was always estimated by means of the following equation:

$$\Delta H_{ex} = \frac{\pi \cdot \Delta T \cdot L_{bed}}{\frac{1}{h_{bed} \cdot D_i} + \ln\left(\frac{D_e}{D_i}\right) \frac{1}{2k_w} + \ln\left(\frac{D_{ins}}{D_e}\right) \frac{1}{2k_{ins}} + \frac{1}{h_{air} \cdot D_{ins}}} \quad (78)$$

$$\Delta T = T_m - T_{ex}$$

$T_{ex}$  is room temperature [K]

$D_i$  and  $D_e$  are inner and external bed diameters respectively [m]

$D_{ins}$  is the unit diameter including insulation material layer [m]

$k_w$  and  $k_{ins}$  are thermal conductivities, respectively for bed walls and insulation material [W/m·K]

$h_{air}$  is the convective heat transfer coefficient for external (air) side. It was calculated as:

$$h_{air} = \frac{Nu_{air} \cdot k_{air}}{D} \quad (79)$$

$k_{air}$  is air thermal conductivity [W/m·K]

$$Nu_{air} = 0,12 \cdot (Pr \cdot Gr)^{1/3} \quad (80)$$

$$Pr = \frac{\mu_{air} \cdot C_p}{k_{air}} \quad (81)$$

$$Gr = \frac{9,81 \cdot \rho_{air}^2 \cdot D^3 \cdot \beta \cdot \Delta T}{\mu_{air}^2} \quad (82)$$

$\beta$  = air thermal compressibility [0,0033K<sup>-1</sup>]

$h_{bed}$  is the overall heat exchange coefficient between bed and inner walls of unit. It is calculated by means of the following relation:

$$h_{bed} = \frac{2k_e^o}{d_g} + 0,05 \cdot c_p \cdot \rho_g \cdot u \quad (83)$$

$$k_e^o = \varepsilon \cdot k_{gas} + (1 - \varepsilon) \cdot k_s \left[ \frac{1}{\phi_w \left( \frac{k_s}{k_{gas}} \right) + \frac{1}{3}} \right] \quad (84)$$

$\phi_w$  represents the film thickness (as a ratio with bed particle size) within the heat exchange is supposed to be developed, It is empirically estimated according to  $k_s/k_{gas}$  ratio [Kunii et al., 1969]

Thermal insulation was necessary for tars cracking and H<sub>2</sub>S chemical adsorption units. In both of the cases and for all the unit sizes, expanded perlite was chosen as insulation material ( $k_{ins} = 0,002 \text{ W/m}\cdot\text{K}$ ) and a layer of 10 cm was estimated enough to keep constant temperature inside the beds.

For cyclone and candle/fabric filter vessels  $\Delta H'_{ex}$  was calculated as:

$$\Delta H'_{ex} = K_{ex} \cdot A \cdot \Delta T \quad (85)$$

$$\Delta T = T_m - T_{ex}$$

A = total external surface of unit [m<sup>2</sup>]

$K_{ex}$  = overall heat exchange coefficient [W / m<sup>2</sup> K]

$$K_{ex} = 1 / (1/h_{gas} + s/k_w + 1/h_{air}) \quad (86)$$

$h_{gas}$  is the heat transfer coefficient for gas side and it is estimated through the following relations:

$$h_{gas} = Nu \cdot k_{gas} / D \quad (87)$$

$$Nu = 0,023 \cdot Re^{0,8} \cdot Pr^{0,333} \quad (88)$$

$$Pr = \frac{\mu \cdot C_p}{k_{gas}} \quad (89)$$

$$Re = \frac{u \cdot \rho_g \cdot D}{\mu} \quad (90)$$

In the case of cyclone, D is the main body diameter of the unit while  $v_i$  is the inlet tangential velocity of gas (in order to take in exam the vortical fluid-dynamics inside the cyclone). For filters vessels, instead, D is still the main diameter of the unit but  $v_i$  is the ratio between gas flow and the cross sectional area of the same vessel.

Only for water scrubber packed column, inlet and outlet temperatures of gas were fixed a priori, and absorption heat was supposed to be totally transferred to water flux (see par. 5.2.8).

Since  $T_{out}$  is present in both of the right and left sides of eq.(77), its estimation was carried out by an iterative procedure (in *Excel* sheets).

### 5.3.2 Clogging of pipes and filters by tars condensation

One of the most usual problems to be solved in gas cleaning operations is represented by the high frequency of filters clogging and narrow sections plugging, especially due to the simultaneous tars condensation and solid particles trapping by the same tars droplets. The sticky material that is formed by this mechanism usually deposits on the colder and narrow sections of the gas cleaning line or in the first layers of packed bed units.

In this latter case, pressure drops of packed beds rapidly increase, even if almost the total bed of filter is still clean. On line methods of filter regeneration are often not sufficient, as well.

Tars condensation is quite detrimental for candle and fabric filters as well, since their droplets can penetrate into the inner layers of filter mediums and blind them irreversibly.

For these reasons, gas cleaning line arrangements were always set up by avoiding tars condensation in any section of the line where fine particles are still present.

Nevertheless, since raw gas temperature at the exit of cyclone (always the first unit in gas cleaning line), is close to the tars condensation one (at least for the heavier compounds), such as around 400-450 °C, fine particles filters (i.e. candle or fabric ones) can't even be put immediately downstream the cyclone without the risk to blind them.

The only solution that was thus accepted to face clogging and plugging problems was the use tars cracking units to be inserted between cyclone and particle filters, in order to eliminate tars instead of enhancing their condensation.

As a consequence, the first three units of gas cleaning line arrangements always resulted to be the same, such as cyclone, catalytic tars cracking unit and fine particles filters.

Among these latter, fabric filters were chosen in all of the cases, especially for their lower pressure drops. Nevertheless, they also show an higher cleaning gas (nitrogen) consumption in respect with candle filters (3÷4 times more), so that this choice could be even better evaluated, on the basis of particles collection efficiency as well.

### **5.3.3 Materials corrosion**

All the materials which gas cleaning equipments are made of are assumed to be resistant to chemical corrosion, even at high temperature. For this reason, ceramic filters would be preferred to metal sintered ones in the case candle filters were used for particles collection.

The most corrosive contaminant species considered in this work are HCl and Alkali metals. Neglecting the corrosive effect of HCl (since it is not involved in nucleation mechanisms), alkali metals were only considered from this point of view. Therefore, they were always supposed to be removed in the first sections of gas cleaning line (see par. 5.2.11). Dry scrubbing was then chosen as the best solution, so as to avoid the insertion of a further single adsorption unit that could increase total pressure drop and have negative effects on temperature profile.

### **5.3.4 Catalyst poisoning**

Catalytic materials are usually poisoned and deactivated by different compounds which react with them in irreversible processes. Among these poisoning substances, sulphur components are certainly some of the most reactive ones and they are also present in syngas stream quite often.

For this reason, all the catalytic materials considered in this work (both for tars cracking and for ammonia partial oxidation) were chosen among the ones which were proven to be sulphur resistant in proper experimental tests. For ammonia partial oxidation catalyst, it was even demonstrated [Jones et al., 2005] that catalytic reaction was enhanced by low H<sub>2</sub>S concentrations in the gas stream.

However, on the basis of the different methods which were in turn used for H<sub>2</sub>S abatement (such as chemical or physical adsorption), catalytic partial oxidation unit for ammonia decomposition was inserted both upstream and downstream the sulphur removing equipments, according to their relative optimal working temperatures,

### **5.3.5 Frequency of regeneration**

As seen in the previous paragraphs, most of the materials used for syngas treatment need to be cleaned or regenerated after an estimated saturation time, which mainly depends on gas flows and inlet contaminant concentrations, as well as maximum allowable pressure drops. Except for catalytic tars cracking unit, the available working time for each other equipment was arbitrarily fixed not less than 24 hours, in order to simulate gas cleaning systems working conditions as similar as possible to real applications.

## 6 RESULTS AND DISCUSSIONS

On the basis of the performances analysis on gas cleaning units described in the previous chapter and according to the methodology adopted for their assembly, several basic arrangements were determined as possible alternatives for overall gas cleaning systems. For simplicity, they are called *paths* thereafter, as it is shown the following figure.

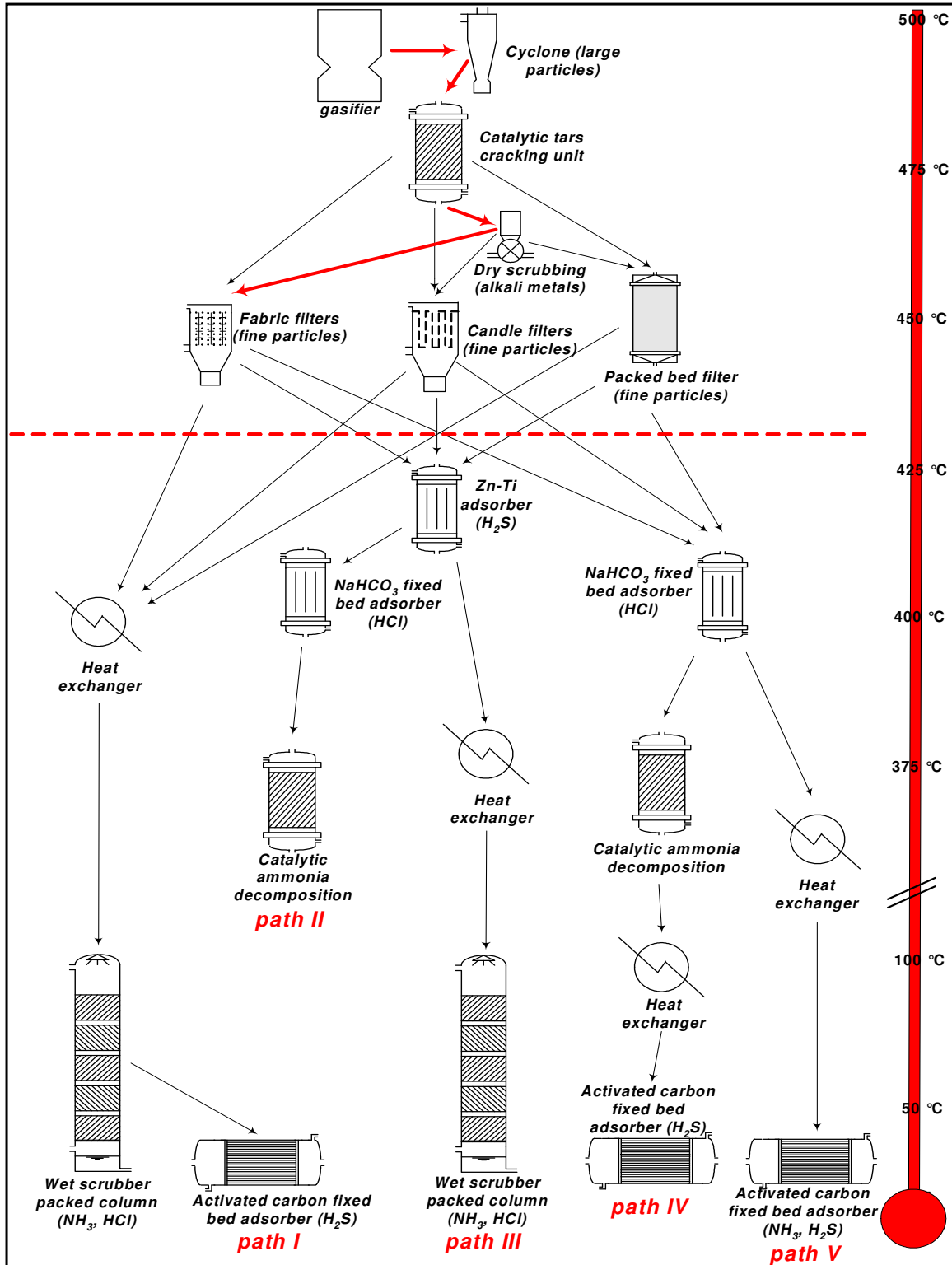


Figure 41: determined arrangements for gas cleaning line (paths)

As explained in par. 5.3.2 and 5.3.3, all these *paths* show cyclone, catalytic tars cracking unit, alkali dry scrubbing device and fabric filters as the first four units of the gas cleaning line. Differences among them are therefore detected for the further downstream equipments only.

By following the analytical procedures described in par. 5.2, gas cleaning units included in each of the five *paths* were dimensioned more than once, according to their relative position in each single cleaning line (which working temperatures and inlet gas flow are affected by) and to the gas flow design values fixed for the three gas cleaning line sizes.

For heat exchangers, instead, thermal energy released by the gas stream cooling operation was calculated only.

Besides dimensions, efficiencies and pressure drops, secondary materials consumptions by the single units were also calculated during both cleaning and regeneration steps, so that each *path* was finally characterized by the estimation of the following parameters:

- Total pressure drop, such as the pressure drop calculated from the exit section of gasifier to the exit section of the last unit in the *path*.
- Total temperature drop, such as gas stream temperature decrease between the exit section of the gasifier (500°C) and the exit section of the last unit in the *path*
- Total enthalpy loss, such as the sum of the enthalpy losses for all the units included in the *path*, calculated in an overall working period as 8000 hours.

The loss of enthalpy for the single unit was thus calculated as:

$$\Delta h_i = m' \cdot c_{p\ gas} \cdot (T_{in} - T_{out}) + Q_{i\ gas} \cdot \Delta p_i + \lambda_{cond} \cdot Q_{w\ cond} \quad (91)$$

$Q_{w\ cond}$  = mass flow of condensed water, calculated as the difference of water vapour content in the gas at the inlet section of the unit and the vapour saturation content in the same unit at gas outlet temperature.

$\lambda_{cond}$  = condensation latent heat of water (2260 kJ/kg)

(The term  $\lambda_{cond} \cdot Q_{w\ cond}$  was calculated for heat exchangers and wet scrubber packed columns only)

- Air consumption, as the total amount of air consumed for the regeneration of tars cracking catalysts and Zn-Ti sulphur adsorbers, during an overall gas cleaning line working period as 8000 hours
- Kaolinite consumption, as the kaolinite mineral quantity consumed for alkali metals dry scrubbing during an overall gas cleaning line working period as 8000 hours
- Nitrogen consumption, as the total amount of nitrogen used in the jet pulse cleaning system of fabric filters, corresponding to an overall gas cleaning line working period as 8000 hours
- Water consumption, as the total amount of water consumed in the wet scrubbing operations, during an overall working period as 8000 hours
- Vapor consumption, as the necessary steam amount consumed for the regeneration of activated carbon material, during an overall gas cleaning line working period as 8000 hours
- Nahcolite consumption, as the nahcolite mineral quantity consumed for HCl dry adsorption, during an overall working time as 8000 hours
- Oxygen consumption, as the total oxygen amount consumed for the catalytic partial oxidation of ammonia, in an overall working period as 8000 hours.

- Number of units, such as the total number of gas cleaning units included in the *path* with the addition of one for each present tandem arrangement (such as in the case of catalytic tars cracking unit and activated carbon H<sub>2</sub>S adsorber)

In the following tables, all these mentioned quantities are reported for all the *paths* and for each gas cleaning line size.

$\Delta p_{TOT}$ (bar)	$\Delta T_{TOT}$ (°C)	$\Delta h_{TOT}$ (W)	kg air	kg Kaolinite	kg N <sub>2</sub>	kg water	kg vapor	kg Nahcolite	kg O <sub>2</sub>	n	<i>path I</i>
0,102	474	1962	17164	300	23585	117216	769	-	-	7 + 2	
$\Delta p_{TOT}$ (bar)	$\Delta T_{TOT}$ (°C)	$\Delta h_{TOT}$ (W)	kg air	kg Kaolinite	kg N <sub>2</sub>	kg water	kg vapor	kg Nahcolite	kg O <sub>2</sub>	n	<i>path II</i>
0,404	175	800	17273	300	23585	-	-	37	2560	7 + 1	
$\Delta p_{TOT}$ (bar)	$\Delta T_{TOT}$ (°C)	$\Delta h_{TOT}$ (W)	kg air	kg Kaolinite	kg N <sub>2</sub>	kg water	kg vapor	kg Nahcolite	kg O <sub>2</sub>	n	<i>path III</i>
0,186	470	2077	17273	300	23585	130435	-	-	-	7 + 1	
$\Delta p_{TOT}$ (bar)	$\Delta T_{TOT}$ (°C)	$\Delta h_{TOT}$ (W)	kg air	kg Kaolinite	kg N <sub>2</sub>	kg water	kg vapor	kg Nahcolite	kg O <sub>2</sub>	n	<i>path IV</i>
0,326	475	2025	17164	300	23585	-	792	37	2560	8 + 2	
$\Delta p_{TOT}$ (bar)	$\Delta T_{TOT}$ (°C)	$\Delta h_{TOT}$ (W)	kg air	kg Kaolinite	kg N <sub>2</sub>	kg water	kg vapor	kg Nahcolite	kg O <sub>2</sub>	n	<i>path V</i>
0,129	475	1956	17164	300	23585	-	3900	37	-	7 + 2	

Table 52a: paths analysis for 8 Nm<sup>3</sup>/h gas flow size

$\Delta p_{TOT}$ (bar)	$\Delta T_{TOT}$ (°C)	$\Delta h_{TOT}$ (W)	kg air	kg Kaolinite	kg N <sub>2</sub>	kg water	kg vapor	kg Nahcolite	kg O <sub>2</sub>	n	<i>path I</i>
0,332	469	30554	269226	5893	355884	731707	10555	-	-	7 + 2	
$\Delta p_{TOT}$ (bar)	$\Delta T_{TOT}$ (°C)	$\Delta h_{TOT}$ (W)	kg air	kg Kaolinite	kg N <sub>2</sub>	kg water	kg vapor	kg Nahcolite	kg O <sub>2</sub>	n	<i>path II</i>
0,464	-202	-5922	270912	5893	355884	-	-	542	40000	7 + 1	
$\Delta p_{TOT}$ (bar)	$\Delta T_{TOT}$ (°C)	$\Delta h_{TOT}$ (W)	kg air	kg Kaolinite	kg N <sub>2</sub>	kg water	kg vapor	kg Nahcolite	kg O <sub>2</sub>	n	<i>path III</i>
0,411	470	30336	270912	5893	355884	800000	-	-	-	7 + 1	
$\Delta p_{TOT}$ (bar)	$\Delta T_{TOT}$ (°C)	$\Delta h_{TOT}$ (W)	kg air	kg Kaolinite	kg N <sub>2</sub>	kg water	kg vapor	kg Nahcolite	kg O <sub>2</sub>	n	<i>path IV</i>
0,359	469	33651	269226	5893	355884	-	11000	536	40000	8 + 2	
$\Delta p_{TOT}$ (bar)	$\Delta T_{TOT}$ (°C)	$\Delta h_{TOT}$ (W)	kg air	kg Kaolinite	kg N <sub>2</sub>	kg water	kg vapor	kg Nahcolite	kg O <sub>2</sub>	n	<i>path V</i>
0,146	466	29759	269226	5893	355884	-	61200	536	-	7 + 2	

Table 52b: paths analysis for 125 Nm<sup>3</sup>/h gas flow size

$\Delta p_{TOT}$ (bar)	$\Delta T_{TOT}$ (°C)	$\Delta h_{TOT}$ (W)	kg air	kg Kaolinite	kg N <sub>2</sub>	kg water	kg vapor	kg Nahcolite	kg O <sub>2</sub>	n	<i>path I</i>
0,351	468	87306	754613	17934	888069	2051282	21863	-	-	7 + 2	
$\Delta p_{TOT}$ (bar)	$\Delta T_{TOT}$ (°C)	$\Delta h_{TOT}$ (W)	kg air	kg Kaolinite	kg N <sub>2</sub>	kg water	kg vapor	kg Nahcolite	kg O <sub>2</sub>	n	<i>path II</i>
0,5	-254	-20852	759264	17934	888069	-	-	1520	112000	7 + 1	
$\Delta p_{TOT}$ (bar)	$\Delta T_{TOT}$ (°C)	$\Delta h_{TOT}$ (W)	kg air	kg Kaolinite	kg N <sub>2</sub>	kg water	kg vapor	kg Nahcolite	kg O <sub>2</sub>	n	<i>path III</i>
0,437	470	86973	759264	17934	888069	2280285	-	-	-	7 + 1	
$\Delta p_{TOT}$ (bar)	$\Delta T_{TOT}$ (°C)	$\Delta h_{TOT}$ (W)	kg air	kg Kaolinite	kg N <sub>2</sub>	kg water	kg vapor	kg Nahcolite	kg O <sub>2</sub>	n	<i>path IV</i>
0,388	468	100159	754613	17934	888069	-	22864	1507	112000	8 + 2	
$\Delta p_{TOT}$ (bar)	$\Delta T_{TOT}$ (°C)	$\Delta h_{TOT}$ (W)	kg air	kg Kaolinite	kg N <sub>2</sub>	kg water	kg vapor	kg Nahcolite	kg O <sub>2</sub>	n	<i>path V</i>
0,156	464	86793	754613	17934	888069	-	172900	1507	-	7 + 2	

Table 52c: paths analysis for 350 Nm<sup>3</sup>/h gas flow size

According to the methodology was used for the *paths* set up (such as the main technical constraints which regulate the units relative positions along the cleaning line), ammonia catalytic partial oxidation technology was found out to be unsuitable for the larger gas cleaning line sizes (125 Nm<sup>3</sup>/h and 350 Nm<sup>3</sup>/h gas flows design values).

Indeed, because of the high exothermic behaviour of ammonia partial oxidation reaction and hydrogen combustion (see par. 5.2.9), catalyst temperature inside the reactor would be unacceptably increased during operation, since the heat losses in the same unit are two orders of magnitude less. Therefore, temperature control devices would be required in order to maintain the constant temperature close to the optimal working condition for catalytic activity, as well as for safety measures. Nevertheless, these devices are not considered as gas cleaning equipments, according to one of the initial assumptions for this analysis. Moreover, as said in par. 5.2.9, partial oxidation of ammonia is undesirably linked to an high hydrogen consumption, so that its use seems to be not properly fitting with the real scope of the application (energy cogeneration).

The analysis and comparison of data reported in tables 52a, 52b and 52c allowed to choose preferential *paths* for each corresponding gas cleaning line size. These choices can be only considered as first indications for the cleaning systems design but they are not representing the overall best arrangements yet. Many other aspects need in fact to be investigated to reach this goal, such as dimensioning and performance analysis of units in regeneration phase, overall reliability of system, maintenance feasibility, costs estimation, and so on.

For the small line size (8 Nm<sup>3</sup>/h gas flow), two different *paths* are presented, respectively called high temperature gas stream option (*path II*) and cold temperature gas stream option (*path V*).

In fact, the first one shows a still relatively high temperature (325°C) of gas at the end of cleaning line, so that clean gas stream could be suitable for such applications where high temperatures are required (i.e. gas turbines utilization for energy cogeneration). It also shows the lowest number of cleaning units together with *path III*, but the highest pressure drops (404mbar). These latter can be mainly ascribed to the ammonia partial oxidation unit (200mbar) and to the sulphur adsorption unit by Zn-Ti adsorber (112mbar), especially because of their small bed materials sizes (see tables 37 and 46). Since they were chosen as the ones adopted for the materials experimental tests (Gupta et al., 1996, Gang Lu et al., 2000), it could be envisaged to reduce pressure drops by only increasing these sizes, but maintaining the same fluid dynamic conditions at which the intrinsic kinetic parameters were obtained.

*Path V* was indicated as the second option for the small size gas cleaning line especially because of its low total pressure drop and in order to still avoid the large water consumption by the scrubber unit for ammonia removal. Indeed, for this small size equipment, a very large waste water production was also estimated. In the better case (*path I*), around 350 waste water litres per day were obtained, while in the worst case (*path III*) even 390 litres of water consumption were calculated, with a frequency of water discharge as about twice per day (200 litres water tank adopted).

On the contrary, by using activated carbon material for abatement of ammonia (together with H<sub>2</sub>S), a water vapour consumption in its regeneration step was estimated as about 12kg per day, with a frequency of regeneration in tandem arrangement as 32h.

For the same reason, *path V* was indicated as the preferable line arrangement for the larger plant sizes, as well. In this case, as said, *path II* and *path IV* did not prove suitable for the overall assessment, since the temperature increase by the ammonia decomposition units.

A very high water consumption was instead calculated for *path I* and *path III*. For 125 Nm<sup>3</sup>/h gas flow line size, a daily frequency of 1000 litres tank recharge was estimated as 2,2 – 2,4 (respectively for *path I* and *path III*) while for the larger size, this frequency rose to 6,15 – 6,8 tanks per day.

*Path V* seems therefore the only practical solution to be adopted in these cases. Moreover, it also shows the lowest pressure drops among all the considered *paths*, at these large sizes.

Nevertheless, the simultaneous adsorption of NH<sub>3</sub> and H<sub>2</sub>S by the activated carbon units causes a deep increase of their regeneration frequency: in the case of 125 Nm<sup>3</sup>/h gas flow size, the activated carbon saturation time decreases from 119h for the only H<sub>2</sub>S adsorption to 24h for both the contaminants retention, while for 350 Nm<sup>3</sup>/h gas flow size, the saturation time drops from 161h to 24h at the same conditions, according to the designed units dimensions for these equipments (see table 41).

As an overall conclusion regarding these first considerations, it can be thus said that dry gas cleaning methods seem to be preferable to the ones including water scrubber technology even in those cases where gas stream needs to be cooled down the same, for its complete purification.

This result is especially connected to the possibility to use activated carbon units for ammonia removal and Nahcolite adsorber for chloride acid. The very high efficiency of this latter material is also remarkable.

Ammonia proved instead as the main considered contaminant affecting the choice of preferable *paths*, from this analysis.

Another overall result to be highlighted is the difficulty of removing tars from gas stream. In this case a catalytic cracking technology was envisaged. Nevertheless, according to the chemical properties of selected material (see par. 5.2.5) a very high regeneration frequency is required in order to still reach a tars conversion factor as 0,9. In fact, a catalysts working time as only two hours could be fixed for the designed units dimensions. As a consequence, a very high air consumption for catalysts regeneration was calculated, as well.

Finally, as an estimation of the overall energy loss pertaining the gas cleaning process, the total enthalpy losses estimated for the three plant sizes were compared with the respective gas streams energy contents, these latter obtained on the basis of low heating value of gas only.

For the small line size, the energy loss was around 7% of gas stream energy content in the case of high temperature gas stream option (*path II*) and 17% for the low temperature gas stream one (*path V*).

For the 125 Nm<sup>3</sup>/h gas flow size, the cleaning line energy loss was estimated as about 15% of gas stream energy content, while for the 350 Nm<sup>3</sup>/h gas flow size this value rose to around 16%, for all the considered possible *paths*.

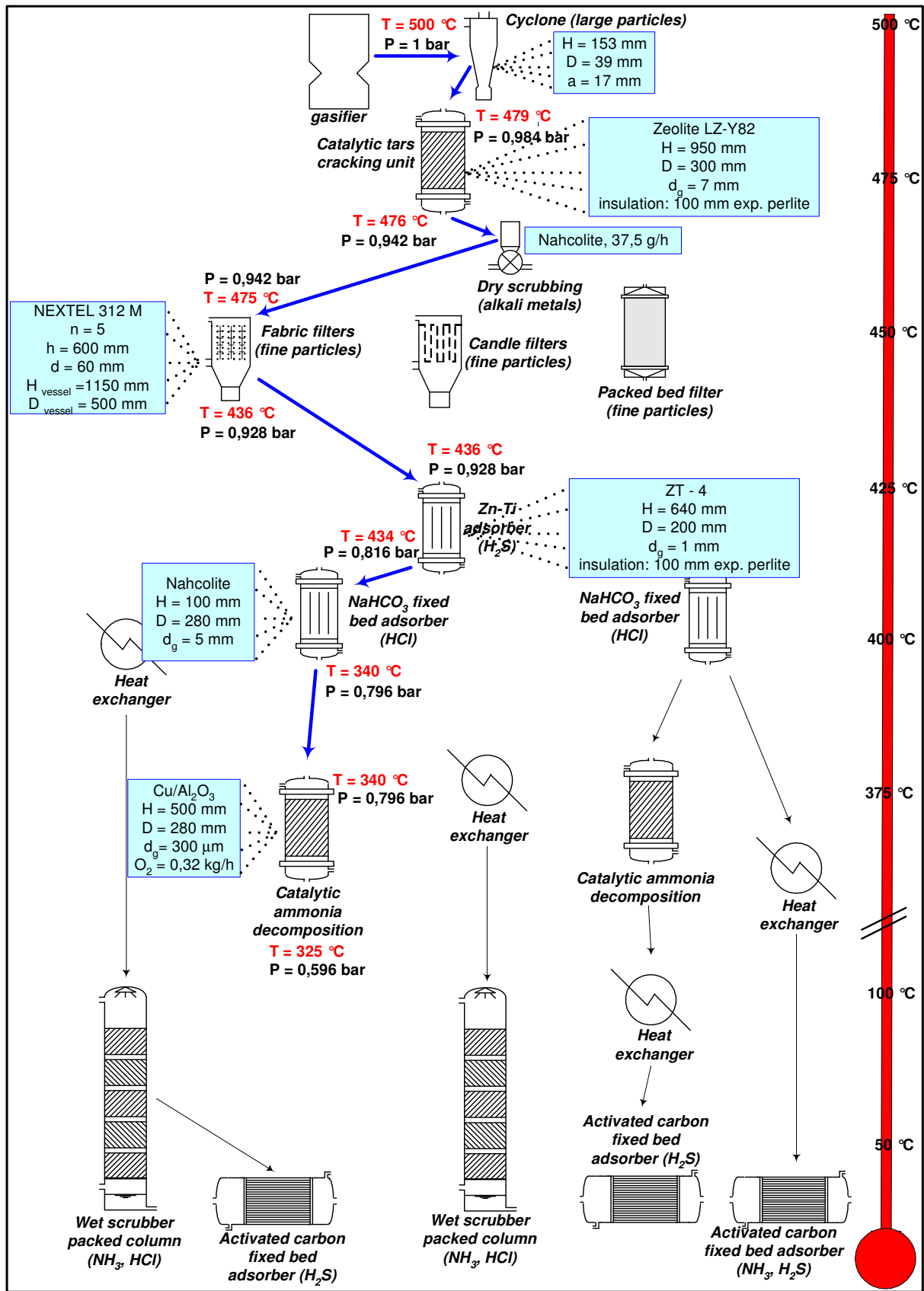


Figure 42a<sub>1</sub>: high temperature gas stream option (path II) for 8 Nm<sup>3</sup>/h gas flow cleaning line

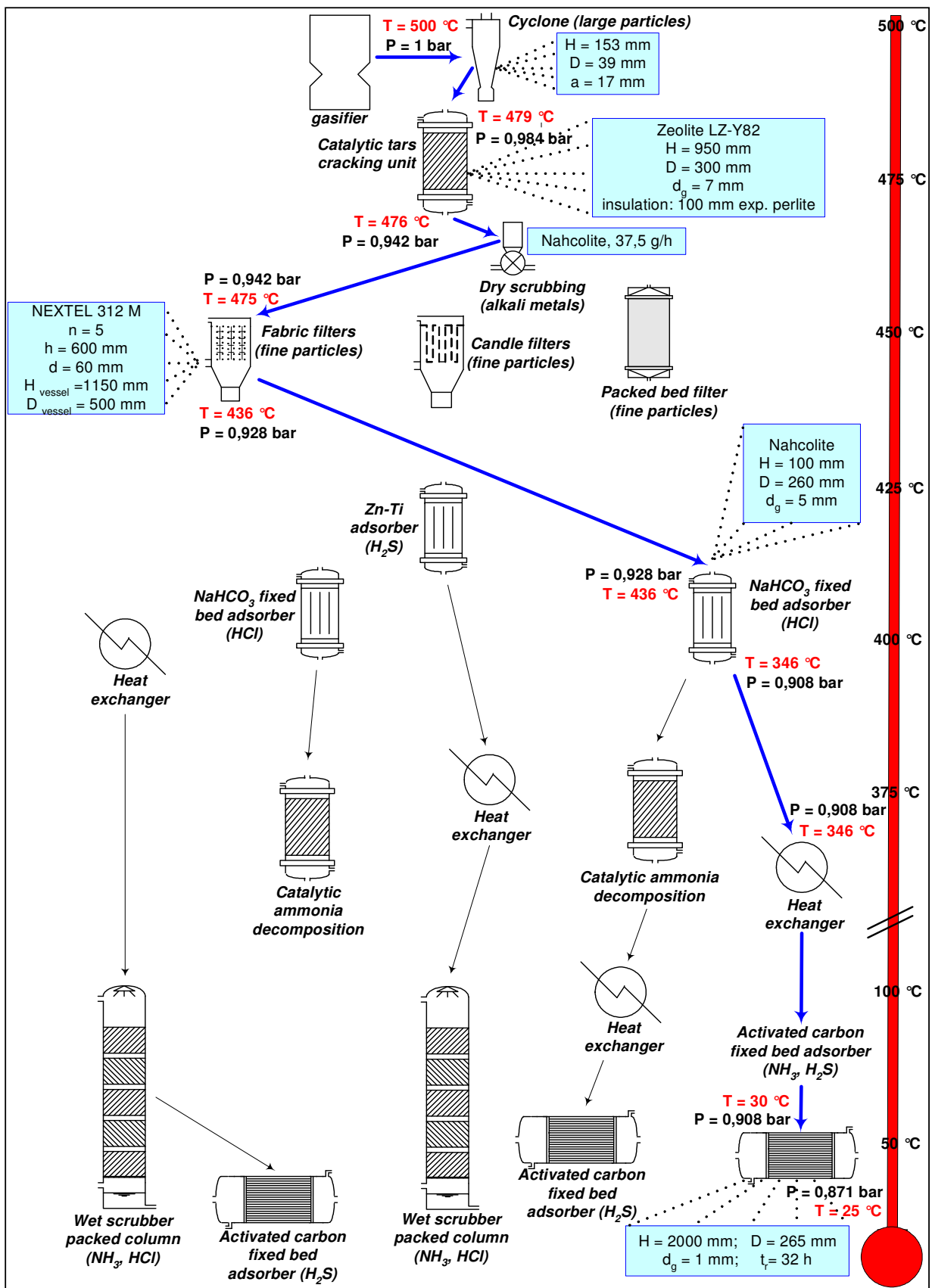


Figure 42a<sub>2</sub>: low temperature gas stream option (path V) for 8 Nm<sup>3</sup>/h gas flow cleaning line



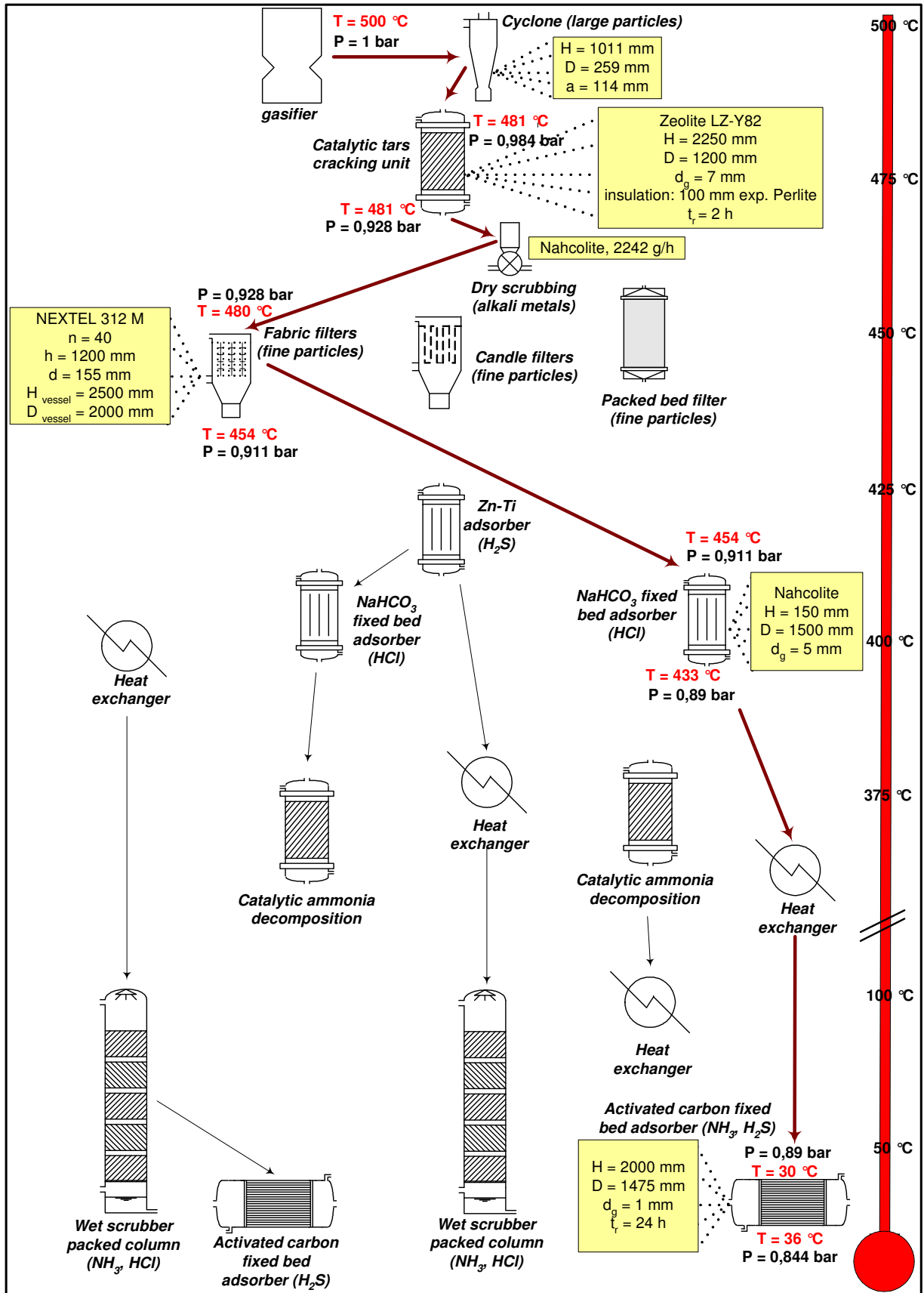


Figure 42c: selected arrangement (pathV) for 350 Nm<sup>3</sup>/h gas flow cleaning line

## 7 OVERALL CONCLUSIONS

Present work was essentially carried out with the scope to estimate flexibility of small scale biomass downdraft gasifiers in accepting different feeding fuels, in order to check out their technical feasibility in rural scenarios (where a lot of heterogeneous agricultural refuses are produced yearly), as integrated units in energy micro-cogeneration systems.

As first step of this study, an overall analysis on gasification of different biomass fuels was carried out in order to learn how some of their properties (composition and particles size, above all) affect the development of this thermo-chemical conversion process and influence gasification units design.

Five biomass species were initially considered: park waste wood, softwood, wheat straw, sewage sludge and refuse derived fuels. Their particles dimensions were chosen as the usual ones observed after their typical pre-treatments, while proximate analyses and elementary compositions were derived from literature data.

An open core air downdraft gasification technology was assumed to be used, especially because of its suitability to even treat small sized materials (as the ones considered in this work), its easy handling and small size units adaptability.

At first, a thermo-chemical kinetic free model for fuels processing was formulated. According to this, gasifier is divided in four reaction zones: biomass heating and drying, pyrolysis, partial oxidation and gasification. The novelty of this analytical approach was the use of the ratio between kinetic constants in order to determine oxygen distribution among the different oxidation reactions (regarding volatile matter only) while equilibrium of *water gas shift* reaction was considered in gasification zone, by which energy and mass balances involved in the process algorithm were linked together, as well.

The main results of this kinetic free model were the yields and compositions of gaseous and solid products at the exit of each reaction zone, as well as the corresponding exit gas temperatures, for every biomass fuel. The analysis was conducted at different equivalence ratios in the range 0.25 – 0.35. Other interesting outcomes of the analytical tool were the distribution of combustion heat among the other endothermic processes and the cold gas efficiency of the overall gasification process.

Good conformity of these results with the other literature data and experimental results was detected for all the materials except for refuse derived fuels. The reason of this limitation is maybe due to the model simplifying assumptions especially concerning pyrolysis step, where some other expected gaseous products should be probably added. Indeed, the particular RDFs elementary composition (low fixed carbon percentage and high C/O ratio, above all) seems to don't properly fit with mass balance expression concerning pyrolysis step. Robustness of the model could be thus improved by means of a more detailed implementation, considering a greater number of possible products in the first steps of thermo-chemical conversion.

Anyway, for the other biomass fuels, the kinetic free model results (corresponding to the highest cold gas efficiencies but presenting gasification temperatures not less than 950K) were also used for the analysis of thermodynamic mechanisms which are at the base of gasification units dimensioning.

In fact, for an initial fresh biomass feeding rate of 100 kg/h, the volume of each reaction zone of gasifier was researched considering the necessary residence time of biomass flow (considered in perfect plug flow regime, in this case) in order that the corresponding process can be completely developed.

Solids residence time was estimated through the investigation of different alternative conversion mechanisms for each step, and it was finally determined by combining together

the corresponding solid conversion times, or even by choosing the longest one when they were not comparable each others.

In this manner, for char gasification process, kinetic rates of gasification reactions were compared with gas mass transfers from bulk gas to the external surface of solid particles, as well as through the inner pores of them.

Kinetic rates of pyrolysis were instead compared with radiative heat transfer from hot combustion gases towards the external surface of particles, and with conductive heat transfer through the inner layers of the same particles.

Drying of biomass was envisaged as water vapour molecular diffusion through the inner pores of particles or even as an internal and external heat transfers limited process, as well.

Finally, biomass heating process was considered as the combination of convective heat transfer between gas and solid phases through the walls of reactor, radiative heat transfer by the same hot walls of reactor and radiative heat transfer from combustion hot gas.

As main outcomes from this analysis, it was shown that gasification step is kinetic rate limited if small/fine biomass particles are fed to the reactor, as in all the examined cases. Working temperature is hence the main controlling parameter of this process.

For pyrolysis, instead, chemical and physical resistances are comparable in the cases of woody biomasses (*Biot* and *Thiele* numbers always included in the range 0.1 – 10), kinetics takes on less importance in wheat straw pyrolysis while heat transfer resistances are negligible in the case of sewage sludge. Therefore, the estimation of pyrolysis times has to be carried out by taking into account different factors according to the particular material is going to be gasified and the particular working conditions are set up inside the reactor. Any only main design parameter is not possible to be detected in this case.

Another very important result is the great variability of gasification and pyrolysis times according to the process temperatures achieved inside their corresponding reaction zones, especially due to the exponential temperature dependence of kinetics expressions. As a consequence, the dimensions of gasification and pyrolysis zones could also undergo great changes with even short temperature variations. For correct design, therefore, a right estimation of temperature profile inside the gasifier is necessary (by means of detailed energy balances and overall thermo chemical models, presumably).

Biomass drying process was found out to be heat transfer limited, while fuel heating is mainly accomplished by radiative heat transfer from the hot walls of reactor.

On the basis of all these results, the reactor heights corresponding to the different conversion steps were calculated for each biomass materials. Gasifier was simply considered as a cylindrical vessel whose diameter was determined according to the gas superficial velocity in gasification zone (0.5 m/s for Nm<sup>3</sup>/h).

It was therefore possible to estimate the relative weight of each conversion step in the total unit height determination. Pyrolysis was the most time demanding process in the case of park waste wood gasification, while biomass heating was the same for sewage sludge and softwood as well, as an unexpected result. As it could be expected, instead, fuel drying is the most rapid process occurring inside the gasifier and it proves almost negligible in the case of sewage sludge gasification. Wheat straw, finally, shows similar unit heights for heating and pyrolysis processes.

As regard gasification units flexibility, it has to be said that each biomass material shows a different volumes distribution, so that any dimensioned gasification unit does not seem to be suitable for more than one biomass species.

Even for the two examined wood species, the reaction zones whose volumes are mainly affected by biomass particles size are quite different each other. Of course, in this case, it would be possible to use the same gasifier by only levelling the size of feedstock materials.

On the contrary, in order to feed the same unit with different biomass species, it can be noted that diameters of reactors are quite similar for all the examined materials, since almost the same gas yields. Therefore, it could be envisaged to adopt the largest diameter and to design an only gasification unit by combining together the maximum heights of each reaction zone, as they were calculated for the different fuels. In this way, a total unit height as 2391 mm would be obtained, that could be still considered acceptable for the size of gasifier.

Besides, this unit could be equipped with air injecting nozzles arranged at different levels along the reactor, in order to properly set up gasification zone (and consequently the upper zones, as well) according to the particular material to be gasified.

Finally, since gasification and pyrolysis times were found to considerably change according to even short temperature variations, it could be also envisaged to regulate air feeding rate for each gasified material (which process temperatures depend on), so as the available reactor volumes would be suitable for the complete development of solid conversion in each case, without even changing fluid dynamics behaviour of the unit as well as air/biomass ratio in noticeable measure.

From the viewpoint of gas cleaning practical necessity for running high efficiency energy cogeneration units, the technical barriers deriving from the use of multi-fuel gasifiers, with a presumably higher number of contaminant compounds in the raw gas stream, seem to be overcome thanks to the large variety of already available or still experimental gas cleaning units.

One of the main issues regarding the gas cleaning process is due to the tars condensation at relatively high temperatures, for which they need to be eliminated in the first sections of gas cleaning line, together with particulate. Nevertheless, because of the risk of blinding or plugging the filter units adopted for fine particles collection, the use of a tars catalytic cracking unit seems to be the only solution to avoid these hold-ups and keep clean the following devices in the line.

At this scope, a catalytic material which is able to work at such temperatures similar to the ones achieved at the exit of gasifier needed to be chosen, as well. Nevertheless, a rapid drop in tars cracking efficiency of this same material was also detected. This therefore leads to an high frequency of catalysts regeneration, so that a maximum working time for these units was possible to be fixed as two hours only, in order to still have acceptable dimensions and pressure drops. Besides, an high air consumption for catalysts regeneration was also estimated.

Similar difficulties are presented for alkali metals compounds, which condense at lower temperatures than tars but they also need to be removed in the first sections of gas cleaning line in order to avoid corrosion of materials. In this case a dry scrubber technology was envisaged, by using the same fine particles filter units and by choosing for them corrosion resistant materials like ceramic ones.

In spite of these two solutions which seem to be unavoidable in gas cleaning line design, several overall arrangements (*paths*) were then designed for the different considered plant sizes (respectively corresponding to 8Nm<sup>3</sup>/h, 125Nm<sup>3</sup>/h and 350Nm<sup>3</sup>/h gas flow values), by which the possibility to clean the gas up to the required standard degree was technically demonstrated, even in the case several contaminants are simultaneously present in the gas stream.

For this design procedure, several technical constraints were fixed a priori, among which the restraint to only have a decreasing gas temperature profile along the cleaning line (in order to reduce the field of investigation and to avoid the use of sophisticated temperature control devices). According to this initial assumption and on the basis of the gas contaminant species considered in the gas stream, high temperature gas cleaning lines were not possible to be achieved for the two larger plant sizes. Indeed, with the scope to still have an high temperature gas flow at the exit of gas cleaning line (such as more than 300 °C), the only suitable solution provided in this study is the use of catalytic oxidation units for ammonia decomposition. Nevertheless, since the high exothermic behaviour of reactions involved in this process, for large size reactors, the increase of working temperature would be not balanced by heat losses and therefore suitable temperature control devices would be required.

On the contrary, for the cleaning line at small size (8Nm<sup>3</sup>/h gas flow), both high and low temperature options were presented as possible solutions.

Besides, all the possible *paths* designed for the different plant sizes were compared each others on the basis of some defined operational parameters, among which total pressure drops, total energy losses, number of units and secondary materials consumption.

As an overall conclusion of this analysis, dry gas cleaning methods proved preferable to the ones including water scrubber technology, especially because of the high water consumption provided by water scrubber units in ammonia adsorption process. This result is yet connected to the possibility to use activated carbon units for ammonia removal and Nahcolite adsorber for chloride acid. The very high efficiency of this latter material is also remarkable.

Finally, as an estimation of the overall energy loss pertaining the gas cleaning process, the total enthalpy losses estimated for the three plant sizes were compared with the respective gas streams energy contents, these latter obtained on the basis of low heating value of gas only. For the small line size, the energy loss was around 7% of gas stream energy content in the case of high temperature gas stream option (*path II*) and 17% for the low temperature gas stream one (*path V*). For the 125 Nm<sup>3</sup>/h gas flow size, the cleaning line energy loss was estimated as about 15% of gas stream energy content, while for the 350 Nm<sup>3</sup>/h gas flow size this value rose to around 16%, for all the considered possible *paths*.

The overall worked out analysis on gas cleaning systems is proposed as an analytical tool by which different gas cleaning line configurations can be valuated according to the particular practical application and cogeneration unit size.

## 8 FUTURE WORK

This work is propaedeutic for an experimental activity by which all the main obtained results could be validated by evident outcomes.

By using the same considered biomass materials in downdraft gasification applications, kinetic free model reliability could be checked out and some implementations could be certainly produced. Such improvements could be probably regarding more sophisticated algorithms for pyrolysis step simulation (by which to add more product components) and the use of proper elementary composition for each biomass char (whereof characteristics would be obtained through the same experimental tests) instead of solid carbon one.

Besides, by also adopting the same initial physical properties of fuels, such as moisture content and particles size, the dimensional aspects mentioned in this analysis could be validated through the observation of temperature profiles inside the gasifier.

However, in order to estimate the real flexibility of gasification units, not only working conditions and available volumes for different fuels conversion need to be checked out, of course. Many other operational aspects have to be considered.

For downdraft units, particular attention needs to be put on feedstock feeding system and bottom grate spacing, on the basis of fuel particles size above all. The control of pressure regime inside the gasifier and the quality of contact between gas and solid phases are also very important issues to take into account, by in case arranging proper devices for gasifying medium injection. The experimental activity would be useful to better face on all these operational issues, as well.

Experimental outcomes would be required for the investigation of gas cleaning units behaviour, as well, in order to better estimate all the working parameters and conditions envisaged in design procedure. Efficiency and reliability of the overall considered arrangements would be also checked out, with particular attention to be focused on catalytic tars cracking units and particles deep filtration devices.

As regard the analytical methodology for the assessment of overall gas cleaning lines, some improvements are suggested to be achieved, too. Especially performances analysis of gas cleaning units in regeneration phase need to be still carried out, and a rating method for the overall system reliability should be defined. Maintenance operations for the different gas cleaning units should be also included in the overall system valuation.

Other cleaning units could be also added to the one considered in this analysis.

Finally, costs estimation should be also carried out for the different *paths* in order to complete gas cleaning lines evaluation, even from financial point of view.

## REFERENCES

- AA.VV., 2007, *Manuale dell'Ingegneria, Nuovo Colombo*, 84<sup>th</sup> ed., Ulrico Hoepli
- Arena U., Volpicelli G., Borrelli S., 1991, *Sistemi di depolverazione delle correnti gassose*, Dept. Chemical Engineering, University of Naples "Federico II"
- Arlabosse P., Chavez S., Prevot C., 2005, *Drying of Municipal Sewage Sludge: from a Laboratory Scale Batch Indirect Dryer to the Paddle Dryer*, Brazilian Journal of Chemical Engineering, 22, n.2, pp.227-232.
- Babu B.V., Sheth P.N., 2006, *Modeling and simulation of reduction zone of downdraft biomass gasifier: effect of char reactivity factor*, Energy Conversion and Management, 47, pp.2602-2611
- Barton S.S., Evans M.J.B., MacDonald J.A.F., 1991, *The adsorption of water vapor by porous carbon*, Carbon vol.29, n.8, pp.1099-1105
- Bass M., Van Stryland E.W., Williams D.R., Wolfe, 1995, *Handbook of Optics*, vol. I, MacGraw-Hill
- Bauen A., 2004, *Biomass Gasification*, Encyclopedia of Energy, vol. I, Elsevier
- Bech W.L.N., Wolff L., Germann L., 1996, *Mathematical Modeling of Straw Bale Combustion in Cigar Burners*, Energy & Fuels, 10, pp.276-283
- Belgiorno V., De Feo G., Della Rocca C., Napoli R.M.A., 2003, *Energy from gasification of solid wastes*, Waste management 23, pp.1-15
- Bellais M., 2007, *Modelling of the pyrolysis of large wood particles*, Doctoral Thesis, KTH Chemical Science and Engineering Department, Stockholm
- Bhoi P.R., Singh R.N., Sharma A.M., Patel S.R., 2005, *Performance evaluation of open core gasifier on multi-fuels*, Biomass and Bioenergy 30, pp. 575–579
- Buah W.K., Cunliffe A.M., Williams P.T., 2007, *Characterization of products from the pyrolysis of municipal solid waste*, Institution of Chemical Engineers, Vol. 85 (B5), pp.450–457
- Bühler R and Hasler P., 1997, *Stand und Entwicklung der Vergasungstechnik*, VDI Berichte Nr. 1319, S81-107, VDI Verlag Düsseldorf GmbH
- Corella J., Sanz A., 2005, *Modeling circulating fluidized bed biomass gasifiers. A pseudo rigorous model for stationary state*, Fuel Processing Technology, vol.86, pp.1021-1053
- Dalai A. K., Batta N., Eswaramoorthi I., Schoenau G.J., 2009, *Gasification of refuse derived fuel in a fixed bed reactor for syngas production*, Waste Management 29, pp.252-258
- Darvell L.I., Heiskanen K., Jones J.M., Ross A.B., Simell P., Williams A., 2003, *An investigation of alumina supported catalysts for the selective catalytic oxidation of ammonia in biomass gasification*, Catalysis Today, 81, pp.681-692
- Davidsson K.O., Pettersson J.B.C., 2002, *Birch wood particle shrinkage during rapid pyrolysis*, Fuel, 81(3), pp.263–270.
- Di Blasi C., 2009, *Combustion and Gasification Rates of Lignocellulosic Chars*, Progress in Energy and Combustion Science, 35, pp.121-140
- Di Blasi C., 2008, *Modeling chemical and physical processes of wood and biomass pyrolysis*, Progress in Energy and Combustion Science, 34, pp.47-90

- Di Blasi C., Branca C., Santoro A., Hernandez E.G.; 2001, *Pyrolytic Behavior and Products of Some Wood Varieties*, Combustion and Flame, 124, pp.165-177
- Di Blasi C., 2000, *Dynamic Behaviour of Stratified Downdraft Gasifiers*, Chemical Engineering Science, 55, pp.2931-2944
- Dokanassionou G.A., Magnoux P., Guisnet M., 1998, *Comparative study of coking and regeneration of HEMT and HFAU zeolites*, Microporous and Mesoporous Materials, vol.22, pp.389-398
- Dubin M.M., 1981, *Isotherm equation for water vapor adsorption by microporous carbonaceous adsorbents*, Carbon, vol.19, n.5, pp.400-403
- ECN, 2009, *Phyllis, Database for Biomass and Waste*, as available at <http://www.ecn.nl/phyllis>, as accessed 09.09.2009
- Eco-Engineering srl, 2009, *Briquetting*, as available at <http://www.ecoeng.eu/en/briquetting.html>, as accessed 26.08.2009
- Ekström C., Lindman N., Pettersson R., *Catalytic Conversion of Tars, Carbon Black and Methane from Pyrolysis/Gasification of Biomass*, The Royal Institute of Technology, Department of Chemical Technology, Stockholm, Sweden.
- EPA, 2008, *Catalogue of CHP Technologies*, U.S. Environmental Protection Agency Combined Heat and Power Partnership
- Erlich C., Björnbom E., Bolado D., Giner M., Fransson T. H., 2006, *Pyrolysis and gasification of pellets from sugar cane bagasse and wood*, Fuel, 85, pp.1535–1540
- Ergudenler A., Weisberg T., Brereton C.M.H., Lim J.C., Grace J.R., Gennrich T.J., 1997, *Performance of high temperature fabric filters under gasification and combustion conditions*, Separation and Purification Technology, vol.11, pp.1-16
- Fair J.R., Steinmeyer D.E., Penney W.R., Crocker B.B., 1997, *Gas adsorption and gas-liquid system design*, Perry's Chemical Engineering Handbook 7<sup>th</sup> ed., McGraw Hill
- Fjellerup J., Henriksen U., Degn Jensen A., Arendt Jensen P. and Glarborg P., 2003, *Heat Transfer in a Fixed Bed of Straw Char*, Energy Fuels, 17 (5), pp.1251-1258
- Galgano A., Di Blasi C., 2004, *Modeling the propagation of drying and decomposition fronts in wood*, Combustion and Flame, 139, pp.16-27
- Gang Lu, Anderson B.G., Van Grondelle J., Van Santen R.A., 2000, *NH<sub>3</sub> oxidation to nitrogen and water at low temperatures using supported transition metal catalysts*, Catalysis Today 61, pp.179-185
- Gang Lu, Anderson B.G., Van Grondelle J., Van Santen R.A., 1999, *Selective low temperature NH<sub>3</sub> oxidation to N<sub>2</sub> on Copper based catalysts*, Journal of Catalysts, pp.100-109
- Geldart D., 1986, *Gas fluidization technology*, John Wiley and Sons
- Germerdonk R., Anzhong W., 1993, *Pollutant adsorption during activated carbon and steam regeneration in technical columns (experiments, modeling). Part 2: influence of process parameters during steam regeneration of activated carbon beds on pollutant exit concentration*, Chemical Engineering and Processing, vol.32, pp 369-377
- Giltrap D.L., Mc Kibbin R., Barnes G.R.G., 2003, *A steady state model of gas-char reactions in a downdraft biomass gasifier*, Solar Energy 74, pp.85–91
- Groeneweld MJ, Van Swaaij WPM, 1980, *Gasification of Char particles with CO<sub>2</sub> and H<sub>2</sub>O*, Chemical Engineering Science, 35, pp.307-313

- Gupta R.P., Gangwal S.K., Cicero D.C., Henningsen G.B., Katta S., 1996, *Hot coal gas desulfurization in fluidized bed reactors using Zinc-Titanate sorbents*, Institut für Mechanische Verfahrenstechnik und Mechanik, Universität Karlsruhe, Germany
- Gupta M., Jang J., Roy C., 2003, *Specific heat and thermal conductivity of softwood bark and softwood char particles*, Fuel, 82, pp.919-927
- Hand D.W., Hokanson D.R., Crittenden J.C., 1999, *Air stripping and aeration*, Mc Graw Hill
- Hartman M., Pohorely M., Trnka O., 2007, *Fluidization of Dried Wastewater Sludge*, Powder Technology 178, pp.166-172
- Hartman M., Pohorely M., Svoboda K., Trnka O., 2005, *Combustion of Dried Sewage Sludge in a Fluidized-Bed Reactor*, Ind. Eng. Chem. Res., vol.44, pp.3432-3441
- Hasler P., Nussbaumer Th., 1999, *Gas cleaning for IC engine applications from fixed bed biomass gasification*, Biomass and Bioenergy, 16, pp.385-395
- He F., Yi W., Bai X., 2006, *Investigation on Caloric Requirement of Biomass Pyrolysis using TG-SC Analyzer*, Energy Conversion and Management, 47, pp.2461-2469
- Hojtahedi W., Konttinen J., Gangwal S., 1996, *Sulfidation-regeneration kinetics on Zinc-Titanate sorbents*, Institut für Mechanische Verfahrenstechnik und Mechanik, Universität Karlsruhe, Germany
- Holman J P., 1990, *Heat transfer*, 7th ed., McGraw-Hill
- Hopkins P.D., Miller J.T., Meyers B.L., Ray G.J., Rojinski R.T., Kuehne M.A., Kung M.M., 1996, *Acidity and cracking activity changes during coke deactivation of ultrastable Y zeolite*, Applied Catalysis A: General 136, pp.29-48
- Hottel H.C., Sarofim A.F., 1967, *Radiative Transfer*, McGraw-Hill
- Inglezakis V. and Pouloupoulos S., 2006, *Physical Properties of Water, Air and Selected Compounds - Appendix I*, Adsorption, Ion Exchange and Catalysis, pp. 551-574
- Jalan R.K. and Srivastava V.K., 1998, *Studies on pyrolysis of a single biomass cylindrical pellet - kinetic and heat transfer effects*, Energy Conversion & Management, 40, pp.467-494
- Janse A.M.C., Westerhout R.W.J., Prins W., 1999, *Modelling of flash pyrolysis of a single wood particle*, Chemical Engineering and Processing, 39, pp.239-252
- Jayah T.H., Aye Lu, Fuller R.J., Stewart D.F., 2003, *Computer simulation of a downdraft wood gasifier for tea drying*, Biomass and Bioenergy, 25, pp.459-469
- Jones J.M., Pourkashanian M., Williams A., Backreedy R.I., Darvell L.I., Simell P., Heiskanen K., Kilpinen P., 2005, *The selective oxidation of ammonia over alumina supported catalysts – experiments and modeling*, Applied Catalysis B: Environmental 60, pp.139-146
- Kim Y.J., Lee J.M., Kim S.D., 2000, *Modeling of coal gasification in an internally circulating fluidized bed reactor with draught tube*, Fuel, 79, pp.69-77
- Kohl, Nielsen A.L., Richard B., 1997, *Gas purification*, 5<sup>th</sup> ed., Elsevier
- Krishnan G.N., Gupta R.P., Cenizales A., Shekular S., Ayala R., 1996, *Removal of Hydrogen Chloride from hot coal gas stream*, Institut für Mechanische Verfahrenstechnik und Mechanik, Universität Karlsruhe, Germany
- Kunii D., Levenspiel O., 1969, *Fluidization Engineering*, John Wiley and Sons inc.
- Lam P. S., Sokhansanj S., Bi X., Lim C. J., Naimi L. J., Hoque M., Mani S., Womac A. R., Ye X. P., Narayan S., 2008, *Bulk Density of Wet and Dry Wheat Straw and Switchgrass Particles*, Applied Engineering in Agriculture, 24(3), pp.351-358

- Lee K.W., Mukund R., 2001, *Filter Collection, Aerosol Measurement Principles, Techniques and Applications*, 2<sup>nd</sup> ed., Wiley Interscience inc.
- Lettner F., Timmerer H., Haselbacher P., 2007, *Biomass gasification – State of the art description*, deliverable of Gasification Guide, Intelligent Energy – Europe (IEE)
- Levenspiel O., 1962, *Chemical reaction engineering*, John Wiley and Sons inc.
- Lilledahl Truls, 2006, *Gasification*, Proceedings of Summerschool *Fuels from biomass*, Industrial Chemistry and Materials Department, University of Bologna, Bertinoro, Italy
- Lindberg J., Hermansson R., 2004, Modification of Reaction Rate Parameters for Combustion of Methane Based on Experimental Investigation at Furnace-like Conditions, *Energy and Fuels*, 18, pp.1482-1484
- Lopez J.M., Lemos F., Riberio F.R., Devouane E.G., Magnoux P., Guisnet M., 1994, *Coke deposition on H-ZSM-20 and USHY zeolites*, *Applied Catalysis A: General* 114, pp.161-172
- Marias F., 2003, *A model of a rotary kiln incinerator including processes occurring within the solid and the gaseous phases*, *Computers and Chemical Engineering* 27, pp. 813-825
- Maschio G., Koufopoulos C., Lucchesi A., 1992, *Pyrolysis, a promising route for biomass utilization*, *Bioresource Technology*, vol. 42, issue 3, pp.219-231
- Naterer G.F., 2003, *Heat Transfer in Single and Multiphase Systems*, CRC Press, LLC
- Okuga A., 2006, *Analysis and operability optimization of an updraft gasifier unit*, *Dept. of Mechanical Engineering*, University of Technology, Eindhoven
- Onda K., Takeuchi M., Okumoto Y., 1967, *Mass transfer coefficient between gas and liquid phases in packed columns*, *Journal of Chemical Engineering of Japan*
- Østberg M., Glarborg P., Jensen A., Johnsson Jan E., Pedersen L. S., Dam-Johansen K., 1998, *A Model of the Coal Reburning Process*, Twenty-seventh Symposium (international) on Combustion, Combustion Institute, pp.3027-3035
- Pantoleonos G., Basinas P., Skodras G., Grammelis P., Pintér J.D., Topis S., Sakellariopoulos G.P., 2009, *A global optimization study on the devolatilization kinetics of coal, biomass and waste fuels*, *Fuel Processing Technology*, doi:10.1016/j.fuproc.2009.03.011
- Pellerano A., Pantaleo A., 2005, *Biomass energy surveying and techno-economical assessment of CHP plants: an application to Basilicata region*, *Agricultural Engineering*, vol.2, pp.25-34
- Perry R.H., Green D., 1985, *Perry's Chemical Engineers' Handbook*, McGraw-Hill
- Ramesh Babu N., Nekere Liben M., 2005, *Sustainable development – Gasification of biomass: an overview*, *ESME journal* vol. V, n.2
- Rao M.S., Singh S.P., Sodha M.S., Dubey A.K., Shyam M., 2004, *Stoichiometric, mass, energy and exergy balance analysis of countercurrent fixed bed gasification of post consumer residues*, *Biomass and Bioenergy*, 27, pp.155-171
- Ratnadhariya J.K., Channiwala S.A., 2009, *Three zone equilibrium and kinetic free modelling of biomass gasifier – a novel approach*, *Renewable Energy*, 34, pp.1050-1058
- Rhine J.M., Tucker R.J., 1990, *Modelling of Gas-Fired Furnaces and Boilers*, McGraw- Hill, as available at [http://www.btinternet.com/~robertjtucker/gas\\_ emissivity.htm](http://www.btinternet.com/~robertjtucker/gas_ emissivity.htm)
- Rodriguez C.C., De Moraes D.Jr., Da Nobrega S.W., Barboza M.G., 2007, *Ammonia adsorption in a fixed bed of activated carbon*, *Bioresources Technology*, 98, pp.886-891

- Sadhukhan A.K., Gupta P., Saha R.K., 2009, *Modelling of Pyrolysis of Large Wood Particles*, Bioresource Technology
- Savage G.M., 1989, *Thermal conductivity and specific heat of densified refuse derived fuel*, Waste Management & Research, Vol.7, Issue 1, pp.83-92
- Schimdt E., Gang P., Pila T., Dittler A., 1996, *High temperature gas cleaning*, Institut für Mechanische Verfahrenstechnik und Mechanik, Universität Karlsruhe, Germany
- Seville J.P.K., 1997, *Gas cleaning in demanding applications*, Blackie Academic & Professional (in print of Chapman and Hall)
- Sharma S.D., Dolan M., Park D., Morphet L., Yliushechkin A., McLennan K., Harris D.J., Thambimuthu K.V., 2008, *A critical review of syngas cleaning technologies – fundamental limitations and practical problems*, Powder Technology 180, pp.115-121
- Suuberg E.M., Aarna I., Milosavljevic I., 2001, *The char residues from pyrolysis of biomass – some physical properties of importance*, Progress in Thermochemical Biomass Conversion, IEA Bioenergy, vol.2, Blackwell Science Ltd., pp.1246-58
- Turku B.S., Gupta R.P., Haas J.C., Wilson K.B., Schulz R.A., 1996, *Controlling contaminants with a moving granular bed filter*, Institut für Mechanische Verfahrenstechnik und Mechanik, Universität Karlsruhe, Germany
- Uberoi M., Punjak W.A., Shadman F., 1990, *The kinetics and mechanism of alkali removal from flue gases by solid sorbents*, Energy Combustion Science vol.16, pp.205-211
- Wakao N., Funazkri T., 1978, *Effect of fluid dispersion coefficients on particle to fluid mass transfer coefficients in packed beds – correlation of Sherwood numbers*, Chemical Engineering Science, vol.33, pp.1375-1384
- Wang J.C.P., Groves F.R., Harrison D.P., 1990, *Modeling high temperature desulfurization in a fixed bed reactor*, Chemical Engineering Science, vol.45, n.7, pp.1693-1700
- Wen-Ching Y., *Handbook of fluidization and fluid particle systems*, Siemens Westinghouse Power Corporation
- Xiao Y., Wang S., Wu D., Yuan Q., 2008, *Experimental and simulation study of hydrogen sulfide adsorption on impregnated activated carbon under anaerobic conditions*, Hazardous Materials 153, pp.1193-1200
- Yang T.R., 1987, *Gas separation by adsorption processes*, Butterworths Series in Chemical Engineering
- Yang Yao Bin, Sliwinski L., Sharifi V., Swithenbank J., 2008, *Dynamic Behaviour of Sewage Sludge Incineration in a Large-scale Bubbling Fluidised Bed in Relation to feeding-rate Variations*, Fuel, vol.87, pp.1552-1563
- Yongwon J., Tien C., 1991, *New correlation for prediction the effect of deposition on collection efficiency and pressure drop in granular filtration*, Journal of Aerosol Science, vol. 22, n.2, pp 187-200.
- Yrjas P., Hupa M., 1996, *Regeneration of sulfided Zn-Titanate by oxidation under pressure*, Institut für Mechanische Verfahrenstechnik und Mechanik, Universität Karlsruhe, Germany
- Zhang Ying, Zhou Rongqi, 2006, *Vapor-liquid equilibria for water + hydrochloric acid + magnesium chloride and water + hydrochloric acid + calcium chloride systems at atmospheric pressure*, Chinese Journal of Chemical Engineering, vol.14, pp.276-280
- Zhou H., Jensen A.D., Glarborg P., Jensen P.A., Kavaliauskas A., 2005, *Numerical Modelling of Straw Combustion in a Fixed Bed*, Fuel 84, pp.389-403

## APPENDIX

### A Single efficiencies for packed bed filters:

*Interception:*

1. 
$$E_i^{\text{interception}} = \frac{(1-\varepsilon) \cdot N_{Ri}^2}{K \cdot (1 + N_{Ri})}$$
2. 
$$N_R = \frac{d_p}{d_g}$$
3. 
$$K = -\frac{1}{2} \ln(\varepsilon) - \frac{3}{4} + \varepsilon - \frac{\varepsilon^2}{4}$$

*Gravitational settling:*

1. 
$$E_i^{\text{gravity}} = \frac{Gr_i}{1 + Gr_i}$$
2. 
$$Gr_i = \frac{V_i^g}{U}$$
3. 
$$V_i^g = \frac{\rho_p \cdot d_{pi}^2 \cdot g \cdot Cu_i}{18 \cdot \mu}$$
4. 
$$Cu_i = 1 + \frac{2 \cdot S_i \cdot \lambda}{d_{pi}}$$
5. 
$$S_i = 1,277 + 0,4 \cdot e^{-1,10} \cdot \frac{d_{pi}}{2\lambda}$$
6. 
$$\lambda = 6,53 \cdot 10^{-8} \quad [\mu\text{m}]$$

*Brownian diffusion:*

1. 
$$E_i^{\text{diffusion}} = 2,58 \cdot \left( \frac{1-\varepsilon}{K} \right)^{1/3} Pe_i^{-2/3}$$
2. 
$$Pe = \frac{d_g \cdot u}{D^{\text{diff}}}$$
3. 
$$D^{\text{diff}} = \frac{k_B \cdot T \cdot Cu}{3\pi \cdot \mu \cdot d_p}$$
4. 
$$k_B = 1,38 \cdot 10^{-23} \text{ J / K}$$

*Inertial impaction:*

1. 
$$E_i^{\text{inertial}} = \frac{\left[ (29,6 - 28 \cdot \varepsilon^{0,62}) \cdot N_{Ri}^2 - 27,5 \cdot N_{Ri}^{2,8} \right] Stk_i}{4 \cdot K^2}$$
2. 
$$St = \frac{Cu \cdot \rho_p \cdot d_p^2 \cdot u}{18 \mu d_g}$$

## **B Jet pulse calculation for cleaning of candle and fabric filters**

When an opposite gas flow is injected to the filtration equipments during operation, the stress (Pa) that acts on the separation surface between the filter medium and the cake can be estimated as the difference between the total pressure drop in the unit and the one pertaining to the only same filter medium. Indeed, this difference also corresponds to the cake pressure drop, that can be in turn written as a function of the jet pulse velocity  $U_c$ .

$$1. \Delta p_{cake} = \kappa \cdot U_c \cdot M_o$$

$$2. M_o = x \cdot m \cdot u \cdot \tau$$

In order to detach the cake from the filter surface, this calculated value has to be at least equal to the so called *detachment stress*, that depends on particle nature and size, but it is not affected by cake thickness. According to the Rumpf's agglomerate strength model [Seville, 1997], the detachment stress can be estimated as follows:

$$3. \sigma_c = \pi \cdot \frac{(1 - \varepsilon)}{\varepsilon} \cdot \frac{\vartheta}{d_p}$$

As a consequence, the minimum necessary jet pulse velocity can be calculated as:

$$4. U_c = \frac{\sigma_c}{\kappa \cdot x \cdot m \cdot u \cdot \tau}$$

And the gas cleaning flow (averaged in a regeneration cycle) is:

$$5. Q_c = \frac{A \cdot t_p \cdot \sigma_c}{\kappa \cdot x \cdot m \cdot u \cdot \tau^2}$$

## C Dimensioning of fluidized bed reactors for catalytic tars cracking

In this work, the same catalyst amounts calculated in the case of fixed bed units design were also considered for sizing fluidized bed catalytic tars cracking units.

Catalyst particles sizes were instead chosen in order to belong to Geldart B Group [Geldart, 1986] (for which bubbling fluid dynamic behaviour of the reactor is easy to be established) and as to achieve the best operating conditions (in terms of tars conversion factor) according to the raw gas flows and the same amounts of catalyst. 200 $\mu\text{m}$  bed material size was chosen for 8 Nm<sup>3</sup>/h gas flow unit and 500  $\mu\text{m}$  particles were envisaged for the other two larger units

Minimum fluidization velocity was calculated by means of the following relation [Kunii, 1969]:

$$1. \quad \frac{1.75}{\varepsilon_{mf}^3 \phi_s} \left( \frac{d_g u_{mf} \rho_g}{\mu} \right)^2 + \frac{150(1 - \varepsilon_{mf})}{\varepsilon_{mf}^3 \phi_s^2} \left( \frac{d_g u_{mf} \rho_g}{\mu} \right) = \frac{d_g^3 \rho_g (\rho_s - \rho_g) g}{\mu^2}$$

The ratio between gas superficial velocity and minimum fluidization velocity was fixed to 4 in the case of 8 Nm<sup>3</sup>/h unit and to 3 in the other two cases.

From the ratio of gas flow design values and gas superficial velocities, cross sections and bed diameters were calculated. Void fraction of the bed  $\varepsilon_{mf}$  at minimum fluidization condition was estimated according to bed material size [Kunii et al., 1969] and, finally, bed heights at minimum fluidization condition were calculated as follows:

$$2. \quad kg_{cat} / [A_{bed} \cdot \rho_s \cdot (1 - \varepsilon_{mf})]$$

According to the two phase bubbling model, fluidized bed is divided in bubbles and emulsion phase. Most of the gas is flowing through the bed as bubbles, while catalyst particles are almost completely included in the emulsion phase.

Bubbles grow and accelerate from the bottom of the bed to its upper surface and they are surrounded by an high solids concentration zone, called *cloud*. Besides, because of the different velocities between bubbles and gas in emulsion phase, a depression zone is also created in the bottom part of bubbles, called *wake*. As a consequence of depression, an higher concentration of solids is detected in this zone, as well.

Both cloud and wake amplitudes depend on bubbles size and velocity. Nevertheless, the most of the catalyst is still considered to be in the emulsion phase, that therefore is also considered as the main zone where catalytic reactions take place.

Reacting gas is on the contrary supposed to be in bubbles only, since the emulsion phase gas is considered at minimum fluidization condition or even stagnant, so that it can be neglected in respect with the total gas flow. For this reason, two phase bubbling model can be only applied in the case gas superficial velocity is quite higher than minimum fluidization velocity. Minimum ratio between them is suggested to be around 2.

In order to estimate the effective tars cracking efficiency of reactor, gas mass transfer phenomena from bubbles to clouds and wakes, and/or from these latter to the emulsion phase need to be considered, besides the intrinsic kinetics of reactions.

Conversion factor for bubbling bed tars cracking units is given by:

$$3. \quad X = \left( \frac{L_{bed} \cdot k}{u_b} \right) \cdot \left[ \gamma_b + \frac{1}{\frac{k}{(K_{bc})_b} + \frac{1}{\gamma_b + \frac{1}{\frac{k}{(K_{ce})_b} + \frac{1}{\gamma_e}}}} \right]$$

$\gamma_b$ ,  $\gamma_c$  and  $\gamma_e$  are respectively the volumes of solids in bubbles, clouds and wakes, and emulsion phase, in respect with the total volume of bubbles.

As already mentioned, solids in bubbles are almost zero. In this case,  $\gamma_b$  is estimated as 0,005, while  $\gamma_c$  and  $\gamma_e$  are calculated as follows:

$$4. \quad \gamma_c = (1 - \varepsilon_{mf}) \left[ \frac{3u_{mf} / \varepsilon_{mf}}{0,711(gd_b)^{0,5} - u_{mf} / \varepsilon_{mf}} + \alpha \right]$$

$$5. \quad \gamma_e = (1 - \varepsilon_{mf}) \cdot \left( \frac{1 - \delta}{\delta} \right) - (\gamma_c + \gamma_b)$$

where  $\alpha$  is the ratio between the volume of the wake and the volume of the corresponding bubble,  $V_{wake} / V_{bubble}$ . It is calculated through the following empirical formula:

$$6. \quad \alpha = 1 - \exp(-0,057 \cdot d_b)$$

$\delta$  is the bed volume consisting on bubbles and it is in turn estimated as:

$$7. \quad \delta = \frac{u_o - u_{mf}}{u_b - u_{mf}}$$

$u_b$  is the bubbles velocity and it is given by:

$$8. \quad u_b = 1,6 \cdot \left[ (u_o - u_{mf}) + 1,13(d_b^s)^{0,5} \right] \cdot D_{bed}^{1,35} + \frac{\sqrt{2}}{3} \cdot \left( \frac{1}{1 - \alpha} \right)^{\frac{1}{6}} \cdot (gd_b)^{0,5}$$

$(K_{bc})_b$  and  $(K_{ce})_b$  are respectively the gas mass transfer coefficients from bubbles to wake and cloud and from these latter to the emulsion phase (in respect with the bubbles volume in the bed). They are estimated by the followings:

$$9. \quad (K_{bc})_b = 4,5 \cdot \left( \frac{u_{mf}}{d_b} \right) + 5,85 \cdot \left( \frac{(D^m)^{1/2} \cdot g^{1/4}}{d_b^{3/4}} \right)$$

$$10. \quad (K_{ce})_b = 6,78 \cdot \left( \frac{\varepsilon_{mf} \cdot D^m \cdot u_b}{d_b^3} \right)^{\frac{1}{2}}$$

As it can be seen, bubble diameter appears in many of these formula. Since they grow from the bottom of the bed to the upper surface, their average value was considered as the bubble size in the overall bed.

Different equations have been found out in order to estimate bubble size at gas distributor,  $d_{b_0}$  (at the bottom of the bed), as well as the ones at the upper surface of the bed,  $d_b^s$ . The formula considered in this work are shown below:

*Darton:*

$$11. \quad d_{b_0} = \frac{0,411 \cdot [A_{or} \cdot (u_o - u_{mf})]^{0,4}}{g^{0,2}}$$

$$12. \quad d_b^s = \frac{0,54 \cdot (u_o - u_{mf})^{0,4} \cdot (L_{bed} + 4\sqrt{A_{or}})^{0,8}}{g^{0,2}}$$

*Geldart:*

$$13. \quad d_{b_0} = \frac{0,361 \cdot [A_{or} \cdot (u_o - u_{mf})]^{0,4}}{g^{0,2}}$$

$$14. \quad d_b^s = d_{b_0} + 0,027 \cdot L_{bed} \cdot (u_o - u_{mf})^{0,94}$$

*Mori and Wen:*

$$15. \quad d_{b_0} = \frac{0,347 \cdot [A_{or} \cdot (u_o - u_{mf})]^{0,4}}{g^{0,2}}$$

$$16. \quad d_b^{\max} = \frac{0,374 \cdot [\pi \cdot D_{bed}^2 \cdot (u_o - u_{mf})]^{0,4}}{g^{0,2}}$$

$$17. \quad \frac{d_b^{\max} - d_b^s}{d_b^{\max} - d_{b_0}} = e^{\left( \frac{-0,3 \cdot L_{bed}}{D_{bed}} \right)}$$

Average values from these relations were considered for both of the case,  $d_{b0}$  and  $d_b^s$ .

$L_{bed}$  was then estimated using an iterative procedure, according to eq. 7, 8 and the following one:

$$18. \quad L_{bed} = L_{mf} \cdot (1 + \delta)$$

Finally, TDH for bubbling beds was estimated by means of the following empirical equations [Geldart, 1986]. The average value was chosen in this case, too.

$$19. \quad TDH = 1000 \cdot u_f^2 / g \quad (\text{Fournol et al.})$$

$$20. \quad TDH = 4,47 \cdot d_b^s{}^{1/2} \quad (\text{Horio et al.})$$

$$21. \quad TDH = 0,85 \cdot u_f^{1,2} (7,33 - 1,2 \log_{10} u_f) \quad (\text{Amitin})$$

$u_f$  is the gas velocity in the freeboard. According to the gas flows considered in this work, in some cases it was reduced by enlarging reactor diameters, in order to obtain acceptable values of TDH.